UNDERSTANDING CONGENITAL BIRTH DEFECTS DEVELOPMENTAL DEFECTS IN THE VESTIBULAR LAMINA

Qiu, Tengyang

Awarding institution:
King's College London

UNDERSTANDING CONGENITAL BIRTH DEFECTS:

DEVELOPMENTAL DEFECTS IN THE VESTIBULAR LAMINA

A thesis submitted for the degree of Doctor of Philosophy

Tengyang Qiu

Faculty of Dentistry, Oral & Craniofacial Sciences

Centre for Craniofacial and Regenerative Biology

King's College London

London SE1 9RT, UK

First Supervisor: Prof. Abigail Tucker

Second Supervisor: Dr. Isabelle Miletich

Mar 2023

Table of Contents

Abstract (P3-P5)

Chapter 1: Introduction (P6-P47)

Chapter 2: Methods (P48-P52)

Chapter 3: (Publication 1 and unpublished supplementary data) Development of the Vestibular Lamina in Human Embryos: Morphogenesis and Vestibule Formation (P53-P67)

Chapter 4: (Publication 2) Mechanisms driving vestibular lamina formation and opening in the mouse (P68-P81)

Chapter 5: (Publication 3 and unpublished supplementary data) Molecular profiling of the vestibular lamina highlights a key role for Hedgehog signalling (P82-P115)

Chapter 6: Supplementary supportive data completed as part of thesis (P116-P156)

Chapter 7: Discussion (P157-P169)

Acknowledgements (P170-P172)

References/Bibliography (P173-P206)

List of Figures (P207-P235)

Abstract

Approximately 3-6% of babies worldwide are born with serious birth defects each year. Among these, craniofacial malformations collectively represent about one-third of all congenital anomalies. The clinical conditions have life-long consequences for the patients, however, the mechanisms of pathology and etiology associated with most craniofacial birth defects are unknown. My PhD project seeks to provide an in-depth analysis focusing on an important but understudied embryonic craniofacial structure the vestibular lamina (VL). Defects in the VL are present in a number of craniofacial syndromes and are associated with the formation of dental tumours (odontomas) in later life.

The VL is an embryonic structure that forms the oral vestibule. It shares a common origin with the neighbouring dental lamina (DL). The development of the VL is disrupted with a high incidence in Ellis-van Creveld (EvC) syndrome. In this syndrome, patients display multiple oral frenula physically linking the lips and teeth. EvC syndrome is a recessive disorder considered as a ciliopathy, which is caused by a mutation in *EVC* or *EVC2*. EVC and EVC2 proteins localize at the base of the primary cilia, and function to regulate hedgehog signalling. To understand the underlying mechanisms linking mutations in *EVC* genes to the physical abnormalities, my PhD project aims to: 1) To examine the early development of VL in mouse and human, and assess the mechanisms underlying furrow formation. 2) To identify the molecular signature for the VL

and to explore the differences in signalling pathway expression in VL and DL. 3) To investigate the development of the VL in *Gas1* and compound mutants and explore the role of Shh signalling in the VL and DL. 4) To compare the VL defects in *Gas1* and *Evc* mice, looking for common underlying mechanisms. The key methods include organ culture, RNA-Scope, DIG *in situ* hybridization, bioinformatic analysis, immunofluorescence, statistical analysis, and histological staining.

I first assessed the VL development in human and mouse, and revealed the mechanisms of furrow formation during normal development. The VL shows a close relationship with DL from initiation to differentiation, with fissure formation caused by terminal differentiation without an obvious contribution from apoptosis. Extension of the VL is driven by localized proliferation at the edges of the VL in the human and mouse. Bulk RNA-Seq was performed to explore the molecules involved during early development of the VL and DL. Novel gene expression data and potential signalling pathways were identified. The highlighted differences of Shh pathway components in the VL and DL drove me to concentrate on the Shh signalling. I have identified that the VL development rely on the Shh signals from the adjacent tooth germ using the Shh pathway mutants (*Gas1* and compound mutants). A deeper understanding of the mechanisms that lead to EvC syndrome defects was achieved through a further comparative analysis of *Evc* mutants and *Gas1* mutants. Despite sharing a

similar truncated VL phenotype, *Gas1* and *Evc* mutants exhibit different pathological mechanisms. Both *Gas1* and *Evc* mutants displayed a reduction in proliferation within the truncated VL. However, the *Gas1* mutants showed decreased expression of *Gli1*, whereas *Evc* mutants exhibited an upregulation of *Gli1*. Additionally, in *Evc* mutants, I have identified other VL and DL defects mimicking the phenotypes seen in EvC patients, such as multiple VL, conical teeth, fused teeth, and supernumerary tooth originated from VL. Moreover, the opening of the short VL occurred as normal and the basic cilia structure appeared unaffected in the *Evc* mutants. These findings will help our understanding of the oral problems in syndromes such as EvC syndrome and other ciliopathies.

The nomenclature used in this thesis adhere to the following rules and guidelines: https://www.informatics.jax.org/mgihome/nomen/

Chapter 1 – Introduction

The craniofacial region consists of a diverse range of tissues, many of which are derived from the neural crest, such as the calvaria and facial bones, odontoblasts, and cranial nerves (**Chai *et al.*, 2000**). Tissues in the craniofacial region that originate from the mesoderm include connective tissue, bones of the cranial base, and muscles (**Yoshida *et al.*, 2008**). The endodermal germ layer forms the pharynx, auditory tube and the middle ear cavity, while the ectoderm forms the inner ear, the skin, and lines the main body of the oral cavity forming the epithelium of the teeth and glands (**Rothova *et al.*, 2012**).

1.1 Embryonic development of the DL and VL in mice and human

The vestibular lamina (VL), also referred to as the labio/bucco-gingival sheet (**Bolk, 1921**) or lip-furrow band (**Schour, 1929**), is a transient epithelial structure that shapes the upper and lower lip furrows (**Hovorakova *et al.*, 2005**). These furrows form the sulcus separating teeth/alveolar portion from the cheeks/lips, known as the vestibulum oris or oral vestibule (**Von and Lozanoff, 2017**) (**Fig. 1**). The VL is encircled buccally/labially by the cheeks and lips mucosa, and internally by the labio-buccal sides of the teeth, gingiva, and alveolar mucosa **(Bolk, 1921; Schour, 1929; Hovorakova *et al.*, 2005**).

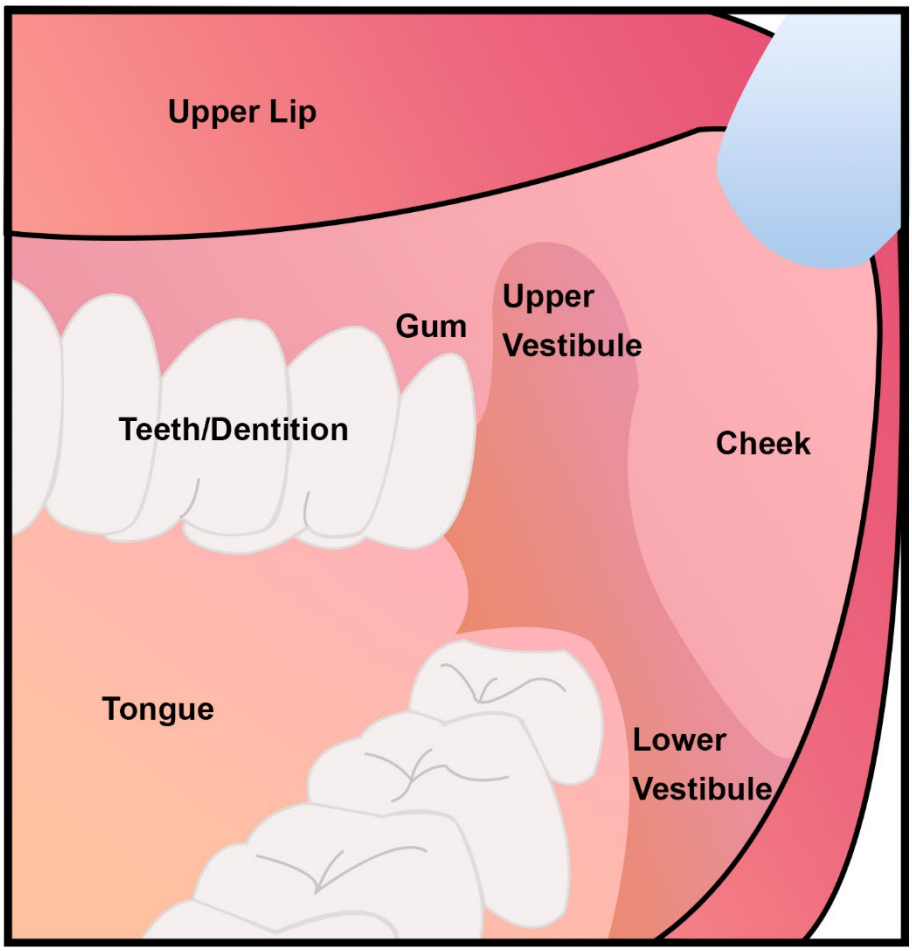

Figure 1. A basic schematic diagram showing the structure of oral cavity. The upper vestibule and lower vestibule are highlighted, which create the sulcus between the cheeks/lips and teeth/gum.

The VL develops on the buccal/labial side of the forming dental lamina (DL), an anlage of the enamel-organs of the tooth primordia and ultimately contribute to the tooth formation. Histologically, the DL consists of a basal layer of columnar cells and superficial squamous cells, separated from the mesoderm by a well-defined basement membrane (**Schour, 1929**). There is a developmental association between the VL and DL, as in mice it has been shown that they

originate from a common primitive epithelial band (**Hovorakova *et al.*, 2016**). In mice, this thickened epithelial band becomes apparent at approximately embryonic day 11 (E11), and subsequently splits into the two laminas (**Peterková, 1985; Tucker and Sharpe, 2004**). Similarly, in human embryos, the primary epithelial band appears around the 6th week during development (**Moore and Persaud 1993**), indicating a comparable developmental process. Contrary to the theories of shared developmental origin of the VL and DL, other research has proposed that these two laminas emerge as distinct structures, with the VL forming either before or after the initial appearance of the DL in both mice and humans **(Orban, 1928; Schour, 1929; Tonge, 1969; Nery, Kraus and Croup, 1970**).

1.2 Initiation and development of the DL

Humans have two sets of dentitions (diphyodont), which exhibit an ordered tooth arrangement of incisors, canines, premolars, and molars. The deciduous or milk teeth are eventually replaced by the permanent teeth, which emerge lingually from the successional dental lamina. These various tooth types with their unique shapes and precise occlusion are thought to adapt to changes in dietary need during evolution (**Miletich and Sharpe, 2003; Tucker and Sharpe, 2004**). Conversely, mice have only single generation of teeth (monophyodont), with a comparatively simpler dentition that lacks canines and premolars, where the incisors and molars are separated by a diastema or toothless gap (**Miletich**

and Sharpe, 2003; Tucker and Sharpe, 2004) (**Fig. 2**).

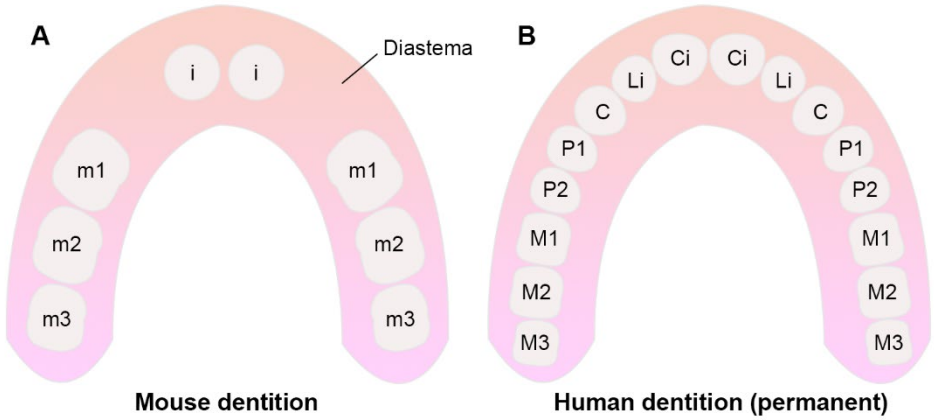

Figure 2. A diagrammatic representation illustrating the arrangement and types of teeth in mice and humans. (**A**) Mouse dentition. In mice, there are one incisor (i) and three molars (m1, m2, m3) positioned in each quadrant, which are distinctly spaced apart by a toothless gap in the dental arch, known as the diastema. (**B**) The human has two sets of dentitions and more complex tooth types. The arrangement of permanent dentition is displayed, which consists eight teeth in each quadrant, including one central incisor (Ci), one lateral incisor (Li), one canine (C), two premolars (P1, P2), and three molars (M1, M2, M3). The third molar (M3) is also called wisdom teeth.

The development of teeth during the embryonic stage involves a series of morphological changes, driven by interactions between the dental epithelium and the underlying mesenchyme. The odontogenesis begins with the initiation of oral epithelial thickening/placode, and the DL originates from this thickened placode as described above at E11. The 3D reconstructions of murine dental primordia and their adjacent structures during embryonic development indicate

that the murine DL and VL were not visible in the mandible and maxilla by E12 (**Radlanski, Mocker and Rahlfs, 1998**). And at approximately E13 in mice, the DL extends downwards into the mesenchyme, and the mesenchyme begins condenses around the DL, leading to the formation of a bulbous epithelial bud, which is termed the bud stage. As the epithelium continues to elongate into the mesenchyme, it takes on a cap-shaped appearance by E14, and the epithelial invagination is filled by the mesodermal tissue called the dental papilla. The tooth germ then proceeds from the "cap-stage" into the "bell- stage" with the onset of differentiation (**Tucker and Sharpe, 2004; Hermans *et al.*, 2021**). Morphogenesis of the tooth germ is regulated by the enamel knot located in the tooth bud tip, which serves as a signaling center during tooth formation (**Jernvall *et al.*, 1998**). The enamel knot expresses Sonic hedgehog (Shh) **(Fig. 3B, C)** (**Seppala *et al.*, 2017**), in addition to a number of other signalling pahways, including Fgfs, Eda, Wnts and Bmps (**Tucker and Sharpe, 2004**). At the late-bell stage (around E18) of tooth development, the condensing mesenchyme is encased within the invaginating epithelium (**Tucker and Sharpe, 2004; Hermans *et al.*, 2021**) (**Fig. 3D**).

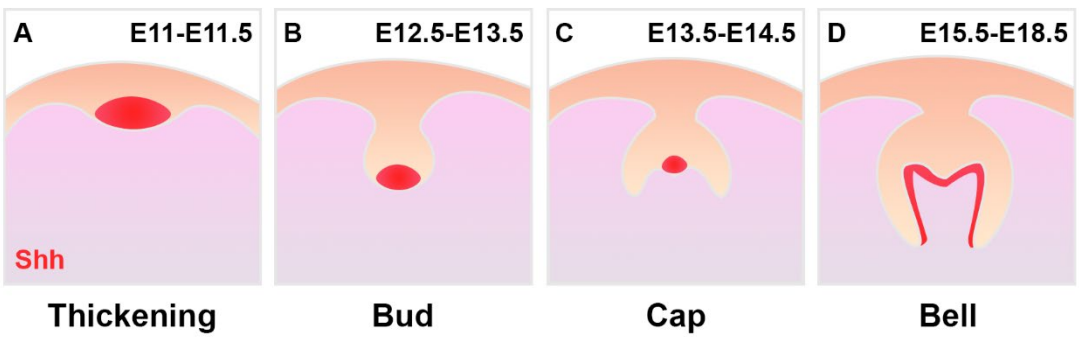

Figure 3. A schematic diagram of *Shh* transcription (red) during early tooth

development. (**A**) Thickening/placode. The DL initiates as a thickened epithelium at embryonic day (E) 11 to E11.5. The *Shh* expression is confined to the epithelial thickening. (**B**) Bud stage at E12.5 to E13.5. The *Shh* expresses in the enamel knot precursor cells located at the tip of the early bud. (**C**) Cap stage at E13.5 to E14.5. The *Shh* expression is observed in the primary enamel knot. (**D**) Bell stage at E15.5 to E18.5. *Shh* expresses is detected in the stratum intermedium, pre-ameloblasts and internal enamel epithelium.

During early tooth development, the expression of Shh expression is confined to the epithelial element of the forming tooth germ (**Seppala *et al.*, 2017**) (**Fig. 3**). Interestingly, evidence has shown in both human and mice that this secreted signaling protein can diffuse into the neighboring mesenchymal and epithelial tooth tissues, which influence reciprocal epithelial–mesenchymal signaling (**Hardcastle *et al*., 1998; Gritli-Linde *et al*., 2002; Hu *et al.*, 2013**).

1.3 Initiation and development of the human VL

Research on the neighboring VL dates back to 1921, when Bolk studied human embryonic development of the VL and DL, spanning the period from the second to fifth month of gestation (**Bolk, 1921**). Early terminology "dento-gingival" and "labio/bucco-gingival" sheets were used to describe these structures. According to the study, the oral epithelium thickening occurs and extends into the underlying tissue at the second month of embryonic development in humans,

forming a lateral labio/bucco-gingival sheet (**Fig. 4A1**) and a medial dento-gingival sheet (**Fig. 4A2**). The dento-gingival sheet gave rise to the ectodermal portion of tooth germs (**Fig. 4B4**) and partial gingiva, while the labio/bucco-gingival sheet (also termed as VL) (**Hovorakova *et al.*, 2005**) (**Fig. 4B3**) developed into the epithelia covering the inner surface of the lip and a part of the gingiva (**Bolk, 1921**). These two epithelial sheets present a complex relationship during development. The labio/bucco-gingival sheet exhibits distinct morphological characteristics as it progresses through the developing deciduous tooth germs in various regions. The labio-tectal furrow is a groove that extends into the joint anlage of the palate and lip (pointed by black arrowhead in **Fig. 4A**). A cleft subsequently formed in the epithelial mass that contributes to the labio/bucco-gingival sheet (**Fig. 4B5**). This cleft, suggested as the true VL furrow, is a lateral prolongation of the bucco-tectal groove, which separates the inner surface of lip from the outer surface of the alveolar ridge. The cleft in the VL that demarcates the dental arch from the surrounding lips/cheeks was believed to be caused by the atrophy of the cells in the labio/bucco-gingival sheet between 12^{th} and 14^{th} weeks in humans (**Bolk, 1921; Coslet and Cohen, 1969**). Despite the significant developmental interplay between the DL and VL, the VL has been largely neglected in odontogenetic studies.

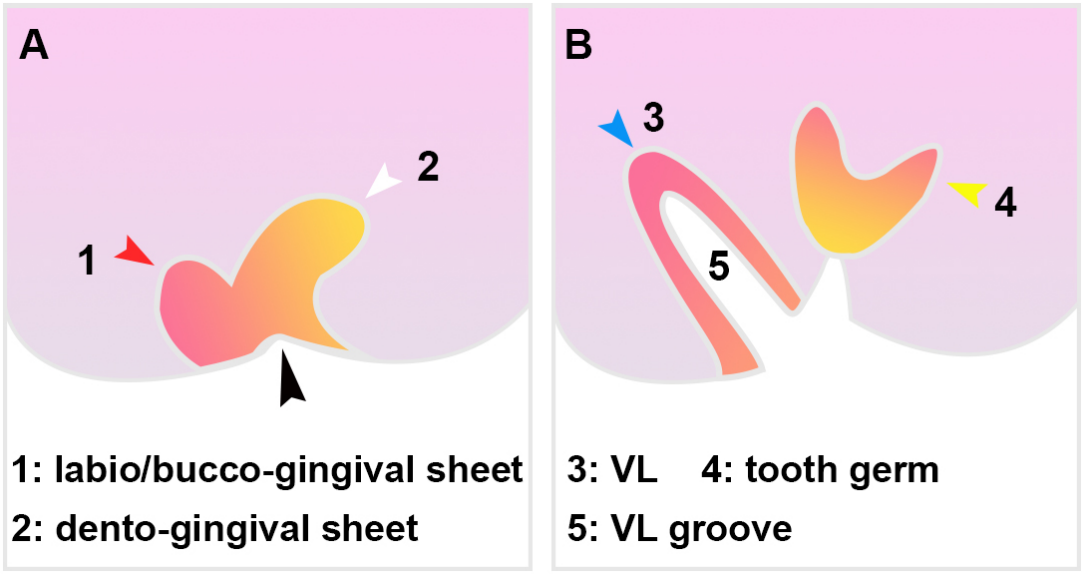

Figure 4. A basic illustration demonstrates the development of dento-gingival sheet and labio-gingival sheet in human embryos. (**A**) During the second month of embryonic development in humans, epithelial thickening grew into the underneath tissue, forming the labio/bucco-gingival sheet (A1) and dento-gingival sheet (A2). The labio-tectal furrow was indicated by a black arrowhead. (**B**) The dento-gingival sheet produced the ectodermal section of tooth germs (B4). Meanwhile, the labio/bucco-gingival sheet developed into the epithelia (B3) that covered the interior surface of the lip and a portion of the gingiva. 1: labio/bucco-gingival sheet (red arrowhead), 2: dento-gingival sheet (white arrowhead), 3: vestibular lamina (VL) (blue arrowhead), 4: tooth germ (yellow arrowhead), 5: VL groove.

1.4 The developmental association of the VL and DL

The VL and DL closely interact during development, and their anatomic relationship is commonly characterized as a classic horseshoe-shaped epithelial structure (**Fig. 6A**). This configuration typically features the VL

situated externally and running parallel to the continuous DL. Such 2-dimentional (2D) view was derived from observations made on serial histological sections in humans, with the VL giving the impression of appearing continuously throughout the dental arch (**Bhaskar, 1980; Schroeder, 1991**). Due to limitations of the 2D observations, the significance of 3D computer-assisted reconstruction was highlighted in comprehending spatial arrangement of oral cavity and surrounding structures such as tooth germ and VL (**Radlanski, 1995**) (**Fig. 5A**). A clear correlation between the tooth primordia and the VL can be observed in human embryos, particularly in the lower central incisor region where a fusion between the VL and dental epithelium was observed (**Fig. 5B**). Additionally, a thick VL was observed in the region of the upper canine primordia (**Fig. 5C**) (**Radlanski, 1995**).

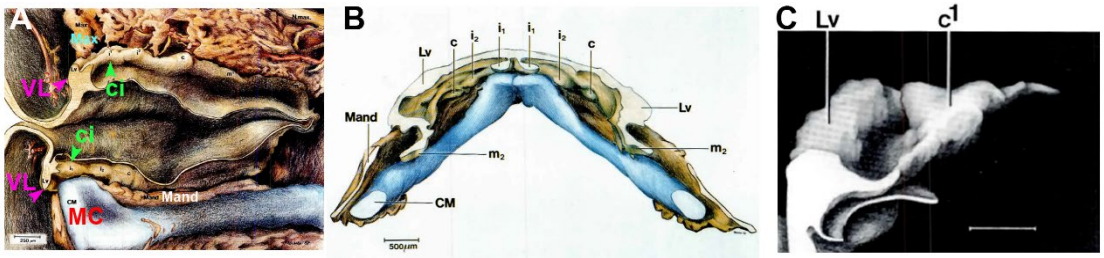

Figure 5. Spatial arrangement of oral cavity and its surrounding structures. (**A**) 37mm crown-rump length (CRL) human embryo. Based on a 3D reconstruction of the right oral cavity and its adjacent tissues, it was observed that the tooth germs i^1 in the maxilla region were in the bud stage, the maxilla extended into the groove between the Lv (VL) and Ld (DL). In the lower jaw, i_1 had developed to the early cap stage. Additionally, the CM (MC) swell had reached adjacent to the bud i_1, and a portion of the Mand was situated in the space between the CM (MC) and other dental germs. (**B**)

21mm CRL human embryo. A 3D reconstruction was used to examine the lower tooth primordia and the surrounding tissues, which revealed that the Lv (VL) runs continuously and externally to the tooth germs. Furthermore, the Lv (VL) was found to be fused with the central incisor. (**C**) 37mm CRL human embryo. A 3D reconstruction of the upper canine primordia and the Lv (VL) showed that the VL was particularly thick in this region. Lv (VL): vestibular lamina; Ld (DL): dental lamina; i1: primary central incisor primordia; i2: primary lateral incisor primordia; c: primary canine primordia; m1: the primary 1st molar primordia; m2: the primary 2nd molar primordia; Mand: mandibular bone; Max: maxilla; CM (MC): Meckel's cartilage (adapted from **Radlanski, 1995**).

More recently, computer-aided 3D reconstructions show that the VL is actually discontinuous in the human maxilla, with the vestibule epithelium dispersing in the VL region during embryonic development (**Hovorakova *et al.*, 2005**) . While the VL consistently appears discontinuous in the mandible of human embryos (**Hovorakova *et al.*, 2007**). The structure of the VL and DL is therefore more complex than previously suggested, as revealed by recent findings (**Hovorakova *et al.*, 2007**) (**Fig. 6**).

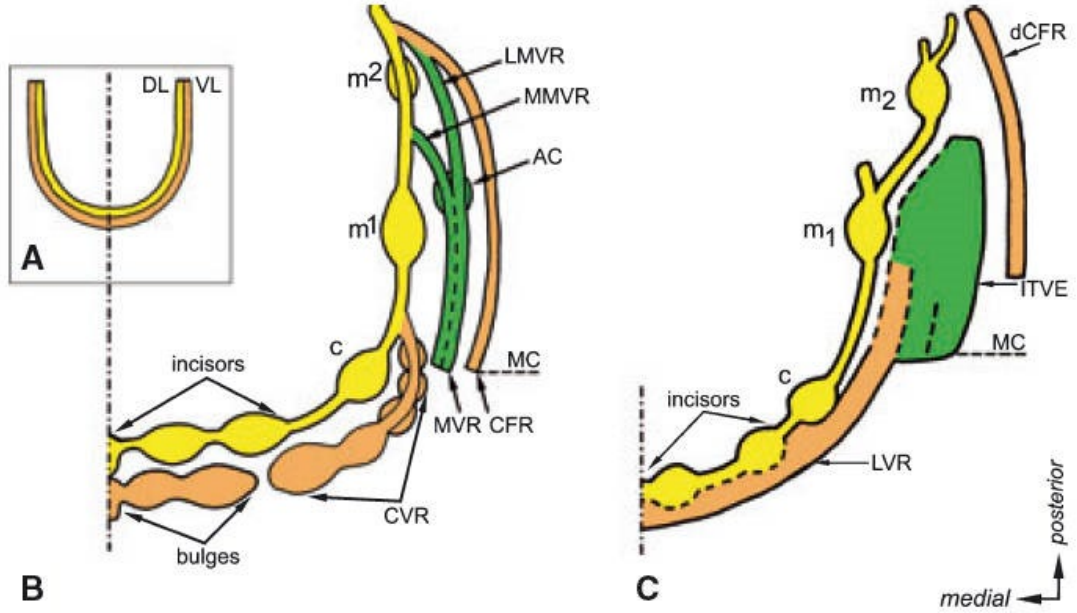

Figure 6. Spatial interactions of the DL and VL in human fetus. The dental epithelium is tinted yellow, and the base of the oral vestibule is shaded in orange. The rest VL epithelium is green. (**A**) The prevailing theory posits that the VL is a continuous entity that runs externally and parallel the DL. (**B**) VL and DL in the upper jaw. Recent findings suggest that the upper VL epithelial bulges initially appear outside of the DL in the lip area. These bulges fuse together and develop into the CVR situated posteriorly. The CVR merges with the dental mound located posterior to the c. Within the cheek area, the vestibular epithelium gives rise to both the MVR and CFR. The CFR refers to the epithelium that lines the mucosal inflection, separating the cheeks and teeth. Posteriorly, the MVR separates into two distinct branches MMVR and LMVR as it extends backwards. (**C**) VL and DL in the lower jaw. The lower vestibular epithelium exhibits several distinct structures, including the LVR, ITVE, and the dCFR. In the lower incisor region, the vestibular and dental epithelium are fused together. VL: vestibular lamina; DL: dental lamina; CVR: canine vestibular ridge; c: deciduous canine

primordium; CFR: cheek-furrow ridge; LMVR: lateral molar vestibular ridge; MMVR: medial molar vestibular ridge; MVR: molar vestibular ridge; AC: accessory epithelial cap; MC: mouth corner; LVR: labial vestibular ridge; ITVE: irregularly thickened vestibular epithelium; dCFR: mandibular cheek furrow ridge; m1: first deciduous molar; m2: second deciduous molar (**Hovorakova *et al.*, 2007**).

The complex interconnection between these two laminas in distinct areas of the jaw may explain the varying descriptions of their development. Nevertheless, evidence suggests that both the VL and DL arise from a shared thickening placode, at least in the lower incisor region of humans (**Bolk, 1921; Hovorakova *et al.*, 2007**). Recent research on lineage tracing of *Shh*-positive cells in the VL and DL has provided further support for their common origin, where both laminas exhibit a shared domain of *Shh* expression in the incisor region of mice (**Hovorakova *et al.*, 2016**). These *Shh* expressing cells in the oral epithelial band were traced by Cre-loxP system, and their descendants were observed in both the DL and the inner epithelial layer of the VL (**Hovorakova *et al.*, 2016**). The investigation on the decisions that determine the fate of this odontogenic placodes has uncovered additional complexity in the VL and DL relationship. During early developmental stages, *Pitx2* and *Shh* have been found to be expressed in this united odontogenic placode (**Thesleff, 2008**). As development progresses, these two laminas start to express different markers, with the VL expressing *Dlx7* at E13.5 while the DL and tooth germs

express *Dlx5* (**Davideau *et al*., 1999; Wang *et al*., 2009**). These Dlx genes show a similar expression profiles at bud and cap stages, with the exception of overlapping expression on the buccal DL at cap stage (**Davideau *et al*., 1999; Wang *et al*., 2009**).

1.5 The VL exhibits species-specific differences in morphology

The anatomy of the VL has been studied in several species, including human, mouse, vole, and sheep, revealing notable differences throughout the jaw across those species (**Pavlikova et al., 1999; Hovorakova *et al*., 2005, 2007, 2016; Witter *et al*., 2005**). As an example, the mouse exhibits distinct variations in the upper and lower VL. Specifically, the lower anterior jaw features a highly prominent VL, while the corresponding upper part has a considerably less pronounced VL (**Peterková, 1985; Hovorakova *et al*., 2016**). On the other hand, the human (**Hovorakova *et al*., 2005, 2007**) and sheep (**Pavlikova et al., 1999**) have much thicker multi-layered VLs in comparison to the thin VLs of vole (**Witter *et al*., 2005**) and mouse (**Hovorakova *et al*., 2016**). Such anatomical discrepancies likely contribute to morphological variations of the presumptive oral cavity and may be indicative of diet diversities among these species. Although the VL present anatomical variations across species, it maintains a close association with the DL during embryonic development, forming from the shared epithelial band as describe previously. In a similar vein, the capacity of this single placode to develop into multiple tissue types has been

noted in reptiles, where the early dental lamina is thought to give rise to both the DL and an adjacent dental gland. This is exemplified in venomous snakes, as the epithelial band can bifurcate into the fang anlage and venom gland (**Kochva, 1963; Vonk *et al.*, 2008**). A comparable arrangement has been identified in lizards, such as chameleons **(Tucker, 2010; Buchtová *et al.*, 2013**). Thus, these placodes can be regarded as the DL-VL lamina in mammals and DL-gland lamina in reptiles, with the early placode having the ability to form teeth, oral vestibule and glands (**Bolk, 1924**) (**Fig. 7**). Additionally, both the VL and glands develop externally to the DL and possibly evolved from an outer row of teeth that share a common ancestor among amniotes (**Hovorakova *et al.*, 2020**).

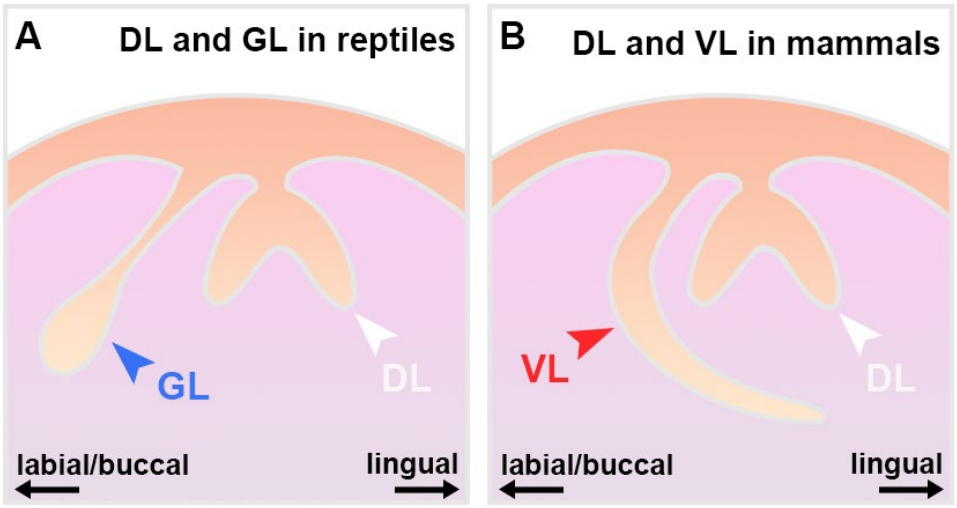

Figure 7. DL-gland lamina in reptiles and DL-VL lamina in mammals. (**A**) In reptiles, the primary epithelial thickening can develop into the DL and an adjacent gland lamina, such as the venom gland in snake and gland in chameleons. (**B**) In mammals, this primary epithelial thickening can develop into the DL and an adjacent vestibular lamina. Both the glands and VL located in the buccal/labial side of the DL. DL: dental lamina;

VL: vestibular lamina; GL: gland lamina.

1.6 VL and odontoma formation

In mammals, rudimentary teeth can develop on the labial/ buccal side of the milk dentition, which is called the pre-milk or pre-lacteal dentition in human (**Röse 1895; Adloff 1909; Leche 1893; Hovorakova *et al.*, 2020**). These rudimentary teeth were also thought as cusps or paramolar externally to the milk molars in human (**Bolk 1914; Adloff 1907; Adloff 1916; Hovorakova *et al.*, 2020**). These tooth-like epithelial structures located labially/buccally to the dental arch have long been associated with the pathological occurrence. For instance, pathologies in patients such as tooth-like tumors, known as odontomas, tend to appear in the oral vestibule. These observations suggest that this region retains some odontogenic potential that can be reawakened in pathological situations **(Hanemann *et al.*, 2013; Hovorakova *et al.*, 2016**). Odontoma, the most frequently occurring odontogenic tumor in the oral cavity, is a benign tumor that comprises various dental tissues such as dentin, enamel, cementum, and pulp (**Boffano *et al.*, 2022**). It is thought to be a developmental anomaly originating from the epithelial and mesenchymal cells (**Boffano *et al.*, 2022**). According to the summary of **Hovorakova *et al*. (2020)**, odontomas can arise in both maxilla **(e.g: Ghandehari-Motlagh *et al.*, 2016**) and mandible **(e.g: Uma, 2017**), with approximately 50% of cases occurring in the anterior maxilla (**Sánchez, Berrocal and González, 2008; Levi-Duque and Ardila,**

2019). Odontomas can be classified as either compound, which resemble tooth-like tissues, or complex, which are disorganized dental structures. Compound odontomas are typically detected more frequently in the anterior portion of maxilla, while posterior region of the mandible is where complex odontomas commonly occur (**Satish *et al.*, 2011**). Research on the VL development has explained why compound odontomas are more frequently found in the anterior upper jaw than lower jaw. Specifically, in the maxilla, the VL forms discrete prominent epithelial bulges that are separate from the dental mound in the lip area (**Hovorakova *et al.*, 2005**). The sites of these distinct VL bulges have been suggested as the locations where tooth-like (compound) odontomas develop in the anterior maxilla (**Fig. 8**) (**Hovorakova *et al.*, 2020**). Conversely, VL in the corresponding region of the mandible presents a closer relationship with the dental lamina, with bulges formed by the dento-vestibular epithelium (**Hovorakova *et al.*, 2007**). The posterior mandible is the site where complex odontomas are more frequently detected, and this region is characterized by an irregularly thickened VL (**Hovorakova *et al.*, 2007**). An accessory cap (AC) observed on the molar vestibular ridge exhibits a similar morphology of the tooth germ at cap stage, which is buccal to the first primary molar primordium in the upper jaw (**Hovorakova *et al.*, 2005**). AC was also found at the level of the second milk molar (**Adloff, 1909**), and a similar structure to AC has been described by **Bolk (1924)**. Such accessory epithelial structures were commonly supposed to be unable to develop into the teeth, and

their further growth is repressed during normal development. AC bulge was suggested to be another region where the compound odontoma might form, which may explain why some odontomas occur in more posterior maxilla (**Hovorakova *et al.*, 2005, 2007**) (**Fig. 8**). The VL is therefore predicted to have potentiality to develop tooth-like odontomas or supernumerary teeth under some pathological circumstances.

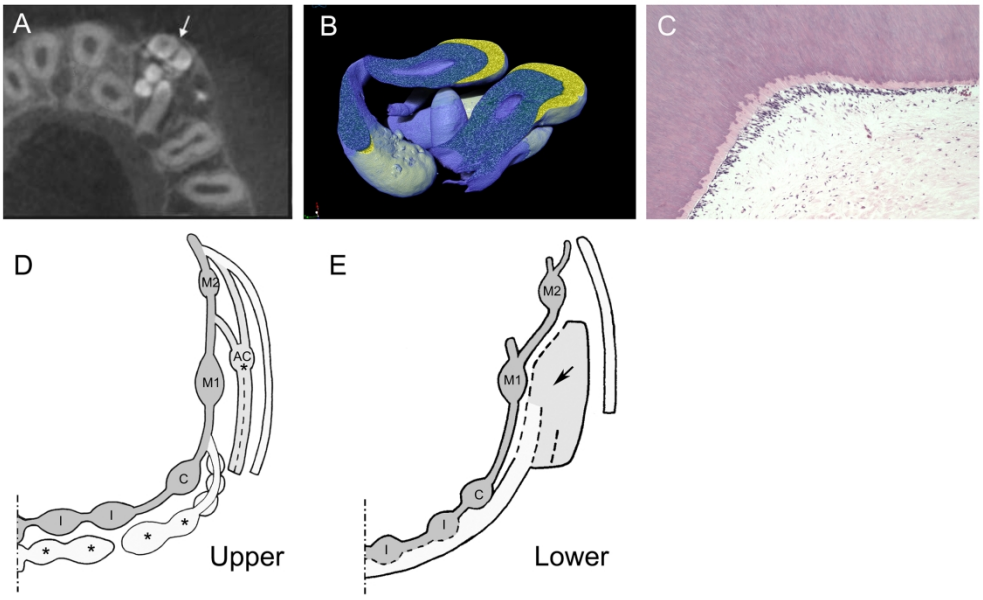

Figure 8. Odontomas formation associated with VL. (**A**) Cone Beam Computed Tomography (CBCT) photograph of a 10-year old patient, showing the odontomas formation located in the anterior upper jaw. (**B**) The MicroCT scan displays the dental structures within odontoma. (**C**) Histological section of odontoma toothlet, which shows a structured odontoblasts layer. (**D, E**) The upper and lower VL/DL in human fetuses are visualized by 3D reconstructions (**Hovorakova *et al.*, 2007**). Dark grey: DL, I: Incisors, C: Canines, M1: the 1st molar, M2: the 2nd molar, AC: accessory cusp. Asterisks: highlights of the areas to form compound odontomas; Arrow: the region where complex odontomas may form (**Hovorakova *et al.*, 2020**).

1.7 The murine VL can develop teeth/tooth-like structures after manipulation

Although the VL does not normally form teeth, it possesses the potential to form teeth when subjected to certain stimuli or conditions. For example, the presence of odontomas and supernumerary teeth has been reported in many syndromes such as Gardner syndrome, which is characterized by an overactivation of the Wnt signalling caused by the adenomatous polyposis coli (APC) mutation (**García and Knoers, 2009; Yu *et al.*, 2018**). The overactivated canonical Wnt signalling in the oral epithelium can induce extra tooth formation in the vestibule area of APC conditional knockouts, accompanied by upregulation of *Fgf8* and *Shh* (**Wang *et al.*, 2009**). And when Wnt signalling was overexpressed in *Sox2*-positive cells, supernumerary teeth were observed in the VL region, which could form mineralised teeth after isolation and culture (**Popa, Buchtova and Tucker, 2019**). Similarly, odontoma formation due to the stimulated Wnt signalling was also observed in mice (**Xavier *et al.*, 2015**). The initiation of odontogenic odontomas is also associated with overactivated Shh (**Rui *et al.*, 2014**), suggesting that the odontomas in non-odontogenic epithelial areas might be triggered by the abnormal activation of Shh in these regions **(Hovorakova *et al.*, 2016**). These effects can be counteracted when the Wnt/β-catenin is overexpressed in the mesenchyme, leading to an inhibition of the tooth number (**Järvinen *et al.*, 2018**). Similar to what has been observed in mice, the

overactivation of Wnt/β-catenin induced by the GSK3β inhibitors in dental culture of snake can lead to more ectopic tooth germs **(Gaete and Tucker, 2013**). These data suggest that the VL can form teeth in some situation, which might be relevant to its common origin with the DL. The odontogenic competence of the oral vestibule can be supported by previous research that shows the formation of dental tumors expressing enamel matrix in transgenic ameloblastin-null mice (**Fukumoto *et al.*, 2004**).

1.8 VL and DL defects are constant phenotypes in Ellis-van Creveld syndrome

Disruptions in the development of VL can occur in certain human disorders, like Ellis-van Creveld (EvC) syndrome (OMIM 225500), resulting in defects in the oral vestibule that may manifest as multiple frenula and labio-gingival adherences **(Sasalawad *et al.*, 2013; Peña-Cardelles *et al.*, 2019**). Other ectodermal dysplasias, like Weyers acrofacial dysostosis (OMIM 193530), have also found to be associated with vestibule defects (**Roubicek and Spranger, 1984**). More recently, abnormalities in oral vestibule and teeth were found in a cryptophthalmos patient caused by the *FREM2* mutation (**Kantaputra *et al.*, 2022**). Among these, oral vestibule defects have been widely reported in individuals with EvC syndrome, however, the underlying mechanisms are still unknown. EvC syndrome is primarily typified by autosomal recessive inheritance, disproportionate dwarfism, short limbs and ribs, polydactyly,

congenital heart malformations, and oral deficiencies (**Ellis and Van Creveld, 1940**). The EvC patients show a wide spectrum of clinical phenotypes related to multisystemic involvement, including skeletal dysplasia, postaxial polydactyly of fingers and lower prevalence of extra toes, ectodermal anomalies, cardiac diseases, respiratory malformation, and oral defects (**Ellis and Van Creveld, 1940; Hattab, Yassin and Sasa, 1998; George *et al.*, 2000; Sasalawad *et al.*, 2013**) (**Fig. 9**). Chondrodysplasia is a condition that shows disproportionate dwarfism with long chunk, short ribs and limbs (**Sasalawad *et al.*, 2013**). Ectodermal dysplasia is characterized by hypoplastic and spoon-shaped nails, occasionally thin scanty hair, and malformed teeth (**Hattab, Yassin and Sasa, 1998; Sasalawad *et al.*, 2013**). Congenital heart anomalies are present in around 50-60% cases, along with respiratory defects that are thought to be responsible for the high neonatal mortality rate, individuals who survive the fragile neonatal period typically exhibit normal emotional and intellectual development, and are generally able to live a normal lifespan (**George *et al.*, 2000; Nakatomi, 2009**). There are also striking oral defects such as abnormal teeth and multiple oral vestibule frenula (**Shaik *et al.*, 2016**). Additionally, fused 5^{th} and 6^{th} metacarpals, fused capitate and hamate of the wrist, valgus deformity of knee, and retarded bone age have been described **(Baujat and Le Merrer, 2007; Nakatomi, 2009**). Several inconstant clinical manifestations have been reported in EvC cases, including epi- and hypospadias, strabismus, and cryptorchidism. Among these, urogenital abnormalities such as

hypospadias were reported to account for 22% of EvC cases (**Kowal *et al.*, 2015**). Renal abnormalities including dysplasia, agenesis, nephrocalcinosis, megaureter and hematologic abnormalities such as dyserythropoiesis (**Scurlock *et al.*, 2005**) and perinatal myeloblastic leukemia **(Miller, Newstead and Young, 1969**) were reported as very rare cases in EvC patients (**Baujat and Le Merrer, 2007**). Multidisciplinary symptomatic management is required for individuals affected with EvC syndrome: 1) treatments of respiratory distress, heart disease, and neonatal teeth extraction during neonatal period; 2) pediatric and orthopedic follow-up for the treatment of short stature and bone deformities; 3) oral and dental treatments. The management of oral manifestations in EvC patients is critical, and dentists play an essential role in this regard. Given the high incidence of cardiac disease associated with this disorder, prophylactic antibiotic treatment should be considered (**Baujat and Le Merrer, 2007**). However, those treatments are still limited to corrective therapy, an enhanced understanding of EvC pathogenesis is needed to improve the management strategies and offer the possibility for targeted therapy.

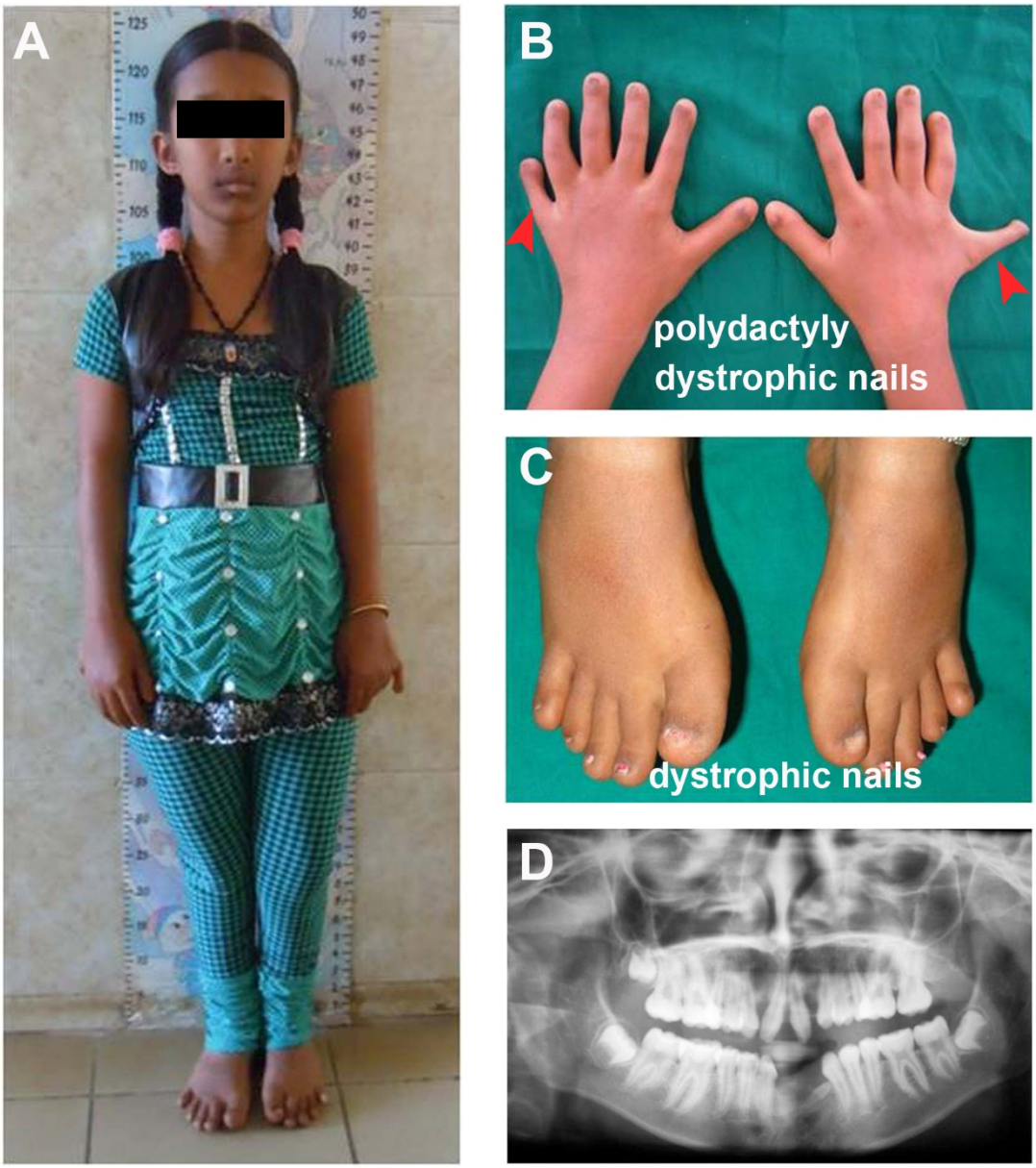

Figure 9. Some typical clinical features of EvC patients. (**A**) The typical characteristics of a 13-year-old patient, who present normal trunk and facial development but with short stature (4 feet). (**B, C**) Supernumerary fingers and hypoplastic, fragile or missing nails. (**D**) A panoramic X-ray displays partial absence of teeth and an impacted incisor in the lower jaw. Red arrowheads point out the supernumerary fingers (adapted from **Sasalawad *et al.*, 2013**).

The mentioned oral manifestations of EvC syndrome are pathognomonic and consistent, particularly with regard to the striking defects in the oral vestibule and teeth, which are essential for the initial diagnosis of the syndrome (**Hattab, Yassin and Sasa, 1998; Mostafa *et al.*, 2005; Sasalawad *et al.*, 2013**). Dysplasia in the oral vestibule in EvC syndrome include the broad median frenum with highly attachment to the gingival margin, multiple broad median and labial frenula, accessory labio-gingival frenula, hypertrophic frenulum, and anteriorly labio-gingival adherences caused by the reduction or obliteration of muco-buccal sulcus (**Hattab, Yassin and Sasa, 1998; Mostafa *et al.*, 2005; Baujat and Le Merrer, 2007; Sasalawad *et al.*, 2013; Nethan, Sinha and Chandra, 2017**) (**Fig. 10**). Gingival inflammation have been noted in areas where frenula attachment is abnormal (**Hattab, Yassin and Sasa, 1998**).

Figure 10. Oral vestibule and tooth defects seen in EvC patients. (**A**) Multiple broad labial frenula and conical incisors in the upper jaw. White arrowheads point out the accessory labio-gingival frenula, and blue arrowheads point out the conical incisors. (**B**) Upper broad median frenum (white arrowhead) with highly attachment to the gingival margin, leading to the increased space between the upper incisors. Tooth defects include malocclusion, conical shaped teeth, and the missing or impacted lower incisors (white asterisk). (**C**) Lower broad median frenum (white arrowhead) with highly

attachment to the gingival margin (adapted from **Sasalawad *et al.*, 2013**; adapted from **Kalaskar and Kalaskar, 2012**).

A diverse array of tooth defects has been identified in EvC patients, which can impact various aspects of tooth development, including eruption, number, morphology, calcification, and arrangement **(Mostafa *et al.*, 2005; Nakatomi, 2009**). Specific manifestations include premature eruption at birth, premature exfoliation, as well as a broad range of eruption timing, from prenatal to delayed (**Hunter and Roberts, 1998; George *et al.*, 2000**). Congenital tooth missing especially in the incisor region (**Fig. 9D,10B**) is a frequent occurrence in individuals with EvC syndrome, fused teeth, supernumerary teeth, and unerupted teeth were also noted in the upper incisor area (**Hunter and Roberts, 1998; Mostafa *et al.*, 2005**). The tooth morphology malformation usually presents conical shape (**Fig. 10**), talon cusps, microdontia, macrodontia, and taurodontism (**Shaik *et al.*, 2016**). Malocclusion (**Fig. 10B**), or the misalignment of teeth, is associated with the misarrangement of teeth that are affected by the diastema or irregular spacing due to hypodontia, as well as by the aberrant location of teeth **(Susami et al., 1999; Nakatomi, 2009)**. Other typical oral characteristics reported in EvC cases include bilateral partial clefts of alveolar ridge in lateral incisor regions, median fissured tongue and bifid tip of the tongue, partial ankyloglossia, and medially notched upper lip caused by the fusion of maxillary gingival margin to the anterior lip (**Cahuana *et al.*, 2004**). Enamel

hypoplasia and hypocalcification suggested as uncommon features in EvC patients are known to be the main causes of severe caries (**Nakatomi, 2009**). Moreover, mandibular prognathism was associated with the mutations in *EVC* and *EVC2* (**Li *et al.*, 2010**). EvC patients have also been reported to exhibit maxillary prognathism (**Shaik *et al.*, 2016**) and mild maxillary hypoplasia with mandibular prognathism (**Nethan, Sinha and Chandra, 2017**).

1.9 *EVC* and *EVC2* are major etiological genes that cause EvC syndrome

As previously stated, EvC syndrome is a chondroectodermal disorder that affects multiple tissues and is inherited in an autosomal recessive pattern, which was described earlier by McIntosh (1933) and first reported by Simon van Creveld and Richard Ellis in 1940 (**Ellis and Van Creveld, 1940**). The patients were of diversified races including Old Order Amish, Dutch, Jewish American, Ecuadorian, Australian Aboriginal, Mexican, Ashkenazi, Asian, British, and Brazilian etc. with parental consanguinity accounting for 30% of cases (**Ellis and Van Creveld, 1940; McKusick *et al*., 1964; Polymeropoulos *et al.*, 1996; Galdzicka *et al*., 2002; Mostafa *et al*., 2005; Tompson *et al*., 2007; Galdzicka, Egeland and Ginns, 2016; Shaik *et al.*, 2016**). Of these, a significant number of cases have been documented within the Old Order Amish community, where the prevalence is estimated to be high at 5 per 1000 individuals in this population (**McKusick *et al*., 1964; Polymeropoulos *et al.*,**

1996). The mapping of this disorder to chromosome 4p16 was initially established in interrelated Amish pedigrees as well as in individual pedigrees from Ecuador, Mexico, and Brazil with EvC syndrome (**Polymeropoulos *et al.*, 1996**). *EVC* and *EVC2* are considered as major etiological genes involved in the pathogenesis of EvC syndrome, mutation in either *EVC* **(Ruiz-Perez *et al.*, 2000**) or *EVC2* (**Galdzicka *et al.*, 2002**) can cause EvC syndrome, which accounts for approximately 70% cases (**Tompson *et al.*, 2007; Aubert-Mucca *et al.*, 2022**). *EVC* and *EVC2* are conserved genes from fish to human, which are tightly genomic linked lying in a divergent head-to-head configuration with transcription start locus separated by 1,647bp in mouse and 2,624bp in human. Affected individuals caused by mutation in either *EVC* or *EVC2* had distinctive spectrum of EvC syndrome characteristics with indistinguishable phenotypes (**Galdzicka *et al.*, 2002; Ruiz-Perez *et al.*, 2003**). It has been proposed that a common mechanism of pathogenesis underlies the developmental abnormalities in *Evc* and *Evc2* mutant mice, as well as in individuals with EvC syndrome (**Thomas *et al.*, 2022**). A number of other ciliopathy-associated genes have been documented to cause EvC syndrome from a recent study of 45 affected families, including *SMO* (2.2%), *DYNC2H1* (6.7%), *PRKACB* (2.2%), and *DYNC2LI1* (2.2%) (**Aubert-Mucca *et al.*, 2022**). Additionally, pathogenic change in *WDR35*, a gene encodes retrograde intraflagellar transport protein 121 (IFT121), was also reported to underlie few EvC cases by interrupting the correct ciliary localization of the SMO and EVC/EVC2 complex (**Caparrós-**

martín *et al.*, 2015).

EvC syndrome is suggested to be mainly caused by *EVC* or *EVC2* homozygous or compound heterozygous mutations (**Ruiz-Perez *et al.*, 2000, 2003**). Whether heterozygous carriers have the phenotypes has been discussed extensively. The large-scale case studies of Amish suggest that there is no manifestation in heterozygote of EvC syndrome (**McKusick, 2000; Baujat and Le Merrer, 2007**). Whereas suspected symptomatic heterozygosity in EvC was suggested by a case whose father also had some EvC features of disproportionate dwarfism, dysplastic nails, and teeth abnormalities (**Spranger and Tariverdian, 1995**). While heterozygous dominant mutation in either *EVC* or *EVC2* result in an allelic disorder Weyers acrofacial dysostosis (WAD) (also called Curry-Hall syndrome, MIM 193530) (**Ruiz-Perez *et al.*, 2000**). WAD is inherited in an autosomal dominant manner, the individuals with WAD typically exhibit a milder version of the EvC phenotype without cardiac defects and have a normal longevity (**Ye *et al.*, 2006; Baujat and Le Merrer, 2007**). Similar to the VL phenotypes in EvC patients, defects in oral vestibule frenulum have also been noted in WAD **(Roubicek and Spranger, 1984**). Based on the evidence that *EVC* mutations were mostly caused by loss of function introduced by the nonsense codon or frameshift (**Tompson *et al.*, 2007**), *Evc* mouse model was then generated by the ablation of gene function which deleted *Evc* exon 1 and inserted a *lacZ* reporter cassette (**Ruiz-Perez *et al.*, 2007**). The *Evc* mutants

mimic the phenotypes of EvC patients, with the exception that they present with no overt cardiovascular defects and polydactyly, which are common characters observed in EvC patients (**Ruiz-Perez *et al.*, 2007**).

1.10 EVC proteins are expressed in craniofacial tissues

Evc extends for 117.9 kb and encodes a 992 amino acid protein, while *Evc2,* a gene orthologous to *LIMBIN (Lbn),* spans 166.4 kb and encodes a 1,308 amino acid protein (**Baujat and Le Merrer, 2007; Ruiz-Perez and Goodship, 2009; Galdzicka, Egeland and Ginns, 2016**). Robust *Evc* and *Evc2* expression are observed in the craniofacial regions and developing skeleton in mice during various embryonic stages and postnatal development (**Ruiz-Perez *et al.*, 2007; Zhang *et al.*, 2015; Kulkarni *et al.*, 2018**). For example, *Evc* expression was observed in the lateral nasal process, maxillary process, nasal septum, mandibular process, cartilaginous components of the skeleton, mesenchyme surrounding the tooth germ, cranial sutures, nails, and skeletal growth plates from E15.5 to P0 (**Ruiz-Perez *et al.*, 2007**). At E15.5, *Evc* expression is predominantly observed in the mesenchyme that surrounds the developing tooth bud and VL. Notably, strong *Evc* expression was also shown in the distal third portion of the VL epithelium (**Ruiz-Perez *et al.*, 2007**) (**Fig. 11**). *Evc2* shows a similar expression pattern to *Evc* at E15.5, being present in the maxilla, mandible, premaxilla, spheno-occipital synchondrosis, and cranial sutures (**Takeda *et al.*, 2002; Badri *et al.*, 2016**). As previously described, the *Evc* and

Evc2 are transcribed divergently and located in close proximity, suggesting that they could be functionally related and coordinately regulated. Mutations in either *EVC* or *EVC2* could interrupt common pathways to cause clinical manifestations seen in EvC patients (**Caparrós-Martín *et al.*, 2013; Galdzicka, Egeland and Ginns, 2016**).

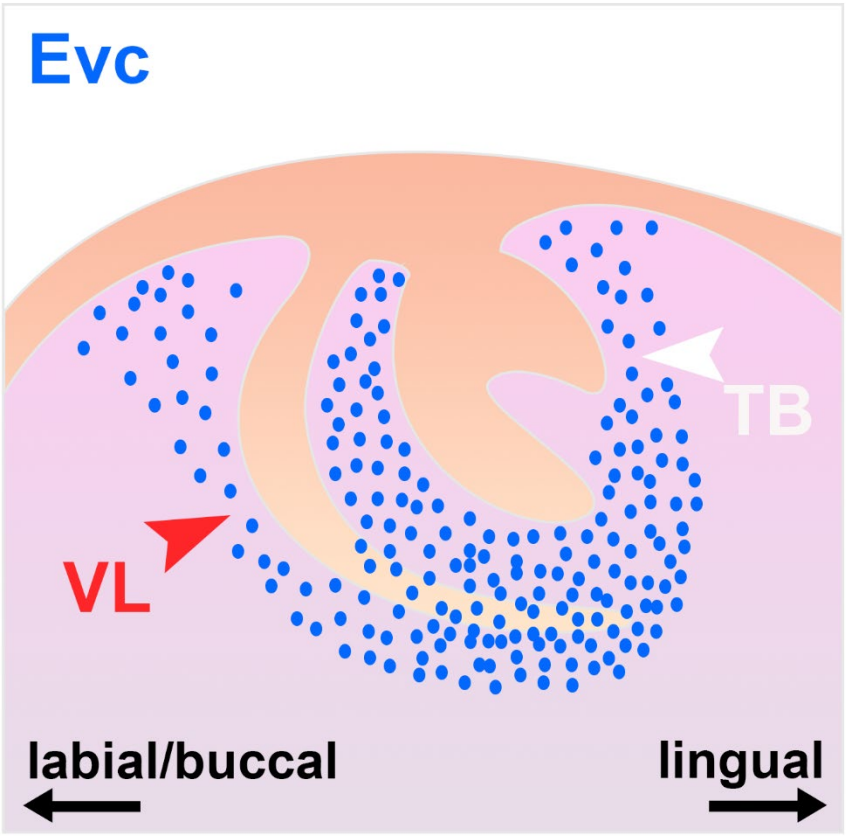

Figure 11. *Evc* expression pattern in the murine VL and TB. At E15.5, the expression of *Evc*, as shown using a reporter for *LacZ*, was mainly concentrated in the mesenchyme surrounding the VL and TB. Within the VL epithelium, robust expression of *Evc* was detected in the distal third region of VL. VL: vestibular lamina; TB: tooth bud.

1.11 EVC is an essential component of the primary cilium

Both *Evc* and *Evc2* genes encode proteins that contain putative transmembrane regions and multiple coiled-coiled domains (**Ruiz-Perez *et al.*, 2003**). EVC and EVC2 are transmembrane proteins with N-terminal anchors that co-localized on the base of the primary cilium by interacting with EFCAB7 through the W domain of EVC2 (**Blair *et al.*, 2011; Louie, Mishina and Zhang, 2020**). EVC and EVC2 are interdependent for ciliary localization, and are critical components of primary cilia involved in various signalling pathways transduction (**Ruiz-Perez *et al.*, 2007; Blair *et al.*, 2011; Louie, Mishina and Zhang, 2020**). The EVC and EVC2 are believed to work as a EVC/EVC2 complex that function as the downstream of SMO activation and upstream of GLI transcription **(Blair *et al.*, 2011; Yang *et al.*, 2012**).

Generally, cilia can be categorized into two types according to their microtubule structures, including primary cilia and motile cilia (**Amack, 2022**). Primary cilium, also referred to as immotile cilium, is a sensory organelle that protrudes in a rod-like shape from the surface of almost every vertebrate cell type. The primary cilium is present on various cell types and acts as a sensor for mechanical and chemical environmental signals and plays a crucial role in regulating cellular differentiation or division, proliferation, cellular signaling, migration and patterning development **(Elliott and Brugmann, 2019; van der Burght *et al.*, 2020**). This ubiquitous cellular microtubule-based organelle is dynamically regulated during the progression of the cell cycle, which is present

in the G0 and G1 phases, and are usually found in cells during the S/G2 phases, however, they are almost invariably resorbed prior to mitotic entry and reappear after cytokinesis (**Plotnikova *et al.*, 2009**). Ciliogenesis, which refers to the formation of the cilium, occurs only during specific cell cycle stages (**Nigg and Stearns, 2011**). The cilium consists of several essential components such as the ciliary membrane, axoneme, EVC zone, and basal body **(Elliott and Brugmann, 2019; Thomas *et al.*, 2022**) (**Fig. 12**).

The basal body comprises a 9 triplets ring of γ- tubulin, with the axoneme protrudes from its apical surface **(Wheway, Nazlamova and Hancock, 2018**). The axoneme is composed of α and β tubulin microtubules that arrange themselves in a ring of nine doublets, whose assembly and sustenance rely on intraflagellar transport (IFT) (**Moore, 2022**). Primary cilium can be distinguished from motile cilium by the lack of central microtubules. Unlike motile cilium, which has a "9+2" structure where dynein arms trigger ciliary movement by acting against the central pair, primary cilium presents as a "9+0" structure due to the lack of this central pair or dynein arms (**Wheway, Nazlamova and Hancock, 2018**) (**Fig. 12**). The transition zone serves as the proximal compartment of the primary cilium, where it connects to the basal body, acting as the ‘cilium gate’ to regulate the entry and exit of molecules at the base of the cilium (**Szymanska and Johnson, 2012**). The EVC zone is the region where the EVC/EVC2 proteins localized as described above. The ciliary tip is the compartment to

regulate the gathering of GLI proteins (**Kong, Siebold, and Rohatgi, 2019**).

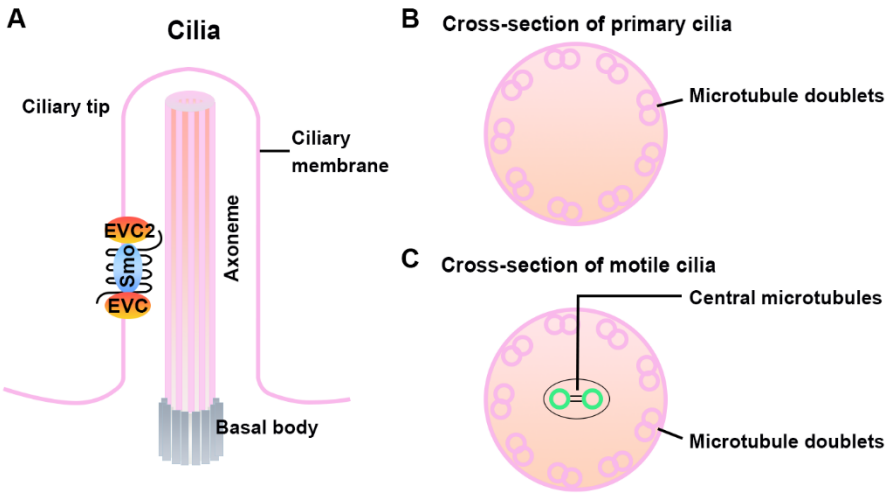

Figure 12. A diagrammatic representation illustrates the structures of primary cilium and motile cilium. (**A**) The cilium's main structural components including ciliary membrane, basal body, axoneme, and EVC zone. (**B**) Specifically, the axoneme within the primary cilium consists of a ring that contains nine microtubule doublets. (**C**) In contrast to primary cilium, the motile cilium exhibits a distinct structural arrangement known as the "9+2" structure, which consists of a central pair of microtubules.

1.12 EvC syndrome belongs to ciliopathies

The primary cilium functions as a complex signalling center that is indispensable for embryonic patterning and organogenesis during development, dysfunction of primary cilium are linked to a diverse array of syndromic disorders, known as ciliopathies (**Berbari *et al.*, 2009**). Both embryonic and postnatal organogenesis are affected in ciliopathies patients, although ciliopathies are rare in each individual case, they are quite common when

considered collectively, with an estimated 1 in 725 individuals affected by these conditions (**Smith, Lake and Johnson, 2020**). Around 30% of these cases exhibit craniofacial abnormalities (**Schock and Brugmann, 2017**). Joubert syndrome, caused by mutations in TALPID3/KIAA0586, is one of the most common syndromes in the ciliopathy spectrum. It has been suggested to have associations with various facial and head defects (**Fraser and Davey, 2019**). Oral-facial-digital (OFD) syndromes are a specific subset of ciliopathies that are considered uncommon hereditary conditions. These syndromes are identified by a cluster of abnormalities that affects face, oral cavity, and digits, accompanied by an extensive range of additional clinical features. Facial features may include cleft lip/palate, low-set ears, and hypertelorism. Oral abnormalities may present abnormal frenula, lobulated tongue, and lingual hamartoma, while digital defects may show brachydactyly and polydactyly (**Bruel *et al.*, 2017**).

The essential roles of the primary cilium in a number of signaling pathways during development have been summarized in **Sreekumar and Norris, 2019**, with the Hedgehog signaling highlighted in the craniofacial development of EvC syndrome (**Thomas *et al.*, 2022**). The primary cilium and Hh pathway were suggested to be linked when the disrupted Hh signaling was found in the ciliary mutants (**Huangfu *et al.*, 2003**). Aberrant SHH signaling has been found to be responsible for the hepatic abnormalities observed in talpid3 ciliopathy mutant,

as indicated by the loss of cilia in its liver (**Davey *et al.*, 2014**). The link between Shh and cilia was further supported by the localization of various Hh components (such as SMO, PTCH1, and GLI) within the cilium **(Corbit *et al.*, 2005; Haycraft *et al.*, 2005; Rohatgi et al., 2007**). Evidence suggests that the loss of *EVC* or *EVC2* function only partially impairs Hedgehog signaling, as indicated by a decrease in the levels of *Gli1* or *Ptch1* expression by approximately two thirds in embryonic fibroblasts (MEFs) or primary chondrocytes of *Evc2* mutants in comparison to controls (**Caparrós-Martín *et al.*, 2013; Zhang *et al.*, 2015**). This is further substantiated by comparing *Gli1* and *Ptch1* mRNA levels across various tissues in *Evc* or *Evc2* mutants and controls **(Ruiz-Perez *et al.*, 2007; Zhang *et al.*, 2016**).

1.13 EVC is essential for hedgehog signalling transduction

The discovery of the Hedgehog (Hh) gene dates back to 1980, when Nüsslein-Volhard and Wieschaus identified it during their genetic analysis of the drosophila melanogaster/ fruit fly (**Nüsslein-Volhard and Wieschaus, 1980**). In the 1990s, researchers identified three main homologs of the Hh gene in vertebrates, known as Sonic hedgehog (Shh), Indian hedgehog (Ihh), and Desert hedgehog (Dhh). These genes are essential for development across various stages, from embryogenesis to adulthood (**Rimkus *et al.*, 2016**). Shh is an important signaling ligand and its expression is widespread in adult tissues (**Ingham and Mcmahon, 2001; Pathi *et al.*, 2001**). The Shh pathway is

essential for proper embryonic development, as it regulates critical processes such as cell proliferation, differentiation, morphogenesis, and patterning. Dysregulated Shh signaling has been linked to various disorders such as EvC syndrome (**Thomas *et al.*, 2022**). Patched (PTCH1) is a transmembrane protein consisting of 12 transmembrane domains and is positioned at the base of the primary cilium. It acts as a primary receptor for the Shh ligand (**Rohatgi, Milenkovic, and Scott, 2007**). There are several co-receptors that can modify the binding affinity of Hh, including GAS1 (Growth arrest specific 1), CDON (Cell adhesion molecule-related/down-regulated by oncogenes), and BOC (Brother of CDON) **(Martinelli and Fan, 2007; Allen *et al.*, 2011; Izzi *et al.*, 2011; Seppala *et al.*, 2017**). When Shh ligands are absent, PTCH1 is embedded in the cilium membrane, where it suppresses the function of Smoothened (SMO), a seven transmembrane protein (**Nakatomi *et al.*, 2013**) (**Fig. 13A**). In this unstimulated state, SUFU (Suppressor of Fused), a protein located in the cytoplasm, directly binds to the GLI (Glioma-associated oncogene homolog) transcription factors. As a result, GLI are sequestered in the cytoplasm and unable to activate target genes regulated by GLI (**Kogerman *et al.*, 1999; Cheng and Michael Bishop, 2002; Paces-Fessy *et al.*, 2004; Tukachinsky, Lopez and Salic, 2010**) (**Fig. 13A**). Specifically, upon translocation to the basal body, the SUFU-GLI complex is phosphorylated at multiple sites by Gylcogen synthase kinase 3 (GSK3), Protein kinase A (PKA) (**Jiang and Struhl, 1995; Li *et al.*, 1995; Hammerschmidt, Bitgood and**

McMahon, 1996), and Casein kinase 1 (CK1) (**Seppala *et al.*, 2017**) (**Fig. 13A**). Following phosphorylation, E3 ubiquitin ligase targets GLI for ubiquitination, leading to its processing by the proteasome into truncated GLI repressor (**Pan *et al.*, 2006; Pan and Wang, 2007**). Once it reaches the nucleus, the SUFU-GLI repressor complex works together with SAP18 and the co-repressor complex to effectively repress the expression of GLI target genes **(Cheng and Michael Bishop, 2002; Paces-Fessy *et al.*, 2004; Zhang *et al.*, 2017**).

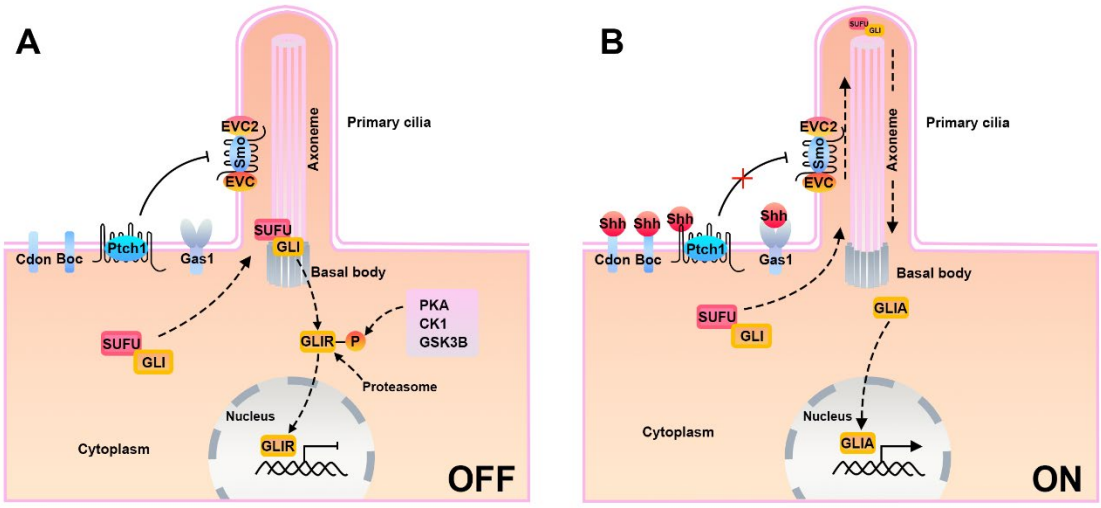

Figure 13. A basic diagram depicting the key steps of Shh signaling transduction in the primary cilium. (**A**) In the inactive (OFF) state, PTCH1 gathers on the primary cilium membrane and suppresses the function of SMO. SUFU sequesters GLI proteins and triggers their phosphorylation by GSK3B, PKA, and CK1. Following phosphorylation, GLI proteins are proteolytically cleaved to truncated repressor forms that suppress the signalling transduction. (**B**) The binding of SHH to PTCH1 activates the Shh signaling pathway (ON), with facilitation from co-receptors CDO, BOC, and GAS1. SMO accumulates in the ciliary membrane and interacts with EVC/EVC2 proteins. The SUFU-GLI complex is transported to the cilium tip and dissociated, full-

length GLI then enters into the nucleus to activate the pathway.

The sequestration of GLI transcription factors by SUFU in the cytoplasm promotes the degradation and processing of GLI proteins, thereby inhibiting Shh pathway transduction (**Kogerman *et al.*, 1999**). Despite being known as a negative regulator of the Shh pathway for a considerable time, recent studies have revealed a more complex role of SUFU. According to research, SUFU plays a significant role in regulating the Shh pathway as a chaperone, shuttling GLI activators into the nucleus while escorting GLI repressors out. Furthermore, these studies suggest that SUFU forms a complex with both GLI isoforms to bind to chromatin and initiate a transcriptional response (**Zhang *et al.*, 2017**).

Vertebrates have three GLI transcription factors: GLI1-3. GLI1 is a full-length transcriptional activator, whereas GLI2/3 can act either as positive or negative regulators, depending on their post-transcriptional and post-translational modifications (**Ruiz i Altaba, 1997; Sasaki et al., 1999**). The GLI family possesses a zinc-finger DNA-binding domain that is highly conserved, which allows for the recognition of a shared DNA element (**Cheng and Michael Bishop, 2002**). GLI proteins' capacity to transcribe Hh target genes is determined by their stabilization as full-length transcription activators in the presence of Hh or their proteolytic cleavage into truncated transcription repressors when Hh is absent. Upon binding with Shh ligand, PTCH1 ceases

to block SMO at the primary cilium. The active SMO enters the primary cilium membrane and positions itself close to the EVC zone. Activated ciliary SMO aided with KIF7, a member of the kinesin protein family, generating a GLI activator that transport to the nucleus and promote the expression of target genes (**Liem *et al.*, 2009**). The increased accumulation of SMO in this region of the cilium membrane repress SUFU, leading to the relief of GLI repression. As a result, this process facilitates the transportation of SUFU/GLI complex towards the tip of the cilium, ultimately triggering its dissociation (**Tukachinsky, Lopez and Salic, 2010**) (**Fig. 13B**). A recent suggestion proposes that GLI activator is accompanied by SUFU when it enters into the nucleus (**Zhang *et al.*, 2017**). The Shh ligand binding causes GLI2 to accumulate within the primary cilium, which leads to transcriptional activation and antagonize the negative regulation by GLI3 (**Kim, Kato and Beachy, 2009**). The generation of GLI activators is inhibited and the GLI proteins are not truncated into repressor forms, such as GLI 3R. As a result, the full form of GLI proteins are translocated into the nucleus, where they activate the transduction of Hh signalling (**Rohatgi, Milenkovic, and Scott, 2007; Tukachinsky, Lopez and Salic, 2010**). GLI transcription factors can trigger the activation of various target genes, including *Gli1* and *Ptch1* involved in Hh pathway, *Myc* associated with cell proliferation, *Bcl-2* related to programmed cell death, *Ang1/2* relevant to angiogenesis, *Snail* engaged in epithelial-to-mesenchymal transition (EMT), and *Nanog* and *Sox2* participating in the self-renewal of stem cells (**Hui and Angers, 2011; Rimkus**

***et al.*, 2016)**.

Apart from the canonical (classical) signaling pathway, Shh signaling also involves non- classical pathways. Non-canonical Shh signaling can be defined in two ways. The first refers to the activation of signaling from PTCH1/SMO in the absence of GLI transcription factors. The second mechanism involves the stimulation of GLI transcription factors without the involvement of the PTCH1/SMO or Shh ligand and is often associated with oncogenic effects with an increased GLI activity (**Rimkus *et al.*, 2016; Pietrobono, Gagliardi and Stecca, 2019**). Targeting SMO has been the main strategy to suppress the Shh pathway. By inhibiting SMO, downstream activation of GLI transcription factors is prevented, leading to the suppression of Shh pathway transduction and genes transcription (**Rimkus *et al.*, 2016**). Cyclopamine, an alkaloid found in V. californicum, has exhibited promising potential for binding to SMO, thereby inhibiting the Shh signaling pathway (**Cooper et al., 1998; Incardona et al., 1998**). Cyclopamine was reported to bind the heptahelical transmembrane domain of SMO, preventing the necessary conformational change required for SMO activation (**Taipale *et al.*, 2000; Zhao, Tong and Jiang, 2007**).

1.14 Primary cilium acts as a positive mediator for Hh signalling transduction

Vertebrate Hedgehog (Hh) signalling transduction has been reported rely on

the primary cilia (**Huangfu *et al.*, 2003; Nakatomi *et al.*, 2013**), as its absence can impede the cellular response to Hh ligands, leading to the development of craniofacial abnormalities (**Bangs and Anderson, 2017**). In vertebrates, cilium is required for the generation of both GLI- activator and GLI-repressor (**Bangs and Anderson, 2017**). The GLI family and SUFU proteins have been found to be enriched at the tip of cilium, disruptions in the components of the cilium can impede the functioning of Hh signal transduction (**Haycraft *et al.*, 2005**). IFT proteins in the primary cilium are crucial for the proper expression of *Ptch1* (**Huangfu *et al.*, 2003**). Disruptions in these proteins can lead to a decrease in *PTCH1* expression (**Beales *et al.*, 2007**) as well as the GLI2/3 gathering at the tip of the cilium (**Qin *et al.*, 2011**). ARL13B, a GTPase from the Arf/Arl family, is a critical component of the cilium membrane for maintaining the normal structure of cilia. The absence of ARL13B has been found to result in shortened cilium length and abnormal axoneme structure (**Caspary, Larkins and Anderson, 2007**). In addition, ARL13B has been identified as a key regulator of the distribution and localization of proteins involved in the Shh signaling pathway within the cilium, when ARL13B is absent, the proper functioning of the Shh signaling pathway can be disrupted, leading to aberrant signal transduction (**Larkins *et al.*, 2011**).

Activation of the Hh pathway leads to the formation of SMO/EVC2 complex, which is restricted in a spatially distinct ciliary compartment, known as EVC

zone (**Dorn, Hughes and Rohatgi, 2012; Bangs and Anderson, 2017**). Precise localization of EVC and EVC2 within primary cilium is critical for their function. Failed ciliary EVC2 localization can cause EvC syndrome and other chondrodysplasias (**Dorn, Hughes and Rohatgi, 2012; Xavier *et al.*, 2016; Thomas *et al.*, 2022**). Additionally, EVC/EVC2 was proposed to function as the upstream of SUFU to modulate Glioma-associated oncogene homolog (GLI) activity, and mediate the balance between GLI^A and GLI^R through accelerating the activation of GLI^A whereas repressing the formation of GLI^R **(Yang *et al.*, 2012; Elliott and Brugmann, 2019**). EVC/EVC2 used to be proposed to localize in the basal body, while current literature commonly suggest the EVC zone is the region where this complex colocalizes **(Thomas *et al.*, 2022**). The EVC/EVC2 complex has been shown to interact with SMO to regulate signalling in the primary cilium, which lead to a diminished response to hedgehog ligands in *Evc* mutant mice. Notably, although the complex is not required for ciliogenesis, the formation of cilia in *Evc* mutant mice appears to be unaffected (**Ruiz-Perez *et al.*, 2007; Caparrós-Martín *et al.*, 2013; Thomas *et al.*, 2022**).

AIMS OF PROJECT

Aim 1: To examine the early development of VL in mouse and human, and assess the mechanisms underlying furrow formation.

Aim 2: To identify the molecular signature for the VL and to explore the

differences in signalling pathway expression in VL and DL.

Aim 3: To investigate the development of the VL in *Gas1* and compound mutants and explore the role of Shh signalling in the VL and DL.

Aim 4: To compare the VL defects in *Gas1* and *Evc* mice, looking for common underlying mechanisms.

Chapter 2 – Methods

2.1 Immunofluorescence

Wax-embedded serial sections were subjected to de-waxing using Histoclear. This involved immersing the sections in Histoclear three times, with each lasting 10 minutes. Following de-waxing, the sections underwent a rehydration process by sequential immersion of the sections in ethanol solutions with decreasing concentrations of 100% (twice), 90%, 70%, 50%, and 30%, with each immersion lasting for 2 minutes. The sections were washed with PBS and then exposed to citric acid (pH 6) antigen retrieval solution in a 92°C water bath for 30 minutes, followed by a 10-minute cooling down period at room temperature. Next, the sections were subjected to a blocking step by incubation with a blocking solution in a humidity chamber at room temperature for 1 hour to prevent nonspecific binding of the primary antibody. The blocking solution comprised of a mixture of PBS, 0.05% Tween20, 10% goat serum (or other serum depending on the secondary antibody used), and 1% bovine serum albumin. The slides were subsequently incubated with primary antibody overnight at 4°C to allow for specific binding of the antibody to its target. The sections underwent a series of four washes with PBT20, with each wash lasting for 5 minutes to remove any unbound primary antibody. PBT20 is a solution made up of PBS and 0.05% Tween20. Subsequently, the sections were incubated with secondary antibodies for a period of 1-2 hours at room

temperature to allow for specific binding of the secondary antibodies to the primary antibodies. To remove any unbound secondary antibodies, the sections were washed four times with PBT20, and each wash lasted for 5 minutes. The sections were treated with Fluoroshield™ containing DAPI (Sigma-Aldrich #SLBV4269) for mounting and subsequently imaged using either a Leica TCS SP5 confocal microscope or a Zeiss ApoTome to visualize the results. Below is a list of primary and secondary antibodies used in the PhD research along with their working concentrations (**Table1 and Table2**). (See details in chapters 3-5).

Table1: Primary antibody list

Antibody Name	**Catalog Number**	**Company**	**Raised in**	**working concentration**
Keratin 14	905501	Covance	rabbit	1:200
keratin 10	ab76318	Abcam	mouse	1:300
keratin 5	PRB-160P	Covance	rabbit	1:300
fillagrin	HPA030188	Cambridge Bioscience	rabbit	1:200
PCNA	ab193965	Abcam	rabbit	1:400
Caspase-3	9579	Cell Signaling	rabbit	1:200
E-cadherin	ab76055	Abcam	mouse	1:400

Loricrin	PRB-145P	Biolegend	rabbit	1:400
Occludin	ab31721	Abcam	rabbit	1:200
BrdU	ab6326	Abcam	rat	1:500
E-cadherin	ab15148	Abcam	rabbit	1:100
Arl13b	17711-1-ap	Novus Biologicals	rabbit	1:200
γ-tubulin	T6557	Sigma-Aldrich	mouse	1:200
β-catenin	610153	BD Biosciences	mouse	1:200

Table2: Secondary antibody list

Antibody Name	**Catalog Number**	**Company**	**working concentration**
Alexa Fluor™ donkey anti-mouse 488	A11001	Invitrogen	1:500
Alexa Fluor™ donkey anti-rabbit 488	ab150073	Abcam	1:500
Alexa Fluor™ donkey anti-rabbit 568	A10042	Invitrogen	1:500
Alexa Fluor™ donkey anti-mouse 488	A21202	Invitrogen	1:500

Alexa Fluor™ donkey anti-mouse 647	A31571	Invitrogen	1:500
Alexafluor donkey anti-rat 647	A21247	Invitrogen	1:500
Alexa Fluor™ goat anti-rabbit 488	A-11008	Invitrogen	1:500

2.2 Histology

Following collection, the samples were fixed in 4% paraformaldehyde (PFA) at 4°C overnight. For human samples and postnatal mice, decalcification was performed using 0.5M ethylenediaminetetraacetic acid (EDTA) at pH = 8. Samples were then dehydrated using a series of increasing ethanol concentrations (30%-50%-70%-90%-100%). After clearing in xylene, the samples were immersed in wax and subsequently embedded in paraffin. The samples were sliced into 5-8 μm thick sections by microtome and sequentially mounted onto charged slides. To perform histological analysis, the slides were subjected to standard staining protocols, including Haematoxylin-Eosin (HE) staining and trichrome staining (Alcian blue, Hematoxylin, and Sirrus red). (See details in chapters 3-5).

2.3 Explant culture

The mandible was harvested from mice at E12.5 or E13, and from humans at

CS19, at a stage when a visible VL/DL could be observed. The McIlwain tissue chopper was utilized to perform a sagittal cut on the dissected mandible at a distance of 200 or 250 μm (**Alfaqeeh and Tucker, 2013**). The incisor region slices were cultured on permeable filters supported by steel meshes, as detailed in the following publications. Slices were kept in a 5% CO_2 environment at 37°C and imaged by microscope. (See details in chapters 3-5).

2.4 Other methods:

Whole mount immunofluorescence: see details in chapters 4;

Statistical analysis: see details in chapters 4 and 5;

RNA isolation and RNA-Seq library construction and sequencing: see details in chapters 5;

Downstream analysis of RNA-Seq: see details in chapters 5;

Radioactive *in situ* hybridization: see details in chapters 5;

RNA-Scope assay: see details in chapters 5.

Chapter 3 – (Publication 1) Development of the Vestibular Lamina in Human Embryos: Morphogenesis and Vestibule Formation

(Frontiers in Physiology, 2020)

Tengyang Qiu[1], Tathyane H. N. Teshima[1], Maria Hovorakova [2,3] and Abigail S. Tucker[1,3]*

1 Centre for Craniofacial and Regenerative Biology, Faculty of Dentistry, Oral and Craniofacial Sciences, King's College London, London, United Kingdom,

2 Institute of Histology and Embryology, First Faculty of Medicine, Charles University in Prague, Prague, Czechia,

3 Institute of Experimental Medicine, Czech Academy of Sciences, Prague, Czechia

Aim: To examine the early development of VL in human, and assess the mechanisms underlying furrow formation.

My contributions: I conducted all of the experiments except the explant culture, including histology and immunohistochemistry. I created all the figures and wrote the draft of the original manuscript. I contributed to the editing of the manuscript.

Abstract:

During early stages of development, the vestibular lamina (VL) is a temporary epithelial structure that later transforms into the oral vestibule, forming the grooves of the upper and lower lips and cheeks. The VL is located on the

buccal/labial aspect of the dental lamina (DL) and have a close developmental relationship. However, our understanding of the developmental processes underlying the VL and its interconnection with DL remains quite limited. In this study, we mainly investigate the development of VL in human embryos, specifically focusing on the period ranging from 6.5 weeks (CS19) to 13 weeks. Our research findings highlighted the close relationship between the VL and DL, revealing their shared origin in humans and a dual origin in mice in the anterior lower region. The VL undergoes intricate morphogenetic transformations during development, resulting in the formation of a branched structure that ultimately segregates to create the vestibule. The dynamic expression of keratins in the VL serves as a key indicator of its differentiation patterns. Notably, the formation of fissures in the VL is closely associated with the onset of filaggrin. Apoptosis plays a crucial role in removing the central portion of the VL, thereby broadening the furrow between the future gum and cheek. This research provides a fundamental foundation for further investigation into developmental abnormalities affecting this specific area of the oral cavity.

frontiers in Physiology

ORIGINAL RESEARCH
published: 16 July 2020
doi: 10.3389/fphys.2020.00753

Development of the Vestibular Lamina in Human Embryos: Morphogenesis and Vestibule Formation

*Tengyang Qiu[1], Tathyane H. N. Teshima[1], Maria Hovorakova[2,3] and Abigail S. Tucker[1,3]**

[1]Centre for Craniofacial and Regenerative Biology, Faculty of Dentistry, Oral and Craniofacial Sciences, King's College London, London, United Kingdom, [2]Institute of Histology and Embryology, First Faculty of Medicine, Charles University in Prague, Prague, Czechia, [3]Institute of Experimental Medicine, Czech Academy of Sciences, Prague, Czechia

The vestibular lamina (VL) is a transient developmental structure that forms the lip furrow, creating a gap between the lips/cheeks and teeth (oral vestibule). Surprisingly, little is known about the development of the VL and its relationship to the adjacent dental lamina (DL), which forms the teeth. In some congenital disorders, such as Ellis-van Creveld (EVC) syndrome, development of the VL is disrupted and multiple supernumerary frenula form, physically linking the lips and teeth. Here, we assess the normal development of the VL in human embryos from 6.5 (CS19) to 13 weeks of development, showing the close relationship between the VL and DL, from initiation to differentiation. In the anterior lower region, the two structures arise from the same epithelial thickening. The VL then undergoes complex morphogenetic changes during development, forming a branched structure that separates to create the vestibule. Changing expression of keratins highlight the differentiation patterns in the VL, with fissure formation linked to the onset of filaggrin. Apoptosis is involved in removal of the central portion of the VL to create a broad furrow between the future cheek and gum. This research forms an essential base to further explore developmental defects in this part of the oral cavity.

Keywords: dental pathologies, keratin, epithelial differentiation, apoptosis, oral mucosa, human development

OPEN ACCESS

Edited by:
Ophir D. Klein, University of California, San Francisco, United States

Reviewed by:
Gareth John Fraser, University of Florida, United States
Heather L. Szabo-Rogers, University of Pittsburgh, United States
Jimmy Hu, University of California, Los Angeles, United States

****Correspondence:***
Abigail S. Tucker
abigail.tucker@kcl.ac.uk

Specialty section:
This article was submitted to Craniofacial Biology and Dental Research, a section of the journal Frontiers in Physiology

Received: *17 April 2020*
Accepted: *11 June 2020*
Published: *16 July 2020*

Citation:
Qiu T, Teshima THN, Hovorakova M and Tucker AS (2020) Development of the Vestibular Lamina in Human Embryos: Morphogenesis and Vestibule Formation. Front. Physiol. 11:753. doi: 10.3389/fphys.2020.00753

INTRODUCTION

The vestibular lamina (VL) or lip furrow band is an embryonic structure that forms the oral vestibule (vestibulum oris), the gap in between the teeth and cheeks and lips. The oral vestibule has been proposed to have evolved to aid suckling, and as such is assumed to be a structure unique to mammals and the evolution of lactation. The VL develops labially/buccally to the dental lamina (DL), which forms the dentition of the jaw. These two laminas have been suggested to originate from a common oral epithelial thickening, which subdivides into the two laminas in the mouse (Peterková, 1985). The thickening of the oral epithelium occurs approximately during the 6th week in human embryos, with a single lamina suggested to split to form two diverticula (Bolk, 1921). However, two independently forming laminas have also been described, with the VL forming before or after the DL (Schour, 1929; Tonge, 1969; Nery et al., 1970). The various theories are summarized in Hovorakova et al. (2005). Tooth buds along the DL progress through bud, cap, and bell stages (Tucker and Sharpe, 2004), while the neighboring VL opens up to create a cleft separating the lips and checks from the dental arch between

the 12th and 14th week (Coslet and Cohen, 1969). Although the VL and DL have a very close early relationship, the VL is largely ignored in odontogenetic studies.

Originally the relationship between the human embryonic VL and DL was represented in a classical "horseshoe-shape," with the VL running in parallel on the outside of the DL. This view was based on histological sections of the upper jaw, where the VL appeared continuous throughout the jaw. Interestingly, however, when viewed in 3D, the human VL is clearly discontinuous, integrating with the DL at distinct points along the jaw, and is therefore a much more complex structure than initially proposed (**Figures 1A, 2A**; Hovorakova et al., 2005, 2007). The complex relationship of the VL and DL in different parts of the jaw probably explains the different accounts of their development, and it appears likely that, at least in the anterior region of the human lower jaw, the VL and DL do share a common origin (Bolk, 1921; Hovorakova et al., 2007). This common origin of the VL and DL is supported by the discovery that both laminas in the anterior area form from a common Shh expressing domain in mice (Hovorakova et al., 2016).

The VL has been described in sheep, mouse, humans, and voles (Pavlikova et al., 1999; Hovorakova et al., 2005, 2016; Witter et al., 2005). Across species, clear anatomical differences are evident along the jaw. For example, in the mouse the VL is very prominent in the anterior lower jaw, while it is almost absent in the anterior upper jaw. The mouse and vole have very thin VLs, while the sheep and human have very thick multi-layered VLs. Such differences are likely to lead to differences in morphology of the final oral cavity and may reflect differences in diet.

The early VL has similarities to other embryonic structures that have a close relationship to the teeth across vertebrates. For example, in reptiles the DL shares a common origin with the adjacent forming dental glands (Vonk et al., 2008; Tucker, 2010). Here, a single epithelial thickening appears to divide to form the DL and a gland, similar to the process described for the VL and DL (Kochva, 1965). Both the VL of mammals and

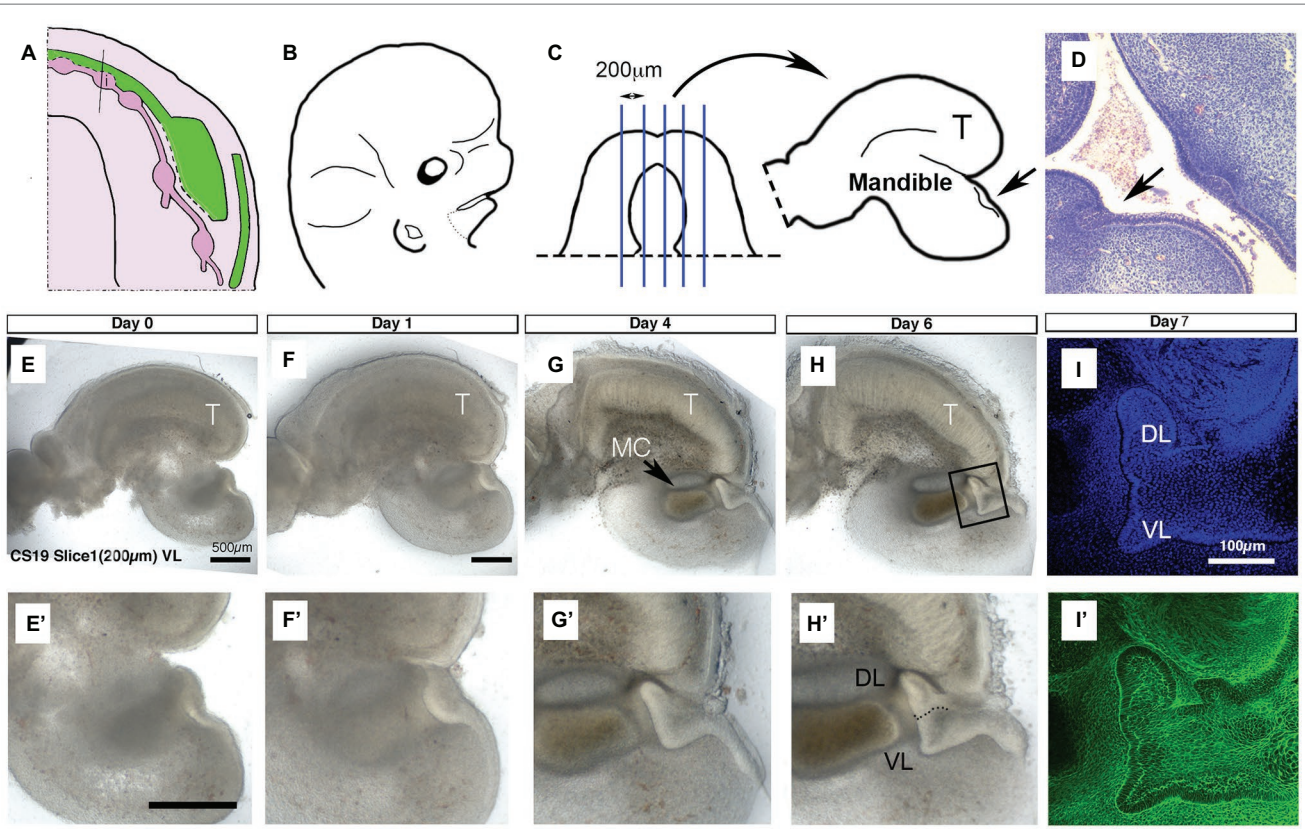

FIGURE 1 | United development of the vestibular lamina (VL) and dental lamina (DL) in the anterior mandible. **(A)** Schematic of the developing VL (green) and DL (pink) during human embryonic lower jaw development. Line through deciduous incisor (i) tooth germ indicates the plane of dissection for culture. **(B)** Schematic of head at CS19 (46 days). Dots indicate dissection of lower jaw. **(C)** Schematic of dissected lower jaw, with blue lines indicating chopping planes to create sagittal live slices. Medial slices contain tongue (T) and single thickening for the DL/VL (arrow). **(D)** Histology section through an embryonic head at 6 weeks. Arrow points to single thickening for the DL/VL. **(E–H)** Developing live sagittal slices of a CS19 mandible. **(E'–H')** Close up of developing VL/DL area shown in **(E–H)**. **(E,E')** Day 0. A single epithelial thickening is evident under the tongue (T). **(F,F')** Day 1. **(G,G')** Day 4. Meckel's cartilage (MC) has condensed and differentiated during the culture period. The tongue (T) has started to fuse with the mandible underneath as an artifact of the culture system. **(H,H')** Day 6. **(I,I')** Day 7 slice fixed and processed for immunofluorescence. Boxed inset in **(H)** shows equivalent regions highlighted in **(I,I')**. **(I)** DAPI, **(I')** Phalloidin stain highlighting F-actin. Schematic in **(A)** based on data in the literature (Hovorakova et al., 2005, 2007). Scale bar in **(E,E',F)** = 500 μm, same scale in **(G,H)** and **(F'–H')**. Scale bar in **(I)** = 100 μm, same scale in **(I')**. VL, vestibular lamina; DL, dental lamina; T, tongue; MC, Meckel's cartilage.

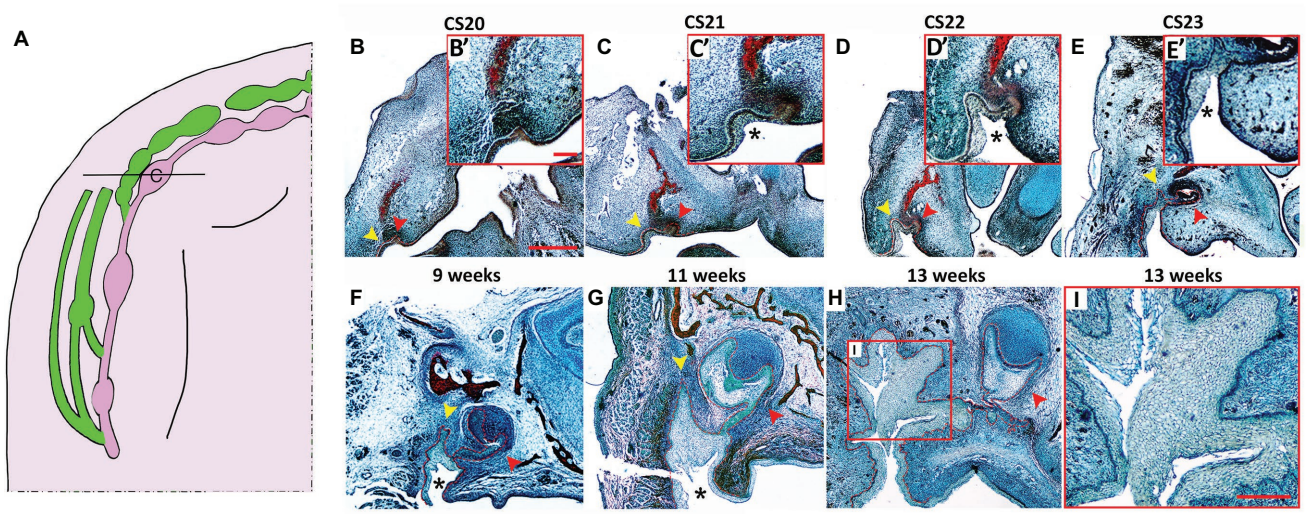

FIGURE 2 | Histological development of the VL and DL in the upper canine region. **(A)** Schematic of the developing VL (green) and DL (pink) during human embryonic upper jaw development. Line through deciduous canine (c) tooth germ indicates the position of the sections in **(B–I)**. **(B–I)** Frontal sections human embryo and fetal tissue stained with a trichrome stain (Alcian blue, Alizarin red, and haematoxylin). **(B)** CS20, **(C)** CS21, **(D)** CS22, **(E)** CS23, **(F)** 9 weeks, **(G)** 11 weeks, **(H,I)** 13 weeks. High power view of VL/DL shown in red inset **(B'–E')**. Boxed area in **(H)** shown in **(I)**. DL and VL outlined by red dashed lines in **(B–H)**. Schematic in **(A)** based on data in the literature (Hovorakova et al., 2005, 2007). Yellow arrowheads indicate forming VL. Red arrowheads indicate forming DL. * = cheek furrow or labio-tectal furrow, which forms from CS21 at the canine. Scale bar in **(B)** = 500 μm, same scale in **(C–H)**. Scale bar in inset **(B')** = 125 μm, same scale in insets **(C',D',E')**. Scale bar in **(I)** = 250 μm.

the dental gland primordium of reptiles form on the outside of the DL and potentially evolved from an outer tooth row from a common amniote ancestor (Hovorakova et al., 2020). This theory is supported by the existence of tooth-germ like bulges that transiently form in the upper VL (**Figure 2A**) and by the high incidence of odontomas and other dental pathologies in the oral vestibule (Hovorakova et al., 2020). In animal models, the VL has the potential to form tooth-like odontomas when signaling in this tissue is perturbed. In mice, supernumerary teeth have been reported to form in the VL region after overexpression of the Wnt pathway in adenomatous polyposis coli conditional knockouts (Wang et al., 2009) and after stabilization of β-catenin in $Sox2^{+}$ positive cells (Popa et al., 2019). The close developmental and evolutionary relationship between the VL and DL may, therefore, explain some of these pathologies.

In addition, the VL is one of the most affected oral tissues in Ellis-van Creveld (EVC) syndrome patients, where defects disrupt the VL development and lead to fusion of the upper lip to the gingiva with multiple frenula (Sasalawad et al., 2013). However, little is known about the development of the VL. We therefore investigated the development of the VL and DL in human embryos and assessed the mechanisms of fissure formation in the vestibular epithelium as the oral vestibule forms. We used organ culture, histology, and immunofluorescence to study the VL development at different stages of human embryos. We have observed that the VL and DL have a very close relationship. We show the complex structure of the VL during development and highlight the roles of epithelial differentiation, proliferation, and apoptosis in the opening of the VL in human embryos. These findings can help our understanding of the normal development of the VL and shed light on the complex relationships between the VL and DL during development, which is crucial for the further exploration of developmental VL defects.

MATERIALS AND METHODS

Human embryos/fetuses were provided by the Human Developmental Biology Resource (HDBR; Project 200504: Characterizing the development of the oral vestibular lamina). Eight stages of human development were examined to study the development of the VL. Samples included CS19 (46 days), CS20 (49 days), CS21 (51 days), CS22 (53 days), CS23 (56 days), 9, 11, and 13 weeks stages. N = 1–2 freshly fixed samples for immunofluorescence were analyzed at each stage (total N = 8). HDBR samples were compared with a larger archival histology collection from the Department of Teratology, IEM, CAS, Prague compiled from the 1960's to the 1980's (recently deposited at First Medical Faculty, Charles University, Prague; N = 53 in total ranging from CS17 to 9 weeks). The stages in the study were selected as they span the period from the initiation of the VL and DL to fissure formation in the VL (Coslet and Cohen, 1969; Hovorakova et al., 2005).

Slice Culture

The lower jaw was isolated from one CS19 and one CS20 human embryo and chopped sagittally at a cutting distance of 200 μm using a McIlwain tissue chopper (Alfaqeeh and Tucker, 2013). A clear DL/VL bud was only evident in the CS19 specimen, so this was used for further analysis for this project. Selected slices from the lower jaw were placed on permeable

membranes (BD) over culture medium [DMEM-Advanced Dulbecco Modified Eagle Medium F12, (Invitrogen); 1% GlutaMAX (Invitrogen); and 1% penicillin-streptomycin solution (10,000 units penicillin and 10 mg streptomycin/ml; Sigma-Aldrich)]. Slices (N = 3 from CS19) were photographed by using a Leica dissecting microscope at day 0 of culture, to record the morphology, and then incubated in 5% CO_2 at 37°C with the culture medium changed every 2–3 days. Slices were photographed at regular intervals for 7 days before fixation in 4% paraformaldehyde (PFA).

Tissue Processing and Histology

The upper jaws of heads were dissected from human embryos (CS20, CS21, CS22, CS23, 9, 11, and 13 weeks) and fixed in 4% PFA. Calcified tissues were decalcified in 0.5 M ethylenediaminetetraacetic acid (EDTA) in PBS. After decalcification, samples were dehydrated in an increasing ethanol concentration and permeated in xylene. Samples were then embedded in paraffin and cut in 10 µm serial sections by Microtome Leica RM2245. One of the sections in the series was stained with trichrome staining (Sirrus red, Alcian blue, and hematoxylin). Stained slides were observed under the Nikon Eclipse 80i light microscope, and images were taken by the attached Nikon Digital Sight DS-Fi1 camera.

Immunofluorescence

Wax embedded serial sections of the VL were de-waxed, rehydrated, and transferred into the citric acid (pH = 6) in 92°C water bath for antigen retrieval. The antibody blocking solution consists of PBS, 0.05% Tween20, 10% goat serum, and 1% bovine serum albumin (1% = 1 g/100 µl). The slides were then incubated with rabbit keratin 14 (K14; 1:200; Covance #905501), mouse keratin 10 (K10; 1:300; Abcam #ab76318), rabbit keratin 5 (K5; 1:300; Covance #PRB-160P), rabbit fillagrin (Cambridge Bioscience #HPA030188), rabbit proliferating cell nuclear antigen (PCNA; Abcam #ab193965), and rabbit Cleaved Caspase-3 (1:200, Cell Signaling #9579) overnight at 4°C. For immunofluorescence, sections were incubated in Alexa Fluor™ donkey anti-mouse 488 (1:500; Invitrogen #A11001), Alexa Fluor™ donkey anti-rabbit 488 (1:500; Abcam ab150073), and Alexa Fluor™ donkey anti-rabbit 568 (1:500; Invitrogen #A10042) for 2 h at RT. Sections were mounted with Fluoroshield™ with DAPI (Sigma-Aldrich #SLBV4269) and imaged with a Leica TCS SP5 confocal microscope or Zeiss ApoTome. To test each antibody, controls were performed where the primary antibodies had been omitted in order to confirm specific staining. Each antibody was repeated at least twice, at different timepoints, using serial sections. To aid comparison, the color of filaggrin was changed to green from red on the ApoTome (13 weeks) or in photoshop (11 weeks), while the K5 was changed on the ApoTome from red to blue.

For wholemount immunofluorescence, explant culture slices were fixed in 4% PFA for 30 min at RT. Samples were permeabilized with PBS Triton 0.5% (PBT) at RT for 1 h, followed by trypsinization for 5 min on ice and incubation in blocking solution for 2 h. After blocking, slices were incubated in Alexa Fluor Phalloidin 488 (Invitrogen; 1:50) and DAPI (1:1,000; Sigma) overnight at 4°C. After washing in PBS, cultures were mounted in glycerol and analyzed by a Leica TCS SP5 confocal microscope.

RESULTS

The Human VL and DL Bud Off From a Single Epithelial Thickening

It has been suggested from 3D reconstructions of histology sections that the human VL and DL are derived from a common oral epithelium in the lower lip region (**Figure 1A**; Hovorakova et al., 2007). To follow the development of these two laminas during development, we made live slices through the dissected mandible of a human embryo at the placode stage (CS19: 6.5 weeks; **Figures 1B,C**; N = 1 embryo). Slices were sectioned in the sagittal plane, and medial slices that contained an epithelial thickening under the developing tongue were selected (N = 3 slices). A single thickening was observed at CS19 (**Figures 1E,E'**), similar to that observed in histology sections through this region of the jaw (**Figure 1D**). The thickening in culture became more pronounced after a day in culture (**Figures 1F,F'**). The thickening extended into the underlying mesenchyme, with a lip of epithelial cells elongating toward the tongue after 4 days (**Figures 1G,G'**). The epithelium divided into two protrusions after 6 days in culture forming the VL and DL (**Figures 1H,H'**). At day 7, a clear bifurcation of the epithelium into a tooth bud and a wider VL was observed when imaged by confocal, with phalloidin staining (green) used to highlight the cell morphology (**Figures 1I,I'**). This confirms the histology findings that, at least in the anterior region of the lower jaw, the human VL and DL form from a single placode and are therefore directly associated with each other.

The Morphology of the Human VL Increases in Complexity During Development

To further investigate the development of the VL and DL in human embryos, we studied the development of VL and DL at embryonic CS20, CS21, CS22, CS23, 9, 11, and 13 weeks. This time period spans the period from defined VL and DL thickenings to proposed formation of the fissure in the VL to create the oral vestibule (Coslet and Cohen, 1969). The relationship between the VL and DL is very complex across the jaw with large variations depending on the A-P position (summarized in **Figures 1A, 2A**). In order to follow how the VL and DL co-develop, we therefore focused on a single region in the jaw. For this, we selected the deciduous canine area of the maxilla. The upper canine and VL are very closely associated in 3D reconstructions (**Figure 2A**), and the VL in this region appears particularly complex in shape (Bolk, 1921, data not shown), thus providing an intriguing area to study further. The primary canine primordia at these stages develop from an oral epithelial thickening at CS20 (**Figures 2B,B'**), bud stage at CS21 (**Figures 2C,C'**) and CS22 (**Figures 2D,D'**), to cap stage at CS23 (**Figures 2E,E'**) and 9 weeks (**Figure 2F**), to a bell stage at 11 (**Figure 2G**) and 13 weeks (**Figure 2H**). At CS20, the VL was visible as a slight thickening on the buccal side of the tooth

germ, forming a prominent thickening by CS21 (**Figures 2B–C'**). By CS22, the whole VL/DL region had invaginated inward to sit within a groove (**Figures 2D,D'**). This groove has previously been described as the labio-tectal furrow and the cheek furrow (Bolk, 1921; Hovorakova et al., 2005). The cheek furrow deepened as the VL/DL developed, with the cap stage canine tooth connected to the VL (**Figures 2E,F**). A narrow fissure in the VL started to form at 11 weeks, extending up from the base of the furrow (**Figure 2G**). By 13 weeks, several fissures had formed that split the VL into a branched structure, with the DL extending from the lingual side of the VL (**Figures 2H,I**).

Epithelial Differentiation Highlights Labial-Lingual Differences in Structure of the VL and May Trigger Furrow Formation

Skin epidermal differentiation occurs in layers from the basal cell layer, where the basal cells sit on the basement membrane adjacent to the surrounding mesenchymal cells, to the superficial cornified layer. K5 and K14 are expressed in more undifferentiated/basal cells; while K10 is expressed in the middle spinous layer with filaggrin expressed in the overlying granular layer (Lee et al., 1999; Coolen et al., 2010). We therefore utilized K5, K14, K10, and filaggrin as markers to investigate the differentiation state of the VL from CS23 to 13 weeks. The expression of various keratins have previously been followed in the human oral mucosa, with expression of K10 in the VL, but not DL, shown at 11 weeks (Pelissier et al., 1992). Where, it was suggested that the boundary between the K10 positive and negative cells in the VL might indicate the site of future fissure formation (Pelissier et al., 1992). At CS23, the buccal oral epithelium within the labio-tectal furrow expressed K5, with very limited expression of K10 and a patchy expression of K14 in the basal epithelial cells, highlighting the undifferentiated state of the epithelium at this stage (**Figures 3A–C**). By 9 weeks, more K10 expressing cells were evident lying in a suprabasal layer on top of the K14 basal layer, with K5 still expressed in most cells (**Figures 3D–F**). By 11 weeks, expression of K10 had spread up into the VL extending from the labio-tectal furrow (**Figure 3G**). Expression was concentrated on the buccal side and was largely absent from the lingual side (**Figures 3G,H,J**), agreeing with the results of Pelissier et al. (1992). The cells of the VL near to the basal lamina and the DL expressed K14 at this stage (**Figure 3G**). The cells in the center of the VL did not express K14, with scattered expression of K10, indicating that the center was more differentiated than the edges (**Figure 3G**). On the buccal side near the oral epithelium, K14 was mainly restricted to the basal layer, with K5 expressed more widely and K10 expressed in a suprabasal layer, with some overlap of expression in the intermediate area between K14 and K10 (**Figures 3H,I**). On the lingual side, the expression of K14 and K5 were similar but with minimal K10, highlighting that the two sides of the lamina appear to differentiate asynchronously (**Figures 3J,K**).

The strong expression of K10 on the buccal side of the VL was maintained at 13 weeks but more K10 positive cells were now found throughout the rest of the lamina (**Figures 4A,B,D**). The expression of K5 reduced, particularly on the buccal side, where expression was mainly restricted to the cells of the basal lamina, overlapping with K14 (**Figures 4C,E**). Some cells again co-expressed K14 and K10, indicating a change in differentiation state (**Figure 4B**). At 13 weeks, a number of fissures had developed in the VL (as seen in **Figure 2H**). To understand how these fissures formed, we looked at expression of filaggrin. Filaggrin has previously been reported as turning on at 22–24 weeks in the interfollicular epidermis and granular layer of the skin, with expression at 14 weeks in developing hair follicles (Dale et al., 1985; Lee et al., 1999). At 13 weeks, filaggrin was strongly expressed in the cells lining the developing fissures (**Figures 4F–J**). As filaggrin expression in keratinocytes results in loss of cell-cell adhesion (Presland et al., 2001), filaggrin upregulation in the VL might trigger fissure formation. To investigate this further, we analyzed filaggrin expression at 11 weeks (**Figures 4K–N**). As at 13 weeks, in areas where fissures had already started to form, filaggrin was expressed (**Figures 4K–M**). Interestingly, however, diffuse expression was also evident in the middle of the VL in regions where fissure formation was yet to initiate (**Figure 4N**), highlighting that filaggrin might be playing a role in fissure initiation. Filaggrin expression in keratinocytes results in decreased proliferation (Presland et al., 2001) and increased susceptibility to apoptosis (Kuechle et al., 2000). Given the links with proliferation and apoptosis, we next investigated how these processes were altered during fissure formation during VL development.

Cells at the Center of the VL Do Not Proliferate and Undergo Cell Death

To investigate proliferation levels, we utilized PCNA as a marker for the S phase of cell proliferation (Dietrich, 1993). At 13 weeks, proliferating cells were generally found associated with the basal layer next to the basal lamina (**Figures 5A,C,D**). Fewer positive cells were observed moving away from the basal lamina (**Figures 5C,D**), with no positive cells in the center (**Figures 5A,B**). Cell death has previously been investigated during the development of the vole VL (Witter et al., 2005). A few scattered apoptotic bodies were evident in the forming VL at E13.5 and E14.5 in the vole, in contrast to high levels in the forming EKs in the DL, suggesting that cell death only played a minor role at these stages (Witter et al., 2005). A lack of degenerating cells in the VL was also described during formation of the furrow in human fetal samples (Coslet and Cohen, 1969), although others have reported localized cellular atrophy as the cause of the split (Bolk, 1921; West, 1924). We utilized Caspase-3 as a marker for apoptosis and correlated to the presence of apoptotic bodies, as identified by condensed nuclei. As in the vole, very few Caspase positive cells were observed at early stages of VL formation (9 and 11 weeks; **Figures 5E–J**). The few positive cells, corresponded to apoptotic bodies, confirming that the cells were undergoing programmed cell death (**Figures 5G,J**). At 13 weeks, there were no positive cells associated with the forming fissures (**Figures 5K–N**); however, a large number of positive cells were found in the V-shaped epithelial tissue at the center of the VL (**Figures 5O–Q2**). Cell death, therefore, appears to play a role in removal of the tissue lying in between the forming fissures but did not play a role in the formation of the fissures themselves.

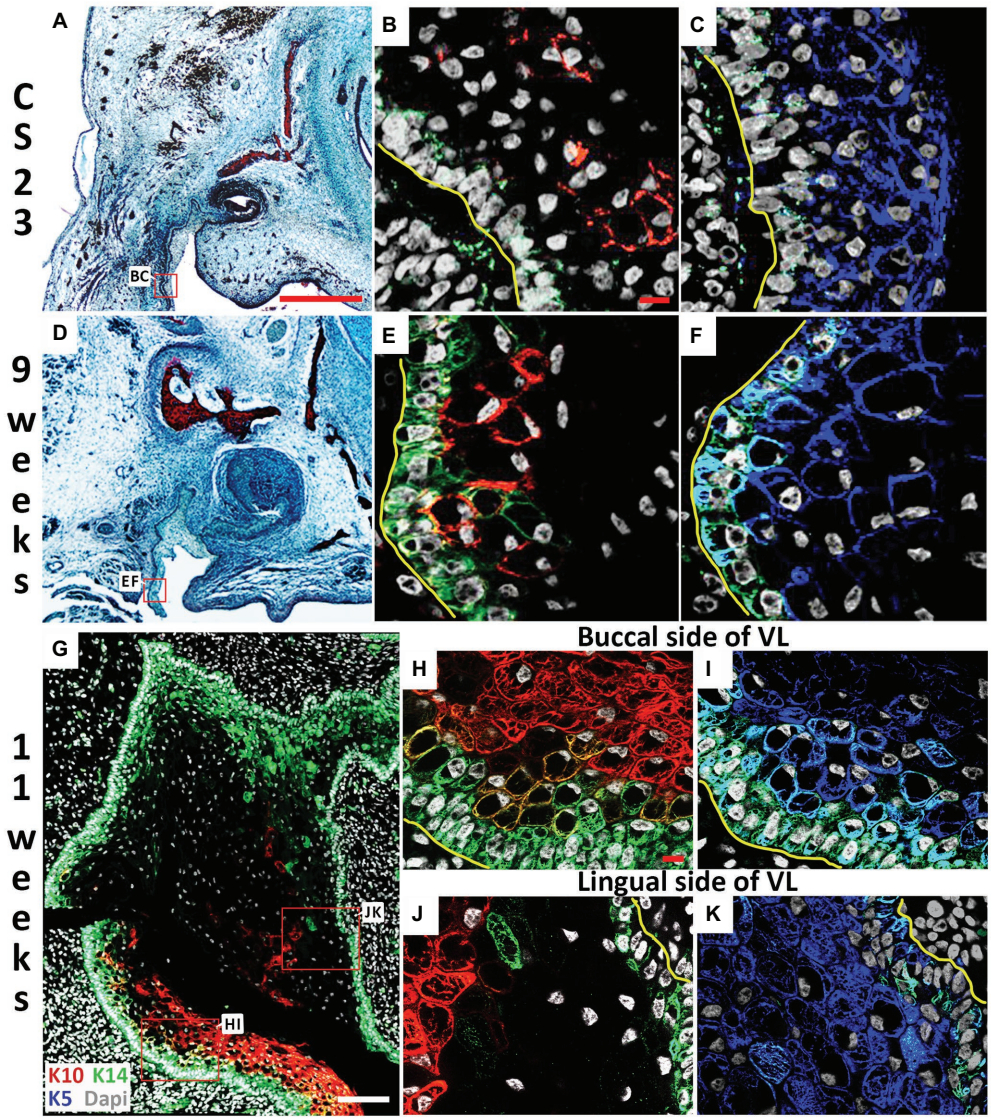

FIGURE 3 | Lingual/buccal differences in VL epithelium. **(A,D)** Histological frontal sections through the upper canine. **(B,C,E–K)** Immunofluorescence. DAPI shows nuclei in white. **(A–C)** CS23. Box in **(A)** highlights regions in **(B,C)**. The buccal side of the cheek furrow comprises cells with **(B)** limited Keratin 14 (K14; Green) and Keratin 10 (K10; red), and **(C)** high levels of Keratin 5 (K5; blue). **(D–F)** 9 weeks. Box in **(D)** highlights regions in **(E,F)**. The buccal side of the cheek furrow comprises cells with **(E)** robust K14 in the basal layer (Green), with K10 turning on in the overlying suprabasal layer (red), and **(F)** high levels of K5 (blue). **(G–K)** 11 weeks. Box in **(G)** highlights regions in **(J,K)**. **(G)** K14 (green) is robustly expressed around the edges of the VL, with K10 (red) observed at high levels mainly on the buccal side only. **(H–K)** High power of the buccal side **(H,I)** and lingual **(J,K)** side of the VL comparing the expression of K5 (blue) and K14 (green) in the basal layer and overlying layer, and K10 (red) in the suprabasal layer. Yellow lines outline the basement membrane separating the epithelial and mesenchymal cells in **(B,C,E,F,H–K)**. Scale bars in **(A)** = 500 μm, same scale in **(D)**. Scales bars in **(B,H)** = 10 μm, same scale in **(C,E,F,I–K)**. Scale bar in **(G)** = 100 μm.

DISCUSSION

A Single Origin of the Anterior VL and DL During Human Development

The DL and VL have a very close relationship during development. In the maxillary canine region, the DL is physically attached to the VL at all stages investigated. In the lower anterior region, our culture experiments confirm that a single epithelial thickening gives rise to both the VL and the DL. Due to the rarity of the material, culture was only attempted for one embryo at CS19 but the results agree with findings indicated from 3D reconstruction of human sections and from lineage tracing in the mouse (Hovorakova et al., 2007, 2016). Although we confirm this dual origin for the lower anterior oral region, the relationship between the DL and VL is dynamic throughout the jaw (**Figures 1A, 2A**). This heterogeneity explains the differing results from papers that have investigated different regions of the jaw (Bolk, 1921; Schour, 1929; Tonge, 1969). We, therefore, suggest that a single thickening, which subsequently divides into the DL and VL, forms in the anterior region, while distinct DL and VL thickenings

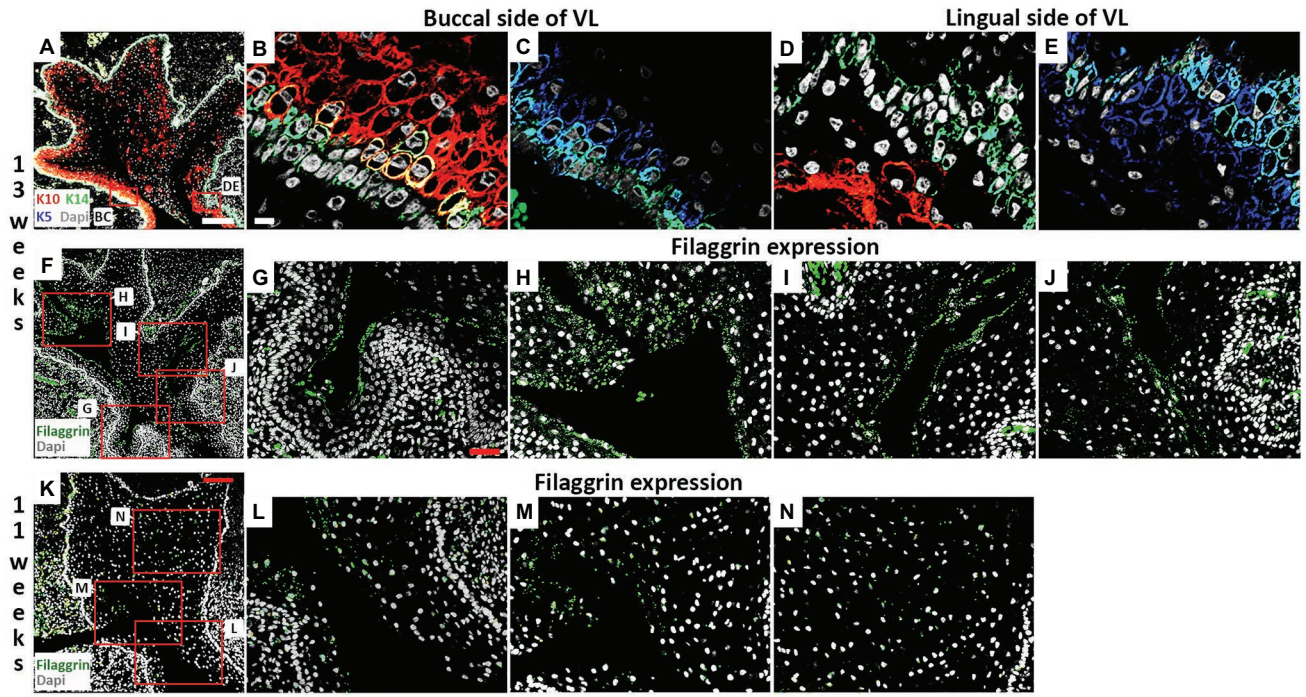

FIGURE 4 | Filaggrin expression is associated with fissure formation in the VL. **(A–J)** Frontal sections through the canine VL at 13 weeks. DAPI shows nuclei in white. **(A)** Branching structure of VL. Boxes in **(A)** highlights regions in **(B–E)**. **(A–E)** K10 (red), K5 (blue), K14 (green). **(B,C)** On the buccal side, K14 is largely limited to the basal layer, with a wider expression of K5, and K10 at high levels in the overlying layer. **(D,E)** On the lingual side, K10 levels remain low, with a less organized layer of K14. **(F–J)** Filaggrin (green) lines the forming fissures at 13 weeks. **(F)** Branching structure of VL. Boxes in **(F)** highlights different parts of the VL in **(G–J)**. **(K–N)** Frontal sections through the canine VL at 11 weeks. DAPI shows nuclei in white. **(K)** VL with evidence of a main fissure running through the structure. Filaggrin (Green). Boxes in **(K)** highlights regions in **(L–N)**. Scale bar in **(A)** = 200 μm, same scale in **(F)**. Scale bar in **(B)** = 10 μm, same scale in **(C–E)**. Scale bar in **(G)** = 50 μm, same scale in **(H–J,L–N)**. Scale bar in **(K)** = 100 μm.

arise more posteriorly. Whether this is a feature across mammals, will be an interesting area for future investigation.

The DL is closely associated with a number of developing structures across vertebrates. In the mouse, a single thickened epithelium has been proposed to be the primordium for the DL, VL, and the rugae of the palate (Peterková, 1985). Similarly, in reptiles the DL and the neighboring dental gland have been suggested to form from a single placode (Vonk et al., 2008; Tucker, 2010). A close relationship between the DL and the neighboring taste bud primordium has also been suggested in the shark and rays, with cells from the taste buds contributing to the cells of the lamina during embryonic development (Martin et al., 2016). The DL should therefore not be thought of in isolation but together with its neighboring epithelial organs. What signals govern the decision to form a VL or DL is an interesting future question. Mistakes in such a process might lead to the VL taking on a DL fate, as in the case when tooth pathologies form in the region of the vestibule (Hovorakova et al., 2020).

The Lingual and Labial/Buccal Sides of the VL Have Different Differentiation Patterns

The VL forms as a block of epithelium which then divides to create the vestibule. Here, we show that the canine VL is not divided by formation of a single fissure but by the development of numerous fissures that split the VL into several pieces. The epithelial cells on the labial/buccal side differentiate earlier, with the expression of the suprabasal marker K10, while this marker was only weakly expressed on the lingual side by 13 weeks when the fissures are apparent. Differences in keratin patterns between the mucosa on either side of the vestibule have also been observed in adult tissue, suggesting that these developmental differences are maintained throughout life (Verlach et al., 2017). It has been proposed that the lingual and labial/buccal sides are divided along the line of the K10 positive and negative expressing cells (Pelissier et al., 1992). There appears to be a slight oversimplification given that many fissures form and do not follow the lines of K10 expression. However, the fissures were lined with the terminal marker filaggrin, with filaggrin expression evident before fissure formation at 11 weeks. Filaggrin has been shown to have a role in cell adhesion (Presland et al., 2001). In epithelial cells, over expressing filaggrin, two desmosome proteins, desmoplakin, and plakoglobin, were lost at the cell interfaces and the cells detached from their neighbors (Presland et al., 2001). The upregulation of filaggrin in the VL, prior to any evidence of a fissure, may therefore lead to the cells at the center losing their adhesion, with the consequence that gaps would appear between the cells, creating the fissures. This is a particularly interesting hypothesis, given that filaggrin expression is observed extremely early in the VL, several weeks before its described upregulation

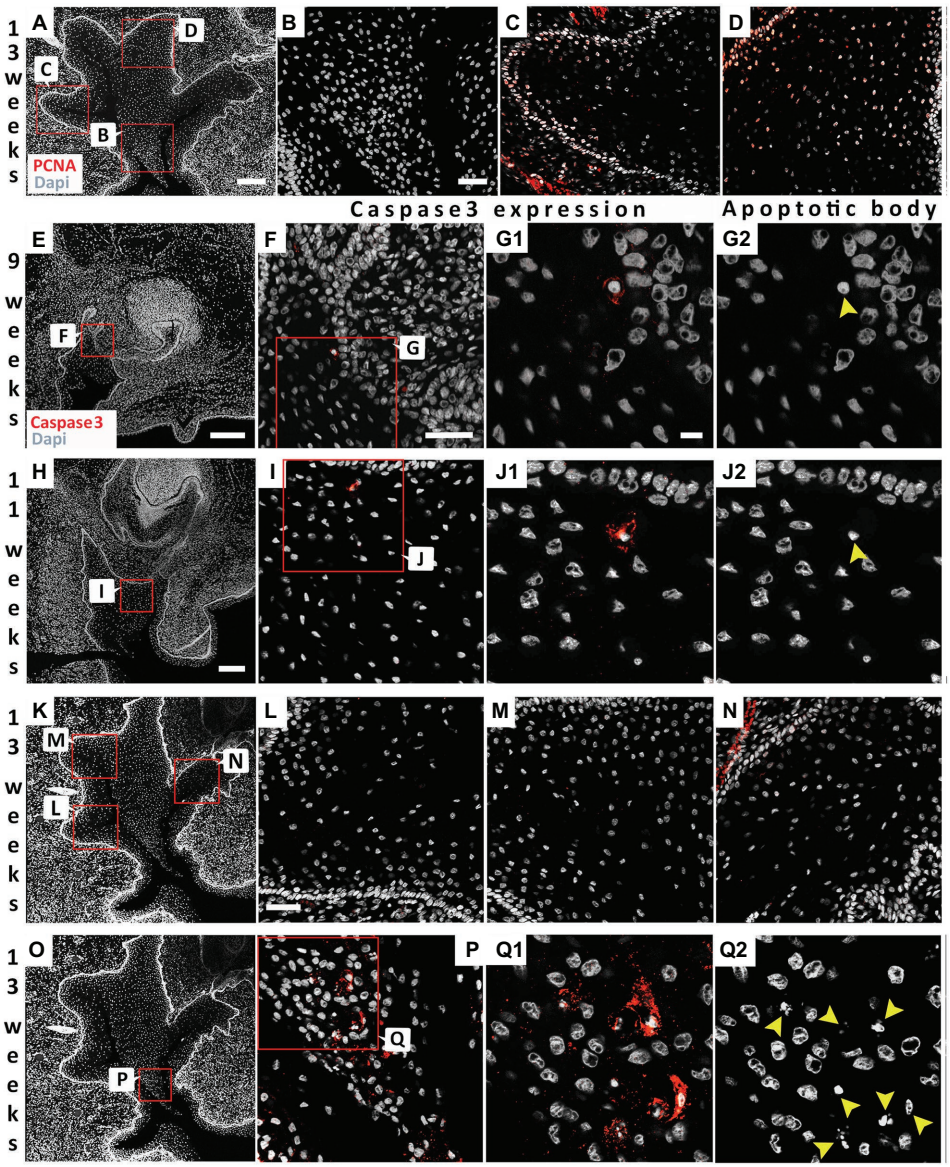

FIGURE 5 | Differential proliferation and apoptosis to remove the central cells to create the vestibule. **(A)** 13 weeks VL. DAPI shows nuclei in white. Boxes in **(A)** highlights regions in **(B–D)**. **(B–D)** PCNA (red). **(B)** Absence of proliferating cells at the center of the VL. **(C,D)** Proliferating cells in the more basal cells at the edges of the VL. **(E–Q2)** Analysis of program cell death. **(F,G1,I,J1,L–N,P,Q1)** activated Caspase-3 immuno (red). **(G2,J2,Q2)** same sections as in **(G1,J1,Q1)** showing the presence of apototic bodies (yellow arrowheads). **(E–G2)** 9 weeks. **(E)** 9 weeks VL. DAPI shows nuclei in white. Box in **(E)** highlights regions in **(F–G2)**. **(H–J2)** 11 weeks. **(H)** 11 weeks VL. DAPI shows nuclei in white. Box in **(H)** highlights regions in **(I–J2)**. **(K–Q2)** 13 weeks. **(K)** 13 weeks VL. DAPI shows nuclei in white. Boxes in **(K)** highlights regions in **(L–N)**. Box in **(O)** highlights regions in **(P–Q2)**. Scale bar in **(A)** = 200 μm, Scale Bar in **(B)** = 50 μm, same scale in **(C,D)**. Scale bar in **(E,H)** = 200 μm, same scale in **(K,O)** as for **(H)**. Scale bar in **(F)** = 50 μm, same scale in **(I)**. Scale bar in **(G1)** = 10 μm, same scale in **(G2,J1,J2,Q1,Q2)**. **(G1)** = 10 μm, same scale in **(G2,J1,J2,Q1,Q2)**. Scale bar in **(L)** = 50 μm, same scale in **(M,N)**.

in forming hair follicles and its expression in fetal skin (Dale et al., 1985; Lee et al., 1999). Division of the VL based on changes in cell adhesion agrees with the hypothesis suggested by Coslet and Cohen (1969) based on cell morphology in histological sections. The upregulation of filaggrin and differentiation of the VL cells agreed with the restriction of proliferation to the more basal parts of the structure. Failure in formation of these fissures along the VL would be predicted to result in the formation of frenulum, with tissue permanently linking the dental arch and lips/cheeks, as observed in EVC syndrome (Sasalawad et al., 2013). EVC syndrome is associated with defects in primary cilia and the Shh signaling pathway (Caparrós-Martín et al., 2013; Nakatomi et al., 2013), suggesting that this pathway may have an important role in development of the VL. In mice, the DL and VL form from a Shh positive placode but then Shh turns off in the VL (Hovorakova et al., 2016). Shh, therefore does not appear to be associated with later development of the VL.

Apoptosis Plays a Role in Removing Tissue From the VL but Not in Fissure Formation

During formation of the fissures, we did not see any evidence of programmed cell death, as evidenced by expression of activated Caspase-3 or of apoptotic bodies. Fissure formation is therefore unlikely to be triggered by death of cells at the center of each fissure, but rather by changes in cell-cell interactions. Several fissures were formed in the VL at the canine, creating a V-shaped wedge of cells at the middle of the VL. It is here that high levels of apoptosis were observed. Removal of the cells in the middle of the VL, created by formation of the fissures, therefore does appear to be dependent on cell death. Cell death in this region would help to broaden the developing vestibule, creating a more pronounced division between the dental arch and surrounding cheeks and lips.

Overall, we show that the DL and VL develop in close association, with the VL as a transient structure, having a perhaps surprisingly complex development. New understanding of development can shed light on dental pathologies associated with the vestibule, and to congenital defects in this region.

DATA AVAILABILITY STATEMENT

The raw data supporting the conclusions of this article will be made available by the authors, without undue reservation.

ETHICS STATEMENT

The studies involving human embryonic and fetal tissue were reviewed and approved by the Human Developmental Biology Resource under the approval of the National Research Ethics Service.

AUTHOR CONTRIBUTIONS

MH and AT conceived the idea. TQ performed the histology and immunohistochemistry. TT performed the explant culture experiments. AT and TQ wrote the manuscript. All authors contributed to the article and approved the submitted version.

FUNDING

This work was supported by the Grant Agency of the Czech Republic (18-04859S to MH and AT). TQ was funded by the China Scholarship Council as part of a PhD studentship at KCL. The human embryonic and fetal material in this paper was provided by the Human Developmental Biology Resource (www.hdbr.org), which is jointly funded by the Medical Research Council and Wellcome Trust (grant #099175/Z/12/Z).

REFERENCES

Alfaqeeh, S. A., and Tucker, A. S. (2013). The slice culture method for following development of tooth germs in explant culture. *J. Vis. Exp.* 81:e50824. doi: 10.3791/50824

Bolk, L. (1921). Odontological essays. *J. Anat.* 57, 55–75.

Caparrós-Martín, J. A., Valencia, M., Reytor, E., Pacheco, M., Fernandez, M., Perez-Aytes, A., et al. (2013). The ceiliary EVC/EVC2 complex interacts with smo and controls hedgehog pathway activity in chondrocytes by regulating Sufu/Gli3 dissociation and Gli3 trafficking in primary cilia. *Hum. Mol. Genet.* 22, 124–139. doi: 10.1093/hmg/dds409

Coolen, N. A., Schouten, K. C. W. M., Middelkoop, E., and Ulrich, M. M. W. (2010). Comparison between human fetal and adult skin. *Arch. Dermatol. Res.* 302, 47–55. doi: 10.1007/s00403-009-0989-8

Coslet, J. G., and Cohen, D. W. (1969). Observations on the development of the vestibular trough in the human fetus part I. The anterior portion of the mouth. *J. Periodontol.* 40, 320–329. doi: 10.1902/jop.1969.40.6.320

Dale, B. A., Holbrook, K. A., Kimball, J. R., Hoff, M., and Sun, T. T. (1985). Expression of epidermal keratins and filaggrin during human fetal skin development. *J. Cell Biol.* 101, 1257–1269. doi: 10.1083/jcb.101.4.1257

Dietrich, D. R. (1993). Toxicological and pathological applications of proliferating cell nuclear antigen (PCNA), a novel endogenous marker for cell proliferation. *Crit. Rev. Toxicol.* 23, 77–109. doi: 10.3109/10408449309104075

Hovorakova, M., Lesot, H., Peterka, M., and Peterkova, R. (2005). The developmental relationship between the deciduous dentition and the oral vestibule in human embryos. *Anat. Embryol.* 209, 303–313. doi: 10.1007/s00429-004-0441-y

Hovorakova, M., Lesot, H., Vonesch, J. -L., Peterka, M., and Peterkova, R. (2007). Early development of the lower deciduous dentition and oral vestibule in human embryos. *Eur. J. Oral Sci.* 115, 280–287. doi: 10.1111/j.1600-0722.2007.00464.x

Hovorakova, M., Lochovska, K., Zahradnicek, O., Tibenska, K. D., Dornhoferova, M., Horakova-Smrckova, L., et al. (2016). One odontogenic cell-population contributes to the development of the mouse incisors and of the oral vestibule. *PLoS One* 11:e0162523. doi: 10.1371/journal.pone.0162523

Hovorakova, M., Zahradnicek, O., Bartos, M., Hurnik, P., Stransky, J., Stembirek, J., et al. (2020). Reawakening of ancestral dental potential as a mechanism to explain dental pathologies. *Integr. Comp. Biol*. icaa053. doi: 10.1093/icb/icaa053

Kochva, E. (1965). The development of the venom gland in the opisthoglyph snake *Telescopus fallax* with remarks on *Thamnophis sirtalis*. *Copeia* 1965, 147–154. doi: 10.2307/1440716

Kuechle, M. K., Presland, R. B., Lewis, S. P., Fleckman, P., and Dale, B. A. (2000). Inducible expression of filaggrin increases keratinocyte susceptibility to apoptotic cell death. *Cell Death Differ.* 7, 566–573. doi: 10.1038/sj.cdd.4400687

Lee, S. C., Lee, J. B., Kook, J. P., Seo, J. J., Nam, K. I., Park, S. S., et al. (1999). Expression of differentiation markers during fetal skin development in humans: immunohistochemical studies on the precursor proteins forming the cornified cell envelope. *J. Invest. Dermatol.* 112, 882–886. doi: 10.1046/j.1523-1747.1999.00602.x

Martin, K. J., Rasch, L. J., Cooper, R. L., Metscher, B. D., Johanson, Z., and Fraser, G. J. (2016). Sox2+ progenitors in sharks link taste development with the evolution of regenerative teeth from denticles. *Proc. Natl. Acad. Sci. U. S. A.* 113, 14769-14774. doi: 10.1073/pnas.1612354113

Nakatomi, M., Hovorakova, M., Gritli-Linde, A., Blair, H. J., MacArthur, K., Peterka, M., et al. (2013). Evc regulates a symmetrical response to Shh signaling in molar development. *J. Dent. Res.* 92, 222–228. doi: 10.1177/0022034512471826

Nery, E. B., Kraus, B. S., and Croup, M. (1970). Timing and topography of early human tooth development. *Arch. Oral Biol.* 15, 1315–1326. doi: 10.1016/0003-9969(70)90020-8

Pavlikova, H., Witter, K., and Misek, I. (1999). Primordium of the upper vestibulum oris in the domestic sheep. *Acta Vet. Brno* 68, 175–178. doi: 10.2754/avb199968030175

Pelissier, A., Ouhayoun, J. P., Sawaf, M. H., and Forest, N. (1992). Changes in cytokeratin expression during the development of the human oral mucosa. *J. Periodontal Res.* 27, 588–598. doi: 10.1111/j.1600-0765.1992.tb01741.x

Peterková, R. (1985). The common developmental origin and phylogenetic aspects of teeth, rugae palatinae, and fornix vestibuli oris in the mouse. *J. Craniofac. Genet. Dev. Biol.* 5, 89–104.

Popa, E. M., Buchtova, M., and Tucker, A. S. (2019). Revitalising the rudimentary replacement dentition in the mouse. *Development* 146:dev171363. doi: 10.1242/dev.171363

Presland, R. B., Kuechle, M. K., Lewis, S. P., Fleckman, P., and Dale, B. A. (2001). Regulated expression of human filaggrin in keratinocytes results in cytoskeletal disruption, loss of cell-cell adhesion, and cell cycle arrest. *Exp. Cell Res.* 270, 199–213. doi: 10.1006/excr.2001.5348

Sasalawad, S. S., Hugar, S. M., Poonacha, K. S., and Mallikarjuna, R. (2013). Ellis-van Creveld syndrome. *BMJ Case Rep.* 2013:bcr2013009463. doi: 10.1136/bcr-2013-009463

Schour, I. (1929). Early human tooth development, with special reference to the relationship between the dental lamina and the lip-furrow band. *J. Dent. Res.* 9, 699–717. doi: 10.1177/00220345290090050801

Tonge, C. H. (1969). The time-structure relationship to tooth development in human embryogenesis. *J. Dent. Res.* 48, 745–752.

Tucker, A. S. (2010). "Salivary gland adaptations: Modification of the glands for novel uses" in *Salivary glands.* eds. A.S., Tucker and I., Miletich (Basel: Karger), 21–31.

Tucker, A., and Sharpe, P. (2004). The cutting-edge of mammalian development: how the embryo makes teeth. *Nat. Rev. Genet.* 5, 499–508. doi: 10.1038/nrg1380

Verlach, J., Foltan, R., Vlk, M., Szabo, P., and Smetana, K. (2017). Phenotypic chacterisation of oral mucosa: what is normal? *J. Oral Pathol. Med.* 46, 834–839. doi: 10.1111/jop.12556

Vonk, F. J., Admiraal, J. F., Jackson, K., Reshef, R., de Bakker, M. A. G., Vanderschoot, K., et al. (2008). Evolutionary origin and development of snake fangs. *Nature* 454, 630–633. doi: 10.1038/nature07178

Wang, X. P., O'Connell, D. J., Lund, J. J., Saadi, I., Kuraguchi, M., Turbe-Doan, A., et al. (2009). Apc inhibition of Wnt signaling regulates supernumerary tooth formation during embryogenesis and throughout adulthood. *Development* 136, 1939–1949. doi: 10.1242/dev.033803

West, C. M. (1924). The development of the gums and their relationship to the deciduous teeth in the human fetus. *Contr. Embroyol. Carnegie Inst.* 16, 25–45.

Witter, K., Pavlikova, H., Matulova, P., and Misek, I. (2005). Relationship between vestibular lamina, dental lamina, and the developing oral vestibule in the upper jaw of the field vole (*Microtus agrestis*, Rodentia). *J. Morphol.* 265, 264–270. doi: 10.1002/jmor.10356

Conflict of Interest: The authors declare that the research was conducted in the absence of any commercial or financial relationships that could be construed as a potential conflict of interest.

Supplementary data to chapter 3: Development of the vestibular lamina in human embryos: morphogenesis and vestibule formation (unpublished)

Dual origin of the murine VL and DL depends on position

The developmental relationship between the VL and DL in humans has been controversial in the literature, with **Hovorakova** (2005) summarizing three proposed explanations. These include independent development, a shared origin, or a common origin in the anterior region with separate development in the posterior region. The results of my thesis have confirmed that in the lower incisor region of humans, the VL and DL share a common developmental origin from a single epithelial thickening (**Qiu *et al.*, 2020**), while their relationship appears to be dynamic and varies depending on the location within the jaw (**Qiu *et al.*, 2020**). This is consistent with the findings from 3D reconstruction of human sections (**Hovorakova *et al.*, 2005, 2007**) and lineage tracing experiments in mice (**Hovorakova *et al.*, 2016**). In order to assess the situation further we used the DiI explant culture system previously used in human embryos in the mouse. DiI lineage labeling indicated that the VL could originate either from the same oral epithelial placode as DL (**Fig. S1**) or from a distinct placode, with the VL located externally to the DL (**Fig. S2**), depending on the age of embryo when sliced and the exact position in the jaw. In some slices one thickening was observed while in others two clear thickenings were evident.

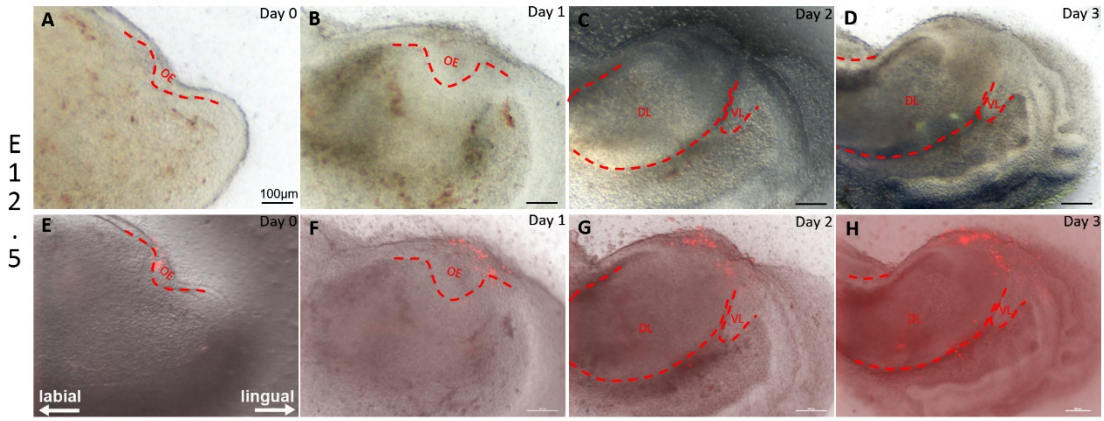

Figure S1. The DiI tracing experiment reveals that the origin of murine VL and DL can be traced back to the same oral epithelial placode. (**A-D**) The development of murine VL and DL at E12.5 after 3 days in culture. At Day0 (E12.5), a single thickened epithelium was observed. (**E-H**) The corresponding slices of VL and DL labeled with DiI (red fluorescence). The caudal portion of the epithelial thickening was labeled with DiI at Day0 (E12.5). The DiI extended to label the oral epithelium associated with the DL, while the non-labelled portion of the placode gave rise to VL. The VL and DL were outlined with red dashed lines. VL: vestibular lamina; DL: dental lamina; OE: oral epithelium. Scale bar in (A-H) = 100μm. Labial-lingual axes shown in E, same plane for all images.

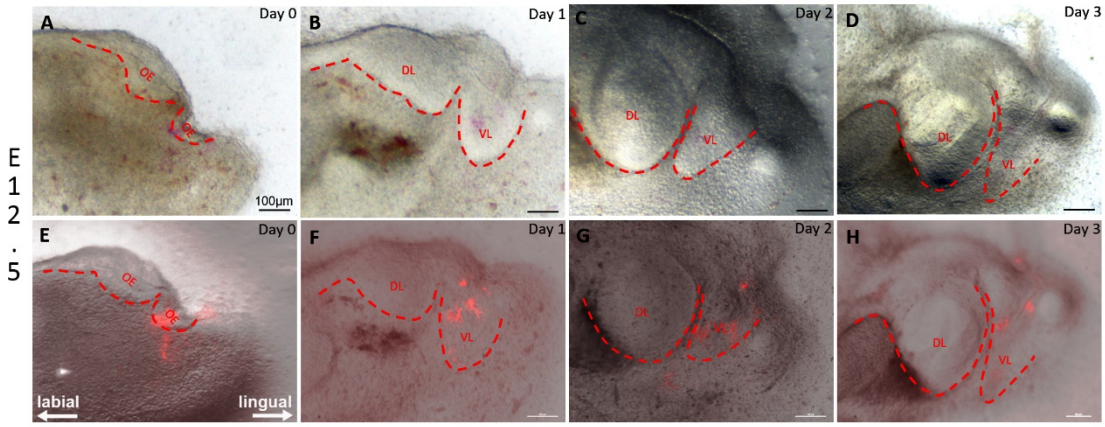

Figure S2. The DiI tracing results demonstrate that VL and DL form from two

distinct adjacent thickenings, and the VL is situated at the labial side of the DL. (**A-D**) The development of murine VL and DL at E12.5 after 3 days in culture. By E12.5, the primordia of VL and DL were already discernible as distinct entities when viewed as sagittal slices. (**E-H**) The corresponding slices of VL and DL labeled with DiI (red fluorescence). DiI labeling of the more rostral thickening revealed an extension of DiI downwards, which was associated with the development of VL. No DiI was observed in the DL that originated from the more caudal placode. The VL and DL were outlined with red dashed lines. VL: vestibular lamina; DL: dental lamina; OE: oral epithelium. Scale bar in (A-H) = 100μm. Labial-lingual axes shown in E, same plane for all images.

The differences observed may be due to subtle differences in age of the embryos, even though they were from the same litter. The two placodes may represent slightly older embryos where a single placode had already separated into two. Alternatively, the differences may represent subtle different positions in the jaw, with medial and lateral slices showing different relationships. To assess this further we could weigh the embryos before dissection, as weigh as been shown to be a good predictor of stage of tooth development (**Peterka, Lesot, and Peterková, 2002**). The exact position in the jaw could also be assessed more carefully by monitoring how the slices related to each other in the mandible.

Chapter 4 – (Publication 2) Mechanisms driving vestibular lamina formation and opening in the mouse

(Journal of Anatomy, 2022)

Tengyang Qiu and Abigail S. Tucker*

Centre for Craniofacial and Regenerative Biology, Faculty of Dentistry, Oral and Craniofacial Sciences, King's College

Aim: To examine the early development of VL in mouse, and assess the mechanisms underlying furrow formation.

My contributions: I conducted all of the experiments, including histology, immunohistochemistry, and explant culture. I created all the figures and wrote the draft of the original manuscript. I contributed to the editing of the manuscript.

Abstract:

The vestibular lamina (VL) forms as an epithelial outgrowth parallel to the dental lamina (DL) in the oral cavity. During late development, it opens to create a furrow that divides the dental tissue from the cheeks and lips and is known as the vestibule. Defects in this process lead to failure in the separation of the teeth from the lips and cheeks, including the presence of multiple frenula. In this paper, the development of the VL is followed in the mouse, from epithelial placode in the embryo to postnatal opening and vestibule formation. During early outgrowth, differential proliferation controls the curvature of the VL as it

extends under the forming incisors. Apoptosis plays a role in thinning the deepest part of the lamina, while terminal differentiation of the epithelium, highlighted by the expression of loricrin and flattening of the nuclei, predates the division of the VL into two to create the vestibule. Development in the mouse is compared to the human VL, with respect to the relationship of the VL to the DL, VL morphology and mechanisms of opening. Overall, this paper provides insight into an understudied part of the oral anatomy, shedding light on how defects could form in this region.

Received: 14 August 2022 | Revised: 8 September 2022 | Accepted: 13 September 2022

DOI: 10.1111/joa.13771

Journal of Anatomy ANATOMICAL SOCIETY WILEY

ORIGINAL ARTICLE

Mechanisms driving vestibular lamina formation and opening in the mouse

Tengyang Qiu | **Abigail S. Tucker**

Centre for Craniofacial and Regenerative Biology, Faculty of Dentistry, Oral and Craniofacial Sciences, King's College London, London, UK

Correspondence
Abigail S. Tucker, Centre for Craniofacial and Regenerative Biology, Faculty of Dentistry, Oral and Craniofacial Sciences, King's College London, London SE1 9RT, UK.
Email: abigail.tucker@kcl.ac.uk

Funding information
China Scholarship Council; Grantová Agentura České Republiky, Grant/Award Number: 18-04859S

Abstract

The vestibular lamina (VL) forms as an epithelial outgrowth parallel to the dental lamina (DL) in the oral cavity. During late development, it opens to create a furrow that divides the dental tissue from the cheeks and lips and is known as the vestibule. Defects in this process lead to failure in the separation of the teeth from the lips and cheeks, including the presence of multiple frenula. In this paper, the development of the VL is followed in the mouse, from epithelial placode in the embryo to postnatal opening and vestibule formation. During early outgrowth, differential proliferation controls the curvature of the VL as it extends under the forming incisors. Apoptosis plays a role in thinning the deepest part of the lamina, while terminal differentiation of the epithelium, highlighted by the expression of loricrin and flattening of the nuclei, predates the division of the VL into two to create the vestibule. Development in the mouse is compared to the human VL, with respect to the relationship of the VL to the DL, VL morphology and mechanisms of opening. Overall, this paper provides insight into an understudied part of the oral anatomy, shedding light on how defects could form in this region.

KEYWORDS
apoptosis, epithelial differentiation, oral mucosa, vestibule

1 | INTRODUCTION

The vestibular lamina (VL) is a transient mammalian structure that forms during embryonic development and creates the vestibule, the gap separating the teeth from the cheeks and lips. It has also been referred to as the lip furrow band and vestibuli oris (Bolk, 1921; Peterkova, 1985; Schour, 1929). In some human syndromes, such as EVC syndrome (OMIM 225500), the development of the VL is compromised, leading to defects in the vestibule, such as multiple frenuli causing labioginival adherences (Nakatomi et al., 2013; Sasalawad et al., 2013). Vestibule defects have also been noted in some ectodermal dysplasias, such as Weyers acrofacial dysostosis (also known as Weyers acrodental dysotosis) (OMIM 193530) (Roubicek & Spranger, 1984) and, most recently, VL abnormalities and dental anomalies were reported in a patient with cryptophthalmos resulting from a mutation in the FREM2 gene (OMIM 23570) (Kantaputra et al., 2022). Shallow vestibules were noted in 3.6% of healthy children in a study of 83 children, with a small number of frenulum abnormaliies observed (Kus-Bartoszek et al., 2022). Such frenulum defects have been linked to later development of some types of periodontal disease (Placek et al., 1974).

In the embryo, the vestibular lamina forms in close relationship to the neighbouring dental lamina (DL). The DL goes on to form the tooth germs, and in some parts of the jaw the two laminas share a common placodal origin in both the mouse and human (Hovorakova et al., 2016; Peterkova, 1985; Qiu et al., 2020). The VL and DL are often thought of horse-shoe structures with the VL running continuously around the jaw parallel to the DL, however in humans 3D

reconstructions reveal that the VL is discontinuous with numerous connections to the DL (Hovorakova et al., 2005, 2007). Interestingly, in some positions along the jaw the VL forms tooth germ-like structures, and in some mouse mutants tooth germs can develop from the VL, suggesting it has the potential to form teeth, similar to the DL (Popa et al., 2019; Wang et al., 2009). Some odontomas (tooth-like tumours) are also associated with the VL in patients, providing further evidence that the VL has dormant tooth-forming potential (Hovorakova et al., 2020).

Recently, the early development of the VL has been followed in human embryonic and foetal tissue, highlighting the relationship between the VL and DL and the process of opening to create the vestibule. In humans, the VL starts to open around 11 weeks by the creation of fissures due to differentiation of the epithelium and loss of epithelial integrity (Qiu et al., 2020). Apoptosis then plays a role in removing cells from the middle of the opening VL to create a large gap between the future teeth and cheeks (Qiu et al., 2020).

Morphology of the developing VL has been followed in a few mammals, such as the sheep, field vole and mouse, highlighting that there are clear species-specific differences in the size and shape of the VL in different parts of the mouth. The morphology of the VL may therefore be shaped by later feeding requirements. The mouse and vole VL forms as a thin lamina and is prominent in the anterior mandible, while in humans and sheep the VL is multi-layered and found associated with all teeth (Hovorakova et al., 2005, 2016; Pavlikova et al., 1999; Qiu et al., 2020; Witter et al., 2005). In the mouse, the early development of the VL has been followed using 3D reconstruction of the incisor region from Embryonic day (E)11.5 to E13.5, highlighting the close relationship of the tooth germ and neighbouring VL (Hovorakova et al., 2011). Later questions about how the VL extends and opens and the timing of such events have not been investigated. A lack of knowledge regarding VL development in the mouse has led to this structure being largely ignored in the description of mouse mutants and being missed out in recent schematics of the oral cavity (Ye et al., 2022).

Here the development of the murine VL has been followed from initiation in the embryo to vestibule formation during postnatal stages. The mechanisms that drive the extension and opening of the VL are described, highlighting the role of epithelial differentiation and distinct differences between the labial and lingual sides of the VL. Overall, this paper provides a systematic description of the formation of the vestibule, which will provide an essential source for further understanding of normal and abnormal development of this structure.

2 | MATERIALS AND METHODS

2.1 | Murine tissue collection

Mouse embryos were collected from wild-type mice of CD1 strain, which were housed in the Biological Services Unit in New Hunts House at King's College London (KCL). Day 0.5 was considered midday on the day that a plug was found. Postnatal stages from P0 to P15 were collected from wild-type mice (CD1 and C57Bl6 background). All animals were culled using schedule one culling methods as approved by the UK Home Office. For proliferation assays, pregnant dams were injected with Bromodeoxyuridine (BrdU) (30 mg/kg) 1 h before culling.

2.2 | Tissue processing and histology

Dissected heads were fixed in 4% paraformaldehyde (PFA), dehydrated through an increasing ethanol concentration, before moving to xylene and embedding in paraffin wax. Postnatal tissues were decalcified in 0.5 M ethylenediaminetetraacetic acid (EDTA) before dehydration. Sections were cut in 8 μm serial sections using a Microtome Leica RM2245, and serially split onto slides. For histology trichrome staining was using: sirius red, Alcian blue and Hematoxylin. Stained slides were photographed using a Nikon Eclipse 80i light microscope attached with a Nikon Digital Sight DS-Fi1 camera.

2.3 | Explant culture

Wild-type pregnant CD1 mice were collected at embryonic stage E12.5 ($n > 3$). The mandibles were dissected, and tongue removed before being chopped sagittally into 250 μm thick slices using a McIlwain tissue chopper (Alfaqeeh & Tucker, 2013). The slices with a clear DL/VL bud in the incisor region were selected. Explants were placed on permeable membranes (BD Falcon cell culture inserts, pore size 0.4 μm) over culture medium (DMEM-Advanced Dulbecco Modified Eagle Medium F12, [Invitrogen]; 1% GlutaMAX [Invitrogen]; and 1% penicillin–streptomycin solution [10,000 units penicillin and 10 mg streptomycin/ml; Sigma- Aldrich]). Slices were photographed using a Leica dissecting microscope at day 0 of culture, and then cultured in a 5% CO_2 at 37°C in an incubator for up to 3 days, with the culture medium changed every 1–2 days. Slices were photographed at regular intervals before fixation in 4% PFA. For whole mount immunofluorescence, explant slices were cultured with Bromodeoxyuridine (BrdU) at a concentration of 30uM for 2 h before fixation in 4% PFA for 40 min at RT.

2.4 | Immunofluorescence/whole mount immunofluorescence

Wax-embedded serial sections of the VL were de-waxed, rehydrated and treated with citric acid (pH 6) antigen retrieval solution in a 92°C water bath followed by 10 min at room temperature. The slides were then incubated with rabbit Cleaved Caspase-3 (1:200, Cell Signaling #9579), mouse anti-E-cadherin (1:400; Abcam, ab76055), rabbit anti-Loricrin (1:400; Biolegend, PRB-145P), rabbit anti-Occludin (1:200, Abcam #ab31721) rabbit anti-PCNA (1:400; Abcam #ab193965), and rat anti-BrdU (1:500, Abcam # ab6326), overnight at 4°C. The sections were then incubated in Alexa Fluor™ donkey anti-mouse 488

(1:500, Invitrogen #A21202), Alexa Fluor™ donkey anti-rabbit 568 (1:500, Invitrogen #A10042) and Alexa Fluor™ donkey anti-mouse 647 (1:500, Invitrogen #A31571) for 1 h at RT. Sections were mounted with Fluoroshield™ with DAPI (Sigma-Aldrich #SLBV4269) and imaged with a Leica TCS SP5 confocal microscope. To test each antibody, controls were performed where the primary antibodies had been omitted in order to confirm specific staining. Each antibody was repeated at least three times, at different timepoints, using serial sections.

For whole mount immunofluorescence, fixed BrdU cultured explant slices were permeabilized with PBS Triton 0.5% (PBT) at RT for 1.5 h followed by trypsinization for 12 min on ice and incubation in blocking solution for 2 h. After blocking, slices were incubated in primary antibodies mouse anti-E-cadherin (1:400; Abcam, ab76055) and rat anti-BrdU (1:500, Abcam # ab6326) overnight at 4°C. Next day, after washing in 0.5% PBT for 3 h at RT, the slices were incubated in the Alexafluor donkey anti-rat 647 (1:500, Invitrogen, A21247), Alexa Fluor™ donkey anti-mouse 488 (1:500, Invitrogen #A11001) and DAPI (1:1000, Sigma) overnight in the fridge. Finally, the slices were washed in 0.5% PBT for 3 h at RT, mounted in PBS and analysed using a Leica TCS SP5 confocal microscope.

2.5 | Cell quantification and statistical analysis

Cells on the lingual and labial sides of the VL were quantified manually using the multiple-point tools of Fiji/ImageJ. Results were plotted using GraphPad Prism software (GraphPad Prism V.8.0.2) and statistical analysis were performed using IBM SPSS Statistics software (IBM SPSS Statistics V.25.0). Statistical significance was calculated using paired *t*-tests (comparing lingual and labial sides of the same VL). Significance was taken as $p < 0.05$ (*), $p < 0.01$ (**) or $p < 0.001$ (***).

3 | RESULTS

3.1 | Development of the mouse VL varies between the upper and lower jaw during development

The VL is prominent in both the upper and lower jaw in humans (Hovorakova et al., 2005, 2007; Qiu et al., 2020). In the mouse, the VL is evident in the anterior of the mouth, but a clear structure was less obvious more posteriorly near the molars (Hovorakova et al., 2011; Peterkova, 1985). We therefore analysed the developing VL in the mouse focusing on the more anterior/incisor region from E (embryonic day) 12.5, the stage when the VL and DL are at the placodal thickening stage. In the anterior part of the upper jaw, only small areas of thickened oral epithelium were observed lateral to the forming DL/tooth primordia from E12.5 to E16.5, which were barely distinguishable from the oral epithelium (Figure 1A–D). At E18.5 the maxillary VL was more evident, forming an epithelial projection lateral to the forming incisors (Figure 1E). In contrast, in the mandible, the VL was much more pronounced at the same embryonic stages. At E12.5 two thickened laminas were evident, the VL positioned lateral to the DL (Figure 1F). By E13.5 the incisor had reached the bud stage, while the adjacent VL had extended down and around the forming tooth (Figure 1G). By E15.5 the VL had extended under Meckel's cartilage, with the two laminas almost touching in the midline by E16.5 (Figure 1H,I). The VL remained a solid structure at E18.5 (Figure 1J). In human embryos, the DL extends from the VL in both the upper and lower jaw (Figure S1; Qiu et al., 2020). In contrast, in the mouse the DL and VL both extended directly from the oral surface at all stages investigated.

3.2 | Asymmetrical proliferation of the extending VL leads to bending of the outgrowth

In histological section, it was evident that the VL curves as it grows so that it extends under the tooth. This directional growth could be followed in slice culture. Here live sagittal slices of the jaw were generated at E12.5, when the VL was evident as a placode (Figure 2A–D). During the culture period, the incisor tooth germ (outlined in magenta) developed from a thickening to a late cap stage tooth, and the neighbouring VL (outlined in green) extended under the forming tooth (Figure 2E–H). To address what drives the VL extension, we explored the role of proliferation during VL development. We utilised BrdU as a marker for detecting the dividing cells during the S phase of the cell cycle. Explants were cultured with BrdU for 2 h at day 2 before fixation and processed for whole mount immunofluorescence ($N > 3$). The morphology of the VL and DL were highlighted by the epithelial cell adhesion marker E-cadherin (Figure 2K). The developing slices had high levels of proliferation, as shown by BrdU-positive cells (in red), with labelled cells in the epithelium and mesenchyme (Figure 2I–L). After counting it was evident that the labial/buccal side of the VL contained significantly more positive cells than the neighbouring lingual side, with differential proliferation of the epithelium potentially driving the shape of the VL (Figure 2M). To confirm this difference, BrdU-positive cells were visualised in frontal sections at E14.5 (Figure 2N). As shown in culture, more positive cells (magenta) were observed on the buccal side of the VL compared to the lingual side near the tooth germ (Figure 2N,O). In section and in culture, the tip of the VL displayed high levels of proliferation throughout, driving the extension towards the midline (Figure 2L,N).

3.3 | The VL opens postnatally to form the vestibule by P15

To follow the creation of the vestibule we analysed the opening process postnatally in the lower jaw. The VL opened in a wave from the posterior to the anterior. At postnatal day (P)6, the anterior VL was still solid, while more posteriorly it had already opened (Figure 3A,E,I). Interestingly the VL did not appear to open from the top in an unzipping mechanism, but holes appeared within the centre of the structure (Figure 3B–D,F,G). The deepest part of the VL,

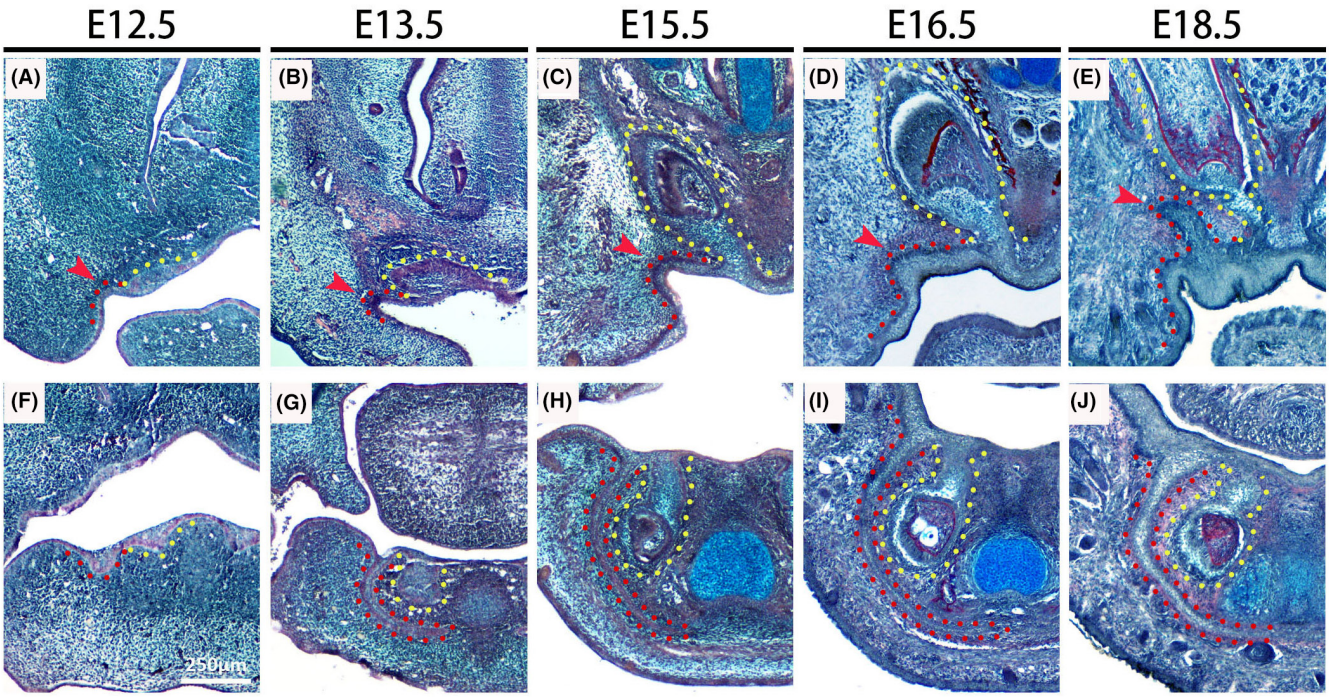

FIGURE 1 Embryonic development of the vestibular lamina (VL) in the murine incisor region. (A–E) Frontal sections of the upper jaw in wild-type (WT) mouse embryos stained with trichrome. (F–J) Frontal sections of lower jaw in WT mouse embryos stained with trichrome. (A, F) E12.5, (B, G) E13.5, (C, H) E15.5, (D, I) E16.5, (E, J) E18.5. Dental lamina/incisors and VL are outlined by yellow and red dashed lines, respectively. Scale bar in (F) = 250 µm, same scale in all other figures

under the forming incisor teeth and Meckel's cartilage, was the last part of the VL to open. Splitting of the VL was complete anteriorly by P12-P15, freeing the tooth-forming region from the neighbouring cheeks (Figure 3D,H,L–N). Interestingly, the splitting of the VL into buccal and lingual sections was not symmetrical, with the buccal side consisting of several epithelial layers while the lingual side was composed of only a few cell layers (Figure 3O–R).

3.4 | Postnatal opening of the VL does not appear to be driven by apoptosis

To understand the opening process in more detail, we focused on P0 to P4, just as the VL is starting to change from a solid structure. At birth (P0), the VL remained solid (Figures 4A and 5A). The first sign of opening was the appearance of small holes in the VL at P2 (Figure 4B). By P4, small holes were observed within the deeper parts of the lamina, with the VL open additionally at the oral surface in more posterior sections (Figures 4C,D and 5D). Ecadherin (Ecad) was used to follow changes to the epithelium during this period. Already by P0 expression of Ecad was reduced in the centre (suprabasal layer) of the VL in the top two thirds of the structure, this becoming more pronounced by P4, where a central core of Ecad-negative cells was observed (Figure 4M,N). The Ecad-positive basal cells were PCNA positive, with reduced proliferation in the core of the VL (Figure 4F,H). The deep part of the VL had high levels of proliferating cells, highlighting that the VL is still growing at this stage (Figure 4J,L). Our previous study on VL opening in human embryos highlighted that apoptosis played a

FIGURE 2 Differential proliferation shapes the developing VL. (A) Schematic of E12.5 mouse head. Red dots show the mandible dissection. (B) Diagram of dissected mandible. Dark lines indicate the chopping planes to create sagittal slices. (C) Medial slices present a tongue (T), and two protrusions, for the VL (green) and DL (magenta) respectively. (D) Histological sagittal section through a mouse embryonic head at E12.5. Magenta dashed line labels DL, and green dashed line outlines VL. (E–H) Developing sagittal slice of the lower jaw from E12.5. (E) Day 0. Two oral epithelial thickenings are prominent at E12.5. (F) Explant slices after 16 h in culture. (G, H) Slices after 48 and 72 h in culture. The VL extended into the mesenchyme and a clear tooth bud could be observed. Whiskers (red asterisks) also develop during the culture period. (I–L) Day 2 slice. Slices were cultured with BrdU for 2 h before fixing and processing for whole mount immunofluorescence. (I) DAPI (white nuclei). Green dashed line presents VL, light blue dashed line divides VL into lingual VL and buccal/labial VL. (J) DAPI (white) and BrdU (red). All BrdU expression is nuclear, confirming specificity. (K) BrdU (red) and E-cadherin (green). (L) BrdU alone (red). (M) Statistical graph for BrdU-positive cells (ratio) in the buccal VL compared to the lingual VL ($n = 3$, $p < 0.001$, error bars are SEM). (N, O) Frontal sections of lower jaw in wildtype mouse (E14.5). (N) BrdU (magenta) and E-cadherin (green) outlines the incisor tooth germ and VL. (O) BrdU (magenta) and DAPI (white). Positive cells are evident on the outer edge of the VL. Scale bar in (D) = 250 µm. Scale bar in (E) = 125 µm, same scale in F–H. Scale bar in (I) = 100 µm, same scale in J–L, N. Scale bar in (O) = 25 µm. *** is the level of significance as $p <$ 0.001. DL, dental lamina; VL, vestibular lamina; VL (B), Buccal VL; VL (L), lingual VL

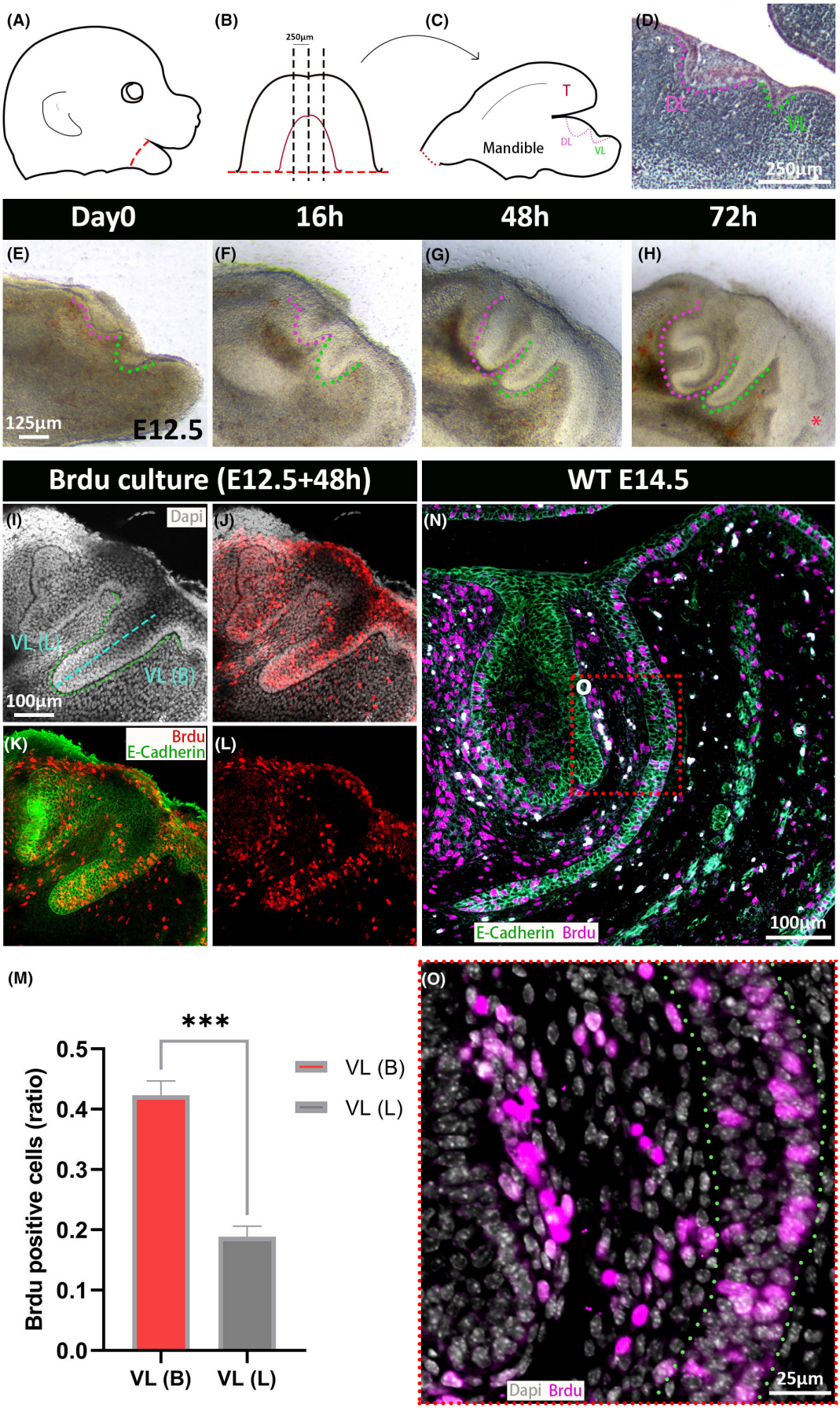
(A)
(B)
250μm
(C)
T
Mandible
DL
VL
(D)
DL
VL
250μm
Day0
16h
48h
72h
(E)
125μm
E12.5
(F)
(G)
(H)
*
Brdu culture (E12.5+48h)
WT E14.5
(I)
Dapi
VL (L)
VL (B)
100μm
(J)
(K)
Brdu
E-Cadherin
(L)
(N)
O
E-Cadherin Brdu
100μm
(M)
***
Brdu positive cells (ratio)
0.5
0.4
0.3
0.2
0.1
0.0
VL (B)
VL (L)
(O)
Dapi Brdu
25μm

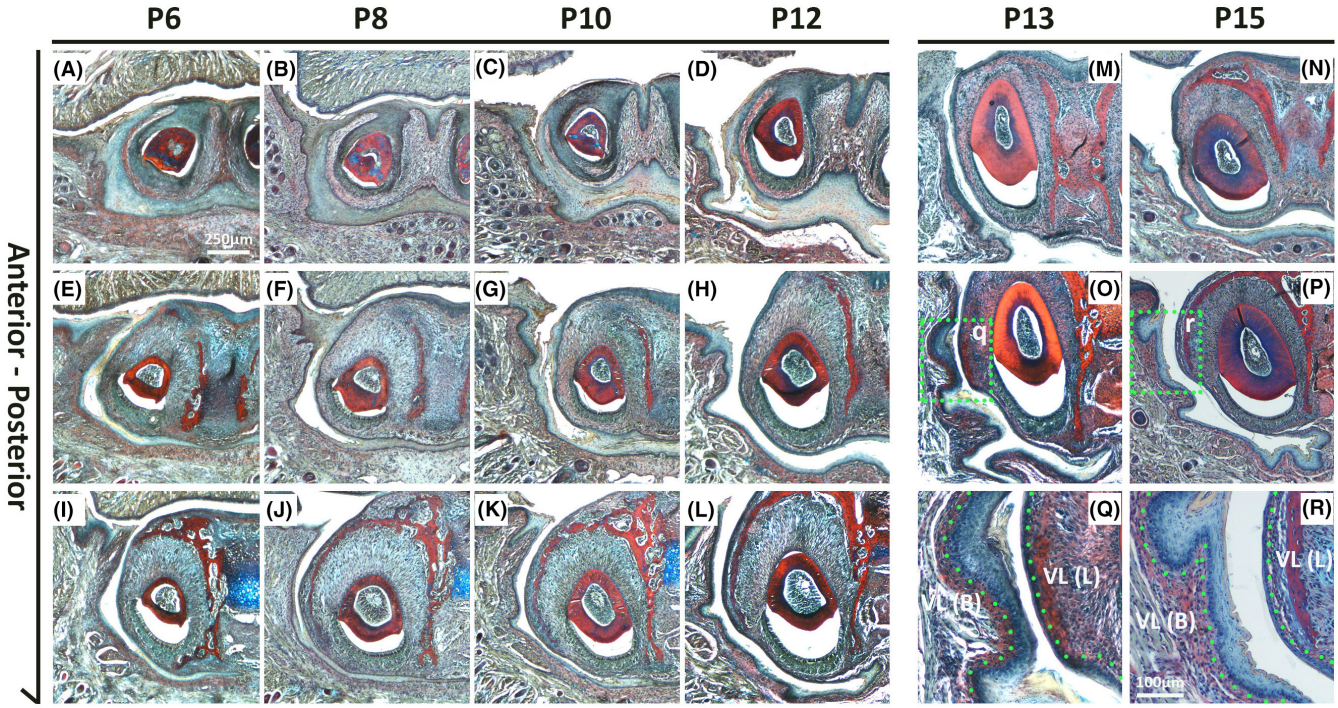

FIGURE 3 Opening of the VL postnatally to create the vestibule. (A–R) Frontal sections of lower jaw in wildtype (WT) mouse embryos stained with trichrome. (A, E, I) Postnatal day (P)6, (B, F, J) P8, (C, G, K) P10, (D, H, L) P12, (M, O, Q) P13, (N, P, R) P15. Anterior end of the VL around the incisors (A–D, M, N), Mid anterior region (E–H, O, P), posterior region (I–L). (Q, R) Higher power view of boxes in O, P to show differences in epithelial thickness on the buccal and lingual sides of the vestibule. Scale bar in (A) = 250 µm, same scale in B–P. Scale bar in (Q, R) = 100 µm. VL, vestibular lamina; VL (B), Buccal VL; VL (L), lingual VL

role in broadening the VL furrow but not in initial fissure formation, although localized cellular atrophy has been thought as the cause of the split in some research (Bolk, 1921; West, 1924). At early embryonic stages of development only scattered apoptotic bodies were observed in the vole VL (Witter et al., 2005). To clarify the mechanisms in the mouse, apoptosis was studied from P0 to P4 using activated caspase 3 as a marker. At P0, prior to opening, a few apoptotic cells were localised to the VL. In the main body of the VL, positive cells were scattered in the epithelium (Figure 4G), while at the tip of the VL many of the epithelial cells were positive (Figure 4K). In contrast, at P4 no apoptotic cells were observed in the VL, despite the presence of caspase-positive cells in adjacent tissues (Figure 4M–P). Apoptosis was not associated with the formation of holes in the VL and did not appear to be a central driver for opening. As previously observed by histology, the tip of the VL does not open until P10 (Figure 3). The cells undergoing apoptosis in this region at P0 are, therefore, unlikely to have a role in opening of the VL, and instead may play a role in thinning of the epithelium in this region.

3.5 | Terminal differentiation may trigger opening of the VL

The changes in Ecad expression prior to opening suggested changes in cell adhesion might be driving the opening process. In human embryos formation of fissures with the VL was linked to the onset of differentiation (Qiu et al., 2020). The identity of the central cells in the VL was therefore followed from P0 to P4 by immuno for occludin and loricrin. Occludin is an integral membrane protein identified at the tight junction and is used as a marker of the granular layer (Zihni et al., 2016). Loricrin is a terminal differentiation marker labelling the cornified layer of the skin (Ishitsuka & Roop, 2020; Koster & Roop, 2004). At P0, prior to any signs of opening, occludin and loricrin were restricted to the top of the VL, where the VL met the oral surface (Figure 5B,C). At P4, the open VL near the oral surface was lined by occludin-positive cells, which formed a layer over the Ecad-positive VL epithelium (Figure 5I,J). Further down the lamina, where the VL had yet to fully open, a similar arrangement was observed with Ecad outer cells flanking occludin positive inner cells around the forming holes (Figure 5E,F) and near to open regions (Figure 5K). The central (suprabasal) cells close to the oral surface were positive for the terminal marker loricrin (Figure 5G,H). During skin development, the skin undergoes terminal differentiation and cornification, a form of cell death (Eckhart et al., 2013). Cornification does not involve caspase 3, but other caspases such as caspase 14 are involved (Lippens et al., 2000). During terminal keratinocyte differentiation, the nuclei become flattened before nuclei degeneration (Eckhart et al., 2013). Interestingly, the nuclei in the centre of the VL had a distinctive flattened appearance, when compared to the rounded cells observed in the basal layers (Figure 5L). Loss of Ecadherin and the onset of occludin and loricrin, therefore, predated opening of the VL, with opening potentially linked to a process of cornification.

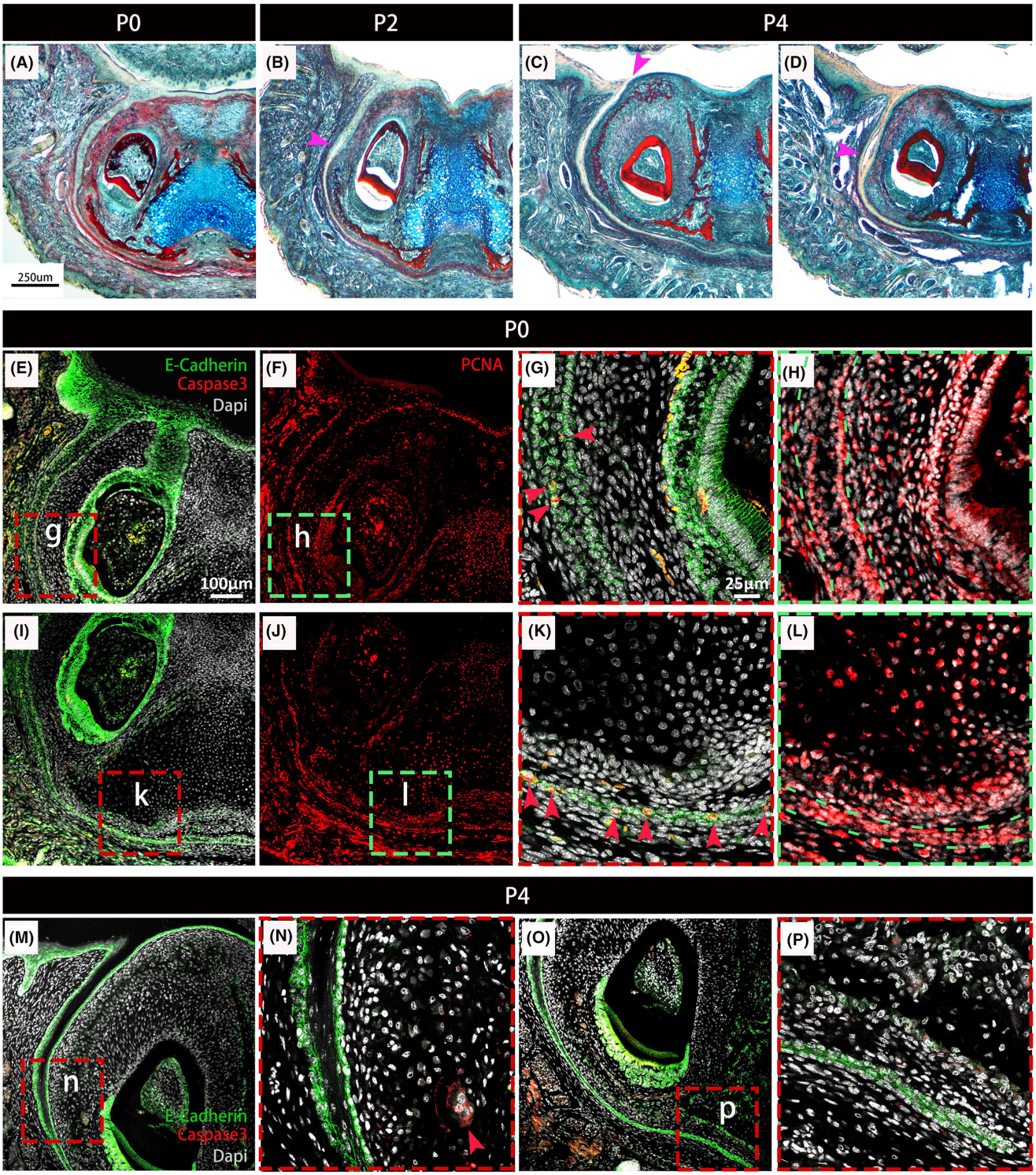

FIGURE 4 Apoptotic cells are not associated with cell clearance during VL opening. (A–D) Trichrome staining of the VL in the anterior lower jaw at P0, P2 and P4. Mouse frontal sections. C is more posterior than D, images taken from within the same mouse. (B) P2. Small holes form in the VL by P2, magenta arrowhead. (C, D) Fissures form in the VL by P4 (Magenta arrowheads), (C) forming from the oral surface, (D) forming as holes within the lamina. (E, G, I, K, M–P) Activated Caspase-3 (red), E-cadherin (green) and Dapi (grey) at P0 (E, G, I, K) and P4 (M–P) in the anterior VL in the murine mandible. (G, K) are higher magnifications of boxes (g, k) in (E, I). (F, H, J, L) PCNA (red) labels proliferating cells in the VL at P0. (H, L) are higher magnifications of boxes (h, l) in (F, J). Green dashes outline VL. (H) In the upper part of the VL PCNA cells are restricted to the basal cell layer L. (L) The lower VL is highly proliferative. A number of caspase3-positive cells were found in the lower 2/3 of the VL (G), with high levels of positive cells at the end of the VL (K) at P0, at which point no obvious fissures were observed. At P4 no caspase3-positive cells were observed throughout the whole lower VL, with only few in the mesenchyme on the lingual side of the VL (N). Red arrowheads indicate caspase3-positive cells. Scale bar in (A) = 250 μm, same scale in B–D. Scale Bar in (E) = 100 μm, same scale in F, I, J, M, O. Scale Bar in (G) = 25 μm, same scale in H, K, L, N, P. VL, vestibular lamina

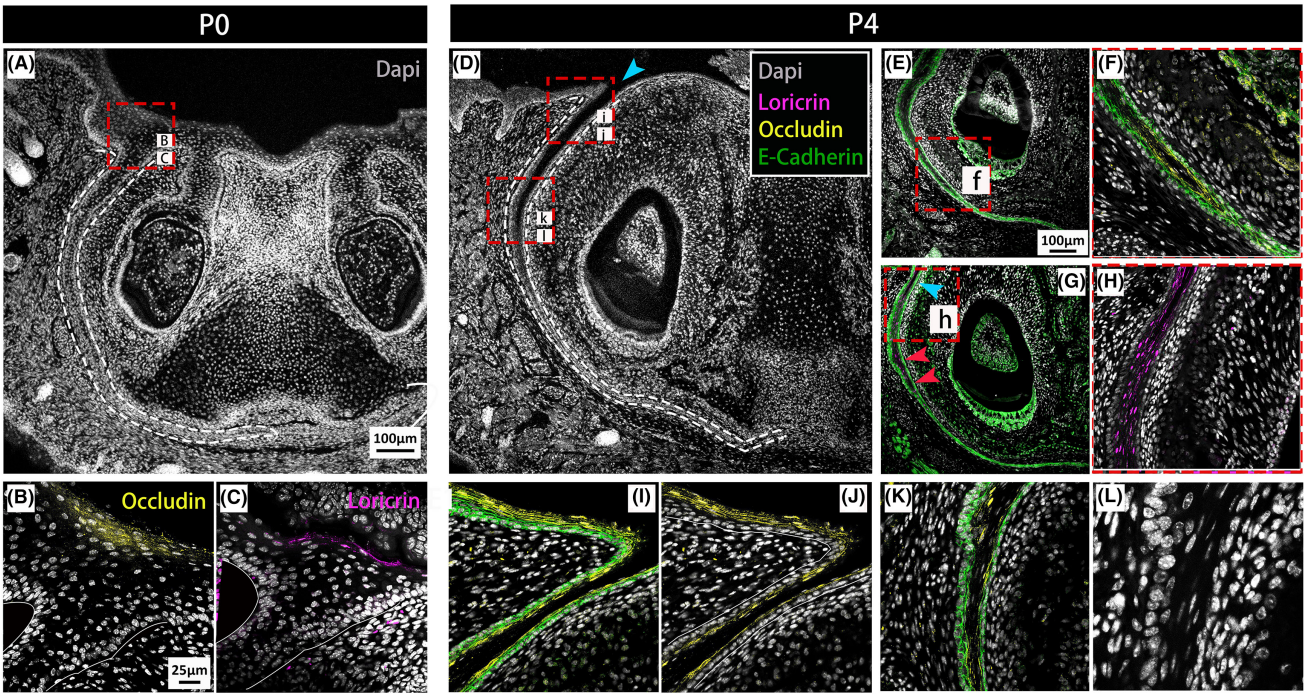

FIGURE 5 Opening of the VL postnatally is associated with terminal differentiation. (A–L) IF for DAPI (grey), Loricrin (magenta), E-cadherin (green), occludin (yellow). (A–C) P0. (A) Anterior VL at P0. (B, C) Higher-power magnification of the oral surface of the VL; occludin and loricrin are expressed in the granular layer and cornified layer, respectively. (D–L) P4. (D) Anterior VL at P4. (E, F, G, I, K) E-cadherin labels the VL and incisor epithelium. Occludin-positive cells surround a small opening within the middle of the VL (E, F, K) and line the opening VL at the top of the VL (I, J). (F) is a higher magnification of (f) in (E). (G, H) Loricrin-positive cells were found in the suprabasal layer prior to opening. (H) is a higher magnification of (h) in (G); (L) highlights the deformation of the nuclei as they flatten in the centre of the VL; cyan arrowheads in (D) point to the main large furrow of the VL, and red arrowheads in (G) indicate small openings separate from the main fissure. Cyan arrows in (G) indicate the area with the main fissure. White dashed lines in (A, D) delineate the VL. Scale bar in (A) = 100 μm, same scale in D. Scales bar in (E) = 100 μm, same scale in F. Scale bar in (B) = 25 μm, same scale in C, F, H, K

4 | DISCUSSION

4.1 | Species-specific differences in VL morphology require distinct mechanisms for vestibule formation

The mouse VL was very different in morphology when compared to the human VL. The human VL was much wider, relatively, with the DL physically attached to it via epithelial bridges throughout the mouth (Qiu et al., 2020) (Figure S1). In contrast, the murine VL was very thin and only prominent in the anterior part of the lower jaw. The murine VL and DL, despite sharing an early common origin in the anterior region (Hovorakova et al., 2016), developed at a distance from each other, with separate connections to the oral cavity. Anteriorly, the murine VL extended much further into the oral cavity than the human VL, with the result that the murine vestibule around the lower incisors would be much deeper than in humans. In contrast, the murine upper incisors were associated with only a rudimentary VL and, therefore, would have a very shallow vestibule on the upper jaw. Such differences are likely to reflect differences in diet and manner of eating.

The different morphologies of the VL resulted in different mechanisms of opening. In human embryos, fissures developed in the wide VL as the epithelial cells underwent differentiation, with the central tissue removed by apoptosis (Qiu et al., 2020). In contrast, the suprabasal cells in the thin murine VL did not appear to be removed by apoptosis but underwent terminal differentiation and possible cornification.

In human embryos, the fissures formed from the oral surface (Figure S1), while in the mouse, there was a combination of splitting of the VL near the oral surface and the formation of small holes along the length of the VL. This process of cavitation therefore shares some similarities with salivary gland lumen formation, where the ducts open by the coalescence of multiple small cavities (Tucker, 2007). The vestibule was completely open by postnatal day 13 to 15, which corresponds to the eruption of the dentition (first molar erupts at P15) and the move to a solid diet (Chlastakova et al., 2011). An incomplete vestibule, therefore, is not a problem for suckling in the first 2 weeks after birth. The differences and similarities in VL and DL formation in mouse and human are highlighted in Figure 6.

4.2 | Lingual-labial differences in the VL are evident from early stages of development

During growth of the murine VL proliferation was observed asymmetrically in the basal epithelial layer, so that more cells were positive

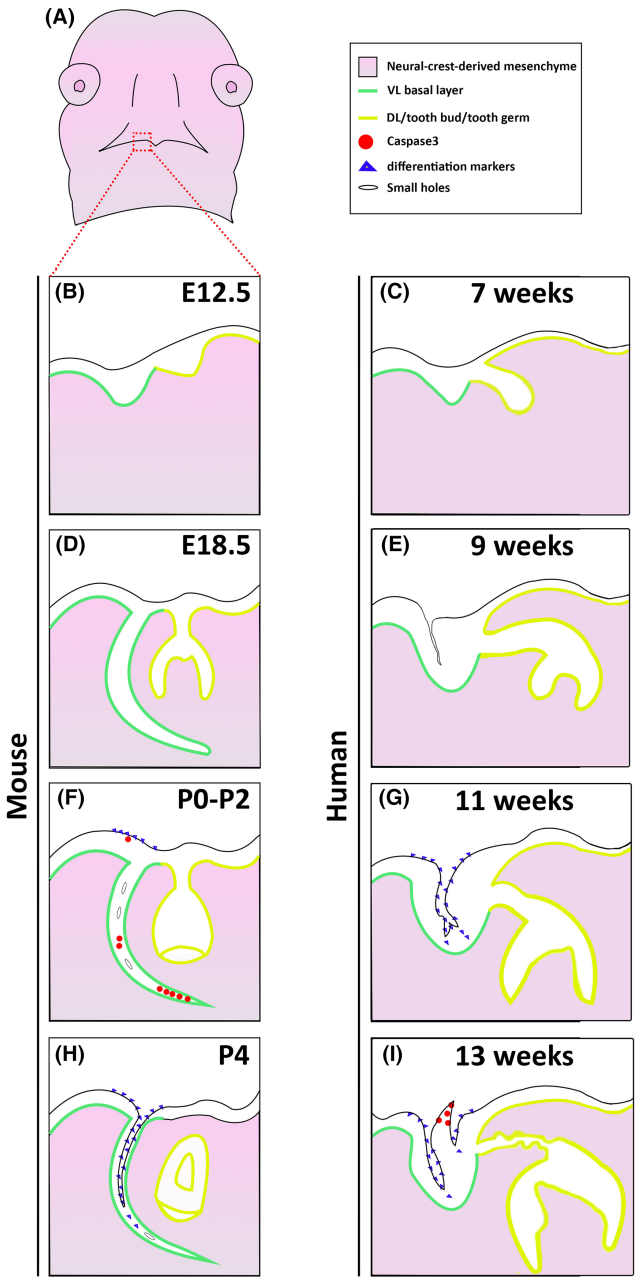

FIGURE 6 Comparison of vestibular lamina (VL) development and opening in human and mouse development. (A) Schematic of developing face highlighting area shown in B-I. (B, D, F, H) Mouse incisor and VL. (C, E, G, I) Human incisor and VL. (B) E(embryonic day) 12.5. (D) E18.5, (F) P (postnatal day) 0-2, (H) P4. (C) 7 weeks gestation, (E) 9 weeks, (G) 11 weeks, (J) 13 weeks

on the labial/buccal side. This is predicted to cause a bend in the developing lamina, directing it under the forming tooth germ, so that the vestibule forms under the incisors. This difference in proliferation may also explain the observed asymmetrical split when the VL opened, with the labial side being much thicker. Due to these differences, the resulting mucosa of the oral cavity is therefore different on the side of the teeth and towards the cheeks. Such differences in thickness of the mucosa may result in differences in robustness, with the cheeks having more layers to counter the forces of chewing. Similar differences between the labial and lingual sides of the lamina were observed in human embryos (Qiu et al., 2020), with differences in keratin patterns on either side of the vestibule maintained in adult tissues (Verlach et al., 2017), suggesting this is a conserved mechanism.

4.3 | Apoptosis and differentiation play distinct roles in VL development

The presence of activated caspase 3-positive cells was not associated with opening of the murine VL at postnatal stages, however, large numbers of apoptotic cells were associated with the bottom third of the VL. These cells undergoing apoptosis were observed over a week before opening of this region and it is proposed that they have a role in thinning, rather than splitting of the VL. This may make later opening of the deep parts of the lamina easier. Opening was associated with loss of Ecadherin, reduced proliferation and upregulation of differentiation markers in the suprabasal layers of the VL. Occludin, as a functional component of tight junctions, marks the granular layer and turns off in the skin to allow shedding of the top layers (Zihni et al., 2016). Similarly, occludin turned off in the middle layers of the murine VL, as loricrin turned on, suggesting a change in cell adhesion. The loricrin expressing suprabasal cells had flattened nuclei, distinct from the rounder Ecad expressing basal cells. This change in cell morphology predated splitting of the VL. A similar change in cell morphology and upregulation of loricrin has been shown in the developing ear canal, another epithelial structure that goes from a solid lamina to an open tube (Fons et al., 2020). Terminal differentiation is therefore potentially a conserved mechanism to open epithelial tubes/laminae. The flattening of the nuclei may suggest that the canal opens due to cornification, with loss of adhesion and epithelial shedding, similar to the process observed in the skin. Cell death mechanisms, other than apoptosis, may therefore regulate this process (Eckhart et al., 2013). It would be interesting to identify whether markers associated with cornification, such as Caspase 14 were upregulated in these cells. Alternatively, the VL may open due to a loss of adhesion between the terminally differentiating cells without cell death. In the human VL, the upregulation of filigrin around the forming fissures suggests that downregulation of tight junctions might cause breaks to form within the epithelium. The murine VL showed upregulation of the terminal marker loricrin postnatally. Interestingly, in the adult oral cavity loricrin has been observed in the palatal but not the buccal epithelium (Ishitsuka & Roop, 2020), suggesting that after opening the loricrin population may not persist. Defects in the extension of the VL or opening of the deepest parts of the VL would be predicted to lead to the formation of a shallow vestibule. Likewise, incomplete separation along the VL could result in the formation of additional frenula, tethering the teeth to the cheeks and lips.

Overall, this paper has shed light on the development of a neglected structure that has an important role in creating the oral

cavity. Here we provide an understanding of the timing of development and mechanisms of murine vestibule formation that can be used to understand defects associated with this region.

ACKNOWLEDGEMENT

Thanks to Maria Hovorakova for discussions on VL development. Thanks to the Human Developmental Biology Resource for human embryonic and fetal tissue used in Supplementary Figure 1.

AUTHOR CONTRIBUTIONS

Abigail S. Tucker conceived the idea. Tengyang Qiu performed the histology and immunohistochemistry and explant culture experiments. Abigail S. Tucker and Tengyang Qiu wrote the manuscript. All authors contributed to the article and approved the submitted version.

FUNDING INFORMATION

This work was supported by the Grant Agency of the Czech Republic (18-04859S to AT). TQ was funded by the China Scholarship Council as part of a PhD studentship at KCL.

CONFLICT OF INTEREST

Abigail Tucker is a member of the Anatomical Society council, and sits on the editorial board of the Journal of Anatomy.

DATA AVAILABILITY STATEMENT

The data that support the findings of this study are shown here and are available from the corresponding author upon request.

ORCID

Abigail S. Tucker https://orcid.org/0000-0001-8871-6094

REFERENCES

Alfaqeeh, S.A. & Tucker, A.S. (2013) The slice culture method for following development of tooth germs in explant culture. *Journal of Visualized Experiments*, 81, e50824.

Bolk, L. (1921) Odontological essays. *Journal of Anatomy*, 55, 219–234.

Chlastakova, I., Lungova, V., Wells, K., Tucker, A.S., Radlanski, R.J., Misek, I. et al. (2011) Morphogenesis and bone integration of the mouse mandibular third molar. *European Journal of Oral Sciences*, 119, 265–274.

Eckhart, L., Lippens, S., Tschachler, E. & Declercq, W. (2013) Cell death by cornification. *Biochimica et Biophysica Acta*, 1833, 3471–3480.

Fons, J.M., Mozaffari, M., Malik, D., Marshall, A.R., Connor, S., Greene, N.D.E. et al. (2020) Epithelial dynamics shed light on the mechanisms underlying ear canal defects. *Development*, 147, dev194654.

Hovorakova, M., Lesot, H., Peterka, M. & Peterkova, R. (2005) The developmental relationship between the deciduous dentition and the oral vestibule in human embryos. *Anatomy and Embryology*, 209, 303–313.

Hovorakova, M., Lesot, H., Vonesch, J.L., Peterka, M. & Peterkova, R. (2007) Early development of the lower deciduous dentition and oral vestibule in human embryos. *European Journal of Oral Sciences*, 115, 280–287.

Hovorakova, M., Lochovska, K., Zahradnicek, O., Domonkosova Tibenska, K., Dornhoferova, M., Horakova-Smrckova, L. et al. (2016) One odontogenic cell-population contributes to the development of the mouse incisors and of the Oral vestibule. *PLoS One*, 11, e0162523.

Hovorakova, M., Prochazka, J., Lesot, H., Smrckova, L., Churava, S., Boran, T. et al. (2011) Shh expression in a rudimentary tooth offers new insights into development of the mouse incisor. *Journal of Experimental Zoology. Part B, Molecular and Developmental Evolution*, 316, 347–358.

Hovorakova, M., Zahradnicek, O., Bartos, M., Hurnik, P., Stransky, J., Stembirek, J. et al. (2020) Reawakening of ancestral dental potential as a mechanism to explain dental pathologies. *Integrative and Comparative Biology*, 60, 619–629.

Ishitsuka, Y. & Roop, D.R. (2020) Loricrin: past, present, and future. *International Journal of Molecular Sciences*, 21, 2271.

Kantaputra, P.N., Wangtiraumnuay, N., Ngamphiw, C., Olsen, B., Intachai, W., Tucker, A.S. et al. (2022) Cryptophthalmos, dental anomalies, oral vestibule defect, and a novel Frem2 mutation. *Journal of Human Genetics*, 67, 115–118.

Koster, M.I. & Roop, D.R. (2004) Genetic pathways required for epidermal morphogenesis. *European Journal of Cell Biology*, 83, 625–629.

Kus-Bartoszek, A., Lipski, M., Jarzabek, A., Manowiec, J. & Drozdzik, A. (2022) Gingival phenotype changes and the prevalence of mucogingival deformities during the early transitional dentition phase-a two-year longitudinal study. *International Journal of Environmental Research and Public Health*, 19, 3899.

Lippens, S., Kockx, M., Knaapen, M., Mortier, L., Polakowska, R., Verheyen, A. et al. (2000) Epidermal differentiation does not involve the pro-apoptotic executioner caspases, but is associated with caspase-14 induction and processing. *Cell Death and Differentiation*, 7, 1218–1224.

Nakatomi, M., Hovorakova, M., Gritli-Linde, A., Blair, H.J., Macarthur, K., Peterka, M. et al. (2013) Evc regulates a symmetrical response to shh signaling in molar development. *Journal of Dental Research*, 92, 222–228.

Pavlikova, H., Witter, K. & Misek, I. (1999) Primordium of the upper vestibulum oris in the domestic sheep. *Acta Veterinaria Brno*, 68, 175–178.

Peterkova, R. (1985) The common developmental origin and phylogenetic aspects of teeth, rugae palatinae, and fornix vestibuli oris in the mouse. *Journal of Craniofacial Genetics and Developmental Biology*, 5, 89–104.

Placek, M., Mskach, M. & Mrklas, L. (1974) Significance of the labial frenum attachment in periodontal disease in man. Part 1. Classification and epidemiology of the labial frenum attachment. *Journal Periodontology*, 45, 891–894.

Popa, E.M., Buchtova, M. & Tucker, A.S. (2019) Revitalising the rudimentary replacement dentition in the mouse. *Development*, 146, dev171363.

Qiu, T., Teshima, T.H.N., Hovorakova, M. & Tucker, A.S. (2020) Development of the vestibular lamina in human embryos: morphogenesis and vestibule formation. *Frontiers in Physiology*, 11, 753.

Roubicek, M. & Spranger, J. (1984) Weyers acrodental dysostosis in a family. *Clinical Genetics*, 26, 587–590.

Sasalawad, S.S., Hugar, S.M., Poonacha, K.S. & Mallikarjuna, R. (2013) Ellis-van Creveld syndrome. *BMJ Case Reports*, 2013, bcr2013009463.

Schour, I. (1929) Early human tooth development, with special reference to the relationship between the dental lamina and the lip-furrow band. *Journal Dental Research*, 9, 699–717.

Tucker, A.S. (2007) Salivary gland development. *Seminars in Cell & Developmental Biology*, 18, 237–244.

Verlach, J., Flotan, R., Vlk, M., Szabo, P. & Smetana, K. (2017) Phenotypic chacterisation of oral mucosa: what is normal? *Journal of Oral Pathology & Medicine*, 46, 834–839.

Wang, X.P., O'connell, D.J., Lund, J.J., Saadi, I., Kuraguchi, M., Turbe-Doan, A. et al. (2009) Apc inhibition of Wnt signaling regulates supernumerary tooth formation during embryogenesis and throughout adulthood. *Development*, 136, 1939–1949.

West, C.M. (1924) The development of the gums and their relationship to the deciduous teeth in the human fetus. *Contributions to Embryology*, 16, 25–45.

Witter, K., Pavlikova, H., Matulova, P. & Misek, I. (2005) Relationship between vestibular lamina, dental lamina, and the developing oral vestibule in the upper jaw of the field vole (*Microtus agrestis*, Rodentia). *Journal of Morphology*, 265, 264–270.

Ye, Q., Bhojwani, A. & Hu, J.K. (2022) Understanding the development of oral epithelial organs through single cell transcriptomic analysis. *Development*, 149, dev200539.

Zihni, C., Mills, C., Matter, K. & Balda, M.S. (2016) Tight junctions: from simple barriers to multifunctional molecular gates. *Nature Reviews. Molecular Cell Biology*, 17, 564–580.

SUPPORTING INFORMATION

Additional supporting information can be found online in the Supporting Information section at the end of this article.

How to cite this article: Qiu, T. & Tucker, A.S. (2022) Mechanisms driving vestibular lamina formation and opening in the mouse. *Journal of Anatomy*, 00, 1–11. Available from: https://doi.org/10.1111/joa.13771

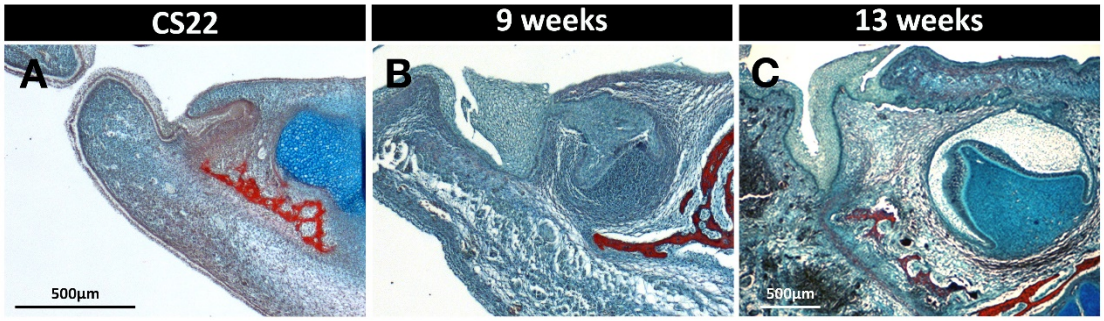

Fig S1. **The DL extends from the VL in the lower jaw in human embryos**. Trichrome staining (Alcian blue, Alizarin red, and haematoxylin) of human frontal sections at CS22(**A**), 9 weeks (**B**), and 13 week (**C**). Scale bar in (A-C) = 500 µm.

Chapter 5 – (Publication 3) Molecular profiling of the vestibular lamina highlights a key role for Hedgehog signalling

(Development, 2023)

Tengyang Qiu[1,2], Barbora Hutečková[3,4], Maisa Seppala[1,5], Martyn T. Cobourne[1,5], Zhi Chen[2], Mária Hovořáková[6], Marcela Buchtová[3,4] and Abigail S. Tucker[1,6,*]

Aim: To investigate the development of the VL in *Gas1* and compound mutants and explore the role of Shh signalling in the VL and DL.

My contributions: I performed the RNA-Seq analysis based on the raw sequencing data, statistical analysis, explant culture (20μM), RNA-Scope in both the manuscript and supplementary materials (*Gli1* expression in the *Gas1* mutants and littermate controls), histology (except the *Gas1* compound mutants, I analysed the slides with Prof. Abigail Tucker), immunohistochemistry, validation of the molecular signature of the murine VL at E14.5 using the Genepaint, I analysed the slides of Radioactive *in situ* hybridization with Prof. Abigail Tucker. I created all the figures in both the manuscript and supplementary materials. I wrote the original manuscript (including supplementary materials) and contributes to the editing of the manuscript and supplementary materials. I uploaded the RNA-Seq data to the Facebase with Prof. Abigail Tucker.

Abstract:

The vestibular lamina (VL) forms the oral vestibule, establishing a distinct space between the teeth, lips, and cheeks. In a number of ciliopathies, the formation of the vestibule is impaired, resulting in the occurrence of multiple frenula. Unlike the adjacent dental lamina, there is a lack of comprehensive knowledge regarding the genes that pattern the VL. In this study, we established a molecular profile for the VL in mice and identified a number of genes and signaling pathways that potentially contribute to its development. Among these pathways, the Sonic hedgehog (Shh) pathway and Wnt signaling pathway are specifically emphasized, and their interaction has been validated through protein-protein interaction (PPI) analysis. In relation to the Shh pathway, we demonstrated the robust expression of co-receptors *Gas1*, *Cdon*, and *Boc* in the VL. Our findings indicated that these co-receptors function to enhance the Shh signals from the developing incisor. *Gas1* mutants displayed a truncated VL, along with the altered *Gli1* expression and decreased proliferation. The severity of this defect was further amplified in *Boc/Gas1* double mutant mice, and a similar phenotype could be reproduced in culture by using cyclopamine. Therefore, signals originating from the developing tooth play a crucial role in regulating the development of neighbouring VL, orchestrating the overall development of the dentition and the oral cavity.

© 2023. Published by The Company of Biologists Ltd | Development (2023) 150, dev201464. doi:10.1242/dev.201464

RESEARCH ARTICLE

Molecular profiling of the vestibular lamina highlights a key role for Hedgehog signalling

Tengyang Qiu[1,2], Barbora Hutečková[3,4], Maisa Seppala[1,5], Martyn T. Cobourne[1,5], Zhi Chen[2], Mária Hovořáková[6], Marcela Buchtová[3,4] and Abigail S. Tucker[1,6,*]

ABSTRACT

The vestibular lamina (VL) forms the oral vestibule, creating a gap between the teeth, lips and cheeks. In a number of ciliopathies, formation of the vestibule is defective, leading to the creation of multiple frenula. In contrast to the neighbouring dental lamina, which forms the teeth, little is known about the genes that pattern the VL. Here, we establish a molecular signature for the usually non-odontogenic VL in mice and highlight several genes and signalling pathways that may play a role in its development. For one of these, the Sonic hedgehog (Shh) pathway, we show that co-receptors *Gas1*, *Cdon* and *Boc* are highly expressed in the VL and act to enhance the Shh signal from the forming incisor region. In *Gas1* mutant mice, expression of *Gli1* was disrupted and the VL epithelium failed to extend due to a loss of proliferation. This defect was exacerbated in *Boc*/*Gas1* double mutants and could be phenocopied using cyclopamine in culture. Signals from the forming teeth, therefore, control development of the VL, coordinating the development of the dentition and the oral cavity.

KEY WORDS: Vestibular lamina, Oral cavity, Sonic hedgehog, Gas1, Dental lamina, Ciliopathies, Mouse

INTRODUCTION

Odontogenesis proceeds through a series of characteristic stages, which are controlled by multiple molecular interactions between the epithelium and underlying mesenchyme. In mammals, the first sign of tooth development is the appearance of a band of thickened epithelium marked by the expression of *Pitx2* and *Shh* (Yu et al., 2020) This band goes on to form the dental lamina (DL), from which the tooth germs will emerge. Lateral to the DL is a second epithelial lamina, known as the vestibular lamina (VL) in mammals. In humans, the VL and DL have a complex relationship during early development, with the two laminas merging and branching as they run along the jaw margin (Hovorakova et al., 2005; 2007). In the anterior parts of the lower jaw, the DL and VL share a common origin, emerging from the same Shh-positive epithelial thickening in both mouse and human (Hovorakova et al., 2007, 2016; Qiu et al., 2020). As these structures diverge in development, Shh signalling is associated with the forming tooth germ, but turns off in the VL (Hovorakova et al., 2016). While the DL produces the teeth, the VL splits down the middle to form a space between the teeth and lips and teeth and cheeks, thereby creating the vestibule of the oral cavity. Given this role, the VL is also known as the labio-gingival ridge, lip-furrow band or cheek furrow ridge (Bolk, 1921; Schour, 1929; Peterková, 1985). During development, the lingual (tongue side) and buccal/labial (cheek/lip) sides of the VL are distinct in both mouse and human, with differences in rates of proliferation and expression of epithelial markers (Qiu et al., 2020; Qiu and Tucker, 2022). These differences may influence the opening of the lamina and they are later reflected by differences in molecular identity of the different parts of the oral mucosa.

The developing mammalian VL has a varied structure across mammals. In human and sheep, the VL is in general thick and wide, whereas in the vole and mouse, the VL is relatively thin and narrow (Pavlikova et al., 1999; Witter et al., 2005; Hovorakova et al., 2005, 2016; Qiu et al., 2020; Qiu and Tucker, 2022). The human VL is prominent throughout the upper and lower jaws and regionalized in parallel with the DL (Hovorakova et al., 2005, 2007). In contrast, the mouse only has a prominent VL in the anterior mandible, and the maxillary VL is almost absent (Qiu and Tucker, 2022). The relationship of the DL and VL also varies, with the DL branching off the VL in humans, while in mice both the DL and VL have a separate connection to the oral cavity. These differences are likely to correspond to the different morphologies of the vestibule and reflect differences in diet and chewing patterns.

A similar laterally situated lamina is also observed in reptiles. This lamina also appears to share a common origin with the adjacent DL. In the chameleon, this more lateral lamina develops into the dental glands that lubricate the teeth, while in poisonous snakes it forms the venom gland (Vonk et al., 2008; Tucker, 2010). It has been suggested that the mammalian VL and the reptilian dental gland lamina have evolved from laterally positioned DLs, similar to those that create the inner and outer dental arches in extant axolotls (Soukup et al., 2021) As the dentition became restricted to a single row of teeth in many tetrapods, the redundant DLs would have been lost or, in the case of the dental glands and VL, repurposed to create other ectodermal structures (Hovorakova et al., 2020).

Despite its shared origin with the DL, the VL does not normally form teeth. However, overexpression of Wnt signalling in the VL does lead to ectopic tooth formation in this structure in mice (Wang et al., 2009; Popa et al., 2019) and may explain the occasional occurrence of odontomas situated in the vestibule of human subjects (Hovorakova et al., 2020). Vestibular deficiencies have been

[1]Centre for Craniofacial & Regenerative Biology, Faculty of Dentistry, Oral & Craniofacial Sciences, King's College London, London, SE1 9RT United Kingdom. [2]The State Key Laboratory Breeding Base of Basic Science of Stomatology & Key Laboratory of Oral Biomedicine, Ministry of Education (Hubei-MOST KLOS & KLOBM), School and Hospital of Stomatology, Wuhan University, 430079 Wuhan, China. [3]Department of Experimental Biology, Faculty of Science, Masaryk University, 625 00 Brno, Czech Republic. [4]Laboratory of Molecular Morphogenesis, Institute of Animal Physiology and Genetics, Czech Academy of Sciences, 602 00 Brno, Czech Republic. [5]Department of Orthodontics, Faculty of Dentistry, Oral & Craniofacial Sciences, King's College London, London, SE1 9RT UK. [6]Institute of Histology and Embryology, First Faculty of Medicine, Charles University, Albertov 4, 128 00 Praha 2, Czech Republic.

*Author for correspondence (abigail.tucker@kcl.ac.uk)

M.T.C., 0000-0003-2857-0315; M.B., 0000-0002-0262-6774; A.S.T., 0000-0001-8871-6094

Handling Editor: Liz Robertson
Received 20 November 2022; Accepted 13 March 2023

Development (2023) 150, dev201464. doi:10.1242/dev.201464

reported in a number of human syndromes; in particular, in the ciliopathy Ellis-van Creveld (EvC) (MIM #225500), where development of the VL is defective, and the gums adhere to the upper lip and cheek with multiple associated frenula (Sasalawad et al., 2013). Recently, VL anomalies along with tooth abnormalities have also been observed in a patient with cryptophthalmos (MIM #123570) due to mutation in the *FREM2* gene (Kantaputra et al., 2022). In addition, a shallow (<4 mm) vestibule and frenula anomalies in the lower incisor region have been noted in a study of gingival phenotypes in healthy children (Kus-Bartoszek et al., 2022). Such deficiencies in frenulum attachment were suggested to be associated with certain periodontal diseases (Placek et al., 1974).

The stages of development of the VL have recently been characterized in mouse and human, with an analysis of proliferation, cell death and epithelial differentiation (Qiu and Tucker, 2022); however, no other data is available regarding the genes involved in shaping and directing the development of this structure. In addition, although the VL and the dentition share a common origin, whether these tissues interact during later development to coordinate oral development is unknown. To address this, a transcriptome of the murine VL at embryonic day (E) 14 was created to identify the molecular signature of this structure and compare it with the neighbouring cap stage incisor tooth germ. This allowed a comparison of odontogenetic and non-odontogenic tissue and identification of genes unique to the VL. At E14, the VL has extended into the lower jaw as a sheet of epithelium with higher proliferation on the labial and buccal sides away from the developing teeth (Qiu and Tucker, 2022). This suggested potential interactions between the tooth and VL. We, therefore, used the transcriptomic dataset to focus on signalling molecules expressed in the tooth and readouts in the VL to further understand how the two tissues might interact. Mouse mutants and explant culture were then used to test the function of identified pathways.

From this analysis, we identified previously unreported markers associated with the VL and highlighted Hedgehog (Hh) signalling from the developing tooth as playing a potential role in patterning the VL during development. Functional studies confirmed the role of Hh signalling in patterning the VL and demonstrated that signals from the tooth have a key role in orchestrating development of neighbouring structures, coordinating development of the teeth and the oral cavity.

RESULTS

A distinct molecular signature for the vestibular lamina at E14

The VL has odontogenic potential but does not normally form teeth (Popa et al., 2019). To identify the molecular signatures that distinguish the VL from the early tooth bud (TB) during development, we dissected the VL and TB from the incisor region of the murine mandible at E14 for analysis through bulk RNA-sequencing (RNA-seq) (Fig. 1A). At this stage, the anterior VL and incisor TB have developed their distinct morphologies and are clearly observed in sagittal slices, facilitating precise dissection. However, despite their morphological differences, the VL can still be induced to form tooth-like structures after stabilization of β-catenin at this late stage (Popa et al., 2019). Fate is, therefore, not yet determined in this structure at E14. The epithelium and mesenchyme were dissected together to provide a comprehensive characterization of the whole structure. The RNA-seq dataset included VL (n=5, VL1-5) and TB (n=5, TB1-5) samples, with the boxplot, violin plot and density plot showing consistent distributions of normalized read counts (counts per million; CPM) (Fig. S1A-C). A correlation plot confirmed that there was a higher correlation between the transcriptomic profile of VL-VL and TB-TB compared with TB-VL (Fig. S1D). Levels of vimentin (a general mesenchymal marker) and *Cdh1* (a general epithelial marker) were used to estimate the relative amounts of mesenchymal and epithelial tissue included in the analysis. No significant difference was observed in expression of these two markers between the TB and VL groups, suggesting that the dissected regions contained approximately equivalent numbers of mesenchymal and epithelial cells (Fig. S1E,F). Principal component analysis (PCA) presented distinct gene expression distributions between the VL and TB datasets at E14 (Fig. 1B). In total, 1788 differentially expressed genes (DEGs) were detected, including 788 upregulated (TB) and 1000 downregulated (VL) DEGs. The top DEGs were visualized by a volcano plot, where absolute value of log2 fold change (abs log2FC)>2 and P-value<0.01 (Fig. 1C). The DEGs were highlighted in a heatmap where abs log2FC>2 and P-value<0.001 (Fig. 1D). Overall, these results confirmed that the VL and TB were significantly different at the molecular level by E14. Our large-scale analysis of gene signatures confirmed that genes known to play a role in early tooth development were upregulated in the TB relative to the VL, including *Shh*, Fgfs, *Pax9*, Dlx homeobox gene-family members, *Runx2*, *Rspo1* and *Scube1* (Zhao et al., 2000; Seppala et al., 2007; Xavier et al., 2009; Kawasaki et al., 2014) (Fig. 1C,D), with gene expression patterns confirmed by RNAscope (Fig. S2). In addition, the screen highlighted a number of genes upregulated in the VL relative to the TB (Fig. 1C,D), with expression in the VL again confirmed by RNAscope (Fig. S3), or by checking expression on Genepaint (https://gp3.mpg.de/), a digital atlas highlighting gene expression in the embryo at E14.5 (Fig. S4) (Visel et al., 2004). These included *Meis1*/*2*, *Otx1* and *Nr4a2* transcription factors, and signalling pathway members *Cd44* and *Wnt7b*, which have not previously been associated with the VL. Interestingly, in keeping with the observed lingual-buccal/labial differences in the VL epithelium at this stage (Qiu and Tucker, 2022), some highlighted genes had clear lingual-buccal/labial differences in expression, such as *Otx1*, which was expressed on the labial side of the VL away from the tooth (Fig. S3L′). In addition, differential expression was evident in the oral and aboral parts of the VL, suggesting additional levels of compartmentalization (Fig. S4). Using this data, we were, therefore, able to create the first molecular signature for the VL.

Differential analysis highlights differences in Shh pathway component expression in the VL and TB

To understand how the tooth bud might impact on development of the VL, we focused on signalling pathways highlighted by the transcriptomics. As expected given its conserved role in tooth development, *Shh* was highlighted as differentially expressed in the tooth germ, along with patched 1 (*Ptch1*) and *Gli1* (Fig. 2A,B; Fig. S5A-F) (Buchtová et al., 2008; Seppala et al., 2017). *Ptch1* is a transmembrane domain protein that acts as the principal receptor for Shh, but also provides a readout of Shh signalling activity, whereas *Gli1* acts as a universal downstream transcriptional target. The Shh pathway is activated when *Shh* binds to *Ptch1*, which is facilitated by a number of co-receptors, including growth arrest-specific 1 (*Gas1*) and Ig/fibronectin subfamily transmembrane proteins *Boc* and *Cdon* (*Cdo*) (Tenzen et al., 2006; Seppala et al., 2022). *Gas1* is a vertebrate-specific glycosylphosphatidylinositol-anchored membrane protein proposed to be a co-receptor for Shh and positive regulator of the signal pathway in vertebrates (Martinelli and Fan, 2007; Seppala et al., 2022). In contrast to *Shh* and *Ptch1*, *Gas1*, *Cdon* and *Boc* were all significantly more

Development (2023) 150, dev201464. doi:10.1242/dev.201464

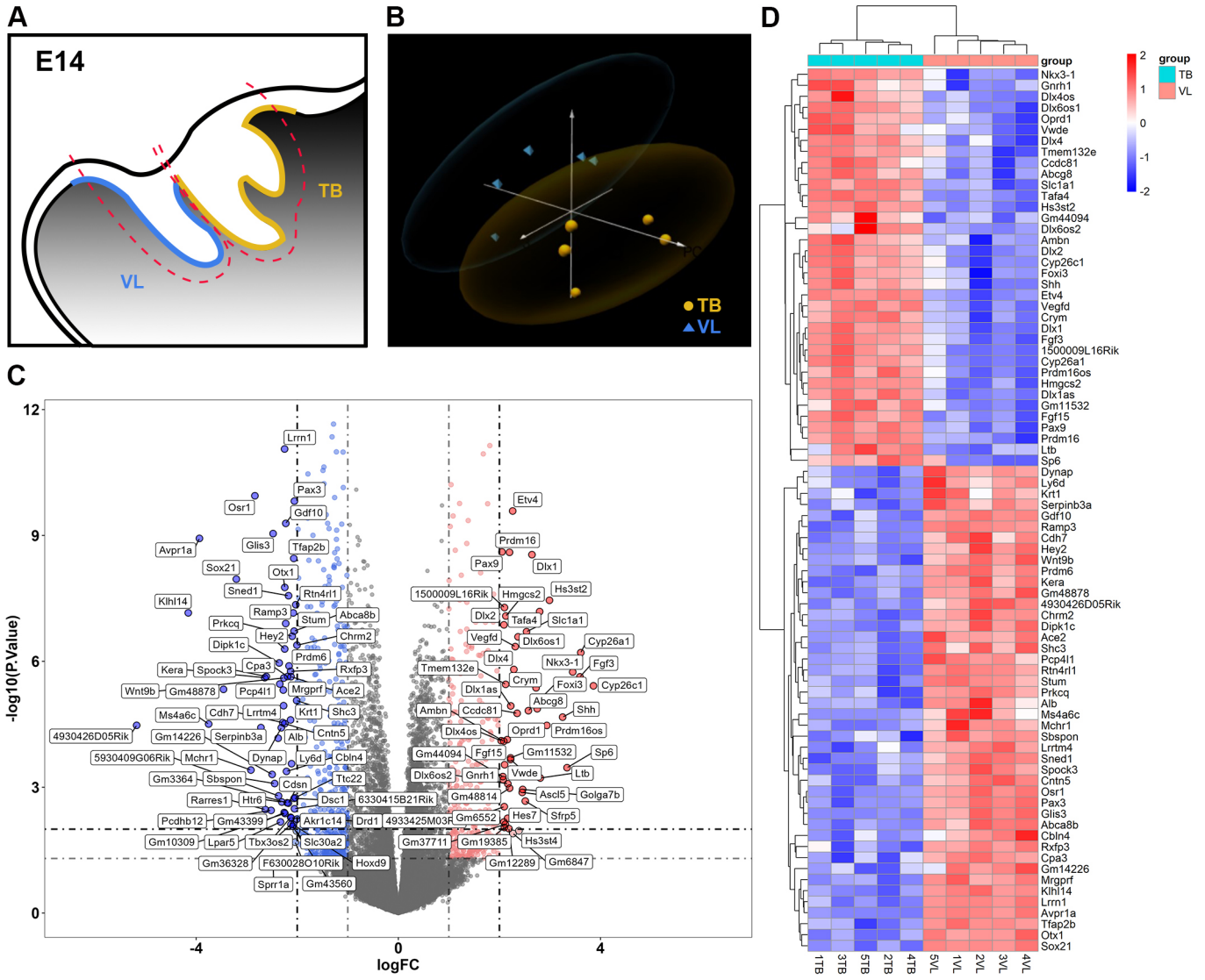

Fig. 1. Distinct gene signatures of the VL and TB at E14 revealed by RNA-seq. (A) Schematic of vestibular lamina (VL) and incisor tooth bud (TB) dissection for RNA-seq. Sagittal view. (B) PCA plot of the RNA-seq dataset for VL and TB samples. Blue and yellow dots represented VL and TB, respectively, in the scatterplot, with the ellipses showing clustering of the samples. Distinct gene expression distributions between the VL and TB were observed. (C) The volcano plot showed a number of upregulated (TB) and downregulated (VL) DEGs. Red represented selected highly expressed genes in TB, whereas blue emphasizes selected highly expressed genes in VL. Abs log2FC_1>1, *P*-value_1<0.05; abs log2FC_2>2, *P*-value_2<0.01. (D) Heatmap of signatures of VL and TB samples. A number of VL and TB markers were identified. Annotations show clustering of the samples. Abs log2FC>2 and *P*-value<0.001. The dissected VL and tooth germs from a single litter (9-15 embryos) were pooled to obtain enough RNA for sequencing. In total, tissue from 11 litters was isolated and pooled samples from five litters with the highest quality scores were used for analysis. These are referred to here as TB1-5 and VL1-5.

highly expressed in the VL (Fig. 2A,B). To further investigate the expression of these Shh pathway-related genes, we compared the expression of *Ptch1*, *Cdon*, *Shh*, *Gas1* and *Boc* in these two laminas at E12.5 (before obvious morphological differences in these structures) and at E15.5 (when the two structures are clearly morphologically distinct) (Fig. 2E-P). The VL runs as a continuous band anteriorly around the incisor tooth germs and, therefore, can be viewed both in sagittal plane for the labial lamina (Fig. 2C) and frontal plane for the buccal lamina (Fig. 2D). At E12.5, the VL (lined by green dashed line) and DL (lined by white dashed line) were evident as two side-by-side epithelial thickenings (Fig. 2E) with *Shh* expression restricted to the DL (Fig. 2H). *Ptch1* was expressed in the epithelium of the VL, DL and strongly in the surrounding mesenchyme (Fig. 2F). In contrast, expression of *Gas1* was mainly observed in the epithelium of the VL and the mesenchyme on the buccal side (Fig. 2I). *Cdon* and *Boc* showed similar expression patterns to *Gas1* (Fig. 2G,J). At E15.5, the VL curves as it extends into the mesenchyme so that it grows under the developing incisors and Meckel's cartilage, while the neighbouring incisor tooth germ has developed from a thickening to reach the late cap stage (Fig. 2K). At this stage, strong transcription of *Shh* was detected in the inner enamel epithelium of the incisors (Seppala et al., 2017); however, the adjacent VL was negative for *Shh* expression (Fig. 2N). *Ptch1* was highly expressed in the developing tooth, in the epithelium and surrounding mesenchyme, but relatively lower *Ptch1* expression was observed in the VL, mainly localized to the lower part of the VL (Fig. 2L). In contrast to the tooth germ-dominant expression of *Shh* and *Ptch1*, *Cdon*, *Gas1* and

Development (2023) 150, dev201464. doi:10.1242/dev.201464

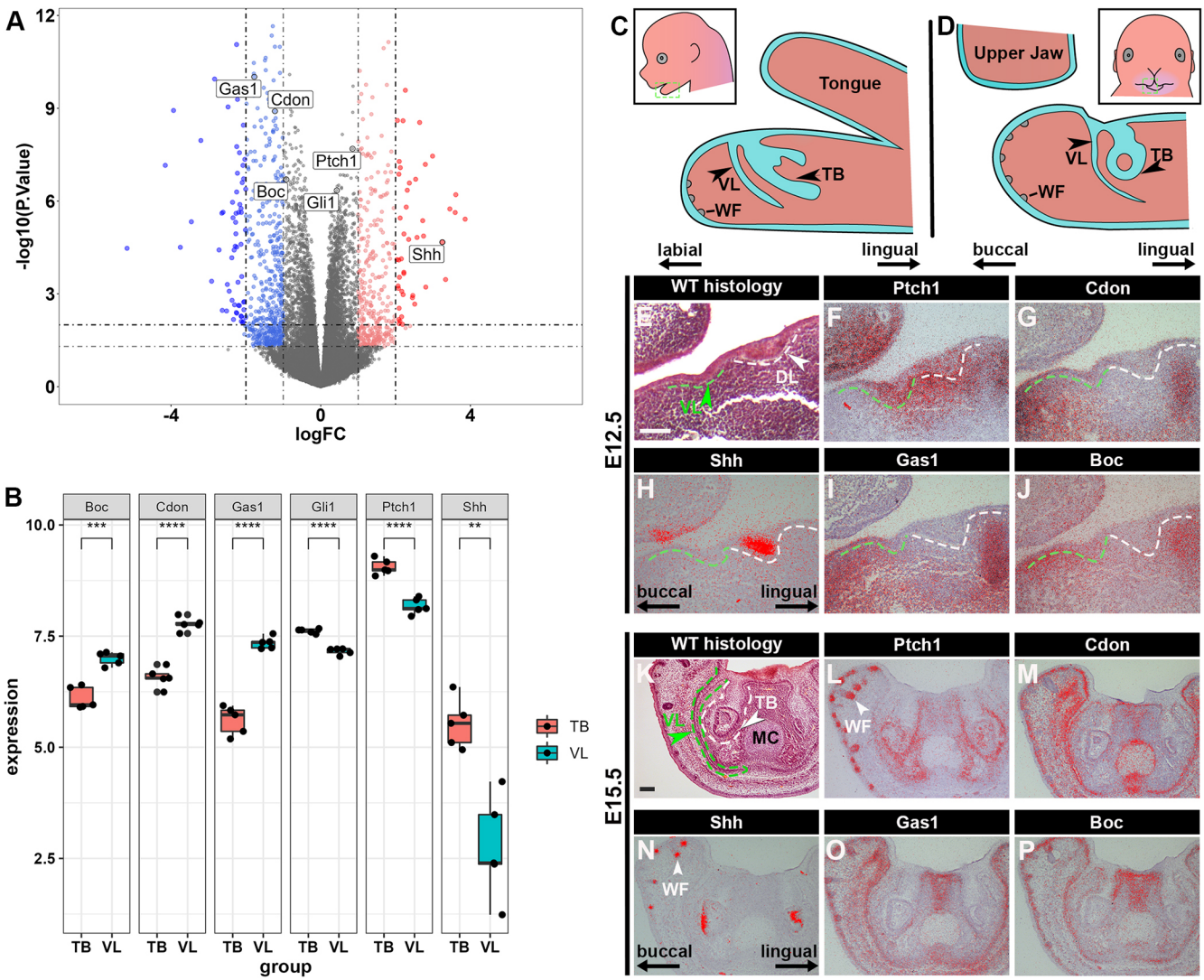

Fig. 2. Differential expression of Shh pathway components in the VL and tooth germ. (A,B) Volcano plot (A) and boxplot (B) highlighting the differences of Shh pathway-related genes in the vestibular lamina (VL) and incisor tooth germ at E14. *Gas1*, *Cdon* and *Boc* were significantly more highly expressed in the VL, whereas *Shh*, *Ptch1* and *Gli1* were significantly more highly expressed in the incisor tooth germ. Abs log2FC_1>1, *P*-value_1<0.05; abs log2FC_2>2, *P*-value_2<0.01. **P*<0.05, ***P*<0.01 and ****P*<0.001 (two-tailed, unpaired *t*-test). In box plots, middle bars represent median values, boxes represent first to third interquartile ranges and dots indicate the expression of each sample. (C) Schematic of E15.5 mouse lower jaw in the sagittal plane, showing the tooth bud (TB) and adjacent VL on the labial (lip) side of the TB. (D) Schematic of E15.5 mouse lower jaw in frontal plane, showing the TB and adjacent VL on the buccal (cheek) side of the TB. (E,K) Trichrome/H&E staining of the VL and dental lamina (DL)/tooth germ in the anterior lower jaw at E12.5 and E15.5. (F-J,L-P) Frontal sections of the lower jaw in the incisor region in WT (CD1) mouse performed with radioactive *in situ* hybridization. Shh pathway gene expression was assessed in the VL and DL/tooth bud/tooth germ at E12.5 and E15.5, respectively. (F,L) *Ptch1*; (G,M) *Cdon*; (H,N) *Shh*; (I,O) *Gas1*; (J,P) *Boc*. WF, whisker follicles; MC, Meckel's cartilage. Lingual-labial axes shown in C. Lingual-buccal axes shown in D,H,N, same plane for E-P. Scale bars: 100 µm.

Boc were reduced in the developing tooth germs but were strongly expressed on the buccal side of the VL in the buccal epithelium and mesenchyme (Fig. 2M,O,P). This buccal/labial bias of *Gas1* expression in the VL epithelium was confirmed at E14 by RNAscope (Fig. S5D-F).

Truncation of the VL in *Gas1* and *Boc* compound mutants

Given the distinct expression pattern of *Gas1* in the VL, we focused on this component of the Shh pathway through the analysis of *Gas1* mutant mice. *Gas1* has been shown to facilitate Shh signalling, particularly with low signal levels at long distance from the source (Martinelli and Fan, 2007). A lack of *Gas1* is associated with a series of midline craniofacial phenotypes including maxillary incisor fusion, midfacial hypoplasia and cleft palate due to reduced Shh signalling in the early craniofacial region (Seppala et al., 2007). At E13.5, the VL (contoured by green dashed lines) has started to extend into the mesenchyme under the forming incisors in wild-type (WT) mice, with full extension under the tooth germ, towards the midline, by E15.5 (Fig. 3A,F). In contrast, in the *Gas1* null mutants ($Gas1^{-/-}$), the VL was shorter and failed to pass under the forming incisors (Fig. 3B,G) (truncated VL observed in N=15/15 $Gas1^{-/-}$ embryos from E13.5 to E15.5). Interestingly, a similar truncated VL was observed in some $Gas1^{+/-}$ embryos at E13.5, although the severity of the defect varied between heterozygous mutants (Fig. 4J-L) (truncation observed in N=5/7 $Gas1^{+/-}$ embryos at E13.5). The reduction in the VL was significant in both homozygous and heterozygous mutants when measured at E13.5 (Fig. 4G).

Development (2023) 150, dev201464. doi:10.1242/dev.201464

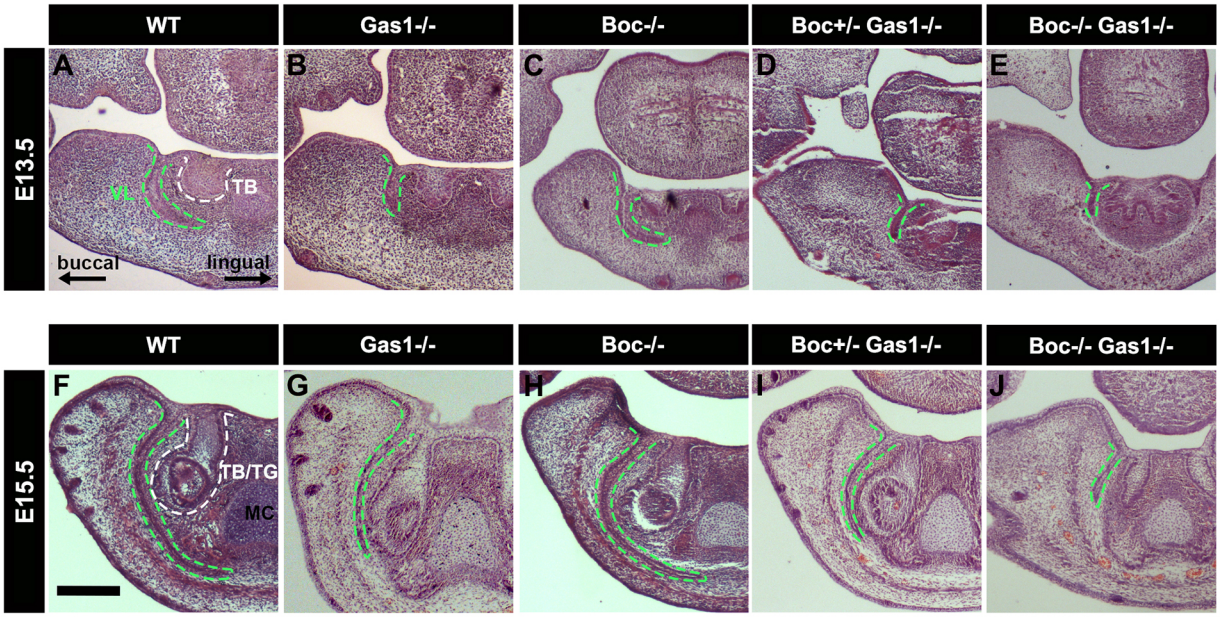

Fig. 3. Truncated VL formation after loss of Shh co-receptors. (A-J) Trichrome/H&E staining of mouse frontal sections through the lower incisor region. (A-E) E13.5. (A) In the WT, the vestibular lamina (VL) had extended into the mesenchyme and around the forming incisor tooth bud (TB). (B) *Gas1*$^{-/-}$. The mutant VL had started to extend but fails to pass the neighbouring incisor tooth bud. (C) *Boc*$^{-/-}$. Normal extension of the VL. (D) *Boc*$^{+/-}$*Gas1*$^{-/-}$. Defective extension. (E) *Boc*$^{-/-}$*Gas1*$^{-/-}$ compound mutant. The VL and tooth germs (TG) were severely affected, with a rudimentary VL and partial fusion of the incisors at the midline. (F-J) E15.5. (F) The WT VL at E15.5 had invaginated further into the mesenchyme and under Meckel's cartilage (MC) in the midline. (G) Similar to E13.5, the *Gas1*$^{-/-}$ had a truncated VL. (H) *Boc*$^{-/-}$. Normal extension of the VL. (I) *Boc*$^{+/-}$*Gas1*$^{-/-}$. Truncated VL. (J) The *Boc*$^{-/-}$*Gas1*$^{-/-}$ compound mutant had an exacerbated VL phenotype with a very short VL and defective incisor tooth germs. Lingual-buccal axes shown in A, same plane in all other images. Mouse numbers analysed: WT (E13.5 *n*>9; E14.5 *n*>3; E15.5 *n*>9; E16.5 *n*>3), *Gas1*$^{-/-}$ *N*=18 (E13.5 *n*=8, E14.5 *n*=4, E15.5 *n*= 3), *Boc*$^{-/-}$ *N*=4 (E13.5 *n*=1; E14.5 *n*=1; E15.5 *n*=1; P0 *n*=1); *Boc*$^{+/-}$*Gas1*$^{-/-}$ *N*=9 (E13.5 *n*=4; E15.5 *n*=3; E18.5 *n*=1; P0 *n*=1); *Boc*$^{-/-}$*Gas1*$^{-/-}$ *N*=3 (E13.5 *n*=1; E15.5 *n*=2). Scale bar: 250 µm.

Gas1 has also been reported to interact with the Hh co-receptor *Boc* in different developmental contexts (Allen et al., 2011). We therefore further explored the function of *Boc* during VL development using mutant mice. Interestingly, analysis of a *Boc* mutant showed a normal VL indistinguishable from WT (Fig. 3C,H) [normal VL observed in *N*=4/4 *Boc*$^{-/-}$ embryos from E13.5 to postnatal day (P) 0]. Loss of a single *Boc* allele in *Gas1*$^{-/-}$ mice did not significantly exacerbate the phenotype compared with *Gas1*$^{-/-}$ mutants (Fig. 3D,I; Fig. 4G) (truncated VL observed in *N*=9/9 *Boc*$^{+/-}$ *Gas1*$^{-/-}$ embryos from E13.5 to P0). In contrast, *Boc/Gas1* double knockouts had exacerbated VL and TB phenotypes, with a severely truncated VL and a developmentally arrested incisor tooth germ (Fig. 3E,J) (severely truncated VL observed in *N*=3/3 *Boc*$^{-/-}$ *Gas1*$^{-/-}$ embryos at E13.5 and E15.5). *Gas1* and *Boc*, therefore, appear to be able to compensate for each other to some extent during VL development.

Downregulation of *Ptch1* and *Gli1* and loss of proliferation in the *Gas1* mutant VL

The identification of a shorter VL in *Gas1*$^{-/-}$ mice suggested that the VL is dependent on Shh signalling for normal development. To confirm this, we assessed expression of *Ptch1* and *Gli1* in these mutants at E13.5, the stage when a clear VL defect is first identifiable in these mice. *Ptch1* was expressed on the labial/buccal side of the VL in WT embryos but, in *Gas1*$^{-/-}$ mice, this expression was lost in the truncated lamina but retained in other regions, including the aboral mesenchyme, underlying the developing whisker follicles (Fig. 4A,D). In the WT, *Gli1*, as viewed by RNAscope, was similarly expressed at significantly higher levels on the buccal side of the VL compared with the lingual side of the VL (Fig. 4B,C,H). Quantification of the RNAscope in the *Gas1*$^{-/-}$ mice revealed that the levels of expression in the buccal epithelium were significantly reduced (Fig. 4E,F,I; Fig. S6) (*N*=3). Given that *Gas1*$^{+/-}$ mice showed a variable truncated VL defect, we assessed changes in *Gli1* in heterozygotes with and without a phenotype at E13.5. In a *Gas1*$^{+/-}$ mouse with no phenotype at this stage, *Gli1* expression appeared as for the WT (Fig. 4M,N). In contrast, *Gas1*$^{+/-}$ mice with a truncated VL still showed *Gli1* expression but had lost the normal buccal-lingual polarity (Fig. 4O). The buccal-lingual difference in Shh response was, therefore, lost in mice with a truncated VL.

To analyse the cause of the truncated phenotype, we investigated the level of proliferation during early development of the VL before the defect in epithelial extension using bromodeoxyuridine (BrdU) to detect cells in the S phase of the cell cycle. At E12.5, the *Gas1*$^{-/-}$ VL and DL were evident as two distinct thickenings, although they appeared to be closer to each other when compared with WT littermates, suggesting part of the phenotype is determined very early in VL development (Fig. 5A-C,G). E-cadherin was used to outline the epithelium and the number of BrdU-positive cells were counted within a defined region, taken from the deepest projection of the DL to the VL (*N*=3) (Fig. 5D-F,H-J, area outlined in D,E,H,I highlights region counted). Proliferation in the epithelium was significantly reduced in the *Gas1*$^{-/-}$ embryos (Fig. 5J,K), with clear reduction of proliferation in the mesenchyme around the forming VL at this stage (Fig. 5D,H).

Loss of *Gas1* activity in the neural crest leads to a truncated VL

Given the strong expression of *Gas1* in both the buccal epithelium and mesenchyme of the VL during development (Fig. 2I,O;

Development (2023) 150, dev201464. doi:10.1242/dev.201464

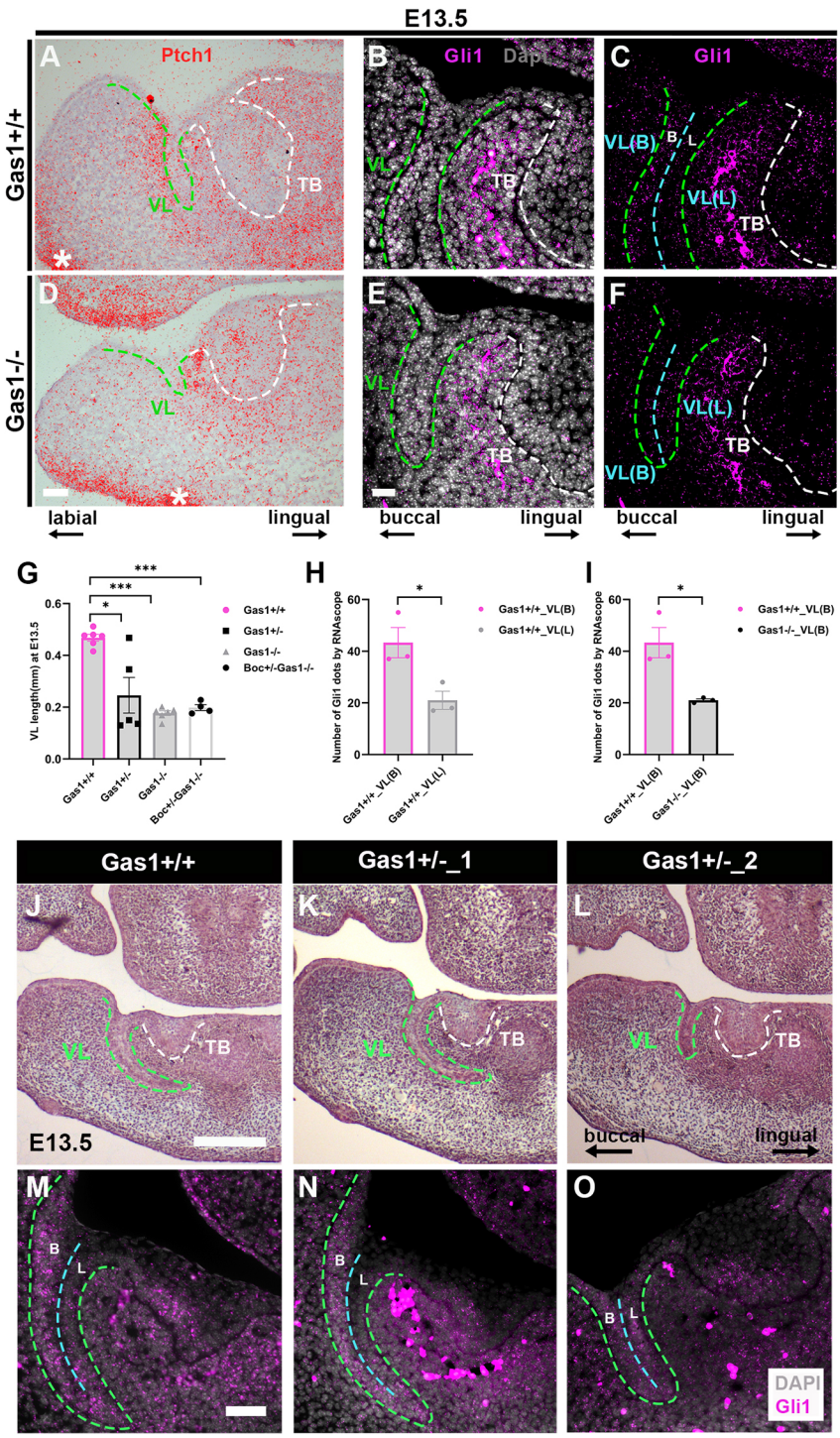

Fig. 4. Altered expression of *Ptch1* and *Gli1* in *Gas1* heterozygote and homozygotes at E13.5. (A,D) Sagittal sections through the lower anterior incisor region showing radioactive *in situ* hybridization of *Ptch1* at E13.5. (A) WT littermate control. (D) *Gas1*$^{-/-}$. Decreased *Ptch1* expression was observed in the shorter vestibular lamina (VL) in *Gas1*$^{-/-}$ mice compared with the littermate controls. White asterisks point to the region where the whisker follicles are forming on the aboral side of the jaw, which is *Ptch1*-positive in both. (B,C,E,F) RNAscope in the lower anterior VL in frontal section at E13.5. DAPI (grey), *Gli1* (magenta). (B,C) DAPI and *Gli1* in the littermate controls; (E,F) DAPI and *Gli1* in the *Gas*$^{-/-}$ mice. The VL was divided by blue dashed lines into two parts: the buccal side [VL(B)], and the lingual side [VL(L)]. (G) Graph showing VL length in WT (*N*=6), *Gas*$^{+/-}$ (*N*=5), *Gas*$^{-/-}$ (*N*=6) and *Boc*$^{+/-}$*Gas1*$^{-/-}$ (*N*=4) at E13.5. The *Gas*$^{+/-}$ mice present variations in VL length, but show a significantly shortened VL compared with the WT. The *Gas*$^{-/-}$ mice showed a strikingly consistent shorter VL, with no additional effect with loss of one copy of *Boc*. (H,I) Graphs quantifying *Gli1* expression in the VL. (H) *Gli1* expression on the buccal VL compared with the lingual VL in WT mice. The *Gli1* expression on the buccal side of the VL was significantly higher than the expression on the lingual side of the VL during normal development. *N*=3, *P*<0.01. (I) *Gli1* expression on the buccal VL in the WT compared with expression on the buccal VL in *Gas*$^{-/-}$ mice. Significantly decreased *Gli1* expression was observed on the buccal side of the VL in the *Gas*$^{-/-}$ mice. (J-L) Trichrome/H&E staining of mouse frontal sections through the lower anterior incisor at E13.5. (J) WT littermate controls. (K) *Gas1*$^{+/-}$ embryo presenting a normal VL. (L) *Gas1*$^{+/-}$ embryo presenting a shorter VL. (M-O) RNAscope in the mandible VL in frontal sections. DAPI (grey), *Gli1* (magenta). (M) *Gli1* in the littermate controls. (N,O) *Gli1* in *Gas1*$^{+/-}$ mice. (N) In the embryo with a WT-shaped VL, the level of *Gli1* was similar to the WT, with higher expression on the buccal side. (O) In the embryo with a truncated VL, the differential expression of *Gli1* on either side of the lamina was lost. Green and white dashed lines delineate the VL and tooth bud (TB), respectively. Lingual-labial axes shown for A,D. Lingual-buccal axes shown for B-F and L, same plane in J,K,M-O. Mouse numbers analysed: WT (E13.5 *n*>9), *Gas1*$^{-/-}$ (E13.5 *n*=8), *Gas1*$^{+/-}$ (E13.5 *n*=7), *Boc*$^{+/-}$*Gas1*$^{-/-}$ (E13.5 *n*=4). **P*<0.05, ***P*<0.01 and ****P*<0.001 (two-tailed, unpaired *t*-test). Error bars represent s.e.m. Scale bars: 50 µm in D (for A,D) and J,M (for J-O); 25 µm in E (for B,C,E,F).

Fig. S5E,F), and reduction of proliferation in both tissues, we wanted to address whether truncation of the VL was caused by loss of *Gas1* in the mesenchyme alone. For this, *Wnt1-Cre;Gas1*$^{fl/fl}$ conditional mutant mice were used. At E16.5, similar to E15.5, the WT VL (labelled by green dashed lines) had extended under the incisors with the ends almost touching each other in the midline in the anterior, and slightly less extended more posteriorly (Fig. 6A,C) (Qiu and Tucker, 2022). Interestingly, *Wnt1-Cre;Gas1*$^{fl/fl}$ mice mimicked the VL phenotype observed in *Gas1*$^{-/-}$ mice, with a significantly truncated VL that failed to reach past the developing incisors (Fig. 3G compared with Fig. 6B,E) (truncation in *N*=3/3). *Wnt1-Cre* mice have been shown to have some brain defects but no craniofacial defects (Heuzé et al., 2014), and in keeping with this the VL was normal in all *Wnt1-Cre* controls (*N*=5/5) (Fig. 6C-E). These findings highlight that loss of *Gas1* in the neural crest-derived mesenchyme alone is sufficient to cause a truncated VL phenotype.

Manipulation of Shh signalling in culture alters VL development

To further manipulate Shh signal levels during early development of the VL, we moved to an *ex vivo* explant culture system, which has previously been used to successfully culture the VL (Qiu and

Development (2023) 150, dev201464. doi:10.1242/dev.201464

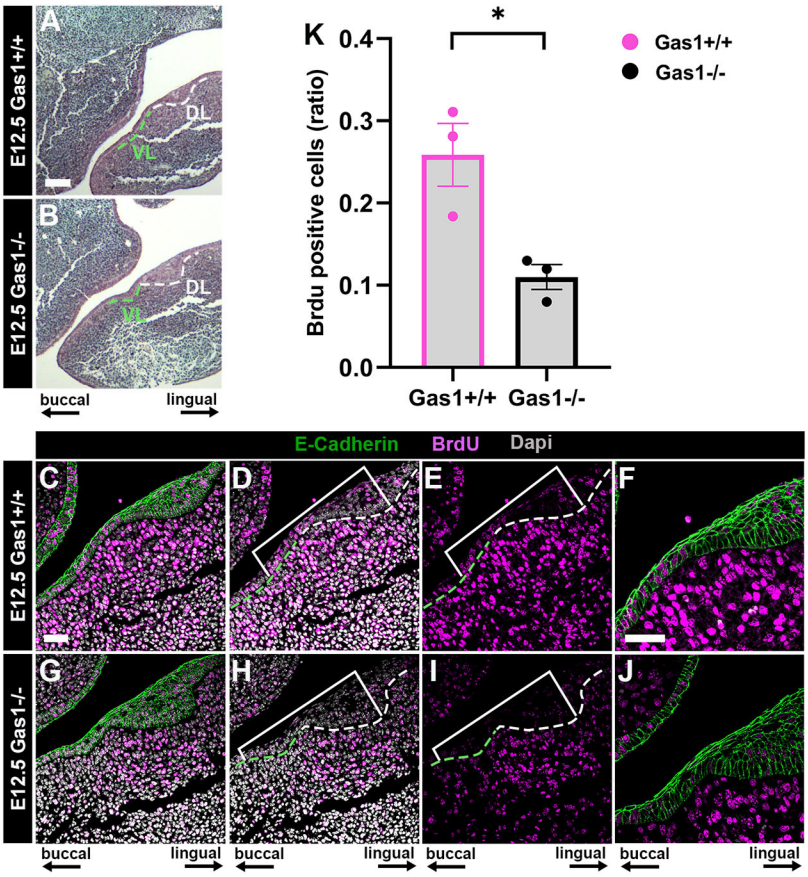

Fig. 5. The truncated VL is associated with reduced proliferation at E12.5. (A,B) Histological (trichrome staining) frontal sections through vestibular lamina (VL) and dental lamina (DL) in the anterior mandible at E12.5. (A) WT littermate control. (B) *Gas1* homozygous mutant. (C-F,G-J) immunofluorescence for E-cadherin (green), BrdU (magenta) and DAPI (grey) in the littermate controls (C-F) and *Gas1*$^{-/-}$ mice (G-J). (C,G) E-cadherin, BrdU and DAPI; (D,H) BrdU and DAPI; (E,I) BrdU; (F,J) Magnification showing a reduced number of BrdU-positive cells in the VL epithelium. (K) Graph comparing the ratio of BrdU-positive cells, where 1=100% of cells are proliferating (N=3, P<0.01, error bars represent s.e.m.). The BrdU-positive cells were significantly decreased in the epithelium in the *Gas1*$^{-/-}$ mice compared with littermate controls. Green and white dashed lines in A,B outline the VL and DL, respectively. The white lines in D, E, H, I define the areas of epithelia selected for counting. Lingual-buccal axes shown for all images. Mouse numbers analysed: WT (E12.5 n>9), *Gas1*$^{-/-}$ (E12.5 n=3). *P<0.05, **P<0.01 and ***P<0.001 (two-tailed, unpaired t-test). Error bars represent s.e.m. Scale bars: 125 µm in A (for A,B); 50 µm in C,F (for C-J).

Tucker, 2022). Here, the mandible harvested at E13.5 was chopped longitudinally into 200 µm thick live slices, and the midline slices containing the VL and incisor tooth germ were selected. Cyclopamine was added at a concentration of 20µM and 50µM to block Shh signalling by interfering with the obligate smoothened receptor (Li et al., 2016). At 20µM whisker follicle development was clearly affected in the slices (Fig. S7), but no obvious VL phenotype was evident (Fig. 7A-D). We therefore increased the concentration to 50µM. Cyclopamine-treated cultures at 50µM continued to grow over the 2 day culture period, with development of a cap stage tooth, but the treated cultures had significantly shorter VLs when compared with slices treated with the carrier solution alone (Fig. 7E-H; Fig. S8) (N=6 control, 6 treated). Confirming loss of Shh signalling, addition of cyclopamine caused an almost complete loss of *Gli1* and *Ptch1* expression (Fig. S10A,C,D,F). To enhance Shh signalling, cultures were treated with SAG (smoothened agonist) at 5µM, which acts to stabilize the key Hh transducer smoothened in the primary cilium. The SAG-treated cultures displayed severe retardation of tooth development and a significant thickening of the forming VL (Fig. 7I-L; Fig. S9) (N=7 control, 7 treated) and was accompanied by an upregulation of *Gli1* in the mesenchyme around the VL and tooth germ and *Ptch1* in the thickened VL (Fig. S10B,E). Targeted loss of Shh signalling at E13.5, therefore, impacted VL development.

DISCUSSION

Distinct lingual-labial/buccal and oral/aboral gene signatures in the VL predate morphological differences

An important aim of this work was to investigate the molecular signature of the VL. The bulk RNA-seq data at E14 provided an interesting set of genes that are likely to play a role in VL development and can be used as markers of the VL in future experiments. Interestingly *Wnt7b* was expressed in the VL, and this gene has been proposed to inhibit Shh expression in non-dental regions (Sarkar et al., 2000). *Meis1/2* were also highlighted in the VL. *Meis1* has been linked to stem cell maintenance and overlaps with *Sox2*-expressing regions, with both *Sox2* and *Meis1* expressed at high levels in the VL (Sanz-Navarro et al., 2019). The VL may, therefore, have some stem cell properties.

One perhaps unexpected result was that many genes exhibited differential expression in the lingual and labial/buccal sides of the VL, suggesting that the epithelium is spatially patterned at this stage, more than 1 week before the VL opens to form the vestibule (Qiu and Tucker, 2022). This differential expression, however, agrees with the observed differences in proliferation rates of the labial/buccal and lingual sides of the VL, which have been proposed to drive the shape of the elongating VL (Qiu and Tucker, 2022). Differences in oral and aboral parts of the VL were also evident, highlighting further compartmentalization of the VL during development. Overall, this is the first molecular analysis of the VL and provides a number of interesting pathways for further exploration.

Shh signalling is essential for correct growth and patterning of the VL

Here, we determined that, although the VL does not express *Shh* after the earliest placodal stages, its development is dependent on Shh signals from the developing tooth. The two laminas are therefore patterning by the same signal. The Shh co-receptors *Gas1*, *Boc* and *Cdon* were shown to have enhanced expression in the

Development (2023) 150, dev201464. doi:10.1242/dev.201464

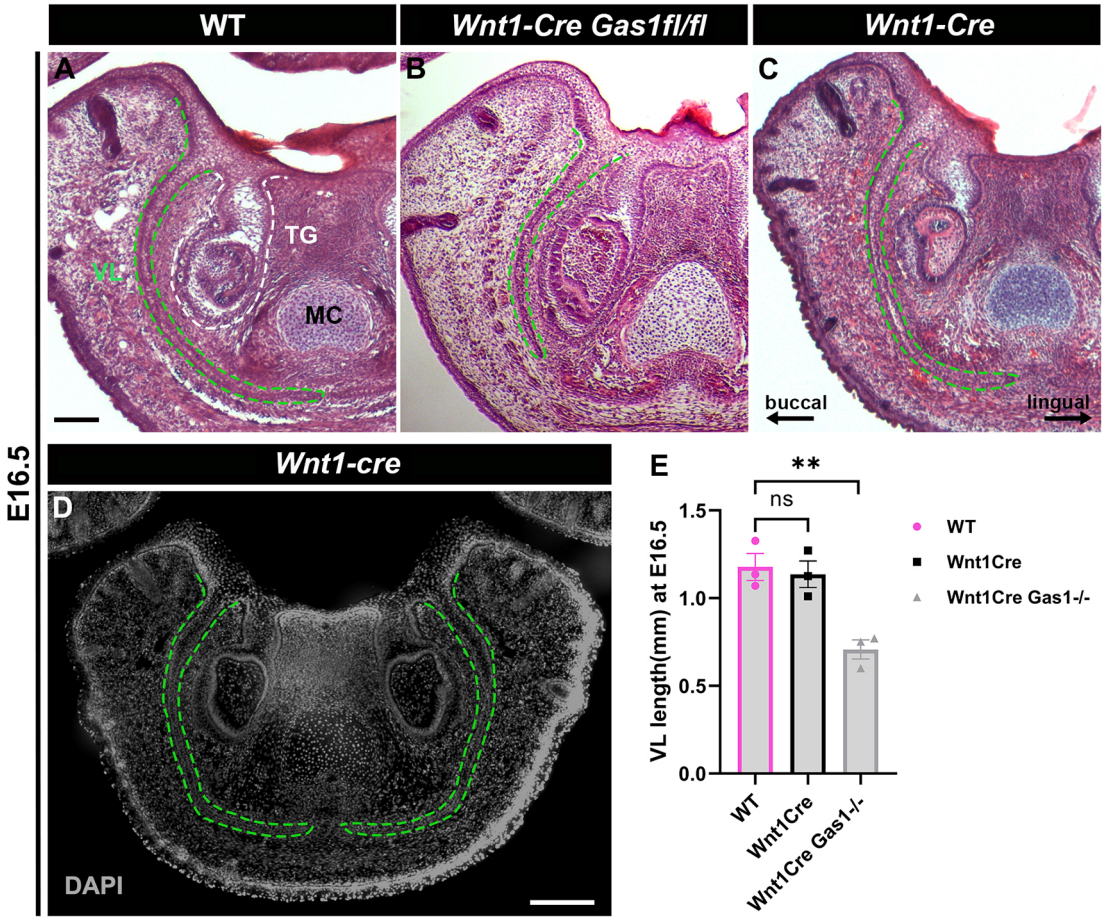

Fig. 6. Lack of *Gas1* in the neural crest in *Wnt1-Cre Gas1$^{fl/fl}$* embryos mimics the shorter VL phenotype in *Gas1* null mutants. (A-C) H&E staining of the anterior lower jaw in frontal sections at E16.5 showing WT (A), *Wnt1-Cre Gas1$^{fl/fl}$* (B) and *Wnt1-Cre* (C) mice. A shorter vestibular lamina (VL) was observed in the *Wnt1-Cre Gas1$^{fl/fl}$* mice compared with the WT and *Wnt1-cre* positive control, mimicking the VL phenotype in the *Gas1$^{-/-}$* mice (Fig. 3B,G). (D) A normal VL was observed in *Wnt1-Cre* mice; DAPI nuclear stain (grey). (E) Graph showing VL length in the WT (*N*=3, s.e.m.), *Wnt1-Cre* (*N*=3, s.e.m.), and *Wnt1-Cre Gas1$^{fl/fl}$* (*N*=3, s.e.m.) mice at E16.5. The VL in the *Wnt1-Cre Gas1$^{fl/fl}$* mice was significantly shorter compared to the WT. Green dashed lines label the VL in A-D. TG, tooth germ; MC, Meckel's cartilage. Lingual-buccal axes shown in C, same axes for all images. **P*<0.05, ***P*<0.01 and ****P*<0.001 (two-tailed, unpaired *t*-test). ns, not significant. Error bars represent s.e.m. Scale bars: 125 µm in A (for A-C); 200 µm in D.

forming VL, and loss of *Gas1* in mouse mutants resulted in truncation of the forming VL. Failure in extension of the VL was driven by a reduction/misexpression of readouts of Hh signalling and a reduction in proliferation. Interestingly, *Gas1* heterozygous mice showed a variable defect in the VL, correlating to changes in *Gli1* expression. *Gas1* heterozygous mice are viable and feed as normal, suggesting that earlier VL defects may be able to correct themselves during later development. This may be linked with developmental stalling, whereby mutant mice display initial defects and a slowing down of development but are able to recover with later accelerated development (Miletich et al., 2011). In both homozygotes and heterozygous *Gas1* mutants the truncated VL was linked to a loss of the differential expression of *Gli1* in the epithelium, suggesting that the lingual-buccal/labial differences are key drivers of vestibular lamina outgrowth.

Gas1 in the VL mesenchyme extends the range of the Shh signal

Gas1 mutants have previously been shown to have tooth defects, which include fusion of the first and second molars, formation of supernumerary teeth in the diastema and cusp defects (Seppala et al., 2022). Loss of one copy of *Boc* in *Gas1* mutants did not exacerbate the phenotype but loss of two copies in the compound mutants resulted in very severe VL defects. *Boc* and *Gas1* have been shown to form distinct complexes with *Ptch1* (Izzi et al., 2011). *Boc$^{-/-}$* are viable, with subtle changes to the cerebellum and a background-dependent mild widening of the facial region (Izzi et al., 2011; Echevarriá-Andino and Allen, 2020). Interestingly, although in many tissues loss of both *Boc* and *Gas1* leads to a worsening of the single mutant phenotype (Seppala et al., 2014), with regards to the width of the face, *Boc* and *Gas1* double mutants had a less severe craniofacial phenotype, suggesting context-dependent effects of these two co-receptors (Echevarriá-Andino and Allen, 2020). Similarly, *Gas1* can restrain, rather than enhance, Hh signalling in the mouse diastema and in presomitic mesoderm explants (Lee et al., 2001a; Cobourne et al., 2004). In the VL, however, *Boc* and *Gas1* appear to act by facilitating Shh signalling in tissue at a distance from the Shh source, with a significant downregulation of *Gli1* in the VL of *Gas1* mutants, particularly on the buccal/labial side. A proposed model of Hh signalling in the VL is shown in Fig. 8, highlighting the known role of the primary cilium. This agrees with findings in the heart, neural tube and limb (Martinelli and Fan, 2007). In these tissues, Shh has been shown to downregulate *Gas1* to constrain its own activity, which may explain

Development (2023) 150, dev201464. doi:10.1242/dev.201464

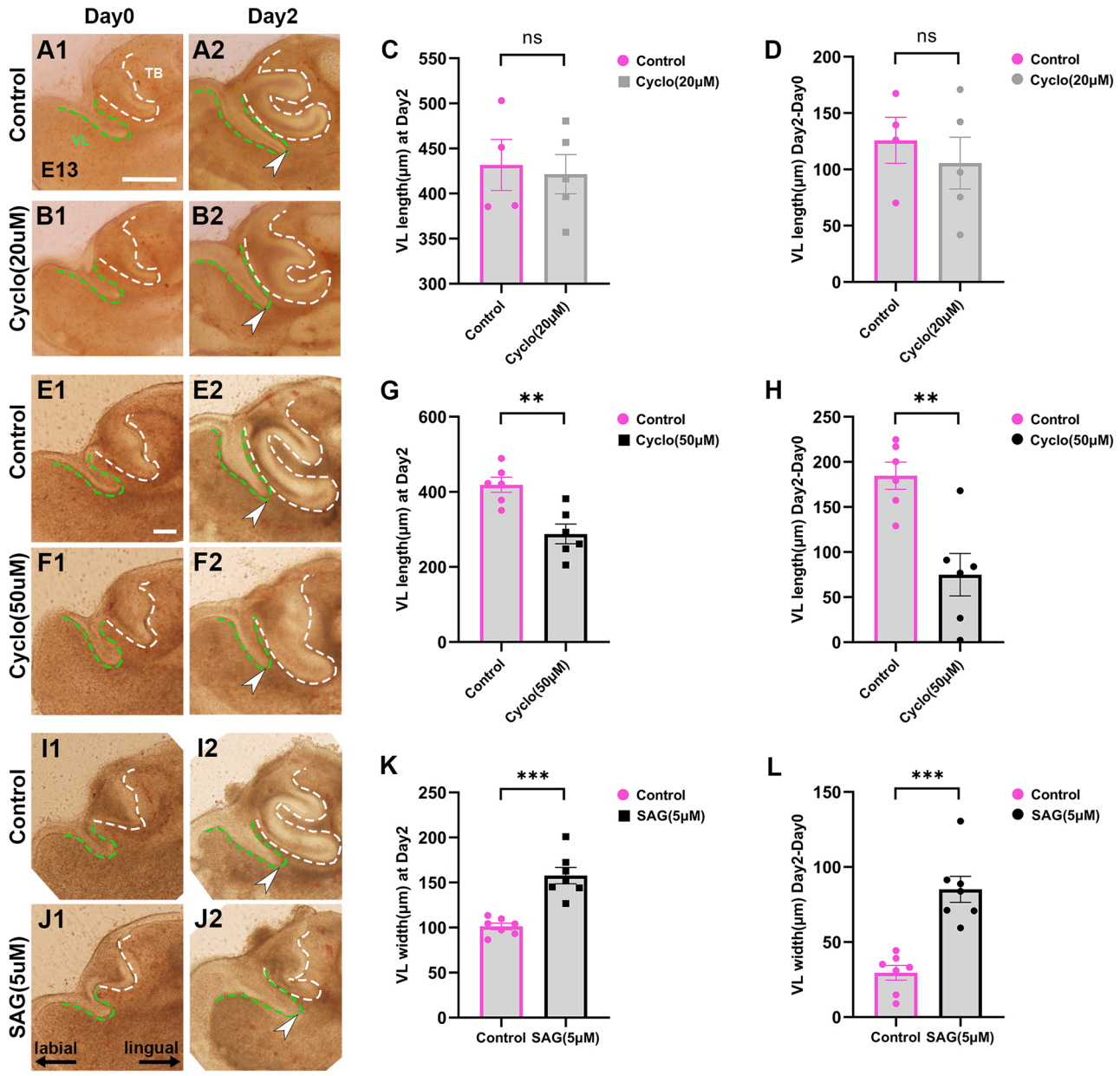

Fig. 7. Manipulation of Shh signalling in explant culture led to changes in VL length and width. (A-J) Sagittal explant slices through the anterior mandible at E13.5. (A1,B1,E1,F1,I1,J1) Day 0. Prominent vestibular lamina (VL) and tooth bud (TB) were observed at E13.5. (A2,B2,E2,F2,I2,J2) Day 2. The VL protruded into the mesenchyme following the curve of the forming tooth germ after 48 h in culture. (A1,2) Control carrier only group for cyclopamine-treated cultures (20 µM). (B1,2) Cyclopamine-treated cultures (20 µM). (E1,2) Control carrier only group for cyclopamine-treated cultures (50 µM). (F1,2) Cyclopamine-treated cultures (50 µM). (I1,2) Control group for SAG-treated cultures (5 µM). (J1,2) SAG-treated group. (B2,C) The VL was not significantly shorter in the cyclopamine-treated cultures at a concentration of 20 µM (N=5) compared with the controls (N=4) after 2 days in culture. (D) To account for any variation at the start of culture we also compared the increase in length during culture by analysing the length at day 2 minus the length at day 0. This also showed no significant difference. (F2,G,H) When treated with 50 µM cyclopamine, the VL was significantly shorter in the cyclopamine-treated cultures (N=6 for both) after 2 days in culture using both measures. (J2,K,L) The VL was significantly thicker in the SAG-treated (5 µM) cultures (N=7 for both) after 2 days in culture (K). In addition, we compared the VL width difference on day 2 minus day 0 and showed a statistical significance (L). Green dashed lines label the VL and white dashed lines outlined the TB. White arrowheads indicate tip of VL after culture. Lingual-labial axes shown in J1, same orientation for all images. *P<0.05, **P<0.01 and ***P<0.001 (two-tailed, unpaired t-test). Error bars represent s.e.m. All experiments were repeated more than six times for SAG and 50 µM cyclopamine, and four times for 20 µM cyclopamine, and differences were compared within a litter. Scale bars: 300 µm in A1 (for A1,A2,B1,B2); 100 µm in E1 (for E1,E2,F1,F2,I1,I2,J1,J2).

the heightened expression of *Gas1* in the VL compared with the tooth in WT embryos.

Gas1 was expressed in both the buccal/labial epithelium of the VL and the surrounding mesenchyme. Perhaps unexpectedly, loss of *Gas1* in the neural crest-derived mesenchyme alone led to truncation of the VL. Expression in the epithelium is therefore not sufficient for VL extension. Tooth number has similarly been found to be dependent on *Gas1* expression in the mesenchyme, with supernumerary teeth developing in the diastema of *Wnt1-Cre; Gas1*$^{fl/fl}$ mice (Seppala et al., 2022).

Development (2023) 150, dev201464. doi:10.1242/dev.201464

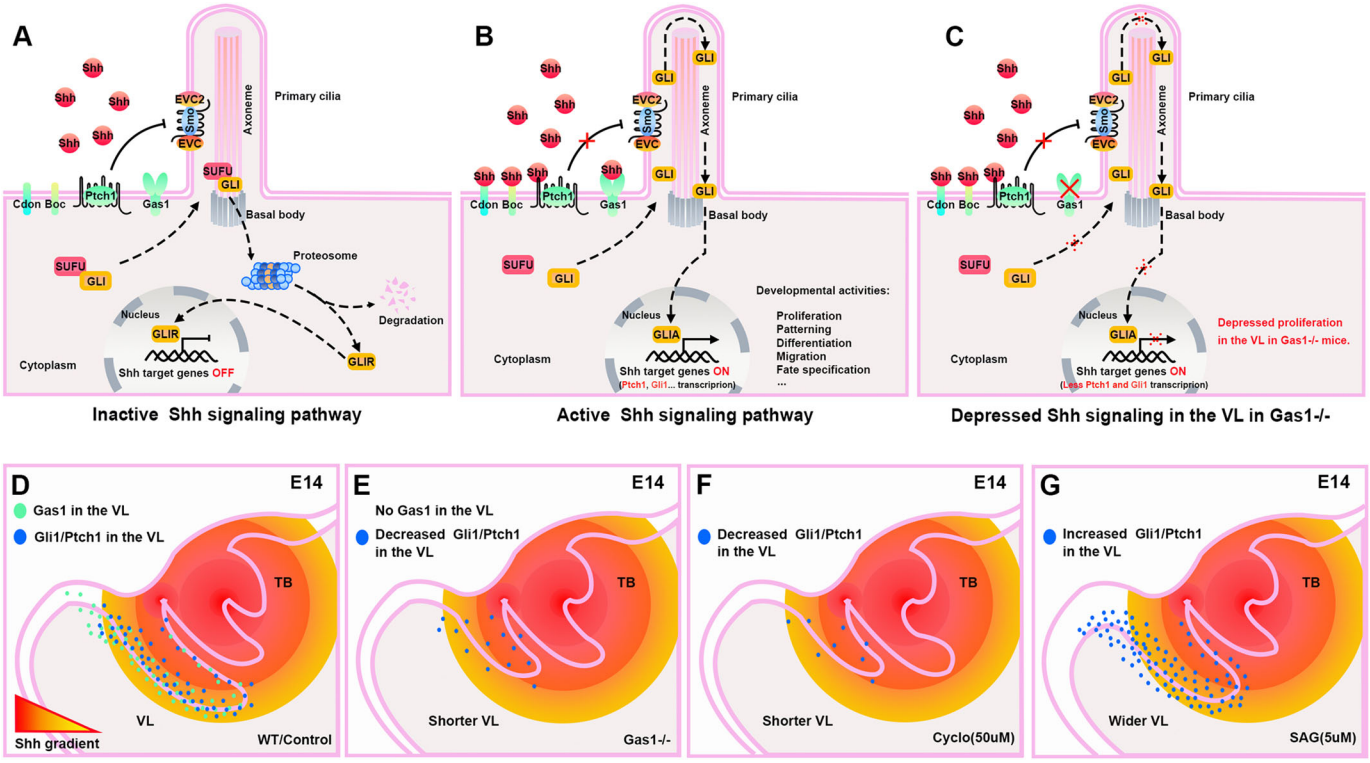

Fig. 8. Schematic of Shh signalling in the VL. (A,B) Review of vertebrate Shh signalling at the cell membrane (Caparrós-Martín et al., 2013; Seppala et al., 2017). (A) Inactive Shh signalling pathway (Off). In the absence of Shh signal, the cell surface receptor Ptch1 accumulates at the primary ciliary membrane and inhibits Smo. GLI proteins are sequestered by SuFu, and proteolytically processed into truncated repressor forms, thus repressing the pathway transcription. (B) Active Shh signalling pathway (On). With the arrival of secreted Shh, the signalling pathway is activated when Shh binds to Ptch1 and releases the inhibition to Smo. This is facilitated by the co-receptors Cdon, Boc and Gas1. The activated Smo enters into the primary cilia and interacts with the EVC/EVC2 complex to trigger the downstream GLI family transcriptional activities. Gli1 translocates into the nucleus to promote the target gene expression. (C) Depressed Shh signalling in *Gas1* homozygous mutants. In the *Gas1*$^{-/-}$ mutant VL, it is proposed that low levels of Shh cannot release the inhibition of Smo owing to loss of a key co-receptor, leading to reduced activation of Gli1 in the VL. (D-G) Schematics of the activity of Shh in the vestibular lamina (VL). (D) In the WT, Shh is produced in the tooth germ and diffuses in a gradient away from the source. High levels of *Gas1* at a distance from the Shh source allow upregulation of *Gli1* and *Ptch1* in the VL. Expression of Hh downstream pathway genes is essential for proliferation and extension of the VL. (E) In *Gas1* mutants, the normal Shh signal at the VL is too weak to elicit activation of *Gli1* and *Ptch1* and the VL fails to grow. (F) In the presence of the smoothened inhibitor cyclopamine, again *Gli1* and *Ptch1* are not activated in the VL and it fails to grow. (G) On stimulation of smoothened by SAG, cells further away from the Shh source can respond and the pathway is upregulated, leading to increase in the width of the VL.

Requirement for Hedgehog signalling in the VL explains the frenula defects observed in EvC patients

Vestibule defects are associated with EvC syndrome, where the gums adhere to the upper lip and cheek with multiple associated frenula (Sasalawad et al., 2013). Interestingly, *Evc* also has a role in the Shh pathway, interacting with smoothened in the primary cilium (Fig. 8). *Evc* regulates Hh signalling by promoting Sufu/Gli3 dissociation and Gli3 ciliary traffic (Caparrós-Martín et al., 2013). A *lacZ Evc* reporter has previously shown expression of *Evc* around the teeth and VL at E15.5 (Ruiz-Perez et al., 2007). The VL has not been studied in *Evc* mutant mice, but a similar truncated VL might be predicted based on a reduction in the Hh pathway and the phenotype from the *Gas1* mutants. VL defects would also be predicted to occur in other ciliopathies and, in keeping with this, frenula defects have been noted in oral-facial-digital (OFD) syndromes (Bruel et al., 2018) and in Joubert syndrome (Penon-Portmann et al., 2022). OFD syndromes can be caused by defects in the ciliary basal body, ciliogenesis or post-ciliary microtubule functions, with at least 20 genes identified in patients (Bruel et al., 2018). It would, therefore, be interesting to study the VL in mouse models where primary cilia function is disrupted. In addition, changes in the vestibule, with defects and accessory frenula, may represent an important additional clinical character for defining ciliopathies in patients.

Variation in Hedgehog signalling may explain species-specific difference in the VL

Our culture experiments allowed the development of the VL and tooth germ to be followed and the Hh pathway to be manipulated at specific time points. Addition of cyclopamine or SAG to target smoothened led to striking defects in the VL. Agreeing with the results from the *Gas1* mutants, addition of cyclopamine caused a shorter VL that failed to extend into the surrounding mesenchyme, strengthening the results that *Gas1* promotes Hh signalling in the VL. Addition of SAG led to a broadening of the VL, which we hypothesize was caused by an extension of the tissue that was able to respond to Shh produced by the neighbouring tooth germ (Fig. 8). The width of the VL varies considerably across mammals, therefore, the wider VL of humans may be driven by enhanced Hh signalling in this tissue compared with mammals such as the mouse, where the VL is very thin.

The results highlight that the tooth germ, through Hh signalling, plays a key role in development of the VL. These two neighbouring laminas, therefore, not only share a common origin in some parts of the jaw but are later patterned together. Defects in the tooth are, therefore, likely to result in defects in the VL. The VL is a fairly unstudied structure, therefore, many published mouse mutants with dental defects may have unreported defects in the VL. From an

Development (2023) 150, dev201464. doi:10.1242/dev.201464

evolutionary perspective, changes to the dentition might not change in isolation but involve secondary effects on the vestibule, linking the evolutionary history of these two structures.

MATERIALS AND METHODS

Mouse strains

Gas1 mutant mice were generated as previously described (Lee et al., 2001b; Seppala et al., 2022). *Gas*$^{+/-}$ (Lee et al., 2001b) and *Boc*$^{+/-}$ (Okada et al., 2006), *Wnt1-Cre*$^{+/-}$ (Danielian et al., 1998) and *Gas1*$^{fl/+}$ (Jin et al., 2015) were crossed to generate compound and conditional mutant mice, respectively. The mice analysed in this research are listed below: WT (E12.5 n>9; E13.5 n>9; E14.5 n>3; E15.5 n>9; E16.5 n>3), *Gas1*$^{-/-}$ N=18 (E12.5 n=3; E13.5 n=8, E14.5 n=4, E15.5 n= 3), *Gas1*$^{+/-}$ N=13 (E12.5 n=3; E13.5 n=7; E14.5 n=3), *Boc*$^{-/-}$ N=4 (E13.5 n=1; E14.5 n=1; E15.5 n=1; P0 n=1); *Boc*$^{+/-}$ *Gas1*$^{-/-}$ N=9 (E13.5 n=4; E15.5 n=3; E18.5 n=1; P0 n=1); *Boc*$^{-/-}$ *Gas1*$^{-/-}$ N=3 (E13.5 n=1; E15.5 n=2); *Wnt1-Cre*;*Gas1*$^{fl/fl}$ N=3 (E16.5), *Wnt1-Cre* N=5 (E16.5). Mutant mice and littermate controls were on a mixed 129sv/C57Bl6 background (Seppala et al., 2022). CD1 mice for transcriptomics, explant culture and *in situ* hybridization were obtained at the Institute of Animal Physiology and Genetics, Czech Academy of Sciences, and King's College London. E0.5 was considered as the day when the plug was detected. All animal procedures were carried out under the guidelines of the Institute of Animal Physiology and Genetics, and King's College London, with Home Office approved Schedule 1 culling methods and conform to ARRIVE guidelines. For proliferation assays, BrdU (30 mg/kg) was injected into the pregnant mouse 2 h before culling.

RNA isolation and RNA-seq library construction and sequencing

VL and neighbouring incisor tooth germs were isolated from the same slices at E14. The dissected VL and tooth germs from a single litter (9-15 embryos) were pooled to obtain enough RNA for sequencing. In total, tissue from 11 litters was isolated at this stage. RNA extraction was performed using the RNeasy Plus Mini Kit (Qiagen, 74136) and pooled samples from five litters with the highest quality scores were used for analysis. These are referred to here as TB1-5 and VL1-5. Sequencing libraries were prepared from total RNA using the Smarter Stranded Total RNA-seq Kit v2 Pico Input Mammalian (Takara), followed by size distribution analysis in the Agilent 2100 Bioanalyzer using a High Sensitivity DNA Kit (Agilent, 5067-4626). Libraries were sequenced using the Illumina NextSeq 500 instrument. Samples were sequenced by the Genomics service at the Institute of Molecular Genetics. Tuxedo protocol was performed for Genome-guided assembly.

Downstream analysis of RNA-seq

The RNA-seq datasets were visualized using R (v4.0.2). Duplicated genes and genes with zero read counts were removed. The counts per gene were normalized to CPM transformed with log2 using an offset of 1. Expression plots such as box plot, violin plot and density plot were generated using package ggplot2 (v3.3.5). Two-tailed, unpaired *t*-test was performed for statistical significance of comparisons in gene expression visualized in box plots. PCA was performed using package pca3d (v0.10.2). Correlation matrix was visualized using package corrplot (v0.90). For differential expression analysis, package limma (v3.46.0) was used to identify the DEGs in TB and VL groups (N=5 in each group). The cut-off criteria for DEGs were set up with the abs log2FC>1.5 and P-value<0.05. Heatmaps and volcano plots were depicted to visualize the results using the packages pheatmap (v1.0.12), ggplot2 (v3.3.5), dplyr (v1.0.7) and ggrepel (v0.9.1). To prioritize genes of interest, two groups of criteria were established in volcano plots with the abs log2FC_1>1, P-value_1<0.05, and abs log2FC_2>2, P-value_2<0.01. The genes were filtered with settings of the abs log2FC>2 and P-value<0.001 in Heatmap showing ranked genes with highest differential expression.

Tissue processing and histological staining

Embryonic heads were fixed in 4% paraformaldehyde (PFA) overnight at 4°C followed by gradient dehydration in ethanol, xylene clearance, wax immersion and paraffin embedding. Samples were then sectioned at 5-8 µm using a microtome (Leica RM2245) and mounted on the charged slides in series sections. For histological analysis, the slides were stained with Haematoxylin and Eosin (H&E) staining, or trichrome staining (Sirrus Red, Haematoxylin and Alcian Blue) using standard protocols. The Nikon Eclipse 80i light microscope was used to photograph the stained slides.

Immunofluorescence staining

Immunostaining was performed using standard protocols as previously described (Qiu et al., 2020; Qiu and Tucker, 2022). The primary antibodies used on sections were: mouse anti-E-cadherin (Abcam, ab76055, 1/400) and rat anti-BrdU (Abcam, ab6326, 1/500). Secondary antibodies were then used to incubate the sections for 1 h at room temperature (RT) at a dilution of 1/500 in the dark: Alexa Fluor donkey anti-mouse 488 (Invitrogen, A21202) and Alexa Fluor donkey anti-rat 647 (Invitrogen, A21247). Slides were mounted with Fluoroshield containing DAPI (Sigma-Aldrich, SLBV4269) and visualized using a Leica TCS SP5 confocal microscope. For BrdU immunofluorescence staining, the mice were injected with BrdU labelling reagent (30 mg/kg, Life Technologies, 000103) 2 h before collection. For E-cadherin immunofluorescence on slices, rabbit anti-E-cadherin (Abcam, ab15148, 1:100) with secondary Fluor goat anti-rabbit 488 (Invitrogen, A-11008, 1:500). Control groups were set up to confirm immunofluorescence staining. Each antibody analysis was carried out at least three times independently.

Radioactive *in situ* hybridization

Radioactive section *in situ* hybridization was performed as previously described (Wilkinson, 1992; Seppala et al., 2014). RNA probes were synthesized using ^{35}S-UTP, and signals were recognized using silver emulsion, which presents positive signals as white grains when viewed under dark-field. Bright-field and dark-field images were photographed using a Nikon Eclipse 80i light microscope. The images were then merged in Photoshop (Adobe 2020), with the colour in dark-field artificially changed to red. The following restriction and polymerase enzymes were used for plasmid DNA linearization and mRNA probe synthesis; EcorI and T7 for *Shh*, BamHI and T3 for *Ptch1*, EcorI and T7 for *Gas1*, XhoI and T7 for *Cdon*, SalI and T7 for *Boc*. We would like to thank Andrew McMahon (Harvard University, USA) for the *Shh* plasmid, Matthew Scott (Stanford University, USA) for the *Ptch1* plasmid, Chen-Ming Fan (Carnegie Institution of Washington, USA) for the *Gas1* plasmid and Robert Krauss (Icahn School of Medicine at Mount Sinai, USA) for the *Cdon* and *Boc* plasmids.

RNAscope assay

Paraffin-embedded embryonic head sections (5 µm) were processed as described above for multiplex fluorescent *in situ* hybridization. Commercially available Multiplex Fluorescent Reagent Kit v2 (323100, Advanced Cell Diagnostics) and RNAscope probes (1:50; Mm-Gli1, 311001; Mm-Meis1, 436361; Mm-Meis2, 436371; Mm-Cd44, 476201; Mm-Nr4a2, 423351; Mm-Wnt7b, 401131; Mm-Otx1, 536041; Mm-Dlx5, 478151; Mm-Runx2, 414021; Mm-Rspo1-O1, 479591; Mm-Scube1, 488131; Mm-Shh, 314361; Mm-Gas1, 547201; Mm-Ptch1, 402811; Advanced Cell Diagnostics) were used for transcript detection according to the manufacturer's protocol. The hybridized probes were visualized using the fluorescein (NEL741001KT, Perkin Elmer) and TSA-Plus Cyanine 3 (NEL744001KT, Perkin-Elmer) system, according to the manufacturer's protocol. All incubation steps were completed using the ACD HybEZ II Hybridization System (321721) at 40°C. In brief, the slides were deparaffinized in xylene, applied in RNAscope Hydrogen Peroxide (322335) at RT for 10 min and submerged in RNAscope Target Retrieval (322001) at 99°C for 30 min. A hydrophobic barrier was then created to circle the interested areas using the ImmEdge Hydrophobic Barrier Pen (310018). Slides were then incubated with RNAscope Protease III (322340) for 15 min followed by the hybridization, amplification and detection steps according to the protocol. Slides were mounted with Fluoroshield with DAPI (Sigma-Aldrich, SLBV4269) and stored at 4°C in the dark.

Development (2023) 150, dev201464. doi:10.1242/dev.201464

Statistics and reproducibility

Quantification of *Gli1* expression levels from RNAscope is outlined in Fig. S6. Morphometrics of structures were performed using Fiji/ImageJ. The length of the VL was assessed by drawing a line parallel to the curved VL from the top to the end using the line tool in Fiji. The width of the VL was measured by drawing a line parallel to the oral epithelium from the junction of VL and DL to the edge of the buccal VL. Results were plotted in GraphPad Prism software (V.8.0.2). Statistical significance was analyzed by IBM SPSS Statistics software (V.25.0) using two-tailed, unpaired *t*-tests. The *P*-values were considered statistically significant if the *P*-value<0.05, with **P*<0.05, ***P*<0.01 and ****P*<0.001. Error bars represent s.e.m.

Explant culture

Slice culture for the tooth germ was carried out as previously described (Alfaqeeh and Tucker, 2013). In brief, embryonic lower jaws were isolated at E13.5, when a very clear VL/DL bud can be observed. The mandibles were then chopped sagittally at 200 µm using a McIlwain Tissue Chopper, and slices in the incisor region were selected and cultured on permeable filters (pore size 0.4 µm, BD Falcon cell culture inserts) held by a steel mesh in Advanced Dulbecco's Modified Eagle Medium F12 (DMEM F12) (Invitrogen) with 1% penicillin-streptomycin (Sigma-Aldrich, Merck) and 1% Glutamax (Invitrogen). To investigate the role of Shh during VL development, slices were cultured with Shh signalling inhibitor cyclopamine (Sigma-Aldrich) at 20 µM or 50 µM (10 mg/ml stock in ethanol), or SAG (smoothened agonist) (Sigma-Aldrich) at 5 µM (stock dissolved in H_20). The explants were cultured at 5% CO_2 and 37°C for 2 days before harvest. Littermate control groups were set up to compare with the experimental groups and cultured under the same conditions but with carrier alone. Litter age can vary depending on mating time, so cultures were only compared within litters. Slices were photographed at day 0 and day 2 using a Leica dissecting microscope to record the morphology. All experiments were repeated more than six times for SAG and 50 µM cyclopamine, and four times for 20 µM cyclopamine.

Acknowledgements

We thank Chen-Ming Fan (Carnegie Institution of Washington) for generously providing us with the *Gas1* mutant line and compound mutant embryos.

Competing interests

The authors declare no competing or financial interests.

Author contributions

Conceptualization: M.H., M.B., A.S.T.; Methodology: T.Q., B.H., M.S., M.T.C., Z.C., M.H., A.S.T.; Formal analysis: T.Q., B.H., M.H., M.B.; Investigation: T.Q., B.H., M.S., M.H.; Resources: M.S., M.T.C., Z.C., A.S.T.; Data curation: M.S., M.H., M.B.; Writing - original draft: T.Q.; Writing - review & editing: M.T.C., Z.C., M.H., M.B., A.S.T.; Supervision: Z.C., M.B., A.S.T.; Project administration: A.S.T.; Funding acquisition: T.Q., Z.C., M.B., A.S.T.

Funding

This work was funded by a grant from the Grantová Agentura České Republiky (21-04178S) awarded to A.S.T. and M.B. Transcriptomics was supported by a previous grant (18-04859S). Additional funds were provided by the National Natural Science Foundation of China (NSFC82230029) and an Open Research Fund Program grant (Hubei-MOST KLOS & KLOBM 2020-04) from Wuhan University to T.Q., A.S.T. and Z.C. T.Q. was funded by the China Scholarship Council as part of a PhD studentship at King's College London. M.T.C. and M.S. are funded by a research grant from the European Orthodontic Society.

Data availability

The transcriptomic dataset used in this study is publicly available at Facebase (https://www.facebase.org/) (Tucker et al., 2023).

Peer review history

The peer review history is available online at https://journals.biologists.com/dev/lookup/doi/10.1242/dev.201464.reviewer-comments.pdf.

References

Alfaqeeh, S. A. and Tucker, A. S. (2013). The slice culture method for following development of tooth germs in explant culture. *J. Vis. Exp.* e50824.

Allen, B. L., Song, J. Y., Izzi, L., Althaus, I. W., Kang, J. S., Charron, F., Krauss, R. S. and Mcmahon, A. P. (2011). Overlapping roles and collective requirement for the coreceptors GAS1, CDO, and BOC in SHH pathway function. *Dev. Cell* **20**, 775-787. doi:10.1016/j.devcel.2011.04.018

Bolk, L. (1921). Odontological Essays. *J. Anat.* **55**, 219-234.

Bruel, A.-L., Levy, J., Elenga, N., Defo, A., Favre, A., Lucron, H., Capri, Y., Perrin, L., Passemard, S., Vial, Y. et al. (2018). INTU-related oral-facial-digital syndrome type VI: A confirmatory report. *Clin. Genet.* **93**, 1205-1209. doi:10.1111/cge.13238

Buchtová, M., Handrigan, G. R., Tucker, A. S., Lozanoff, S., Town, L., Fu, K., Diewert, V. M., Wicking, C. and Richman, J. M. (2008). Initiation and patterning of the snake dentition are dependent on Sonic Hedgehog signaling. *Dev. Biol.* **319**, 132-145. doi:10.1016/j.ydbio.2008.03.004

Caparrós-Martín, J. A., Valencia, M., Reytor, E., Pacheco, M., Fernandez, M., Perez-Aytes, A., Gean, E., Lapunzina, P., Peters, H., Goodship, J. A. et al. (2013). The ciliary EVC/EVC2 complex interacts with smo and controls hedgehog pathway activity in chondrocytes by regulating Sufu/Gli3 dissociation and Gli3 trafficking in primary cilia. *Hum. Mol. Genet.* **22**, 124-139. doi:10.1093/hmg/dds409

Cobourne, M. T., Miletich, I. and Sharpe, P. T. (2004). Restriction of sonic hedgehog signalling during early tooth development. *Development* **131**, 2875-2885. doi:10.1242/dev.01163

Danielian, P. S., Muccino, D., Rowitch, D. H., Michael, S. K. and Mcmahon, A. P. (1998). Modification of gene activity in mouse embryos in utero by a tamoxifen-inducible form of cre recombinase. *Curr. Biol.* **8**, 1323-1326. doi:10.1016/S0960-9822(07)00562-3

Echevarrıá-Andino, M. L. and Allen, B. L. (2020). The hedgehog co-receptor BOC differentially regulates SHH signaling during craniofacial development. *Development (Camb.)* **147**, dev189076. doi:10.1242/dev.189076

Heuzé, Y., Singh, N., Basilico, C., Jabs, E. W., Holmes, G. and Richtsmeier, J. T. (2014). Morphological comparison of the craniofacial phenotypes of mouse models expressing th Apert FGFR2 S252W muation in neural crest or mesoderm derived tissues. *Bone* **63**, 1001-1109. doi:10.1016/j.bone.2014.03.003

Hovorakova, M., Lesot, H., Peterka, M. and Peterkova, R. (2005). The developmental relationship between the deciduous dentition and the oral vestibule in human embryos. *Anat. Embryol.* **209**, 303-313. doi:10.1007/s00429-004-0441-y

Hovorakova, M., Lesot, H., Vonesch, J.-L., Peterka, M. and Peterkova, R. (2007). Early development of the lower deciduous dentition and oral vestibule in human embryos. *Eur. J. Oral Sci.* **115**, 280-287. doi:10.1111/j.1600-0722.2007.00464.x

Hovorakova, M., Lochovska, K., Zahradnicek, O., Domonkosova Tibenska, K., Dornhoferova, M., Horakova-Smrckova, L. and Bodorikova, S. (2016). One odontogenic cell-population contributes to the development of the mouse incisors and of the oral vestibule. *PLoS ONE* **11**, e0162523. doi:10.1371/journal.pone.0162523

Hovorakova, M., Zahradnicek, O., Bartos, M., Hurnik, P., Stransky, J., Stembirek, J. and Tucker, A. S. (2020). Reawakening of ancestral dental potential as a mechanism to explain dental pathologies. *Integr. Comp. Biol.* **60**, 619-629. doi:10.1093/icb/icaa053

Izzi, L., Lévesque, M., Morin, S., Laniel, D., Wilkes, B. C., Mille, F., Krauss, R. S., Mcmahon, A. P., Allen, B. L. and Charron, F. (2011). Boc and Gas1 each form distinct Shh receptor complexes with Ptch1 and are required for Shh-mediated cell proliferation. *Dev. Cell* **20**, 788-801. doi:10.1016/j.devcel.2011.04.017

Jin, S., Martinelli, D. C., Zheng, X., Tessier-Lavigne, M. and Fan, C. M. (2015). Gas1 is a receptor for sonic hedgehog to repel enteric axons. *Proc. Natl. Acad. Sci. USA* **112**, E73-E80. doi:10.1073/pnas.1418629112

Kantaputra, P. N., Wangtiraumnuay, N., Ngamphiw, C., Olsen, B., Intachai, W., Tucker, A. S. and Tongsima, S. (2022). Cryptophthalmos, dental anomalies, oral vestibule defect, and a novel FREM2 mutation. *J. Hum. Genet.* **67**, 115-118. doi:10.1038/s10038-021-00972-4

Kawasaki, M., Porntaveetus, T., Kawasaki, K., Oommen, S., Otsuka-Tanaka, Y., Hishinuma, M., Nomoto, T., Maeda, T., Takubo, K., Suda, T. et al. (2014). R-spondins/Lgrs expression in tooth development. *Dev. Dyn.* **243**, 844-851. doi:10.1002/dvdy.24124

Kus-Bartoszek, A., Lipski, M., Jarzä…Bek, A., Manowiec, J. and Droździk, A. (2022). Gingival phenotype changes and the prevalence of mucogingival deformities during the early transitional dentition phase—a two-year longitudinal study. *Int. J. Environ. Res. Public Health* **19**, 3899. doi:10.3390/ijerph19073899

Lee, C. S., Buttitta, L. and Fan, C. M. (2001a). Evidence that the WNT-inducible growth arrest-specific gene 1 encodes an antagonist of sonic hedgehog signaling in the somite. *Proc. Natl. Acad. Sci. U.S.A.* **98**, 11347-11352. doi:10.1073/pnas.201418298

Lee, C. S., May, N. R. and Fan, C. M. (2001b). Transdifferentiation of the ventral retinal pigmented epithelium to neural retina in the growth arrest specific gene 1 mutant. *Dev. Biol.* **236**, 17-29. doi:10.1006/dbio.2001.0280

Li, J., Chatzeli, L., Panousopoulou, E., Tucker, A. S. and Green, J. B. A. (2016). Epithelial stratification and placode invagination are separable functions in early morphogenesis of the molar tooth. *Development (Camb.)* **143**, 670-681. doi:10.1242/dev.130187

Martinelli, D. C. and Fan, C. M. (2007). Gas1 extends the range of Hedgehog action by facilitating its signaling. *Genes Dev.* **21**, 1231-1243. doi:10.1101/gad.1546307

Miletich, I., Yu, W.-Y., Zhang, R., Sharpe, P. T., Caixeta De Andrade, S., Pereira, S. F. A., Ohazama, A., Mock, O. B., Buchner, G., Sealby, J. et al. (2011). Developmental stalling and organ-autonomous regulation of morphogenesis. *Proc. Natl. Acad. Sci. USA* **108**, 19270-19275. doi:10.1073/pnas.1112801108

Okada, A., Charron, F., Morin, S., Shin, D. S., Wong, K., Fabre, P. J., Tessier-Lavigne, M. and Mcconnell, S. K. (2006). Boc is a receptor for sonic hedgehog in the guidance of commissural axons. *Nature* **444**, 369-373. doi:10.1038/nature05246

Pavlikova, H., Witter, K. and Misek, I. (1999). Primordium of the upper vestibulum oris in the domestic sheep. *Acta Veterinaria Brno* **68**, 175-178. doi:10.2754/avb199968030175

Penon-Portmann, M., Eldomery, M. K., Potocki, L., Marafi, D., Posey, J. E., Coban-Akdemir, Z., Harel, T., Grochowski, C. M., Loucks, H., Devine, W. P. et al. (2022). De novo heterozygous variants in SLC30A7 are a candidate cause for Joubert syndrome. *Am. J. Med. Genet. A* **188**, 2360-2366. doi:10.1002/ajmg.a.62872

Peterková, R. (1985). The common developmental origin and phylogenetic aspects of teeth, rugae palatinae, and fornix vestibuli oris in the mouse. *J. Craniofac. Genet. Dev. Biol.* **5**, 89-104.

Placek, M., Mskach, M. and Mrklas, L. (1974). Significance of the labial frenum attachment in periodontal disease in man. Part 1. Classification and epidemiology of the labial frenum attachment. *J. Periodontol.* **45**, 891-894. doi:10.1902/jop.1974.45.12.891

Popa, E. M., Buchtova, M. and Tucker, A. S. (2019). Revitalising the rudimentary replacement dentition in the mouse. *Development* **146**, dev171363. doi:10.1242/dev.171363

Qiu, T. and Tucker, A. S. (2022). Mechanisms driving vestibular lamina formation and opening in the mouse. *J. Anat.* **242**, 224-234. doi:10.1111/joa.13771

Qiu, T., Teshima, T. H. N., Hovorakova, M. and Tucker, A. S. (2020). Development of the vestibular lamina in human embryos: morphogenesis and vestibule formation. *Front. Physiol.* **11**, 753. doi:10.3389/fphys.2020.00753

Ruiz-Perez, V. L., Blair, H. J., Rodriguez-Andres, M. E., Blanco, M. J., Wilson, A., Liu, Y.-N., Miles, C., Peters, H. and Goodship, J. A. (2007). Evc is a positive mediator of Ihh-regulated bone growth that localises at the base of chondrocyte cilia. *Development* **134**, 2903-2912. doi:10.1242/dev.007542

Sanz-Navarro, M., Delgado, I., Torres, M., Mustonen, T., Michon, F. and Rice, D. P. (2019). Dental epithelial sem cells express he developmental regulator Meis1. *Front. Physiol.* **10**, 249. doi:10.3389/phys.2019.00249

Sarkar, L., Cobourne, M., Naylor, S. and Sharpe, P. T. (2000). Wnt/Shh interactions regulate ectodermal boundary formation during mammalian tooth development. *Proc. Natl. Acad. Sci. USA* **97**, 4520-4524. doi:10.1073/pnas.97.9.4520

Sasalawad, S. S., Hugar, S. M., Poonacha, K. S. and Mallikarjuna, R. (2013). Ellis-van Creveld syndrome. *BMJ Case Rep.* **2013**, bcr2013009463. doi:10.1136/bcr-2013-009463

Schour, I. (1929). Early human tooth development, with special reference to the relationship between the dental lamina and the lip-furrow band. *J. Dent. Res.* **9**, 699-717. doi:10.1177/00220345290090050801

Seppala, M., Depew, M. J., Martinelli, D. C., Fan, C.-M., Sharpe, P. T. and Cobourne, M. T. (2007). Gas1 is a modifier for holoprosencephaly and genetically interacts with sonic hedgehog. *J. Clin. Investig.* **117**, 1575-1584. doi:10.1172/JCI32032

Seppala, M., Xavier, G. M., Fan, C.-M. and Cobourne, M. T. (2014). Boc modifies the spectrum of holoprosencephaly in the absence of Gas1 function. *Biology Open* **3**, 728-740. doi:10.1242/bio.20147989

Seppala, M., Fraser, G., Birjandi, A., Xavier, G. and Cobourne, M. (2017). Sonic hedgehog signaling and development of the dentition. *Journal of Developmental Biology* **5**, 6. doi:10.3390/jdb5020006

Seppala, M., Thivichon-Prince, B., Xavier, G. M., Shaffie, N., Sangani, I., Birjandi, A. A., Rooney, J., Lau, J. N. S., Dhaliwal, R., Rossi, O. et al. (2022). Gas1 regulates patterning of the murine and human dentitions through sonic hedgehog. *J. Dent. Res.* **101**, 473-482. doi:10.1177/00220345211049403

Soukup, V., Tazaki, A., Yamazaki, Y., Pospisilova, A., Epperlein, H.-H., Tanaka, E. M. and Cerny, R. (2021). Oral and palatal dentition of axolotl arises from a common tooth-competent zone along the ecto-endodermal boundary. *Front. Cell Dev. Biol.* **8**, 622308. doi:10.3389/fcell.2020.622308

Tenzen, T., Allen, B. L., Cole, F., Kang, J.-S., Krauss, R. S. and Mcmahon, A. P. (2006). The cell surface membrane proteins cdo and boc are components and targets of the hedgehog signaling pathway and feedback network in mice. *Dev. Cell* **10**, 647-656. doi:10.1016/j.devcel.2006.04.004

Tucker, A. S. (2010). Salivary gland adaptations: modification of the glands for novel uses. In *Salivary Glands*, pp. 21-31. Basel: Karger.

Tucker, A. S., Qiu, T., Buchtová, M. and Hovořáková, M. (2023). Transcriptional profiles (RNA-seq) of incisor tooth germ and adjacent vestibular lamina of E14 murine embryos. *FaceBase Consortium* doi:10.25550/2T-8JMG

Visel, A., Thaller, C. and Eichele, G. (2004). GenePain.org: an atlas of gene expression paterns in the mouse embryo. *Nuclie Acids Res.* **32**, D552-D556. doi:10.1093/nar/gkh029

Vonk, F. J., Admiraal, J. F., Jackson, K., Reshef, R., De Bakker, M. A. G., Vanderschoot, K., Van Den Berge, I., Van Atten, M., Burgerhout, E., Beck, A. et al. (2008). Evolutionary origin and development of snake fangs. *Nature* **454**, 630-633. doi:10.1038/nature07178

Wang, X. P., O'connell, D. J., Lund, J. J., Saadi, I., Kuraguchi, M., Turbe-Doan, A., Cavallesco, R., Kim, H., Park, P. J., Harada, H. et al. (2009). Apc inhibition of Wnt signaling regulates supernumerary tooth formation during embryogenesis and throughout adulthood. *Development* **136**, 1939-1949. doi:10.1242/dev.033803

Wilkinson, D. G. (1992). *In Situ Hybridisation: A Practical Approach*. Oxford: IRL Press.

Witter, K., Pavlikova, H., Matulova, P. and Misek, I. (2005). Relationship between vestibular lamina, dental lamina, and the developing oral vestibule in the upper jaw of the field vole (Microtus agrestis, Rodentia). *J. Morphol.* **265**, 264-270. doi:10.1002/jmor.10356

Xavier, G. M., Sharpe, P. T. and Cobourne, M. T. (2009). Scube1 is expressed during facial development in the mouse. *J. Exp. Zool. B Mol. Dev. Evol.* **312**, 518-524. doi:10.1002/jez.b.21260

Yu, W., Sun, Z., Sweat, Y., Sweat, M., Venugopalan, S. R., Eliason, S., Cao, H., Paine, M. L. and Amendt, B. A. (2020). Pitx2-Sox2-Lef1 interactions specify progenitor oral/dental epithelial cell signaling centers. *Development (Camb.)* **147**, dev186023. doi:10.1242/DEV.186023

Zhao, Z., Stock, D. W., Buchanan, A. V. and Weiss, K. M. (2000). Expression of Dlx genes during the development of the murine dentition. *Dev. Genes Evol.* **210**, 270-275. doi:10.1007/s004270050314

Supplementary Figure 1 |
Distribution features of the normalized read counts (Cpm) of VL (N=5) and TB (N=5) from the RNA-seq dataset. (**A**) boxplot, (**B**) violin plot, and (**C**) density plot showed consistent distributions of VL and TB expression. (**D**) Correlation plot. Higher correlation between the transcriptomic data of VL-VL and TB-TB were observed when compared to TB-VL. (**E**) Vimentin, a mesenchymal marker, showing similar expression between the dissected VL and TB. (**F**) *Cdh1*, an epithelial marker, showing no significant expression differences in the dissected VL and TB. VL: vestibular lamina; TB: tooth bud.

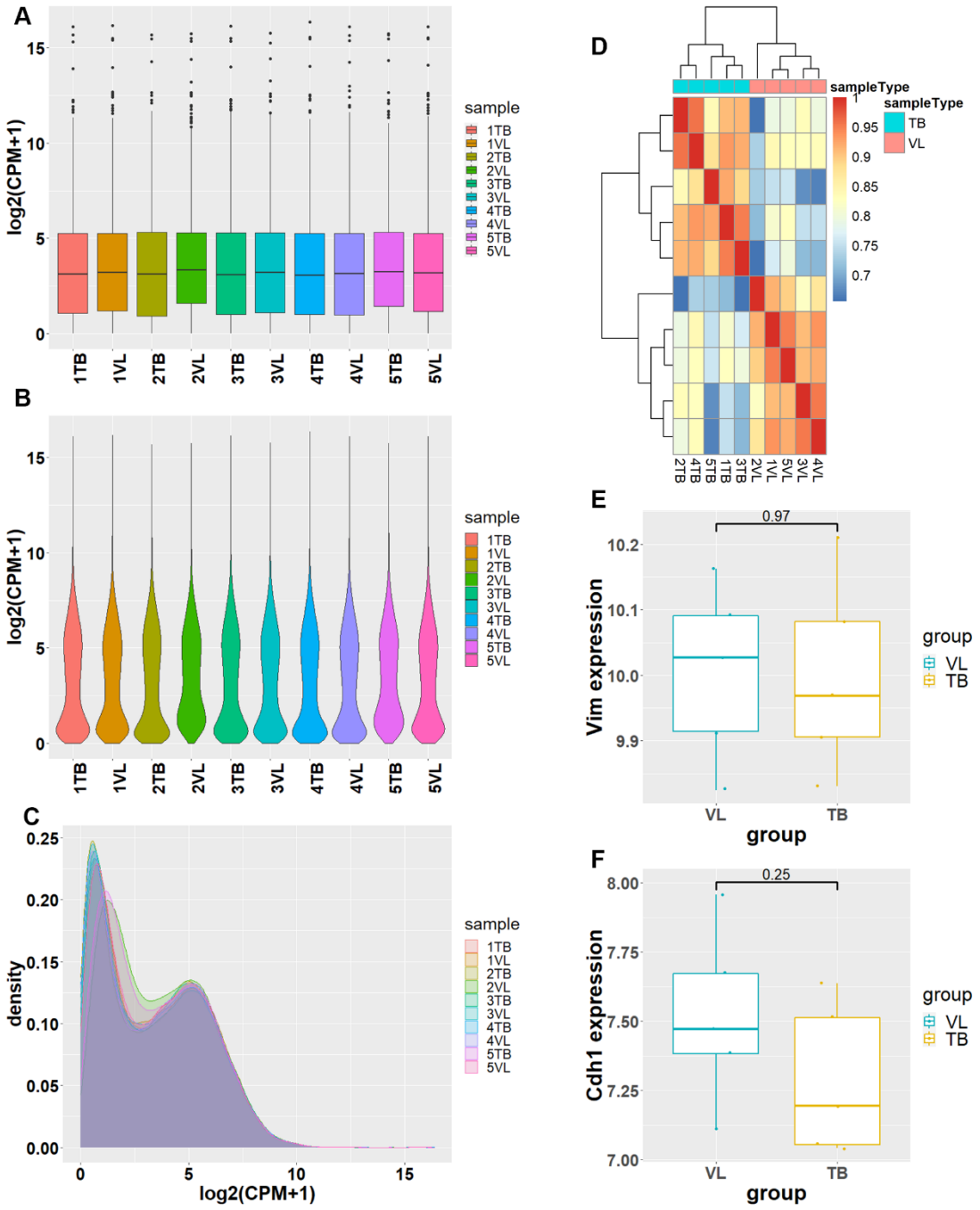

Supplementary Figure 2 |
Highlighted genes in the tooth germ at E14.5.
(**A, C, E, G**) Box plots of genes highlighted as being differentially expressed in the tooth germ. Unpaired t-tests were performed in R to assess statistical significance. N = 5VL and 5TB. *Dlx5*, *Runx2*, *Rspo1*, and *Scube1* were significantly expressed in the TB compared to the expression in the VL. (**B, B', D, D', F, F', H, H'**) Mouse sagittal sections through the anterior lower incisor tooth germ. RNAscope performed for the identification of TB markers. (**B, B'**) *Dlx5*, (**D, D'**) *Runx2*, (**F, F'**) *Rspo1*, (**H, H'**) *Scube1*. (**B', D', F', H'**) Higher power view of white boxes labeled areas (**b', d', f', h'**) in (**B, D, F, H**). Magenta and white dashed lines outlined the VL and TB respectively. VL: vestibular lamina; TB: tooth bud. Scale bars in (**B, D, F, H**) = 100 μm. Scale bars in (**B', D', F', H'**) = 50 μm. Lingual-labial axes shown in H, same plane for all images.

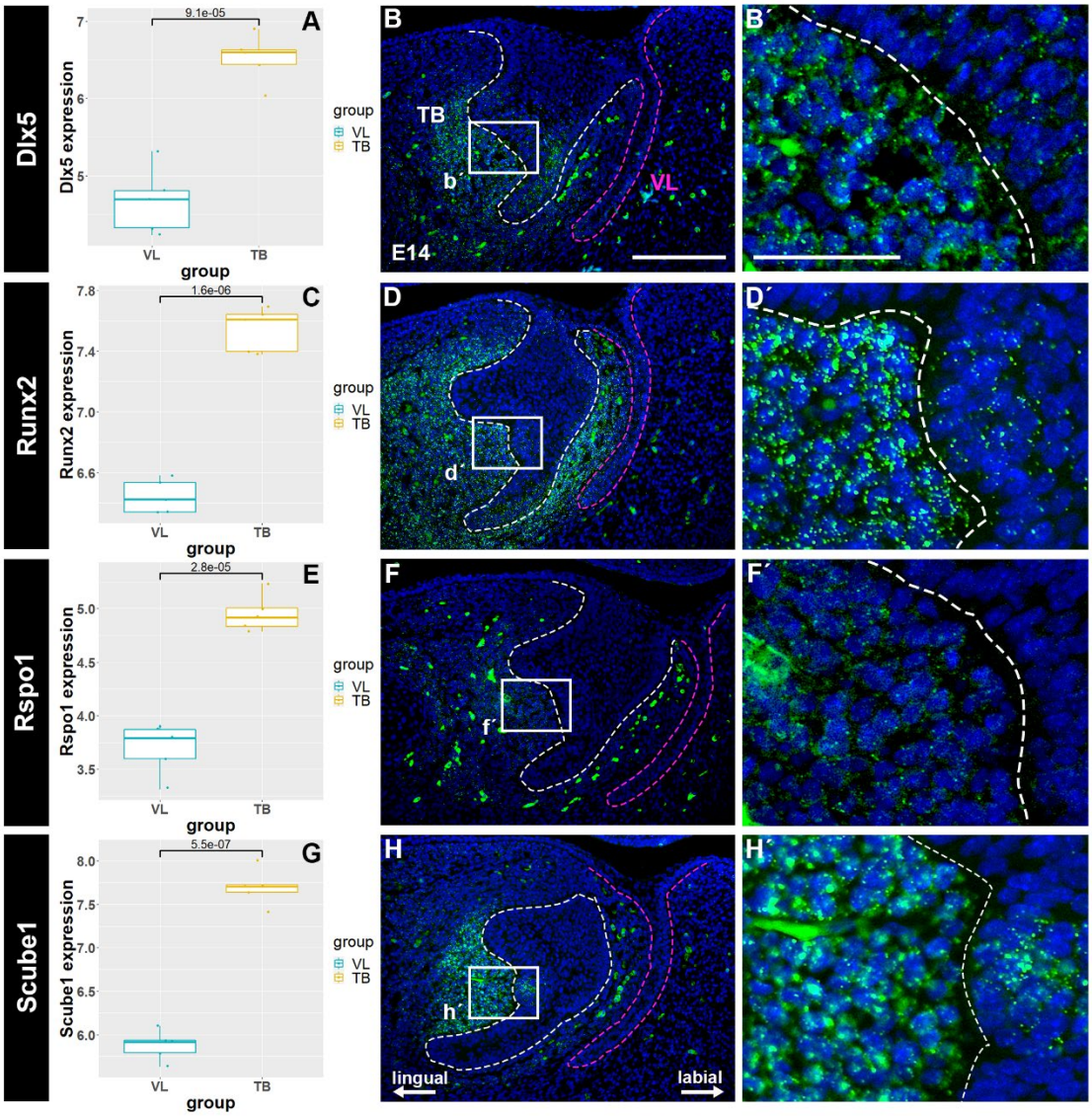

Supplementary Figure 3 |
The expression pattern of novel markers of the VL at E14.
(**A, C, E, G, I, K**) Box plots of genes highlighted as being differentially expressed in the vestibular lamina. Unpaired t-tests were performed in R to assess statistical significance. N = 5VL and 5TB. The expression levels of *Meis1*, *Meis2*, *Cd44*, *Nr4a2*, *Wnt7b*, and *Otx1* in the VL were significantly higher than in the TB. (**B, B', D, D', F, F', H, H', J, J', L, L'**) Mouse sagittal sections through the anterior lower incisor tooth germ. RNAscope performed for the identification of VL markers. (**B, B'**) *Meis1*, (**D, D'**) *Meis2*, (**F, F'**) *Cd44*, (**H, H'**) *Nr4a2*, (**J, J'**) *Wnt7b*, (**L, L'**) *Otx1*. The magenta arrowheads in L' pointed out the strong expression of *Otx1* on the labial side of the VL. (**B', D', F', H', J', L'**) Higher power view of white boxes labeled areas (**b', d', f', h', j', l'**) in (**B, D, F, H, J, L**). Magenta and white dashed lines outlined the VL and TB respectively. VL: vestibular lamina; TB: tooth bud. Yellow dashed lines divided the VL into two parts: labial side of VL (La), and lingual side of the VL (Li). Scale bars in (**B, D, F, H, J, L**) = 100 μm. Scale bars in (**B', D', F', H', J', L'**) = 50 μm. Lingual-labial axes shown in L, same plane for all images.

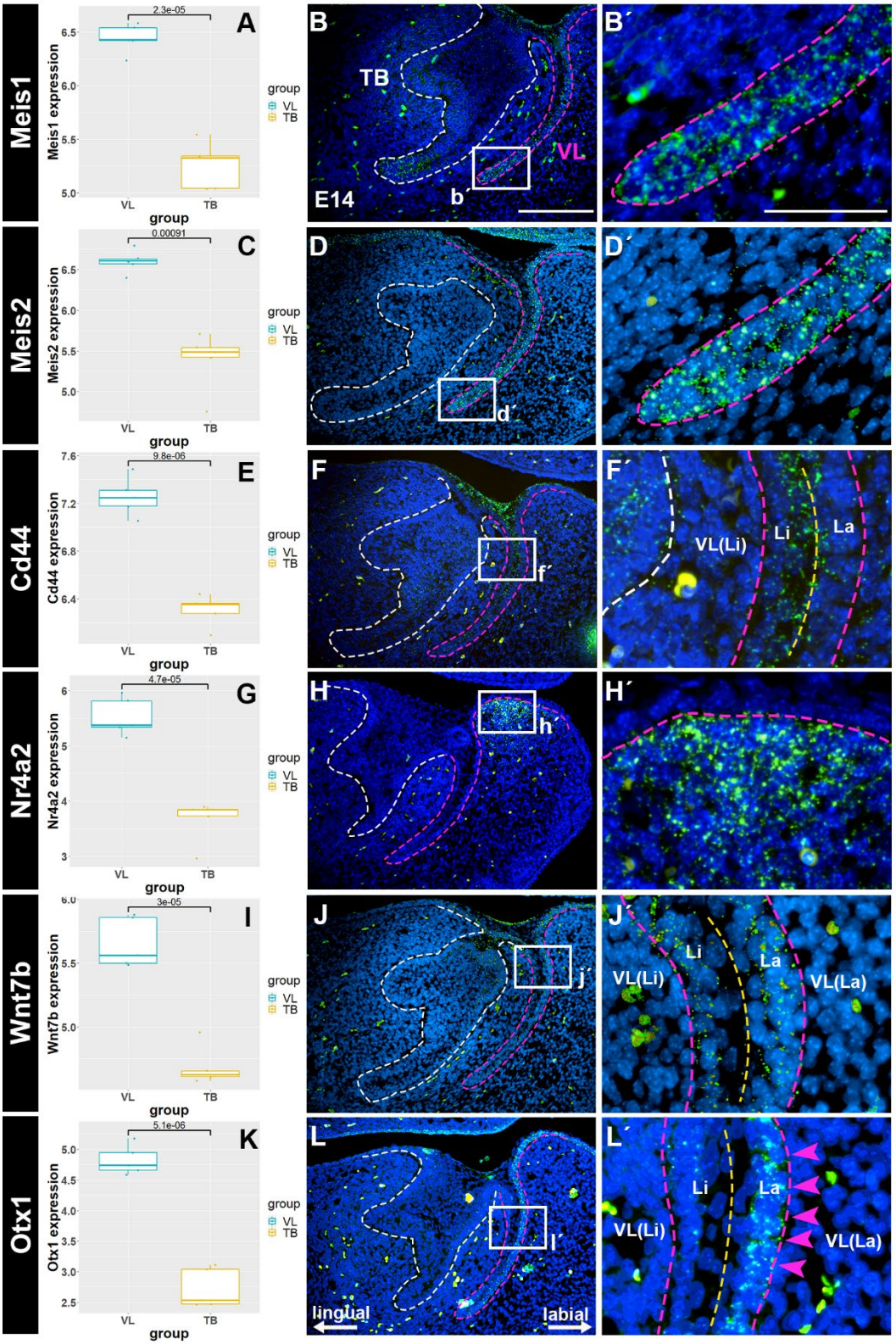
Meis1
Meis1 expression
2.3e-05
A
group
VL
TB
B
TB
VL
E14
b´
B´
Meis2
Meis2 expression
0.00091
C
D
d´
D´
Cd44
Cd44 expression
9.8e-06
E
F
f´
F´
VL(Li)
Li
La
Nr4a2
Nr4a2 expression
4.7e-05
G
H
h´
H´
Wnt7b
Wnt7b expression
3e-05
I
J
j´
J´
VL(La)
Otx1
Otx1 expression
5.1e-06
K
L
l´
L´
lingual
labial

Supplementary Figure 4 |
Molecular signature of the murine VL at E14.5.
Sagittal sections through the anterior incisor area of the mouse at E14.5 (background strains used C57BL/6J and NMRI). (**A-T**) Expression of *Otx1*, *CD44*, *Oxtr*, *Wnt9b*, *Wnt7b*, *Meis1*, *Meis2*, *Abca8b*, *Serpinb3a*, *lrrn1*, *Ace2*, *Klhl14*, *Nr4a2*, *Kera*, *Hey2*, *Gas1*, *Gdf10*, *Sned1*, *Osr1*, *Ramp3* in the murine oral cavity. (**A'**) *Otx1*. Higher power of (A) of the lower incisor tooth bud (TB) and vestibular lamina (VL), showing the strong expression of *Otx1* in the buccal side of the VL. The green dashed line labeled the VL, and the white dashed line labeled the lower incisor TB. (**B'-H'**) Higher magnification of (B-H) of the lower incisor TB and VL, showing the *CD44*, *Oxtr*, *Wnt9b*, *Wnt7b*, *Meis1*, *Meis2*, *Abca8b* were mainly expressed in the whole epithelial VL. (**I'-N'**) Higher magnification of (I-N) of the lower incisor TB and VL, showing robust expression of *Serpinb3a*, *lrrn1*, *Ace2*, *Klhl14*, *Nr4a2*, *Kera* at the top of epithelial or/and mesenchymal VL. (**O', P'**) Higher power of (O, P) of the incisor TB and VL, high expression of *Hey2* and *Gas1* in the buccal VL and mesenchyme were observed. (**Q'-T'**) Higher power of (Q-T) of the lower incisor TB and VL with strong expression of *Gdf10*, *Sned1*, *Osr1*, *Ramp3* in the mesenchyme surrounding the buccal side of the VL. (**U**) Table of gene expression. VL: vestibular lamina; TB: tooth bud; T: tongue. Mes: mesenchyme. Images from https://gp3.mpg.de/ (Visel et al., 2004).

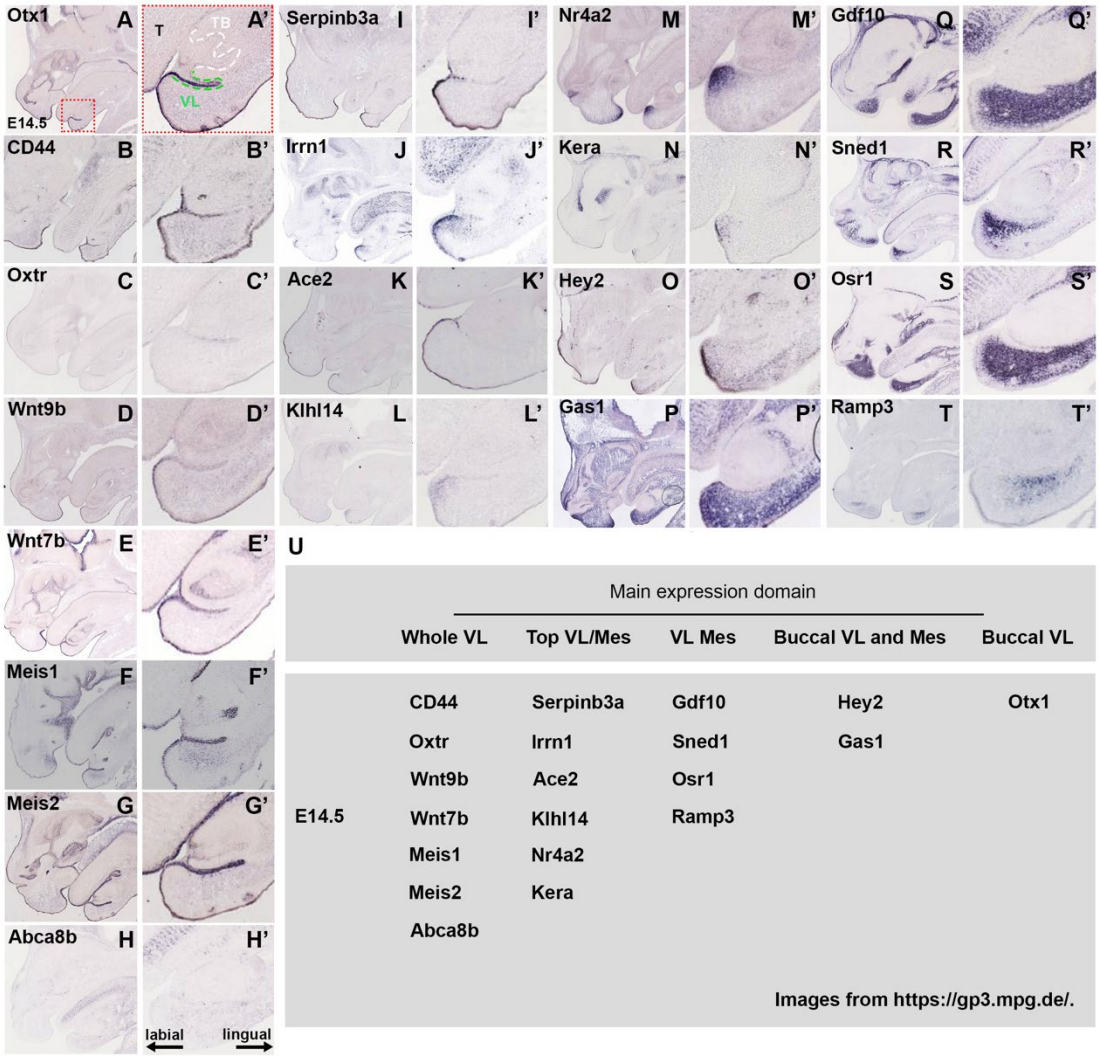

U

	Main expression domain				
	Whole VL	Top VL/Mes	VL Mes	Buccal VL and Mes	Buccal VL
E14.5	CD44	Serpinb3a	Gdf10	Hey2	Otx1
	Oxtr	Irrn1	Sned1	Gas1	
	Wnt9b	Ace2	Osr1		
	Wnt7b	Klhl14	Ramp3		
	Meis1	Nr4a2			
	Meis2	Kera			
	Abca8b				

Images from https://gp3.mpg.de/.

Supplementary Figure 5 |
Expression of Shh pathway genes in the VL and TB at E14.
(**A, D**) Box plots of genes highlighted from the Hedgehog pathway. Unpaired t-tests were performed in R to assess statistical significance. N = 5VL and 5TB. The expression levels of *Shh* was significantly higher in the TB, while *Gas1* was higher in the VL. (**B, C, E, F**) Mouse sagittal sections through the anterior lower incisor tooth germ. RNAscope performed for Hh pathway genes. (**B, C**) *Shh*. *Shh* expression was restricted to the enamel knot, showing statistically higher expression in the TB when compared to the neighboring VL. (**E, F**) *Gas1*. *Gas1* was mainly expressed in the VL, with the magenta arrowheads pointing out the robust expression in the labial side of the VL. (**C, F**) Higher magnification of white boxes labeled regions (**c, f**) in (**B, E**). VL and TB were contoured by magenta and white dashed lines respectively. VL: vestibular lamina; TB: tooth bud. Yellow dashed line divided the VL into two parts: labial side of VL (La), and lingual side of the VL (Li). Scale bars in (**B, E**) = 100 μm. Scale bars in (**C, F**) = 50 μm. Lingual-labial axes shown in B, same plane for all images.

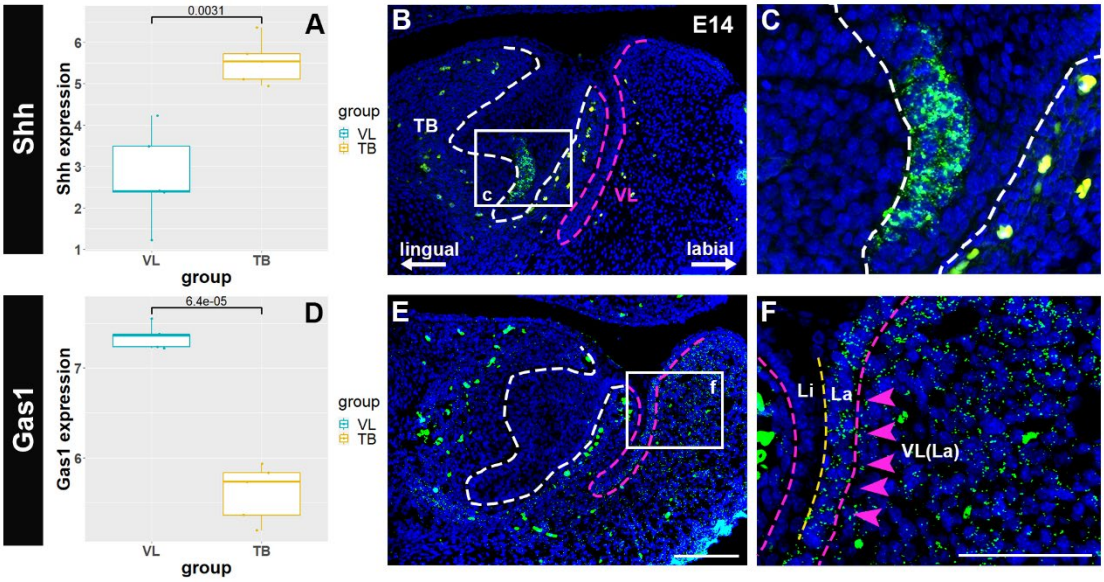

Supplementary Figure 6 |
Quantification of *Gli1* expression levels by RNAscope.
Frontal sections of the VL and TB at E13.5. (**A-F**) Dapi (grey). (**A-C**) Litter mate controls (N=3); (**D-F**) *Gas1* homozygous mutants (N=3). (**G-L**) *Gli1* (magenta). (**G-I**) Litter mate controls (N=3); (**J-L**) *Gas1* homozygous mutants (n=3). VL was contoured by green lines and the VL was divided into buccal (B) and lingual (L) parts by red dashed lines. The yellow/blue boxes define the selected regions (of the same volume) for counting of the *Gli1* expression on the buccal and lingual sides of the VL. VL: vestibular lamina. Scale bars in (**A-L**) = 50 µm. Buccal-lingual axes shown in J, same plane for all images.

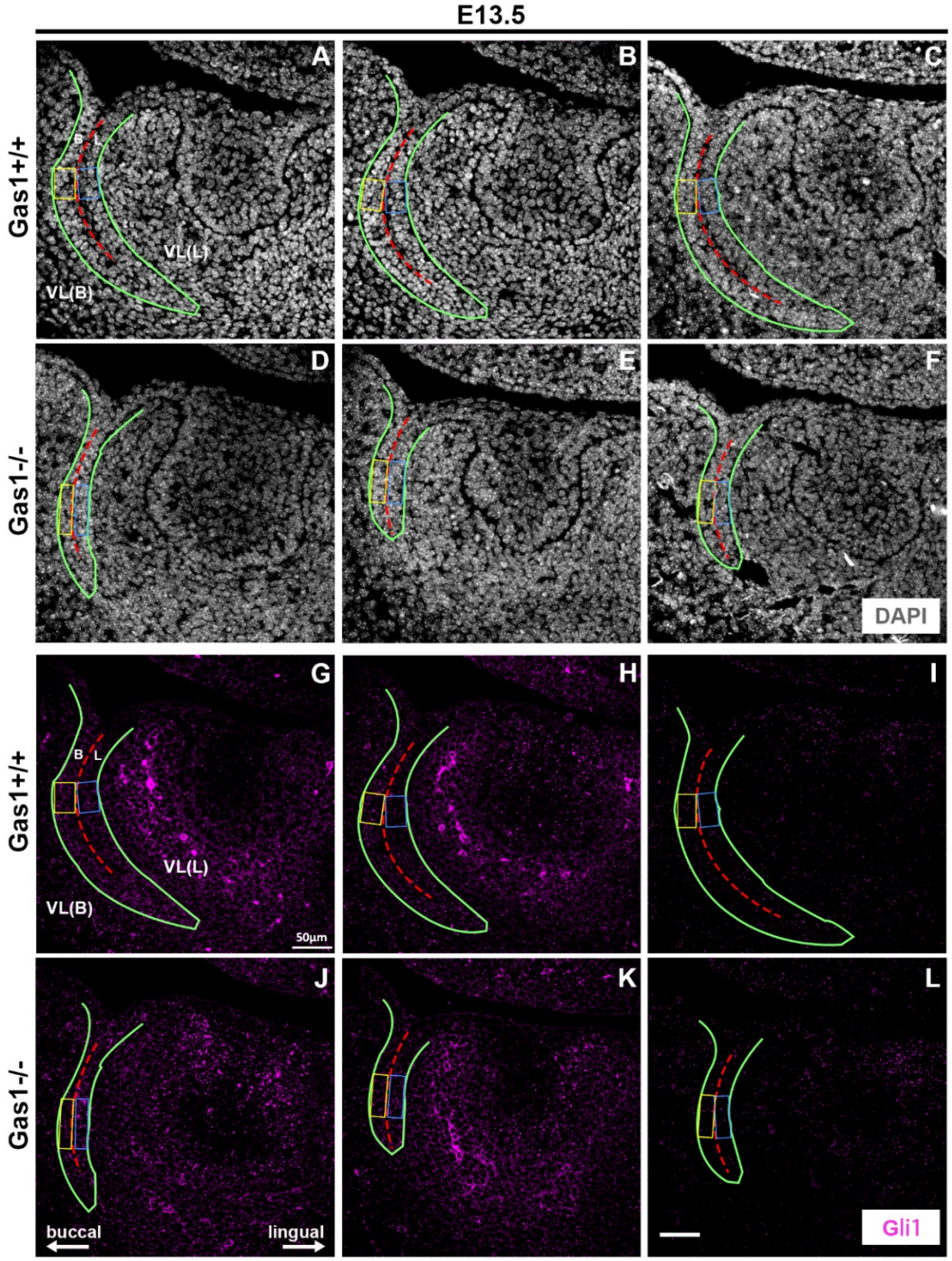

Supplementary Figure 7 |
No consistent change in VL length after treatment of explant slices with 20μM cyclopamine at E13.5.
Sagittal slices through incisor region of mouse embryonic mandibles at E13.5. (**A1, C1, E1, G1; B1, D1, F1, H1, I1**) Day0. (**A2, C2, E2, G2; B2, D2, F2, H2, I2**) Day2 (48 h culture). (**A, C, E, G**) Control carrier only group. Black arrowhead points out the developing whisker follicles after 2 days' culture in the control group. (**B, D, F, H, I**) Cyclopamine-treated groups (20μM). Magenta arrowheads point out the less well-developed whisker follicles after 2 days in culture with 20μM cyclopamine; while the VL showed no consistent phenotype. VL and TB were outlined by green and white dashed lines respectively in A1. VL: vestibular lamina; TB: tooth bud. Scale bars in (**A**) = 300 μm. Same scale in all images. Labial-lingual axes shown in I2, same plane for all images.

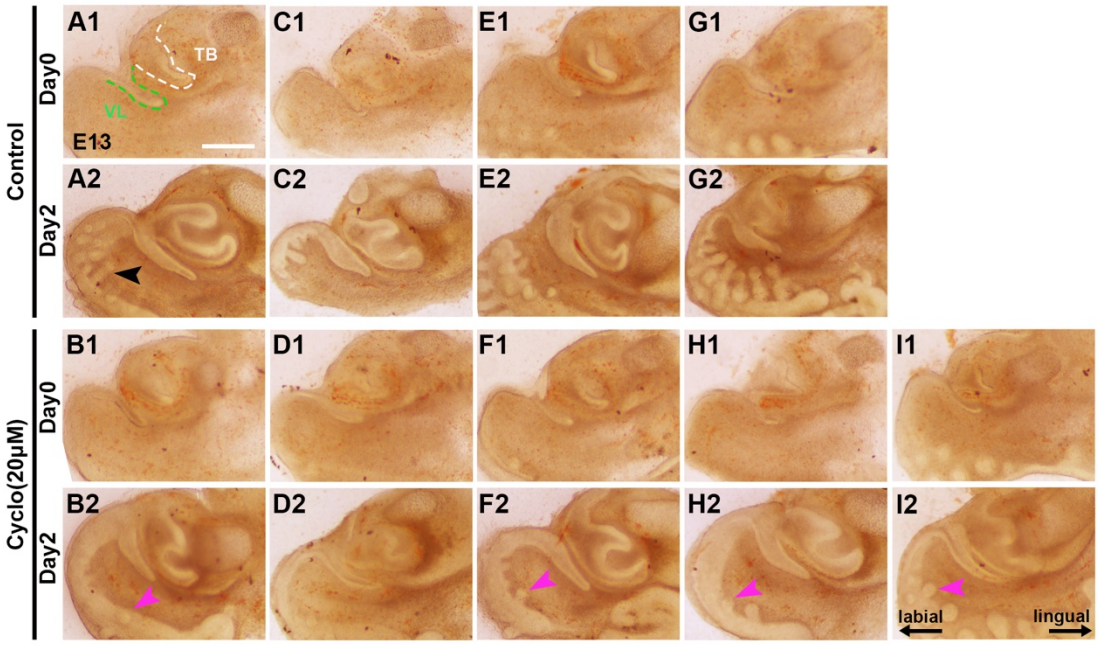

Supplementary Figure 8 |
Shorter VL in 50µM cyclopamine treated slices.
Sagittal slices through incisor region of mouse embryonic mandibles at E13.5. (**A1, C1, E1, G1, I1, K1; B1, D1, F1, H1, J1, L1**) Day0. (**A2, C2, E2, G2, I2, K2; B2, D2, F2, H2, J2, L2**) Day2 (48 h culture). (**A, C, E, G, I, K**) Control carrier only group. (**B, D, F, H, J, L**) Cyclopamine-treated groups (50µM). A shorter VL was observed in the cyclopamine-treated groups after 2 days in culture. VL and TB were outlined by green and white dashed lines respectively in A1. VL: vestibular lamina; TB: tooth bud. White arrowheads indicate tip of the VL. Scale bars in (**A**)= 100 µm. Same scale in all images. Labial-lingual axes shown in L2, same plane for all images.

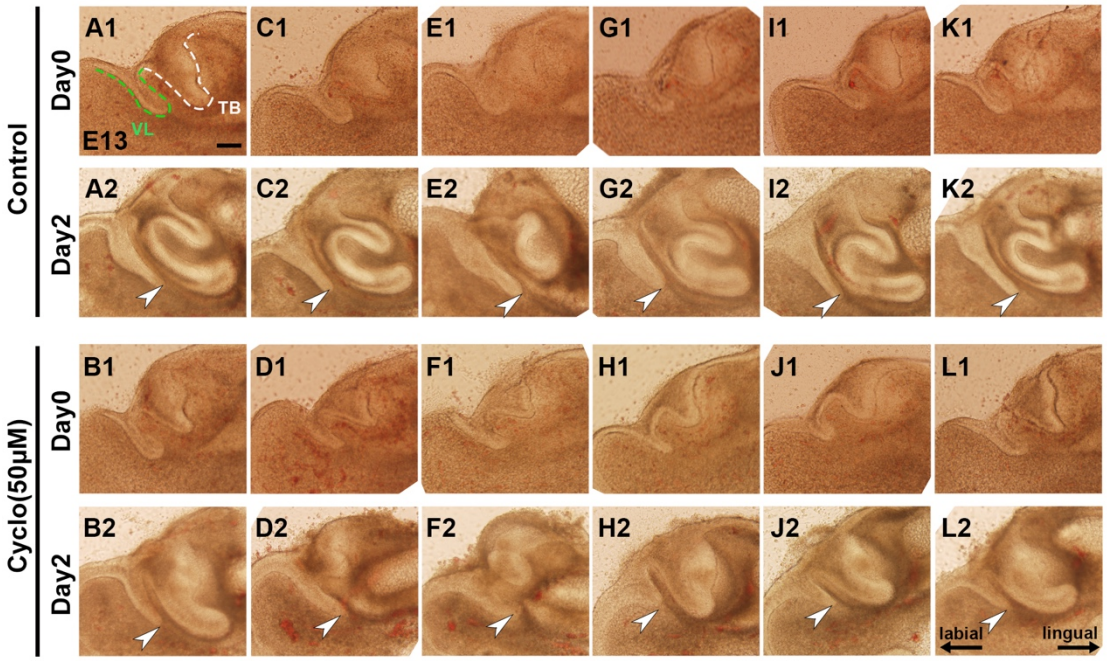

Supplementary Figure 9 |
Thicker VL in SAG-treated slices.
Sagittal slices through incisor region of mouse embryonic mandibles at E13.5. (**A1, C1, E1, G1, I1, K1, M1; B1, D1, F1, H1, J1, L1, N1**) Day0. (**A2, C2, E2, G2, I2, K2, M2; B2, D2, F2, H2, J2, L2, N2**) Day2 (48 h culture). (**A, C, E, G, I, K, M**) Control carrier only group. (**B, D, F, H, J, L, N**) SAG-treated groups (5μM). A thicker VL was observed in the SAG-treated groups after 2 days in culture. VL and TB were outlined by green and white dashed lines respectively in A1. VL: vestibular lamina; TB: tooth bud. Scale bars in (A) = 100 μm. Same scale in all images. Labial-lingual axes shown in N2, same plane for all images.

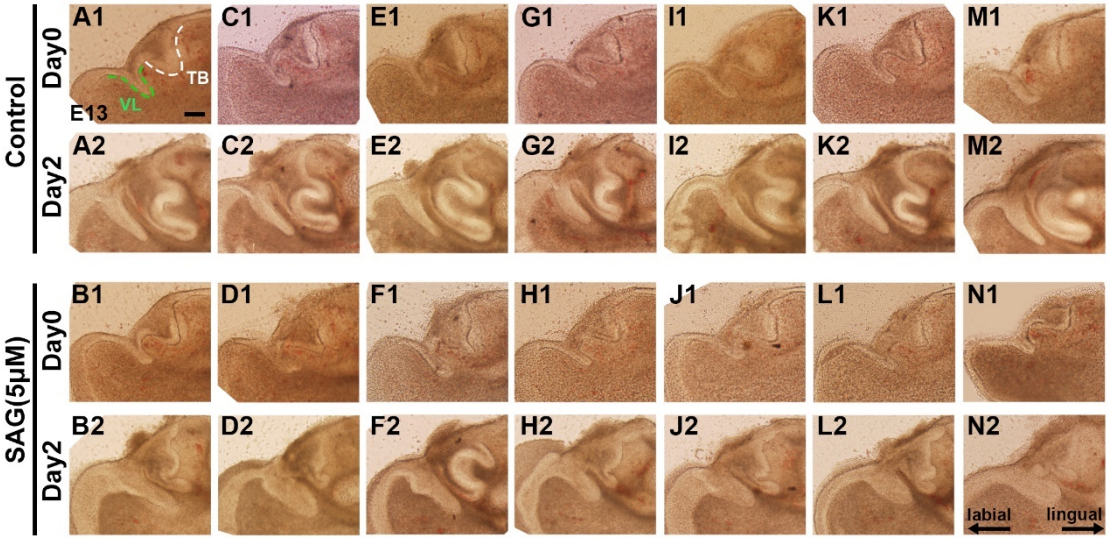

Supplementary Figure 10 |
Changes to *Gli1* and *Ptch1* expression in SAG and cyclopamine treated slices. Sagittal sections through lower anterior incisor region at E13. RNAscope for *Gli1* and *Ptch1*. DAPI (blue); *Gli1* (green, A, B, C); *Ptch1* (green, D, E, F). (**A, D**) Control carrier only group. (**B, E**) SAG-treated group (5μM). (**B**) A thicker VL was observed with increased expression of *Gli1* in the mesenchyme around the VL. (**E**) Increased expression of *Ptch1* particularly in the VL epithelium after SAG-treatment. (**C, F**) Cyclopamine-treated group (50μM). A shorter VL was observed with decreased expression of *Gli1* and *Ptch1* after 2 days in culture compared to the control groups. (**G**) IF was carried out for DAPI (blue) and E-cadherin (green) as a positive control to confirm the viability of the slices in cyclopamine at 50uM. E-cadherin labeled the VL and incisor epithelia. Large dots in the mesenchyme are auto-fluorescent blood vessels. VL and TB were outlined by magenta and white dashed lines respectively. VL: vestibular lamina; TB: tooth bud. Scale bars in (D) = 100 μm. Same scale in all other images. Labial-lingual axes shown in C, same plane for all images.

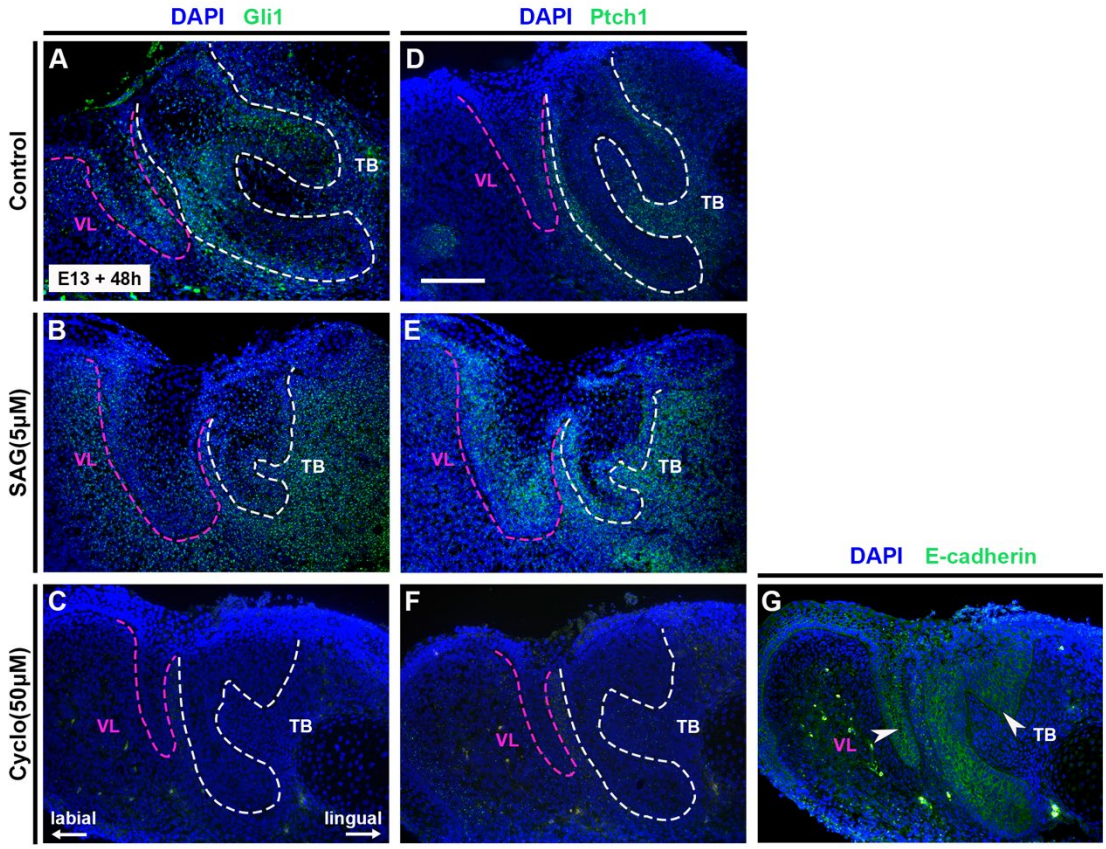

Supplementary data to chapter 5: Molecular profiling of the vestibular lamina highlights a key role for hedgehog signalling (unpublished)

1) Bioinformatics of the VL at E13

In addition to the RNA-Seq data presented in Chapter 5 which showed results from a comparison of E14 VL and incisor tooth germ, we also performed analysis at E13. The dissection and extraction of RNA was performed by collaborators in the Czech Republic. I performed the RNA-Seq analysis based on the raw sequencing data.

E13 is the bud stage of tooth development, and the VL and DL are already distinct. At this stage, a large number of genes exhibited overlapping expression patterns in both laminas (**Fig. S3**), in contrast to the later stage (E14) when the VL and DL had already taken on their own specific morphologies and presented distinct marker expressions (**Qiu *et al*., 2023**). According to the top genes screened by the RNA-Seq analysis at E14, a large number of VL and DL markers was validated by examining gene expression in the E14.5 embryo using Genepaint (https://gp3.mpg.de/) (**Visel, Thaller and Eichele, 2004**), a digital atlas that displays gene expression, or by reviewing the E13.5 and E15.5 datasets in the Allen Mouse Brain Atlas (mouse.brain-map.org) (**Fig. S4,5,6,7**).

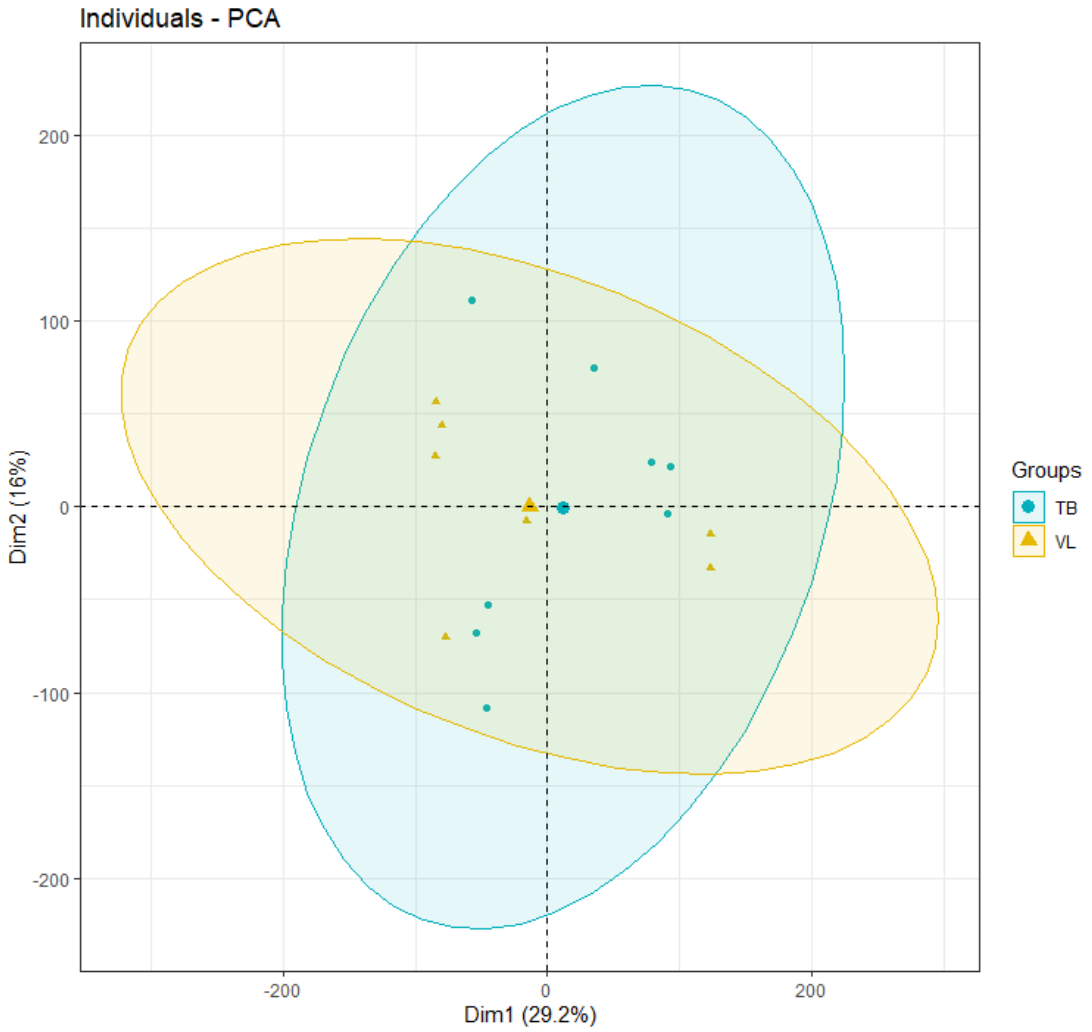

Figure S3. Principal component analysis (PCA) plot exhibited significant overlap of gene expression distributions of VL-TB datasets at E13. The scatterplot displayed blue dots representing TB samples and yellow dots representing VL samples. The clustering of the samples was shown by ellipses.

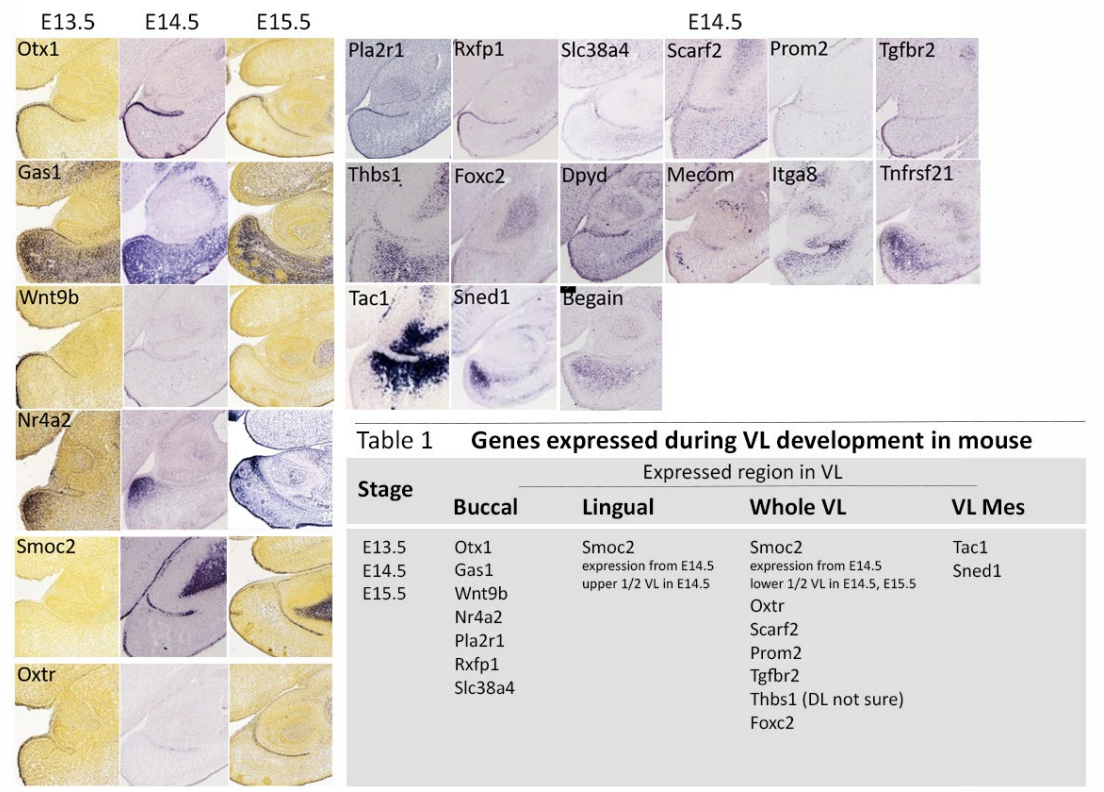

Table 1 **Genes expressed during VL development in mouse**

Stage	Expressed region in VL			
	Buccal	**Lingual**	**Whole VL**	**VL Mes**
E13.5 E14.5 E15.5	Otx1 Gas1 Wnt9b Nr4a2 Pla2r1 Rxfp1 Slc38a4	Smoc2 expression from E14.5 upper 1/2 VL in E14.5	Smoc2 expression from E14.5 lower 1/2 VL in E14.5, E15.5 Oxtr Scarf2 Prom2 Tgfbr2 Thbs1 (DL not sure) Foxc2	Tac1 Sned1

Figure S4. The molecular profile of the murine VL at E13.5, E14.5, and E15.5. The markers specific to VL at E14.5 were identified using Genepaint (https://gp3.mpg.de/) (**Visel, Thaller and Eichele, 2004**), while for E13.5 and E15.5, the datasets available in the Allen Mouse Brain Atlas (mouse.brain-map.org) were referred to.

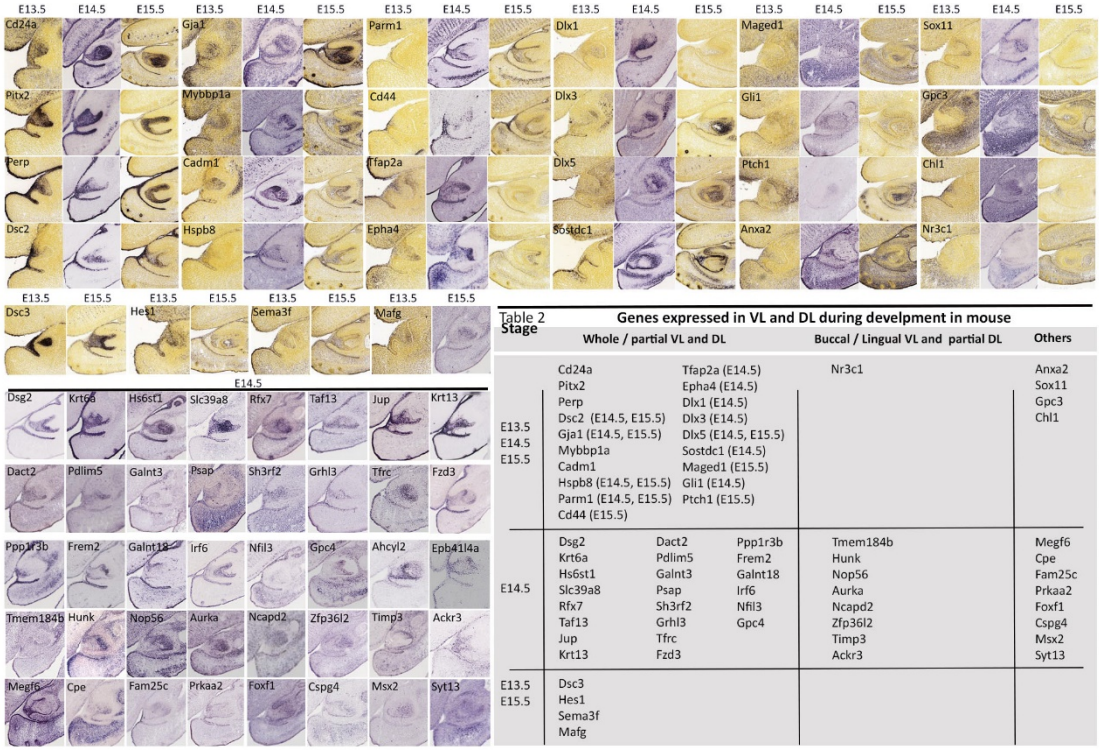

Table 2 **Genes expressed in VL and DL during develpment in mouse**

Stage	Whole / partial VL and DL			Buccal / Lingual VL and partial DL	Others
E13.5 E14.5 E15.5	Cd24a Pitx2 Perp Dsc2 (E14.5, E15.5) Gja1 (E14.5, E15.5) Mybbp1a Cadm1 Hspb8 (E14.5, E15.5) Parm1 (E14.5, E15.5) Cd44 (E15.5)	Tfap2a (E14.5) Epha4 (E14.5) Dlx1 (E14.5) Dlx3 (E14.5) Dlx5 (E14.5, E15.5) Sostdc1 (E14.5) Maged1 (E15.5) Gli1 (E14.5) Ptch1 (E15.5)	Nr3c1		Anxa2 Sox11 Gpc3 Chl1
E14.5	Dsg2 Krt6a Hs6st1 Slc39a8 Rfx7 Taf13 Jup Krt13	Dact2 Pdlim5 Galnt3 Psap Sh3rf2 Grhl3 Tfrc Fzd3	Ppp1r3b Frem2 Galnt18 Irf6 Nfil3 Gpc4	Tmem184b Hunk Nop56 Aurka Ncapd2 Zfp36l2 Timp3 Ackr3	Megf6 Cpe Fam25c Prkaa2 Foxf1 Cspg4 Msx2 Syt13
E13.5 E15.5	Dsc3 Hes1 Sema3f Mafg				

Figure S5. The molecular profile of the murine VL and DL at E13.5, E14.5, and E15.5 (1). Genepaint (https://gp3.mpg.de/) (**Visel, Thaller and Eichele, 2004**) was used to identify the markers that are specific to VL and DL at E14.5. However, for E13.5 and E15.5, the Allen Mouse Brain Atlas datasets (mouse.brain-map.org) was used.

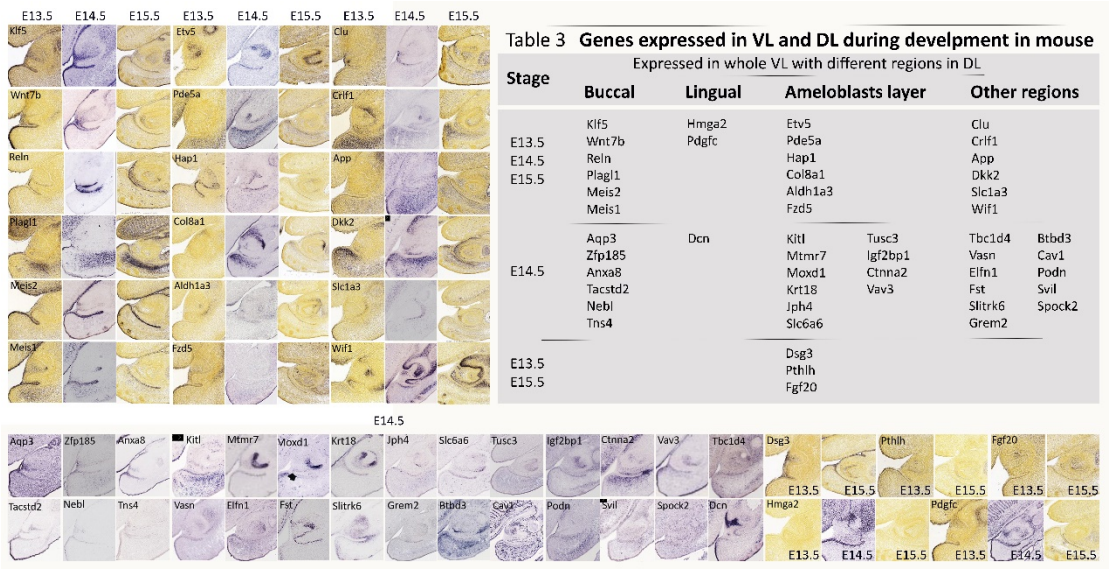

Table 3 **Genes expressed in VL and DL during develpment in mouse**

Expressed in whole VL with different regions in DL

Stage	Buccal	Lingual	Ameloblasts layer		Other regions	
E13.5 E14.5 E15.5	Klf5 Wnt7b Reln Plagl1 Meis2 Meis1	Hmga2 Pdgfc	Etv5 Pde5a Hap1 Col8a1 Aldh1a3 Fzd5		Clu Crlf1 App Dkk2 Slc1a3 Wif1	
E14.5	Aqp3 Zfp185 Anxa8 Tacstd2 Nebl Tns4	Dcn	Kitl Mtmr7 Moxd1 Krt18 Jph4 Slc6a6	Tusc3 Igf2bp1 Ctnna2 Vav3	Tbc1d4 Vasn Elfn1 Fst Slitrk6 Grem2	Btbd3 Cav1 Podn Svil Spock2
E13.5 E15.5			Dsg3 Pthlh Fgf20			

Figure S6. Molecular signature of the murine VL and DL at E13.5, E14.5, and E15.5 (2). To identify the specific markers for VL and DL at E14.5, Genepaint

(https://gp3.mpg.de/) (**Visel, Thaller and Eichele, 2004**) was utilized, while the datasets available on the Allen Mouse Brain Atlas (mouse.brain-map.org) were used to identify the specific markers for E13.5 and E15.5.

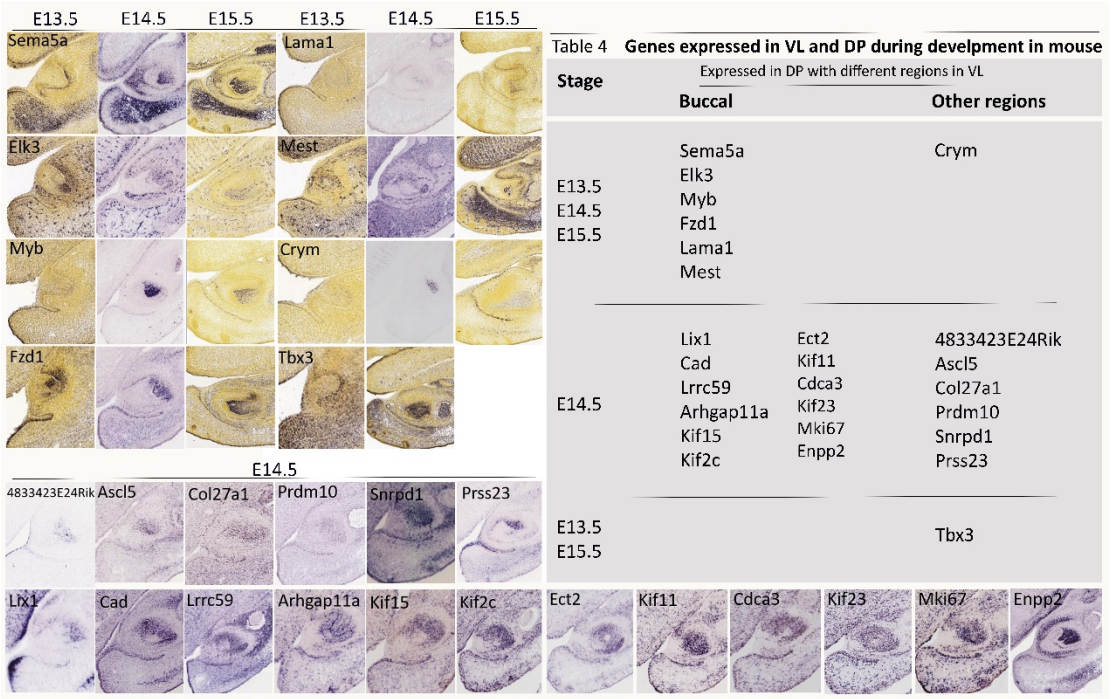

Table 4 **Genes expressed in VL and DP during develpment in mouse**

Stage	Expressed in DP with different regions in VL		
	Buccal		**Other regions**
E13.5 E14.5 E15.5	Sema5a Elk3 Myb Fzd1 Lama1 Mest		Crym
E14.5	Lix1 Cad Lrrc59 Arhgap11a Kif15 Kif2c	Ect2 Kif11 Cdca3 Kif23 Mki67 Enpp2	4833423E24Rik Ascl5 Col27a1 Prdm10 Snrpd1 Prss23
E13.5 E15.5			Tbx3

Figure S7. Molecular signature of the murine VL and DL at E13.5, E14.5, and E15.5 (3). During E14.5, Genepaint (https://gp3.mpg.de/) (**Visel, Thaller and Eichele, 2004**) was used to determine the markers that are specific to VL and DL. On the other hand, for E13.5 and E15.5, the datasets available on the Allen Mouse Brain Atlas (mouse.brain-map.org) was referenced.

This analysis highlighted that the VL and incisor tooth germ were molecularly less distinct from each other at earlier stage (E13). The findings from the analysis also brought to light several intriguing genes that merit further exploration. One such gene is *Nr4a2*, also referred to as *Nurr1*, which belongs to the NR4A orphan nuclear receptor (NR) family (**Volakakis *et al.*, 2010**) and

has been linked to retinoic acid signaling (**Perlmann and Jansson, 1995**).

2) Bioinformatics of the VL at E14 highlights a link with Wnt signalling

In addition to the analysis shown in Chapter 5, further exploration of the E14 dataset emphasized the significance of the Wnt signaling pathway during the early development of the VL and DL (**Fig. S8**), with the protein–protein interaction (PPI) network highlighting the interplay between the Shh and Wnt signaling (**Fig. S9**). Exploring the Wnt signaling pathways involved in the development of the VL would, therefore, be an interesting topic for future research.

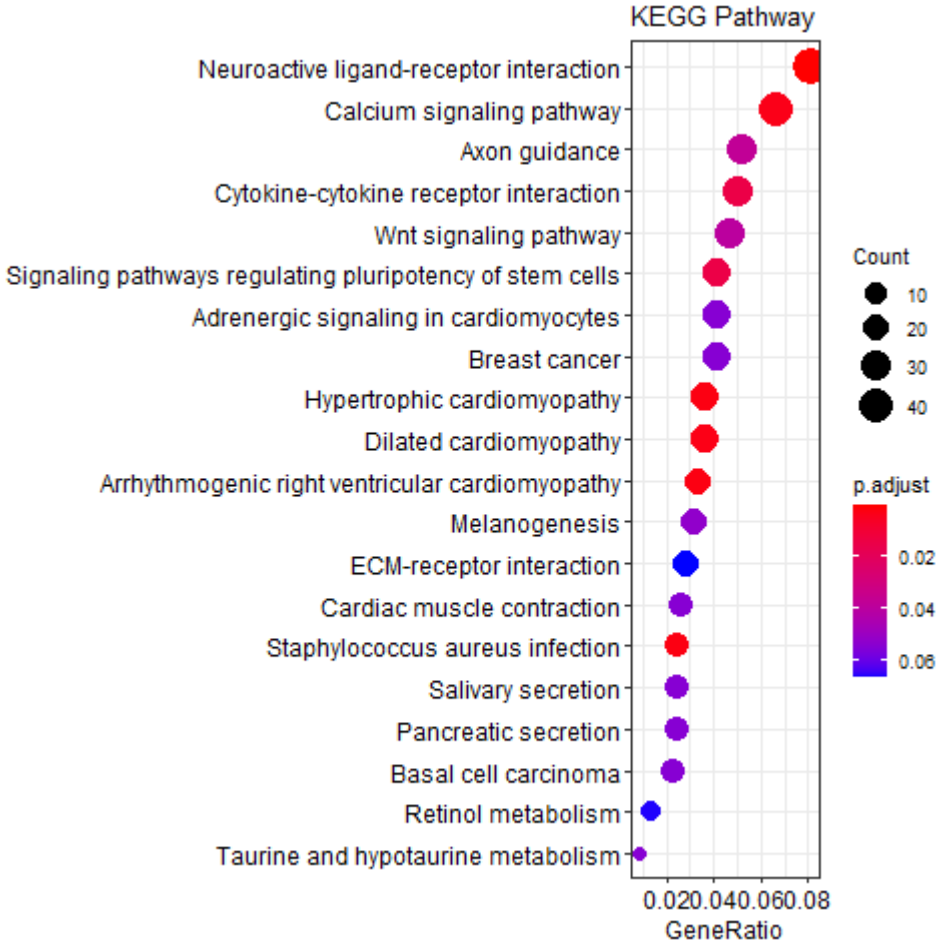

Figure S8. KEGG (Kyoto Encyclopedia of Genes and Genomes) pathway enrichment anlysis highlights the involvement of Wnt signalling pathway during VL and DL early development.

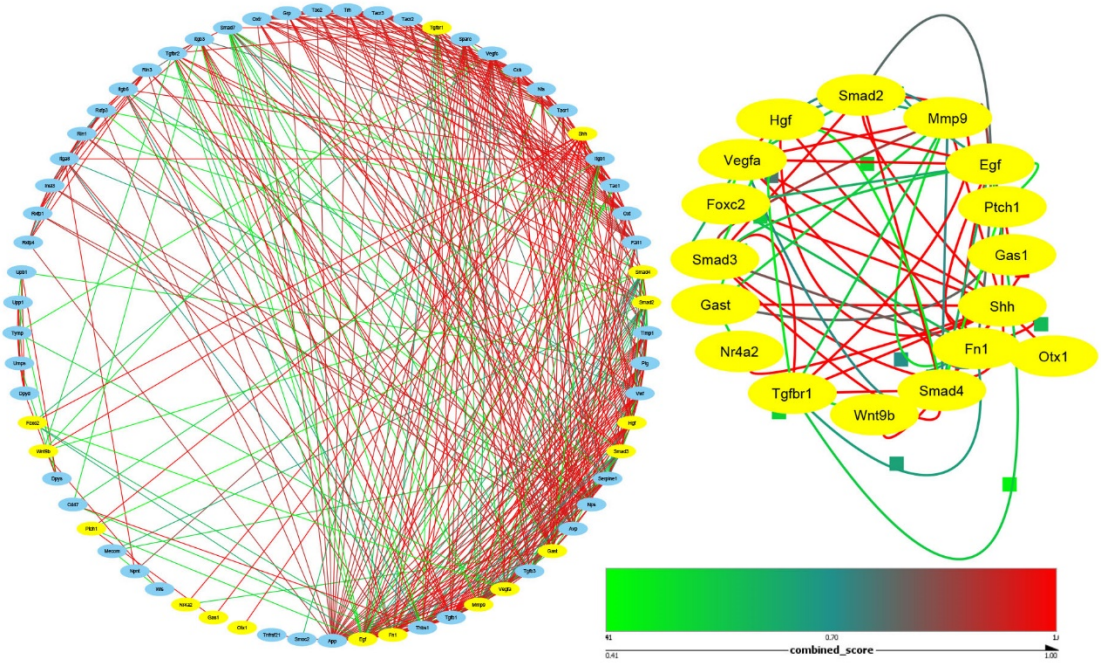

Figure S9. Protein–protein interaction (PPI) network emphasizes the interaction between the Shh and Wnt signaling.

Chapter 6: Supportive data completed as part of thesis (unpublished)

Abstract

Individuals diagnosed with ciliopathies such as EvC syndrome, often experience impaired formation of both the vestibule and teeth, resulting in abnormal frenula formation such as multiple frenula and anomalous tooth generation like supernumerary teeth. *EVC*, the primary gene responsible for EvC syndrome, plays a vital role in the primary cilium and is essential for the transduction of hedgehog signaling. Despite the significance of *EVC* in EvC syndrome, there is currently limited understanding of the underlying developmental mechanisms responsible for causing defects especially oral defects in individuals with the condition. In this study, we utilized *Evc* mouse as a model to investigate the mechanisms underlying the phenotype of EvC patients. Our research findings indicated that *Evc* mutants exhibit a variety of oral abnormalities, including multiple VL, shortened VL, fused teeth, and supernumerary teeth, which closely resemble the clinical oral symptoms seen in individuals with EvC syndrome. The observed defects in *Evc* mutants were caused by changes in proliferation and disruptions in the Shh signaling pathway, with unexpected increase in readouts of Hh signalling. This study improves our comprehension of the mechanisms underlying the development of frenulum defects and tooth-like odontomas, offering new perspectives into the causes of EvC syndrome and other ciliopathies.

Introduction

Ellis-van Creveld syndrome (EvC, MIM 225500) is an autosomal recessive chondroectodermal disorder that affects multiple systems and was originally identified by Richard Ellis and Simon van Creveld in 1940 (**Ellis and Van Creveld, 1940**). EvC syndrome has been reported to occur in individuals of various race or ethnic background (**Galdzicka *et al.*, 2002; Tompson *et al.*, 2007; Shaik *et al.*, 2016**), however, it is particularly prevalent in the Old Order Amish community, with an estimated prevalence of 5 cases per 1000 individuals within this population (**McKusick et al., 1964; Polymeropoulos et al., 1996**). Mutations in the genes *EVC* (**Ruiz-Perez *et al.*, 2000**) and *EVC2* **(Galdzicka *et al.*, 2002**) are predominant etiological factors in the pathogenesis of EvC syndrome, contributing to approximately 70% of cases (**Tompson *et al.*, 2007**). *EVC* and *EVC2* are highly conserved across species, from fish to humans, and are located in close proximity to each other on the genome, arranged head-to-head in a divergent configuration (**Ruiz-Perez *et al.*, 2003**). Mutations in either *EVC* or *EVC2* result in the unique characteristics specific to EvC syndrome, with affected individuals exhibiting indistinguishable phenotypes (**Ruiz-Perez *et al.*, 2003**). These clinical phenotypes include disproportionate dwarfism, shortened limbs and ribs, hypoplastic nails, congenital heart disease, respiratory malformations, and oral defects (**Nakatomi, 2009; Sasalawad *et al.*, 2013**).

The distinct oral features of EvC syndrome are pathognomonic and remain consistent, specifically regarding the prominent defects in the oral vestibule frenula and teeth. These defects are critical in early diagnosis of the syndrome (**Hattab, Yassin and Sasa, 1998; Mostafa *et al.*, 2005; Sasalawad *et al.*, 2013**). The dysplastic changes observed in the oral vestibule of EvC syndrome patients include presence of a wide median frenulum with strong attachment to the gingival margin, several broad median and labial frenula, accessory labio-gingival frenula, hypertrophic frenula, and anterior labio-gingival adhesions resulting from reduced or obliterated muco-buccal sulcus (**Hattab, Yassin and Sasa, 1998; Mostafa *et al.*, 2005; Baujat and Le Merrer, 2007; Sasalawad *et al.*, 2013; Nethan, Sinha and Chandra, 2017**). Inflammation of the gingiva has also been observed in regions with anomalous frenula attachment (**Hattab, Yassin and Sasa, 1998**). A wide range of dental anomalies has been detected in individuals with EvC syndrome, such as early eruption of teeth at birth, premature exfoliation, congenital absence of teeth, fused teeth, supernumerary teeth, malformed tooth, and malocclusion (**Hunter and Roberts, 1998; George *et al.*, 2000; Mostafa *et al.*, 2005; Nakatomi, 2009; Shaik *et al.*, 2016**). Similar vestibule defects are also associated with some other ectodermal dysplasias, such as Weyers acrofacial dysostosis (OMIM 193530) (**Roubicek and Spranger, 1984**). Additionally, a recent study also linked anomalies in the oral vestibule and teeth with cryptophthalmos resulting from a mutation in *FREM2* (**Kantaputra *et al.*, 2022**).

The generation of an *Evc* mouse model was based on evidence suggesting that *EVC* mutations were primarily caused by loss of function due to nonsense codons or frameshifts (**Tompson *et al.*, 2007**). To achieve this, researchers deleted *Evc* exon 1 and inserted a *lacZ* reporter cassette to eliminate gene function (**Ruiz-Perez *et al.*, 2007**). The *Evc* mutant mouse model has been developed as a representative model of EvC syndrome and is reported to closely mimic the physical traits observed in individuals with this condition (**Ruiz-Perez *et al.*, 2007**). Strong expression of *Evc* has been observed specifically in craniofacial regions and in the developing skeleton of mice at various embryonic stages (**Ruiz-Perez *et al.*, 2007**). Specifically, *Evc* expression has been observed in the lateral nasal process, nasal septum, skeletal growth plates, mesenchyme surrounding the tooth germ, maxillary process, mandibular process, cartilaginous components of the skeleton, nails, and cranial sutures from E11.5 to P0 (**Ruiz-Perez *et al.*, 2007**). *Evc* expression is particularly prominent in the mesenchyme surrounding the VL and developing tooth bud at E15.5. Interestingly, the distal third section of the VL epithelium also showed strong *Evc* expression during this stage (**Ruiz-Perez *et al.*, 2007**).

The *Evc* and *Evc2* genes encode proteins that have several coiled-coil domains and potential transmembrane regions (**Ruiz-Perez *et al.*, 2003**). *EVC* and *EVC2* are co-dependent for localization in the cilia, and they play a crucial role

as primary cilia components that are involved in the transduction of various signaling pathways (**Ruiz-Perez *et al.*, 2007; Blair *et al.*, 2011; Louie, Mishina and Zhang, 2020**). EVC and EVC2 proteins interact with one another and are involved in regulating hedgehog signaling in the primary cilium, with a reduced response to hedgehog ligands in chondrocytes in mouse mutants **(Caparrós-Martín *et al.*, 2013**). The primary cilium acts as a critical signaling hub that is essential for embryonic patterning and organogenesis during development (see Introduction and *Gas1* chapter). Dysfunctions of the primary cilium have been associated with various syndromic disorders, referred to as ciliopathies (**Berbari *et al.*, 2009**). Besides EvC syndrome, various craniofacial defects including abnormal frenula were also observed in Oral-Facial-Digital (OFD) syndromes, a specific subset of ciliopathies **(Bruel *et al.*, 2017**).

As described previously, during embryonic development, the vestibular lamina (VL) and dental lamina (DL) originate from the same epithelial band and are closely associated with each other (**Hovorakova *et al.*, 2016; Qiu *et al.*, 2020**). The oral vestibule has been reported as a common site for the appearance of odontomas/tooth-like tumors that may develop in patients, highlighting that the VL has the potential to develop tooth-like odontomas or supernumerary teeth under specific pathological conditions (**Hovorakova *et al.*, 2020**). The development of odontomas and supernumerary teeth have been observed in Gardner syndrome, due to an overactivation of Wnt signaling caused by the

adenomatous polyposis coli (APC) mutation (**García and Knoers, 2009; Yu *et al.*, 2018**). In APC conditional knockouts, excessive canonical Wnt signaling in the oral epithelium prompted development of extra tooth germs in the vestibule region, along with increased expression levels of *Fgf8* and *Shh* (**Wang *et al.*, 2009**). When Wnt signaling was overexpressed in Sox2-positive cells, supernumerary teeth were observed in the oral vestibule region, which could ultimately form mineralized teeth after isolation and culture **(Popa, Buchtova and Tucker, 2019**). In mice, the induction of odontomas through stimulated Wnt signaling has also been observed (**Xavier *et al.*, 2016**). Overactivated Shh is also implicated in the onset of odontogenic odontomas (**Rui *et al.*, 2014**), and it has been suggested that abnormal activation of Shh in non-odontogenic epithelial areas could trigger odontoma formation in these regions (**Hovorakova *et al.*, 2016**). Overexpression of Wnt/β-catenin in the mesenchyme can counteract these effects, resulting in a reduction in the number of teeth (**Järvinen *et al.*, 2018**). In dental cultures of snakes, similar to the phenotype observed in mice, overstimulation of Wnt/β-catenin pathway by GSK3β inhibitors could promote the development of additional ectopic tooth germs (**Gaete and Tucker, 2013**). These gathered data indicate that the VL has the capacity to generate teeth under certain circumstances, which could be associated with its shared origin with the DL.

In this chapter, we investigate the dental and vestibule phenotype of *Evc* mutant

mice. We first characterize the postnatal phenotype, then investigate the underlying mechanisms behind the dental and VL defects in order to explain the underlying causes of defects in patients.

Methods

Mouse strains

Evc mice were obtained from Victor Luis Ruiz (Institute de Investigaciones Biomedicas de Madrid). Both the mutant mice and littermate controls were bred on a mixed CD1 background. The day of plug detection was marked as E0.5, and all animal procedures were conducted following the guidelines set forth by King's College London. To label proliferating cells, BrdU (30 mg/kg) was administered through injection to the pregnant mouse two hours prior to culling.

Tissue processing and histological staining

Embryonic heads were fixed overnight at 4°C in 4% paraformaldehyde (PFA) followed by decalcification in 0.5M EDTA (pH = 8) for a duration of 3 days (P0) and 10 days (P4). The samples were then subjected to a series of steps including gradient dehydration in ethanol, xylene clearance, wax immersion, and paraffin embedding for histological analysis. The samples were subsequently sectioned at a thickness of 5-8μm using a microtome (Leica RM2245). These sections were then mounted on charged slides in sequential

order for further analysis. The slides were prepared for histological analysis and stained using standard protocols for trichrome staining, which mainly involved the use of Sirrus Red, Haematoxylin, and Alcian Blue. Photographs of the stained slides were captured using the Nikon Eclipse 80i light microscope.

Immunofluorescence staining

Immunostaining was conducted following established protocols as previously outlined (**Qiu *et al*., 2020; Qiu and Tucker, 2022; Qiu *et al*., 2023**). The sections were subjected to primary antibodies as follows: rat anti-BrdU (Abcam, ab6326, 1/500), rabbit anti-Arl13b (Novus Biologicals, 17711-1-ap, 1:200) , mouse anti-γ-tubulin (Sigma-Aldrich, T6557, 1:200), mouse anti-β-catenin (BD Biosciences, 610153, 1:200), and mouse anti-E-cadherin (Abcam, ab76055, 1/400). Subsequently, the sections were incubated with secondary antibodies diluted at 1/500 in the dark at room temperature (RT) for 1 hour: Alexa Fluor donkey anti-mouse 488 (Invitrogen, A21202), Alexa Fluor™ donkey anti-rabbit 568, and Alexa Fluor donkey anti-rat 647 (Invitrogen, A21247). After mounting the slides with Fluoroshield containing DAPI (Sigma-Aldrich, SLBV4269), the slides were visualized using a Leica TCS SP5 confocal microscope for observation. To perform BrdU immunofluorescence staining, the mice were administered BrdU labeling reagent (30 mg/kg, Life Technologies, 000103) via injection 2 hours prior to sample collection. Control groups were established to validate the immunofluorescence staining. Each antibody analysis was

independently conducted a minimum of three times to ensure reliability and consistency.

In situ hybridization

The *in situ* hybridization process was performed according to the standard protocol, as previously described (**Fons Romero *et al.*, 2017**). The *Gli1* plasmid was linearized using SalI (R6051, Promega) by incubating it for 2 hours at 37°C, and then purified with Monarch PCR&DNA cleanup kit (T1030G, NEB).

RNA-Scope assay

The Multiplex Fluorescent Reagent Kit v2 (323100, Advanced Cell Diagnostics) was employed in accordance with the manufacturer's instructions, as previously described (**Qiu *et al.*, 2023**). The RNA-Scope probe used was (1:50; Mm-Gli1, 311001).

Results

Evc mutants replicate the physical characteristics observed in EvC patients

As mentioned in the introduction, Ellis-van Creveld (EvC) syndrome is primarily characterized by short limbs and ribs, disproportionate dwarfism, congenital heart malformations, polydactyly, and oral defects (**Ellis and Van Creveld, 1940**). *Evc* homozygous mutants displayed a comparable phenotype, where

they were observed to be smaller in size than their littermates at P20 (**Fig. 14A**). *Evc* heterozygous mutants appeared to have no notable physical differences (**Fig. 14A**). The *Evc* homozygous mutants displayed very pronounced dental abnormalities (**Fig. 14G, magenta arrowheads; Fig. 15D-F, green arrowheads**). This is in line with the phenotypes of *Evc* mutants that have been previously reported (**Ruiz-Perez *et al.*, 2007; Nakatomi *et al.*, 2013**). As previously mentioned in the introduction, oral vestibule defects are a consistent feature of EvC syndrome, but have not been assessed in *Evc* mice. Analysis of the homozygous mutants showed a clear defect in the oral vestibule of the lower jaw at P20 (**Fig. 14D,G**), including a hyperplastic lower medial vestibule that was highly attached to the gingival margin (**Fig. 14D,G, red arrowheads**), which results in increased spacing between the two incisors (**Fig. 14B-G**).

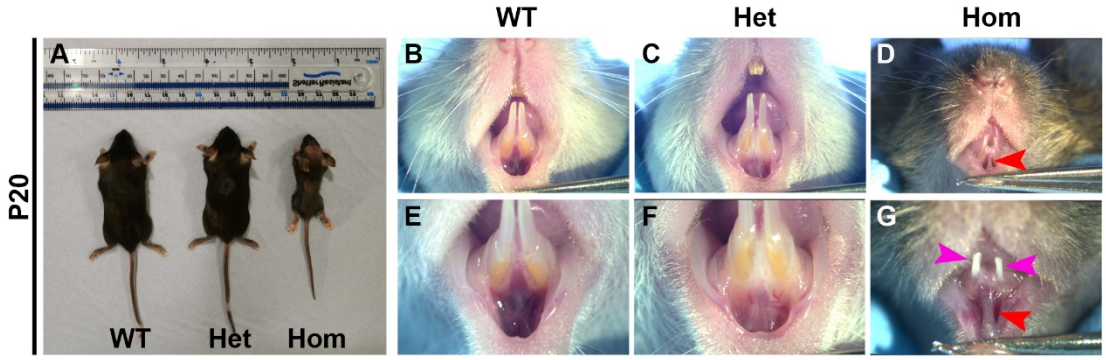

Figure 14. The observed characteristics of the *Evc* mutants at P20. (**A**) Body size differences in $Evc^{-/-}$ (N=7), $Evc^{+/-}$ (N=7), and WT littermates (N=5). The *Evc* homozygous mutants exhibit a substantially reduced body size compared to the littermate controls, while the body size of *Evc* heterozygous mutants is similar to that of their littermate controls. (**B-G**) Frontal view of the incisors and oral vestibule. (**B, E**) WT littermates; (**C, F**) *Evc* heterozygous mutants (Het); (**D, G**) *Evc* homozygous

mutants (Hom); Observations in *Evc* homozygous mutants (**D, G**) showed the presence of rudimentary incisors (indicated by magenta arrowheads) and a hyperplastic lower medial vestibule that displayed high attachment to the gingival margin (indicated by red arrowheads), resulting in wider spacing between the two incisors. However, the incisors and vestibule in *Evc* heterozygous mutants (**C, F**) appeared normal and comparable to WT littermates (**B, E**).

The *Evc* homozygous mutants exhibit defects in development of tooth germ and the VL

Given the phenotype in juveniles, the development of the VL was then assessed during development. In mice, the VL is noticeable in the front part of the mouth, however, it is less discernible towards the posterior region near the molars (**Peterková, 1985; Hovorakova *et al.*, 2011**). We therefore analysed the developing VL in the mouse focusing on the more anterior/incisor region. Similar to the phenotype in *Gas1* mutants (**Qiu and Tucker, 2022**), we observed a rudimentary VL in *Evc* homozygous mutant ($Evc^{-/-}$) mice compared to the robust VL in the lower jaw in wild-type (WT) littermates (**Fig.15**) (truncated VL observed in N=21/21 $Evc^{-/-}$ mice from E14.5 to P4). By E14.5, in WT mice, the VL has extended into the mesenchyme and displays a full extension of the VL that almost reaches towards the midline under Meckel's cartilage (**Fig. 15G**). However, in *Evc* homozygous mutants, the extension of VL was stunted and unable to pass under the forming incisors, remaining shorter than in WT litter

mates at the same developmental stage (**Fig. 15J**) (truncated VL observed in N=6/6 *Evc*$^{-/-}$ embryos at E14.5). By P0, the VL in WT mice had undergone further extension, resulting in the two laminas touching at the midline (**Fig. 15H,I**). On the other hand, *Evc* homozygous mutants continued to display a shortened VL at P0 and P4 (**Fig. 15K,L**) (truncated VL observed in N=5/5 *Evc*$^{-/-}$ mice at P0 and N=4/4 *Evc*$^{-/-}$ mice at P4). At birth (P0), the VL in WT mice remained solid (**Fig. 15H**), however, by P4, small holes within the deeper parts of the lamina start to form (**Qiu and Tucker, 2022**) (**Fig. 15I**). Interestingly, the *Evc* homozygous mutants exhibited a similar pattern of VL opening (**Fig. 15K,L**) (normal opening of VL observed in N=4/4 *Evc*$^{-/-}$ mice at P4), suggesting that opening of the VL was not compromised in the mutants. Furthermore, *Evc*$^{-/-}$ mice exhibited additional branches in the VL compared to the WT littermate at P4 (**Fig. 15L**) (branched VL observed in N=3/4 *Evc*$^{-/-}$ mice at P4), which may explain the multiple frenula observed in EvC patients (**Sasalawad *et al.*, 2013**).

The *Evc*$^{-/-}$ mice also exhibited dental defects, which included fused upper incisor germs (**Fig. 15**) (fused upper incisor germs observed in N=7/17 *Evc*$^{-/-}$ mice from E14.5 to P4). Such midline fusions suggest a midline defect similar to the premaxillary incisor fusion observed in *Gas1*$^{-/-}$ mice (**Seppala *et al.*, 2007**), suggesting narrowing of the midline tissues as a mild form of holoprosencephaly. These findings underscore the close relationship between these two genetic mutations. It is noteworthy that at E14.5, P0, and P4 stages

of development, the VL and DL/tooth germs were observed normal in *Evc* heterozygous mutants (data not shown) (normal VL and DL observed in N=7/7 *Evc*$^{+/-}$ mice from E14.5 to P4).

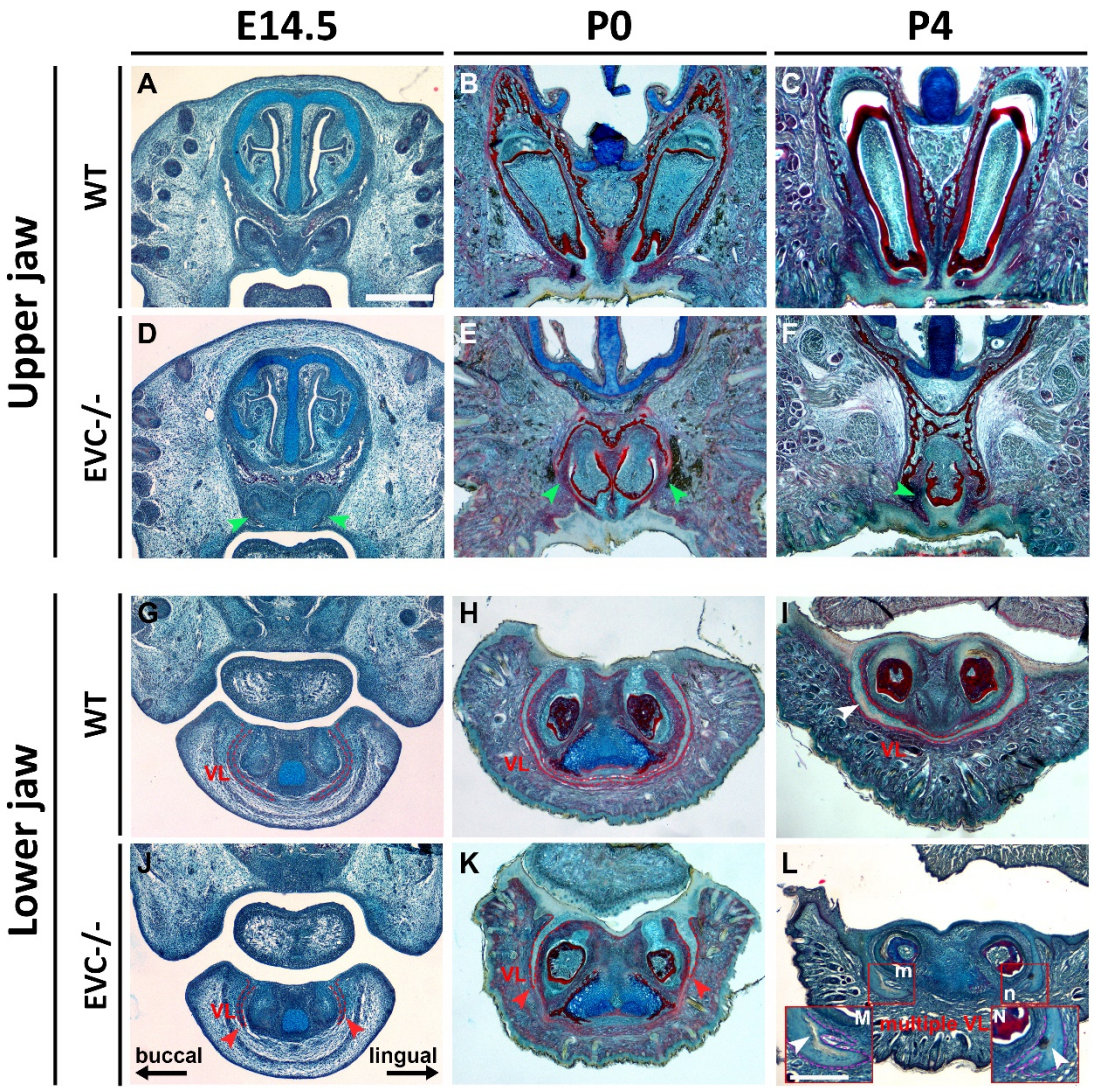

Figure 15. The *Evc*$^{-/-}$ mice exhibit defects in both tooth germ and VL in the incisor region. (**A-L**) Histological trichrome staining was utilized to examine frontal sections of the VL and tooth germ in the anterior maxilla and mandible at E14.5, P0, and P4. (**A-F**) Anterior upper jaw. Compared to littermate controls with normal incisor tooth germ (A-C), the *Evc*$^{-/-}$ mice displayed fused incisor tooth germs at E14.5, P0, and P4 (**D-F**, green arrowheads). (**G-L**) Anterior lower jaw. (**G-I**) The VL in the littermate

controls extends into the mesenchyme and surround the tooth germ, with both sides touching each other at the midline by P0. (**J-L**) A shortened VL is observed in the *Evc*$^{-/-}$ mice (red arrowheads). (**L**) Multiple VLs are observed in the *Evc*$^{-/-}$ mice. (**M, N**) in (**L**) are Higher power view of boxes m and n. VL is outlined by red dashed lines. Lingual-buccal axes are displayed in J, with the same axes utilized for all images. Scale bar in (A-L) = 500μm; Scale bar in (M, N) = 250μm.

Basic structure of the primary cilium is maintained in the VL in *Evc*$^{-/-}$ mice

The overall structure of the primary cilium has been shown to be unaffected in *Evc*$^{-/-}$ mice in chondrocytes (**Ruiz-Perez *et al.*, 2007; Caparrós-Martín *et al.*, 2013**). To confirm this was also true in the craniofacial region, the basic structure of the primary cilium was assessed using ARL13B and γ-tubulin. In keeping with other tissues, primary cilia were present in the affected VL in *Evc*$^{-/-}$ mice at E12.5 (**Fig. 16A,B**) and E18 (**Fig. 16C,D**).

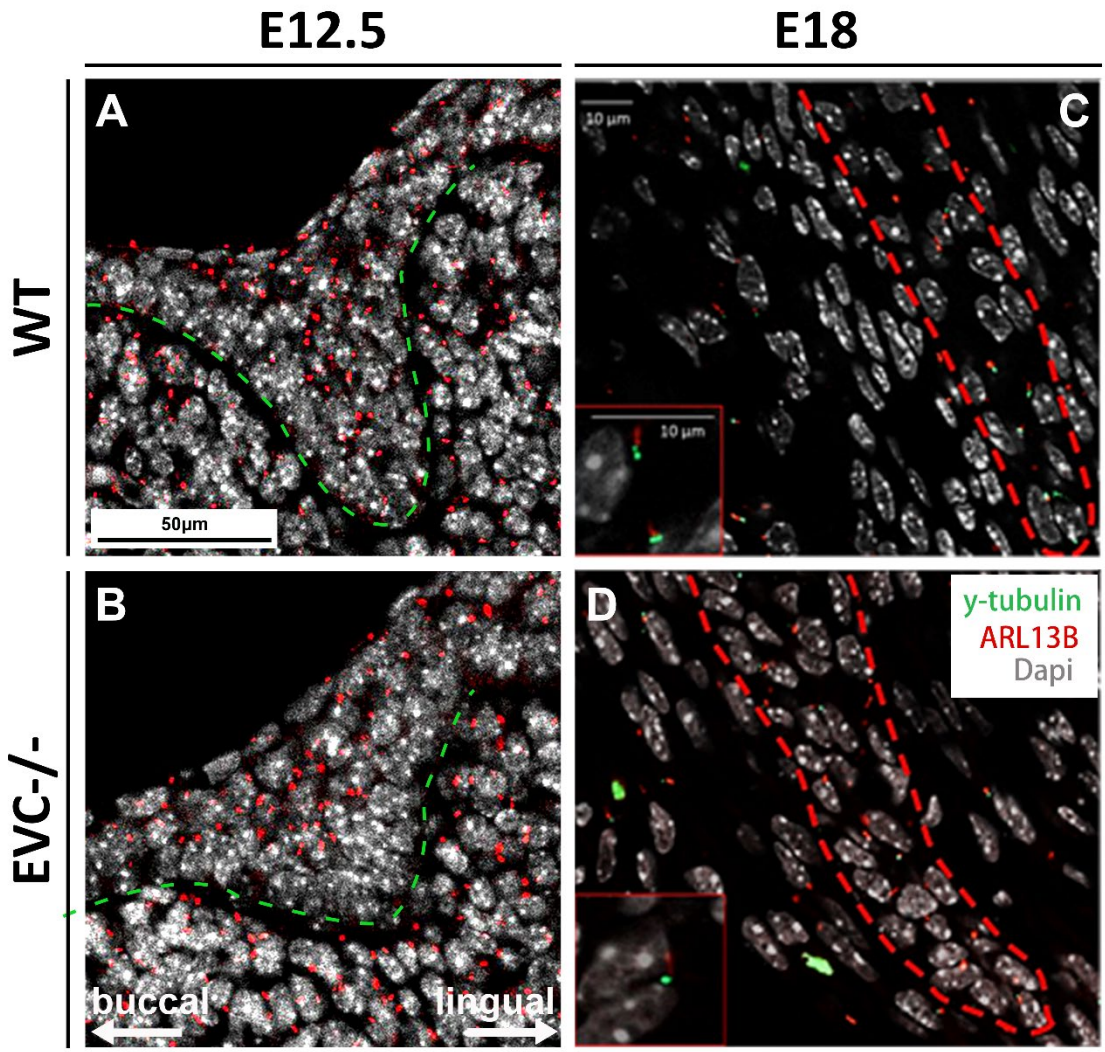

Fig 16. The ARL13B-posive cells are present in the *Evc*$^{-/-}$ mice in comparison to the WT littermates. IF for DAPI (grey), ARL13B (red), and γ-tubulin (green). (**A, B**) E12.5. ARL13B-Positive cells are detected in *Evc*$^{-/-}$ mice compared to their WT littermates. (**C, D**) E18. Magnification (red boxes in C and D) showed that the structure of primary cilia appears normal in the *Evc*−/− mice, as labelled by ARL13B and γ-tubulin. Buccal-lingual axes in panel B shown for all images. Scale bar in (A, B) = 50µm; Scale bar in (C, D) = 10µm; Scale bar in red boxes in panels C and D = 10µm.

Evc$^{-/-}$ mice exhibit defects in proliferation

In the *Gas1* mutants the truncated VL was linked to a reduction in proliferation at early developmental stage (E12.5) (**Qiu *et a*l., 2023**). To investigate the mechanisms behind the truncated VL phenotype observed in these mutants, the proliferation level was analysed at E12.5 and E14.5 using the proliferation marker bromodeoxyuridine (BrdU). At E12.5, the VL and DL were distinguishable as two separate thickenings (**Qiu and Tucker, 2022**). The VL and DL were outlined by E-cadherin in *Evc*$^{-/-}$ mice, the VL appeared slightly shorter than the WT littermates (**Fig. 17A,D**). Although the truncated VL in *Gas1* and *Evc* homozygous mutants have different effects on the labial/buccal-lingual expression pattern, both mutations lead to impaired proliferation at an early stage (E12.5) in the truncated VL (**Qiu *et al*., 2023; Fig. 17B,C,E,F**). Moreover, at this stage, there was an evident decrease in mesenchymal proliferation surrounding the developing VL in the *Evc* homozygous mutants (**Fig. 17B,C,E,F**) (decrease in mesenchymal proliferation observed in N=4/4 *Evc*$^{-/-}$ embryos at E12.5).

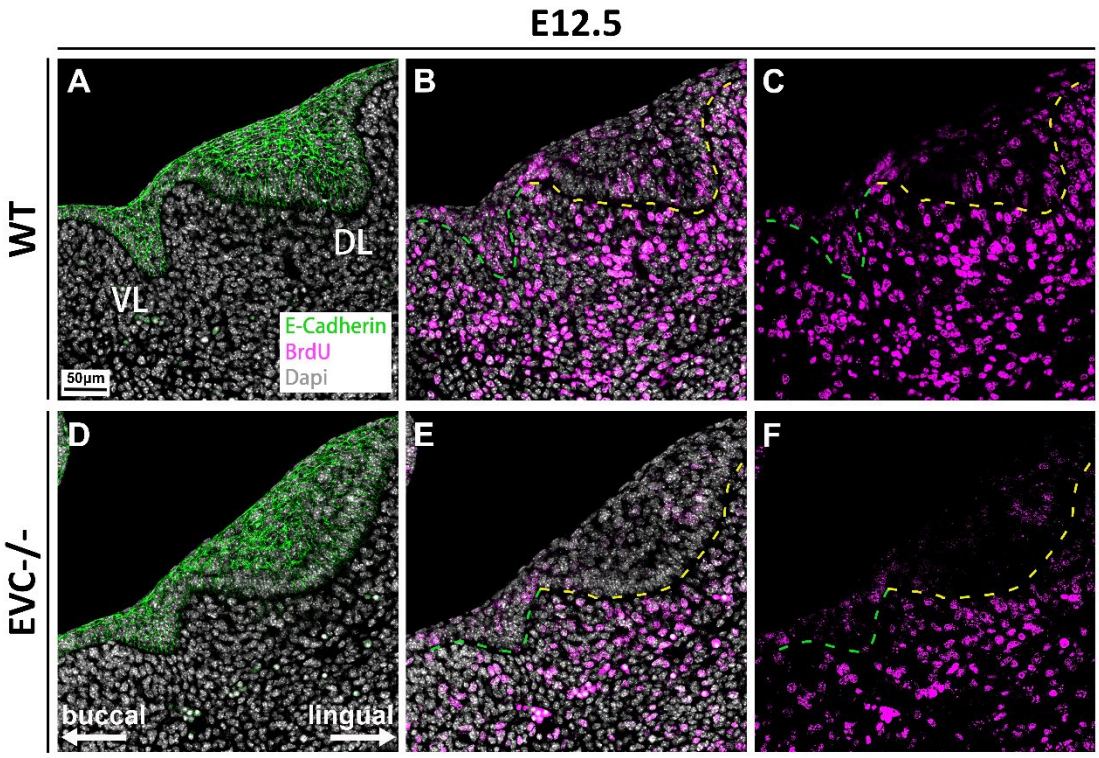

Figure 17. The truncated VL observed in *Evc* homozygous mutants was linked to a decrease in proliferation at E12.5. Immunofluorescence (IF) for BrdU (magenta), DAPI (grey), and E-cadherin (green) in the WT littermates (**A-C**) and *Evc*$^{-/-}$ mice (**D-F**). E-cadherin labelled the VL and DL (**A, D**), and a rudimentary VL was observed in the *Evc*$^{-/-}$ mice. The number of BrdU-positive cells in the VL epithelium was reduced in the *Evc*$^{-/-}$ mice (**E, F**) compared to the WT littermates (**B, C**). Buccal-lingual axes in panel D shown for all images. Scale bar in (A-F) = 50µm.

By E14.5, the VL has already bent to form a curve that surrounds the tooth germ, proposed to be driven by asymmetrical proliferation (**Qiu and Tucker, 2022; Qiu *et al*., 2023**). However, the high level of proliferation at the tip of the VL, which drives its extension towards the midline, continues at least until P0 (**Qiu and Tucker, 2022**). To gain deeper insights into how impaired proliferation

contributes to the truncated VL in *Evc*$^{-/-}$ mice, proliferation was also assessed at E14.5. By utilizing β-catenin to label the VL and tooth germ, a shorter VL (**Fig. 18A,D,G)** was clearly observed in the *Evc*$^{-/-}$ mice, while the characteristic bending of the VL (indicated by rectangular boxes in **Fig. 18B,H)** was still present. Within the bending region of the VL (indicated by the rectangular boxes in B and H), the *Evc* homozygous mutants displayed a proliferation pattern that follows the buccal-lingual differential expression, similar to that of the WT littermates (**Fig. 18**). Nevertheless, a reduction in proliferation was detected at the distal end of the truncated VL in *Evc* homozygous mutants (pointed out by yellow arrowheads in E and H) during this stage (**Fig. 18**) (N=4/4 *Evc*$^{-/-}$ embryos at E14.5). We aim to quantify the changes in proliferation to confirm these findings.

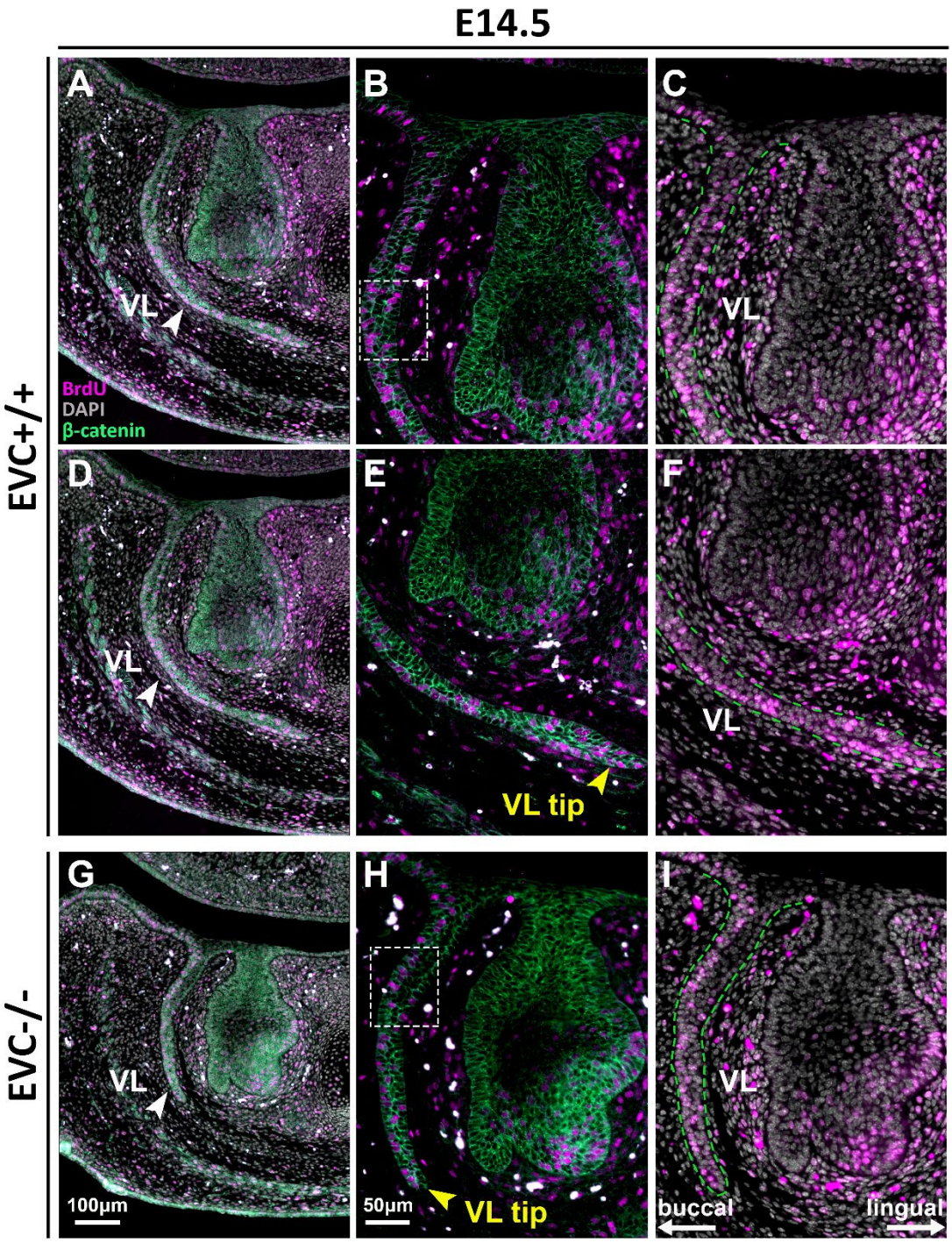

Figure 18. A reduction in proliferation at the tip of the VL at E14.5 is observed in conjunction with the truncated VL of *Evc*$^{-/-}$ mice. (**A-I**) Immunofluorescence staining was performed for β-catenin (green), BrdU (magenta), and DAPI (grey) in both the littermate controls (**A-F**) and *Evc*$^{-/-}$ mice (**G-I**). β-catenin (green) outlines the incisor tooth germ and VL in panels A, B, D, E, G ,H. Compared to the littermate controls, a

shorter VL was observed in the *Evc* homozygous mutants, along with a significant decrease in the number of BrdU-positive cells was observed in the epithelium at the end of the VL in the $Evc^{-/-}$ mice (yellow arrowheads). The rectangular boxes in B and H indicate the bending region of the VL, where both the *Evc* homozygous mutants and WT littermates exhibit the buccal-lingual expression pattern of proliferation. The VL is outlined by green dashed lines in panels C, F, and I. Lingual-buccal axes are displayed in I, with the same axes utilized for all images. Scale bar in (A, D, G) = 100μm; Scale bar in (B, C, E, F, H, I) = 50μm.

Upregulation of *Gli1* in the *Evc* homozygous mutant VL

Evidence suggests that the loss of *EVC* or *EVC2* function results in impaired Hedgehog signaling, as evidenced by a significant decrease in the expression levels of *Gli1* or *Ptch1* in the developing long bones in mouse mutants when compared to controls (**Caparrós-Martín *et al.*, 2013; Zhang *et al.*, 2015**). Given the similar VL defects in *Gas1* and *Evc* homozygous mutants, it was hypothesized that the *Evc* mutants would show diminished readout of Shh signalling in the tooth and VL, as revealed by a reduction in *Gli1* in *Gas1* mutants (**Qiu *et al.*, 2023**). Perhaps unexpectedly, the truncated VL in *Evc* and *Gas1* mutants were found not to share the same pathological mechanism. Unlike the decreased *Gli1* expression in the shortened VL of *Gas1* mutants (**Qiu *et al.*, 2023**), the truncated VL in the *Evc* mutants had an upregulation of *Gli1*, particularly at the tip of the VL (**Fig. 19**). This was shown both by RNA-Scope

and DIG *in situ* hybridization (**Fig 21**). We aim to follow this interesting result up by quantification of the RNA-Scope expression to confirm changes in expression in different parts of the lamina.

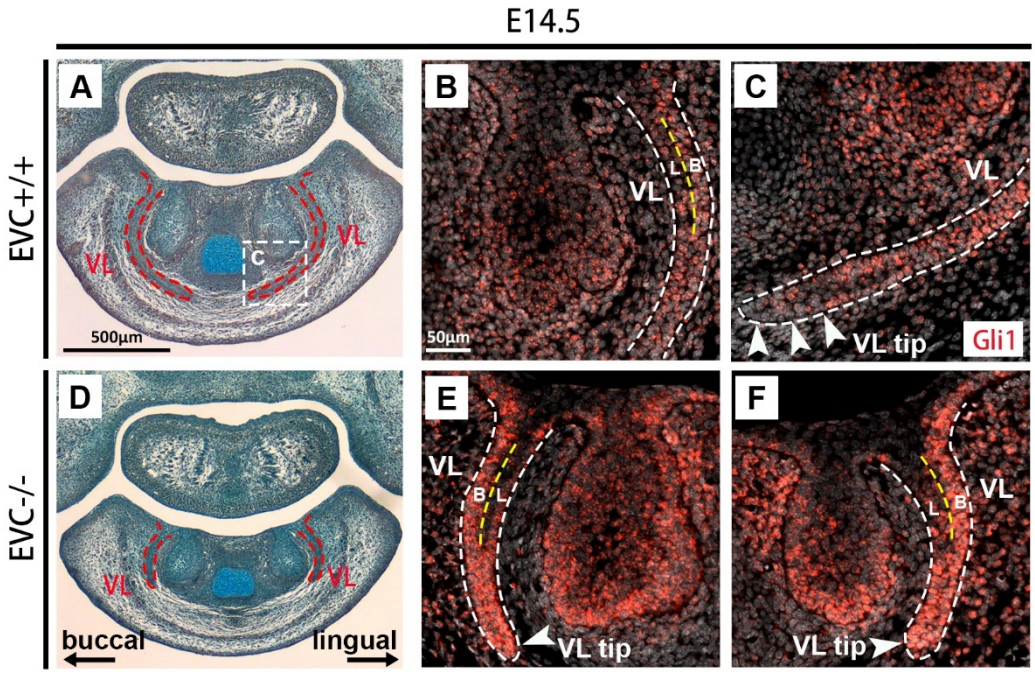

Figure 19. Upregulated expression of *Gli1* in *Evc* mutants at E14.5. (**A**, **D**) Trichrome staining of VL and DL in the lower incisor region at E14.5. Compared to the WT littermates (**A**), a decreased length of the VL was observed in the *Evc*$^{-/-}$ mice. (**B**, **C, E, F**) RNA-Scope for Gli1 (red) and DAPI (grey). (**B, C**) The WT littermates exhibited higher expression of *Gli1* on the buccal side (B) of the VL in the bending region, compared to the lingual side (L), whereas minimal expression of *Gli1* was observed at the tip of the VL (white arrowheads in C). (**E, F**) Despite the truncated VL observed in *Evc*$^{-/-}$ mice, differential expression of *Gli1* between the buccal (B) and lingual (L) sides in the bending region of the VL was still present. *Gli1* expression at the tip of the VL was significantly increased, as indicated by the white arrowheads in panels E and F. White dashed lines outlined the boundaries of the VL, and yellow dashed lines were

added to divide the VL into buccal and lingual sections. Buccal-lingual axes in panel D shown for all images. Scale bar in (A, D) = 500μm; Scale bar in (B, C, E, F) = 50μm.

Supernumerary tooth germs and multiple VLs observed in *Evc* mutants are consistent with the oral features of EvC syndrome

Although the VL was truncated in the *Evc* homozygous mutants (**Fig. 15**), the later morphology of the VL did not completely phenocopy that of the *Gas1* mutants (**Qiu *et al*., 2023**). In particular, the VL appeared to branch in the *Evc* mutants at E16.5 (**Fig. 20**) and P4 (**Fig. 15L**) (branched VL observed in N=3/3 $Evc^{-/-}$ embryos at E16.5 and N=3/4 $Evc^{-/-}$ mice at P4), a phenotype never observed in the *Gas1* mutants (**Qiu *et al*., 2023**). By E16.5, the VL had elongated beneath Meckel's cartilage, and the two laminae were in close proximity to each other at the midline in the frontal sections **(Qiu and Tucker, 2022**). Similarly, in E16.5 sagittal sections of WT littermates, it was observed that the VL had extended under Meckel's cartilage and surrounded the developing incisor germ (**Fig. 20A**). However, *Evc* homozygous mutant sagittal sections at E16.5 displayed a significantly abbreviated VL, accompanied by the presence of an additional branch of the VL (**Fig. 20E**), resembling the branches found in the forming gland. By P4, tiny openings were noted within the VL in the anterior frontal sections (**Qiu and Tucker, 2022**). In the anterior frontal sections at P4, the *Evc* mutants displayed comparable microscopic apertures in the multiple VL (**Fig. 15L, white arrowheads**), as seen in the VL of the WT

littermates (**Fig. 15I, white arrowheads**). To investigate the mechanism of multiple VL formation, the expression of *Gli1* was examined in the multiple VLs. At E16.5, there was a shift in the *Gli1* expression pattern in comparison to the earlier stage (E14.5) (**Fig. 19**). In WT littermates, *Gli1* expression was predominantly observed in the middle region of the VL and the whisker follicles (WF), with minimal expression in the upper and distal ends of the VL (**Fig. 20B-D**). Interestingly, in the *Evc* homozygous mutants, the *Gli1* expression in the VL additional branches was reduced (**Fig. 20F-H, pointed by white arrowheads**), while the VL still displayed a significant increase in *Gli1*, particularly at the end of the VL (**Fig. 20F-H, pointed by yellow arrowheads**), similar to the *Gli1* expression observed in the shorter VL (**Fig. 19E,F, pointed by white arrowheads**) (increased *Gli1* expression in the shortened VL observed in N=5/5 *Evc*$^{-/-}$ embryos from E14.5 to E18).

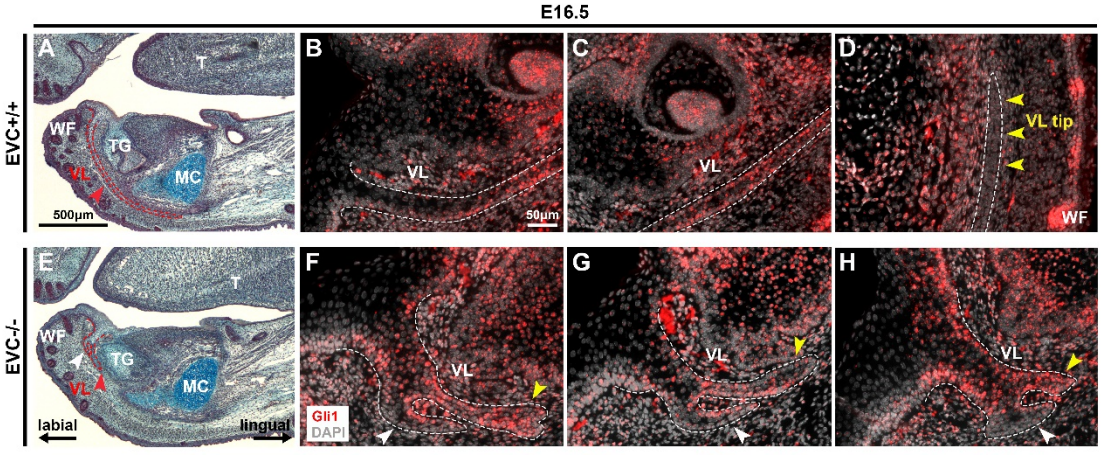

Figure 20. The defective VL of *Evc* homozygous mutant mice showing altered expression of *Gli1* at E16.5. (**A, E**) Trichrome staining performed on sagittal sections of the lower incisor region of mice at E16.5. The VL had extend under the Meckel's cartilage in the WT littermates (**A**); while shorter VL along with the additional VL were

observed in the *Evc* mutants (**E**). (**B-D; F-H**) RNA-Scope for Gli1 (red) and DAPI (grey). In WT littermates (**B-D**), *Gli1* expression was mainly detected in the middle region (C) of the VL, with only a few detected in the top (B) and bottom (yellow arrowheads in D) regions. In *Evc* mutants (**F-H**), the expression of *Gli1* in the additional branches of the VL (white arrowheads in F, G, H) was suppressed, but there was a significant increase in *Gli1* expression in the VL, particularly at the end of the VL. The VL is demarcated by white dashed lines. VL: Vestibular lamina; TG: Incisor tooth germ; MC: Meckel's cartilage; WF: Whisker follicles; T: Tongue. Labial-lingual axes in panel E shown for all images. Scale bars in (A, E) = 500μm; Scale bar in (B-D; F-H) =50μm.

Interestingly, in addition to the branching VL, the area between the VL and the tooth was the site of formation of an additional tooth germ in some *Evc* homozygous mutant mice (**Fig. 21**) (additional tooth germ observed in N=2/28 $Evc^{-/-}$ mice from E14.5 to P20), mimicking the supernumerary tooth reported in the incisor regions of EvC patients (**Mostafa *et al.*, 2005**). Unlike the supernumerary teeth that have been reported to form in the toothless diastema region of *Gas1* mutants (**Seppala *et al.*, 2022**), the *Evc* mutants exhibited a supernumerary tooth germ from the VL in the incisor region at E18 (**Fig. 21C-G**). The origin of this ectopic tooth germ appeared to be from the common epithelium shared with the truncated VL (**Fig. 21D**). Additionally, Meckel's cartilage appears to be twisted on the side with the extra tooth germ (**Fig. 21**). It is noteworthy that at E18, the expression of *Gli1* in the VL of the WT littermate

was significantly decreased (**Fig. 21H**), as compared to the earlier developmental stages of E14.5 (**Fig. 19B,C**) and E16.5 (**Fig. 20B-D**). Nevertheless, during this stage, *Gli1* expression remained present in other developing areas, such as the whisker follicles, Meckel's cartilage, and tooth germ (**Fig. 21H**). Similar to the observations mentioned above, the $Evc^{-/-}$ mice exhibited an increase in *Gli1* expression in both the truncated VL and the VL that contributed to the supernumerary tooth germ, particularly at the end of the VL (**Fig. 21H-K**). Additionally, there was a decrease in *Gli1* expression observed in the whisker follicles of the *Evc* homozygous mutants (**Fig. 21H-K**). Nonetheless, the expression of *Gli1* in the supernumerary tooth germ appeared to be normal (**Fig. 21H-K**).

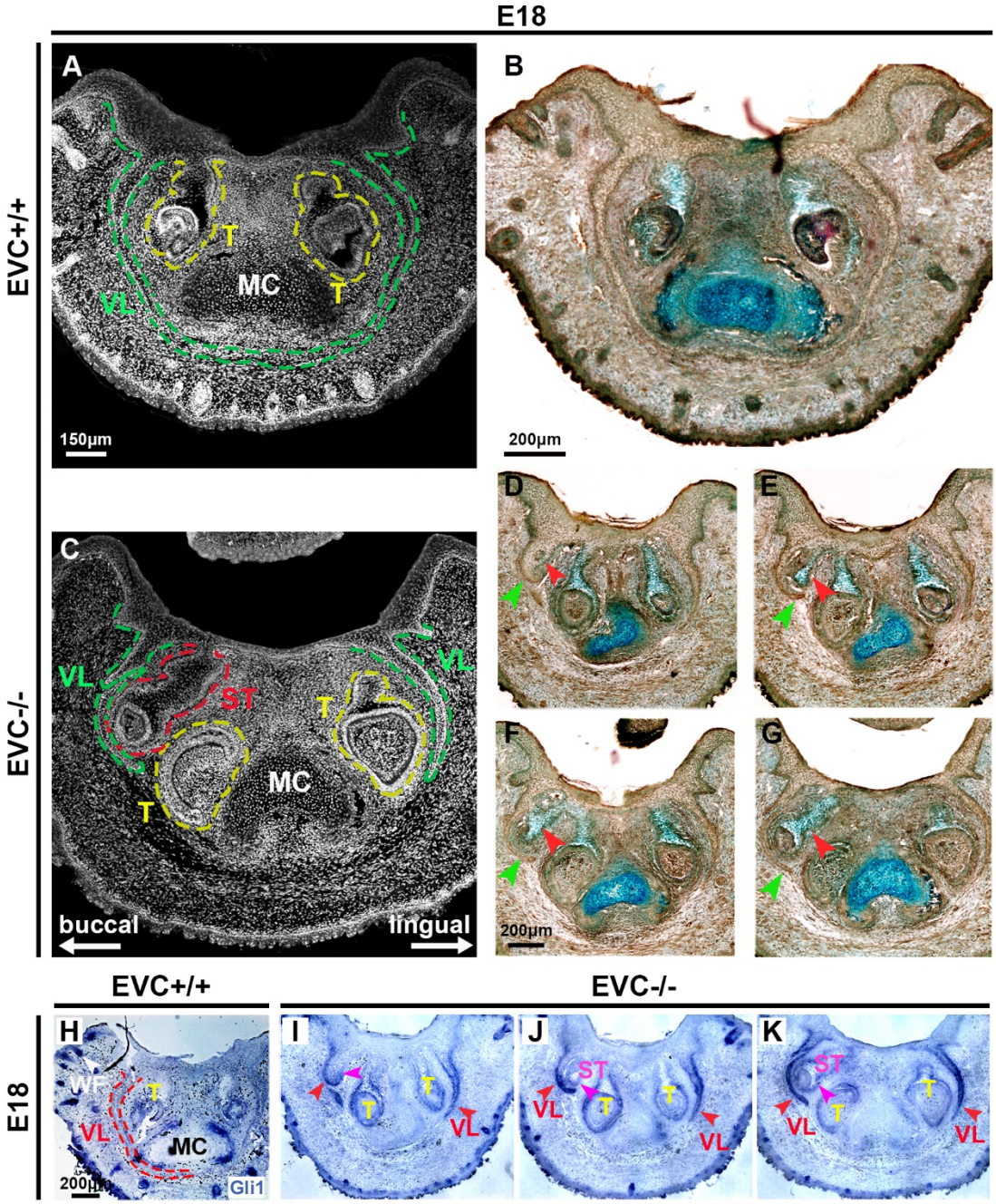

Figure 21. Extra tooth germ formed in the *Evc* homozygous mutants, with upregulated *Gli1* expression in the truncated VL and the normal *Gli1* expression in the extra tooth at E18. (**A, C**) Immunofluorescence for DAPI (grey). (**A**) WT littermate control. (**C**) *Evc* homozygous mutant displays a supernumerary tooth germ on the lingual side of the truncated VL. (**B, D-G**) To provide further insight, histological frontal sections of the anterior mandible were obtained using trichrome staining. (**B**)

WT littermate control. (**D-G**) *Evc* homozygous mutant show an extra tooth germ (pointed by red arrowheads) formed from the VL (indicated by green arrowheads). (**H-K**) DIG *in situ* hybridization for Gli1, with positive stain in blue. (**H**) WT littermates. *Gli1* expression was notably decreased in the VL, but it continued to be present in other developing regions, including the whisker follicles, Meckel's cartilage, and tooth germ. (**I-K**) *Evc* mutants. There is an upregulation of *Gli1* expression in both the truncated VL and the VL giving rise to the extra tooth germ, especially at the end of the VL. VL: Vestibular lamina; T: Incisor tooth germ; MC: Meckel's cartilage; WF: Whisker follicles; ST: supernumerary tooth germ. Buccal-lingual axes displayed in C shown for all images. Scale bars in (A, C) = 150μm; Scale bar in (B) = 200μm; Scale bar in (D-G) = 200μm; Scale bar in (H-K) = 200μm.

Overall, the analysis of the *Evc* mutant mice emphasized the important role of Hedgehog signalling in both VL and tooth formation and helped to explain the phenotype observed in EvC patients. These mice are an excellent model for further exploration of the VL and to understand the complex and tissue specific changes to *Gli1*.

Discussion

Analysis of a ciliopathy mutant (*Evc*) in this chapter highlighted interesting similarities and differences between the mechanisms involved in VL defects when compared to *Gas1* mutants

During mouse development, the DL and VL originate from a placode that expresses *Shh*, but *Shh* expression is subsequently silenced in the VL (**Hovorakova *et al.*, 2016**). Despite the fact that the VL stops expressing *Shh* after the initial placodal stages showed in chapter 5 that the VL development relies on Shh signals from the adjacent forming tooth, with the upregulation of Shh co-receptors, *Cdo*, *Boc*, and *Gas1* observed in the developing VL (**Qiu *et al.*, 2023**). The absence of *Gas1* affected VL development, as shown by a truncated VL detected in *Gas1*$^{-/-}$ mice along with a decrease/misexpression of Shh signalling readouts and a reduction in cellular proliferation (**Qiu *et al.*, 2023**). As previously noted in the introduction, EVC is a key protein involved in Shh signaling transmission through the primary cilium (**Ruiz-Perez *et al.*, 2007**). As predicted, given the impact on Hedgehog signaling, the *Evc*$^{-/-}$ mice display a similar pattern of VL shortening to *Gas1* mutants (**Fig. S11; Qiu *et al.*, 2023)**, potentially resulting from decreased Shh pathway activity. The midline phenotype of a fused upper incisor in *Evc* mutant mice (**Fig. S11**) closely mimics the premaxillary incisor fusion observed in *Gas1*$^{-/-}$ mice (**Seppala *et al.*, 2007**). The close relationship between these two genetic mutations is highlighted by our results. It is intriguing to note that although *Evc* and *Gas1* mutants display comparable VL truncation patterns, they exhibit different pathological mechanisms. Interestingly, similar to *Gas1* mutants, a truncated VL was also observed in *Evc* mutants with reduced proliferation, but instead of loss of *Gli1* we observed an increase in this readout of Hh signalling in *Evc*

mutants. This is also in contrast to published research which has shown significant decrease of *Gli1* expression in the skeleton in *Evc*$^{-/-}$ mice (**Ruiz-Perez *et al.*, 2007**), and sequentially diminished response to Shh signaling from the buccal to lingual direction during the development of first lower molars in *Evc*$^{-/-}$ mice (**Nakatomi *et al.*, 2013**). Although primary cilia have a conserved structure and are commonly thought to be homogeneous in function, recent research has highlighted an appreciation that defects in the same cilia machinery have different impacts on different tissues (**Elliott and Brugmann, 2019; Brooks *et al.*, 2021**). Our most recent studies have validated a comparable decrease in *Gli1* expression pattern in the first molar of *Evc*$^{-/-}$ mice (data is not shown), suggesting the response to loss of *EVC* is context dependent. It would be fascinating to further examine other Shh response indicators such as *Ptch1* and *Shh* in other craniofacial tissues in *Evc*$^{-/-}$ mice.

Vestibule changes, such as accessory frenula are critical clinical indicators that can aid in the diagnosis of ciliopathies in patients

Vestibular defects are a prevalent oral clinical manifestation observed in individuals with EvC syndrome, which are often characterized by the presence of multiple frenula and the attachment of gums to the upper lips and cheeks (**Sasalawad *et al.*, 2013**). Few previous studies have also reported vestibular frenula defects in oral-facial-digital (OFD) syndromes (**Bruel *et al.*, 2018**) and Joubert syndrome (**Penon-Portmann *et al.*, 2022**). This implies that other

ciliopathies may also have vestibular abnormalities, which could have been overlooked in previous case studies. The phenotypes observed in *Evc* mutants closely resemble those found in EvC patients, particularly the oral defects, which is consistent with previous studies (**Ruiz-Perez *et al.*, 2007; Nakatomi *et al.*, 2013**).

The new identified shorter VL phenotypes in *Evc* mutants, as observed in our latest findings, could be potentially considered as a possible mechanism leading to the formation of shallower oral vestibule. Although we expected that the gums and lips adherence could be associated with the failure opening of VL, our findings showed that $Evc^{-/-}$ mice were still able to create a vestibule by opening the VL normally at least in the anterior region, with the presence of small holes in the multiple VL (**Fig. 15; Qiu and Tucker, 2022**). This suggests that the differentiation mechanisms of the VL opening may remained unaffected. The shallower oral vestibule observed in postnatal *Evc* mutants is most likely due to an incomplete extension of the VL, rather than a failure to open it. However, further research on the differentiation process in *Evc* mutants is necessary to confirm this hypothesis.

3D reconstructions of the VL in humans have revealed that the VL is a highly intricate structure that branches out to connect with the DL during development (**Hovorakova *et al.*, 2005, 2007; Qiu *et al.*, 2020**). However, in mice, the

anterior VL appears as a single extension only (**Hovorakova *et al.*, 2016**). The branching of VL observed in our studies on *Evc* mutants may be associated with the development of accessory frenula in individuals with EvC syndrome. Epithelial tissue branching is a common phenomenon in various organs, such as the kidneys, salivary glands, and lungs, which is regulated by Fgf signaling (**Zhang *et al*., 2014; Chatzeli, Gaete, and Tucker, 2017**) . It would be intriguing to further investigate whether an increase in Fgf signaling is responsible for the development of multiple VL formations observed in *Evc* mutants.

Overall, vestibule changes, including accessory frenula, altered attachment, shallower oral vestibule, and other defects, could serve as crucial clinical indicators for diagnosing ciliopathies in patients.

Supernumerary tooth formation in *Evc* mutants provide new insights into odontoma formation and dental defects in EvC syndrome

It has been reported that in mice, the VL and DL share a Shh expressing domain (**Hovorakova *et al.*, 2016**), suggesting a potential common developmental origin. Our previous research has confirmed that the human VL and DL have a significant developmental correlation, particularly in the lower incisor region, where these two laminas share a common origin (**Qiu *et al.*, 2020**). As we have discussed in the introduction, the tooth-like tumors could be formed under some pathological conditions. Studies have demonstrated that an overactive Wnt

signaling pathway in the epithelium can lead to an upsurge in tooth development (**Järvinen *et al.*, 2006; Popa, Buchtova and Tucker, 2019**). However, mesenchymal Wnts have been shown to suppress tooth development. Reducing Wnt activity in the mesenchyme in mice has led to the formation of ectopic teeth by enabling other regions of the epithelium to contribute to tooth formation (**Järvinen *et al.*, 2018**). Hh and Wnt signaling pathways have a complex relationship in various tissues, and alterations in Hh signaling may have an effect on Wnt signaling (**Sarkar *et al.*, 2000; Kumar *et al.*, 2021**). The emergence of supernumerary tooth germs in *Evc* mutants may result from an imbalance of Wnt signaling between the ectoderm and neural crest-derived mesenchyme.

Dental abnormalities found in *Evc* mutants such as fused upper teeth and supernumerary teeth, resembling the dental defects observed in EvC patients (**Mostafa *et al.*, 2005**). In *Gas1* mutants, the upper fused teeth and supernumerary tooth formation in toothless diastema region were observed, along with the reduced levels of Shh transduction (**Seppala *et al.*, 2022**). Unlike the *Gas1* mutants, the occurrence of extra tooth germs from the VL in *Evc* mutants coincides with an increase in *Gli1* expression observed in the truncated VL, suggesting an alternative possibility of potential activation of the non-canonical Shh signaling pathway. A common feature of non-canonical Shh signaling pathway is the independent activity of GLI transcription factors without

requiring PTCH1/SMO or Shh ligand, which often results in oncogenic effects caused by increased GLI activity **(Pietrobono, Gagliardi and Stecca, 2019**). Therefore, it is crucial to further investigate the expression of *Ptch1* in both the shortened VL and supernumerary tooth.

To summarize, the examination of VL and DL defects in *Evc* mouse models provides new insights into the mechanisms underlying ciliopathies, especially EvC syndrome. Further studies are necessary, including quantifying the shortened VL, quantifying proliferation and *Gli1* expression in the truncated VL, using explant culture of VL to rescue the phenotype, verifying *LacZ* expression in *Evc* mice, analyzing the Wnt signaling pathway to understand the mechanisms behind supernumerary tooth formation in *Evc* mutants, examining the Fgf signaling pathway to understand the mechanisms of multiple VL formation, and exploring the context-dependent effects of other Hh signaling components.

References:

Baujat, G. and Le Merrer, M. (2007) ‘Ellis-van creveld syndrome’, *Orphanet Journal of Rare Diseases*, 2(1), pp. 1–5. doi: 10.1186/1750-1172-2-27.

Berbari, N. F. *et al.* (2009) ‘The Primary Cilium as a Complex Signaling Center’, *Current Biology*, 19(13), pp. 526–535. doi: 10.1016/j.cub.2009.05.025.

Blair, H. J. *et al.* (2011) ‘Evc2 is a positive modulator of Hedgehog signalling that interacts with Evc at the cilia membrane and is also found in the nucleus’, *BMC Biology*, 9, pp. 1–13. doi: 10.1186/1741-7007-9-14.

Brooks, E. C. *et al.* (2021) ‘Mutation in the ciliary protein c2cd3 reveals organ-specific mechanisms of hedgehog signal transduction in Avian Embryos’, *Journal of Developmental Biology*, 9(2). doi: 10.3390/jdb9020012.

Bruel, A. L. *et al.* (2017) ‘Fifteen years of research on oral-facial-digital syndromes: From 1 to 16 causal genes’, *Journal of Medical Genetics*, 54(6), pp. 371–380. doi: 10.1136/jmedgenet-2016-104436.

Bruel, A. L. *et al.* (2018) ‘INTU-related oral-facial-digital syndrome type VI: A confirmatory report’, *Clinical Genetics*, 93(6), pp. 1205–1209. doi: 10.1111/cge.13238.

Caparrós-Martín, J. A. *et al.* (2013) ‘The ciliary EVC/EVC2 complex interacts with smo and controls hedgehog pathway activity in chondrocytes by regulating Sufu/Gli3 dissociation and Gli3 trafficking in primary cilia’, *Human Molecular Genetics*, 22(1), pp. 124–139. doi: 10.1093/hmg/dds409.

Chatzeli, L., Gaete, M., & Tucker, A. S. (2017). Fgf10 and Sox9 are essential for the establishment of distal progenitor cells during mouse salivary gland development. Development (Cambridge, England), 144(12), 2294–2305. https://doi.org/10.1242/dev.146019.

Elliott, K. H. and Brugmann, S. A. (2019) ‘Sending mixed signals: Cilia-dependent signaling during development and disease’, *Developmental*

Biology, 447(1), pp. 28–41. doi: 10.1016/j.ydbio.2018.03.007.

Ellis, R. W. B. and Van Creveld, S. (1940) 'A syndrome characterized by ectodermal dysplasia, polydactyly, chondro-dysplasia and congenital morbus cordis: Report of three cases', *Archives of Disease in Childhood*, 15(82), pp. 65–84. doi: 10.1136/adc.15.82.65.

Fons Romero, J. M. *et al.* (2017) 'The Impact of the Eda Pathway on Tooth Root Development', *Journal of Dental Research*, 96(11), pp. 1290–1297. doi: 10.1177/0022034517725692.

Gaete, M. and Tucker, A. S. (2013) 'Organized Emergence of Multiple-Generations of Teeth in Snakes Is Dysregulated by Activation of Wnt/Beta-Catenin Signalling', *PLoS ONE*, 8(9). doi: 10.1371/journal.pone.0074484.

Galdzicka, M. *et al.* (2002) 'A new gene, EVC2, is mutated in Ellis-van Creveld syndrome', *Molecular Genetics and Metabolism*, 77(4), pp. 291–295. doi: 10.1016/S1096-7192(02)00178-6.

García, E. B. G. and Knoers, N. V. (2009) 'Gardner's syndrome (familial adenomatous polyposis): a cilia-related disorder', *The Lancet Oncology*, 10(7), pp. 727–735. doi: 10.1016/S1470-2045(09)70167-6.

George, E. *et al.* (2000) 'MIM 22550) in three siblings from a non-consanguineous mating', 28, pp. 425–427.

Hattab, F. N., Yassin, O. M. and Sasa, I. S. (1998) 'Oral manifestations of Ellis-van Creveld syndrome: Report of two siblings with unusual dental anomalies', *Journal of Clinical Pediatric Dentistry*, 22(2), pp. 159–165.

Hovorakova, M. *et al.* (2005) ‘The developmental relationship between the deciduous dentition and the oral vestibule in human embryos’, *Anatomy and Embryology*, 209(4), pp. 303–313. doi: 10.1007/s00429-004-0441-y.

Hovorakova, M. *et al.* (2007) ‘Early development of the lower deciduous dentition and oral vestibule in human embryos’, *European Journal of Oral Sciences*, 115(4), pp. 280–287. doi: 10.1111/j.1600-0722.2007.00464.x.

Hovorakova, M. *et al.* (2011) ‘Shh expression in a rudimentary tooth offers new insights into development of the mouse incisor’, *Journal of Experimental Zoology Part B: Molecular and Developmental Evolution*, 316 B(5), pp. 347–358. doi: 10.1002/jez.b.21408.

Hovorakova, M. *et al.* (2016) ‘One Odontogenic Cell-Population Contributes to the Development of the Mouse Incisors and of the Oral Vestibule’, pp. 1–16. doi: 10.1371/journal.pone.0162523.

Hovorakova, M. *et al.* (2020) *Reawakening of Ancestral Dental Potential as a Mechanism to Explain Dental Pathologies*, *Integrative and Comparative Biology*. doi: 10.1093/icb/icaa053.

Hunter, M. L. and Roberts, G. J. (1998) ‘Oral and dental anomalies in Ellis van Creveld syndrome (chondroectodermal dysplasia): Report of a case’, *International Journal of Paediatric Dentistry*, 8(2), pp. 153–157. doi: 10.1046/j.1365-263X.1998.00069.x.

Järvinen, E. *et al.* (2006) ‘Continuous tooth generation in mouse is induced by activated epithelial Wnt/β-catenin signaling’, *Proceedings of the National*

Academy of Sciences of the United States of America, 103(49), pp. 18627–18632. doi: 10.1073/pnas.0607289103.

Järvinen, E. *et al.* (2018) 'Mesenchymal Wnt/β-catenin signaling limits tooth number', *Development (Cambridge)*, 145(4), pp. 1–12. doi: 10.1242/dev.158048.

Kantaputra, P. N. *et al.* (2022) 'Cryptophthalmos, dental anomalies, oral vestibule defect, and a novel FREM2 mutation', *Journal of Human Genetics*, 67(2), pp. 115–118. doi: 10.1038/s10038-021-00972-4.

Kumar, V. *et al.* (2021) 'The Role of Notch, Hedgehog, and Wnt Signaling Pathways in the Resistance of Tumors to Anticancer Therapies', *Frontiers in Cell and Developmental Biology*, 9(April), pp. 1–24. doi: 10.3389/fcell.2021.650772.

Louie, K. W., Mishina, Y. and Zhang, H. (2020) 'Molecular and cellular pathogenesis of ellis-van creveld syndrome: Lessons from targeted and natural mutations in animal models', *Journal of Developmental Biology*, 8(4), pp. 1–15. doi: 10.3390/jdb8040025.

Mostafa, M. I. *et al.* (2005) 'Unusual pattern of inheritance and orodental changes in the Ellis-Van Creveld syndrome', *Genetic Counseling*, 16(1), pp. 75–83.

Nakatomi, M. (2009) 'Ellis-van Creveld (EvC) Syndrome: Unusual Oral Defects in Humans and Evc Mutant Mice', *Journal of Oral Biosciences*, 51(3), pp. 151–157. doi: 10.1016/s1349-0079(09)80023-6.

Nakatomi, M. *et al.* (2013) ‘Evc regulates a symmetrical response to Shh signaling in molar development’, *Journal of Dental Research*, 92(3), pp. 222–228. doi: 10.1177/0022034512471826.

Nethan, S. T., Sinha, S. and Chandra, S. (2017) ‘Ellis-van creveld with an unusual dental anomaly: A case report’, *Iranian Journal of Medical Sciences*, 42(5), pp. 501–504.

Penon-Portmann, M. *et al.* (2022) ‘De novo heterozygous variants in SLC30A7 are a candidate cause for Joubert syndrome’, *American Journal of Medical Genetics, Part A*, 188(8), pp. 2360–2366. doi: 10.1002/ajmg.a.62872.

Peterková, R. (1985) ‘The common developmental origin and phylogenetic aspects of teeth, rugae palatinae, and fornix vestibuli oris in the mouse.’, *Journal of craniofacial genetics and developmental biology*, 5(1), pp. 89–104. Available at: http://www.ncbi.nlm.nih.gov/pubmed/2580855 (Accessed: 13 April 2020).

Pietrobono, S., Gagliardi, S. and Stecca, B. (2019) ‘Non-canonical hedgehog signaling pathway in cancer: Activation of GLI transcription factors beyond smoothened’, *Frontiers in Genetics*, 10(JUN), pp. 1–20. doi: 10.3389/fgene.2019.00556.

Popa, E. M., Buchtova, M. and Tucker, A. S. (2019a) ‘Revitalising the rudimentary replacement dentition in the mouse’, *Development (Cambridge, England)*, 146(3). doi: 10.1242/dev.171363.

Popa, E. M., Buchtova, M. and Tucker, A. S. (2019b) ‘Revitalising the

rudimentary replacement dentition in the mouse', *Development (Cambridge, England)*, 146(3). doi: 10.1242/dev.171363.

Qiu, T. *et al.* (2020) 'Development of the Vestibular Lamina in Human Embryos: Morphogenesis and Vestibule Formation', *Frontiers in Physiology*, 11(July). doi: 10.3389/fphys.2020.00753.

Qiu, T., & Tucker, A. S. (2022). Mechanisms driving vestibular lamina formation and opening in the mouse. Journal of anatomy, 242(2), 224–234. https://doi.org/10.1111/joa.13771.

Qiu, T., Hutečková, B., Seppala, M., Cobourne, M. T., Chen, Z., Hovořáková, M., Buchtová, M., & Tucker, A. S. (2023). Molecular profiling of the vestibular lamina highlights a key role for Hedgehog signalling. Development (Cambridge, England), 150(7), dev201464. https://doi.org/10.1242/dev.201464.

Roubicek, M. and Spranger, J. (1984) 'Weyers acrodental dysostosis in a family', *Clinical Genetics*, 26(6), pp. 587–590. doi: 10.1111/j.1399-0004.1984.tb01108.x.

Rui, Z. *et al.* (2014) 'Smoothened gene alterations in keratocystic odontogenic tumors', *Head and Face Medicine*, 10(1), pp. 1–7. doi: 10.1186/1746-160X-10-36.

Ruiz-Perez, V. L. *et al.* (2000) 'Mutations in a new gene in Ellis-van Creveld syndrome and Weyers acrodental dysostosis', *Nature Genetics*, 24(3), pp. 283–286. doi: 10.1038/73508.

Ruiz-Perez, V. L. *et al.* (2003) ‘Mutations in two nonhomologous genes in a head-to-head configuration cause Ellis-van Creveld syndrome’, *American Journal of Human Genetics*, 72(3), pp. 728–732. doi: 10.1086/368063.

Ruiz-Perez, V. L. *et al.* (2007) ‘Evc is a positive mediator of Ihh-regulated bone growth that localises at the base of chondrocyte cilia’, *Development*, 134(16), pp. 2903–2912. doi: 10.1242/dev.007542.

Sarkar, L. *et al.* (2000) ‘Wnt/Shh interactions regulate ectodermal boundary formation during mammalian tooth development’, *Proceedings of the National Academy of Sciences of the United States of America*, 97(9), pp. 4520–4524. doi: 10.1073/pnas.97.9.4520.

Sasalawad, S. S. *et al.* (2013) ‘Ellis-van Creveld syndrome’, *BMJ Case Reports*, pp. 1–4. doi: 10.1136/bcr-2013-009463.

Seppala, M. *et al.* (2007) ‘Gas1 is a modifier for holoprosencephaly and genetically interacts with sonic hedgehog’, *Journal of Clinical Investigation*, 117(6), pp. 1575–1584. doi: 10.1172/JCI32032.

Seppala, M *et al.* (2022) ‘Gas1 Regulates Patterning of the Murine and Human Dentitions through Sonic Hedgehog’. doi: 10.1177/00220345211049403.

Seppala, M. *et al.* (2022) ‘Gas1 Regulates Patterning of the Murine and Human Dentitions through Sonic Hedgehog’, *Journal of Dental Research*, 101(4), pp. 473–482. doi: 10.1177/00220345211049403.

Shaik, S. *et al.* (2016) ‘Ellis-van Creveld syndrome with unusual oral and

dental findings: A rare clinical entity', *Dental Research Journal*, 13(2), pp. 193–197. doi: 10.4103/1735-3327.178213.

Tompson, S. W. J. *et al.* (2007) 'Sequencing EVC and EVC2 identifies mutations in two-thirds of Ellis-van Creveld syndrome patients', *Human Genetics*, 120(5), pp. 663–670. doi: 10.1007/s00439-006-0237-7.

Wang, X. P. *et al.* (2009) 'Apc inhibition of Wnt signaling regulates supernumerary tooth formation during embryogenesis and throughout adulthood', *Development*, 136(11), pp. 1939–1949. doi: 10.1242/dev.033803.

Xavier, G. M. *et al.* (2016) 'Hedgehog receptor function during craniofacial development', *Developmental Biology*, 415(2), pp. 198–215. doi: 10.1016/j.ydbio.2016.02.009.

Yu, F. *et al.* (2018) 'A novel mutation of adenomatous polyposis coli (APC) gene results in the formation of supernumerary teeth', *Journal of Cellular and Molecular Medicine*, 22(1), pp. 152–162. doi: 10.1111/jcmm.13303.

Zhang, H. *et al.* (2015) 'Generation of Evc2/Limbin global and conditional KO mice and its roles during mineralized tissue formation', *Genesis*, 53(9), pp. 612–626. doi: 10.1002/dvg.22879.

Chapter 7: Discussion

My thesis has followed the development of the VL taking advantage of murine and human samples, and a variety of transgenic mice that can be used to model human diseases/syndromes. It offers comprehensive insights into the development of the VL, encompassing its morphological and molecular aspects. The key findings of my thesis are as follows:

1) Extra tooth germs formed from the VL in the mouse highlight the evolutionary and developmental origins of the anterior VL and DL.

2) Differences in Shh signalling level may reflect the varying VL morphology across different vertebrate species.

3) Species with varying VL morphologies undergo distinct mechanisms of vestibule formation.

4) The similar truncated VL in two Shh models (*Gas1* and *Evc* mutants) show distinct pathological mechanisms.

5) VL defects related to disrupted Shh signalling shed light on the pathological mechanisms of ciliopathies, particularly EvC syndrome.

7.1 Extra tooth germs formed from the VL in the mouse highlight the evolutionary and developmental origins of the anterior VL and DL

The DL is closely related to various developing structures in vertebrates as discussed in the introduction (**Fig. 7**). Thus, it is essential to consider the DL together with its neighboring epithelial organs, rather than in isolation. My PhD

research has identified, at least in the lower incisor region, the human VL and DL share a common origin (**Qiu *et al.*, 2020**), while DiI labelling of the murine VL and DL gave mixed results suggesting both a single and dual origin (**Fig. S1,2, Qiu and Tucker, unpublished**). Additional research such as explant culture is therefore necessary to determine the developmental relationships of these two laminae in other regions, especially the posterior jaw. The VL development and evolutionary knowledge combined with clinical pathogenesis shed light on the underlying mechanisms of additional tooth rows adjacent to the dental arch. As we have discussed, the origin of these anomalies may be explained by a “reawakening” of epithelial tissues in non-dental regions during early embryogenesis. Under pathological conditions, these epithelial tissues can exhibit odontogenic potential, leading to the formation of odontogenic cysts or tumors. The formation of extra tooth germ formed from the VL (**Fig. 21, Qiu and Tucker, unpublished**) could be part of the evolutionary history and rationalise the origin of dental pathologies that occur around the dentition.

Our preliminary RNA-Seq analysis of E13 showed that there is a close association between the VL and DL during early development, as evidenced by the expression of overlapping genes (**Fig. S3,5-7, Qiu and Tucker, unpublished**). It is therefore intriguing to explore the decisions that determine the fate of odontogenic placodes during development. Recently, a single cell RNA-Sequencing (scRNA-Seq) of the mandibular epithelium at E12 has

identified a number of distinct cell populations in spatial distinct regions of the anterior jaw (**Ye, Bhojwani and Hu, 2022**). The VL is not mentioned in this study, although the specific region of the VL is analysed. Further analysis could be carried comparing our datasets with the one of Ye et al., to identify the VL-associated cell populations and to illustrate their relationship to the DL-associated cell populations. In keeping with our study identifying novel VL markers (**Qiu *et al*., 2023**), some markers such as *Meis1* were also highlighted at a similar anatomical region in this scRNA-Seq analysis (**Ye, Bhojwani and Hu, 2022**).

Our molecular analysis focused on the anterior VL and incisor tooth germ, as the VL is prominent in this region in mice. The occurrence rate of compound odontomas or complex odontomas varies in the anterior and posterior regions of the jaw in humans (**Satish *et al*., 2011**). To understand the difference in incidence, it would be worthwhile comparing the populations of VL-cells and DL-cells in both the anterior and posterior jaw regions. Findings in this thesis provide a fundamental basis to challenge the fate decisions of VL and DL in this early placode by signalling manipulation in murine explant culture. In addition, further research can be carried out in reptiles to investigate whether the early gland-tooth relationship shares similar gene signatures to the VL-DL relationship in mice. This would allow for exploration of a conserved mechanism for fate decisions across vertebrates.

7.2 Differences in Shh signalling level may reflect the varying VL morphology across different vertebrate species

The distinct morphologies of the VL across various species, such as sheep, field voles, and mice, are summarized in **Qiu and Tucker 2022**. My PhD research primarily focused on identifying the morphology of the VL in mice and humans. The results confirmed that there are significant differences between the two species, with humans having a relatively wider VL (**Qiu *et al.*, 2020**) and mice having a thinner VL (**Qiu and Tucker, 2022**). The considerable variation in VL width observed among mammals could be explained by varying level of Shh signalling within the tissue. This is supported by my recent PhD research showing that enhanced Shh signallng induced by SMO agonist SAG could lead to significant abnormalities in the VL, presenting an expansion of the VL with an increase in Shh readouts (**Qiu *et al.*, 2023**). The anatomical relationship between the VL and the neighboring tooth germ is highly intricate and varies significantly across the jaws **(Hovorakova *et al.*, 2005, 2007; Qiu *et al.*, 2020**). Throughout my PhD research, my primary focus centered on the anterior region, particularly the lower incisor region in mouse, where the two laminas share a common placode expressing *Shh* domain (**Hovorakova *et al.*, 2016**). However, it would be valuable to extend the molecular investigation of the VL to other regions, particularly the posterior regions.

7.3 Species with varying VL morphologies undergo distinct mechanisms of vestibule formation

The contrasting morphologies of the VL gave rise to disparate opening mechanisms. The VL starts off as a solid block of epithelial tissue which subsequently undergoes division to form the oral vestibule. Opening of the human VL started from the oral surface as the cells underwent differentiation, resulting in division of the VL into multiple distinct pieces (**Qiu *et al.*, 2020**). Apoptosis was then involved in the removal of the central "V-shaped" tissue formed by the multiple fissures (**Qiu *et al.*, 2020**). In contrast, mice opened their vestibule through differentiation and merging of small cavities throughout the VL (**Qiu and Tucker, 2022**), a process that is similar to lumen formation in salivary glands (**Tucker, 2007**). Apoptosis also appeared to play a role in the mouse but in reducing the thickness of the end VL, rather than as part of opening (**Qiu and Tucker, 2022**). In both mouse and human the opening mechanism was driven by terminal differentiation of the epithelium, causing a change in cell-cell adhesions. However, the format of fissure formation differed slightly. Failure in opening in the VL would likely lead to frenulum formation, where the gingiva are permanently attached to the lips/cheeks, as seen in EvC patients **(Sasalawad *et al.*, 2013**).

7.4 The similar truncated VL in two Shh models (*Gas1* and *Evc* mutants) show distinct pathological mechanisms

As mentioned in the introduction, EVC plays a crucial role in the primary cilium by facilitating the transmission of Shh signaling. As expected, my latest PhD study shows that the *Evc* mutants exhibit a comparable pattern of VL truncation (**Fig. 15, Qiu and Tucker, unpublished**) to the *Gas1* mutants, which might be caused by the diminished Shh pathway. The fused upper incisor observed in *Evc*$^{-/-}$ mice (**Fig. 15, Qiu and Tucker, unpublished**) is a midline phenotype that closely resembles the premaxillary incisor fusion seen in *Gas1*$^{-/-}$ mice (**Seppala *et al.*, 2007**). These findings emphasize the close association between these two genetic mutations. Interestingly, the truncated VL observed in *Evc* and *Gas1* mutants exhibit distinct pathological mechanisms, despite their similarities.

Gas1 and *Evc* mutant mice both exhibit a truncated VL, but the VL in *Gas1*$^{-/-}$ mice is considerably shorter without obvious bending at E13.5 (**Qiu *et al.*, 2023**) and E14.5 (**data is not presented**). In contrast, the truncated VL in *Evc* mutants is relatively less severe at E13.5 (**data is not shown**) and E14.5 (**Fig. 15, Qiu and Tucker, unpublished**), with a curved shape but an incapacity to reach the midline. Additionally, *Gas1* mutants show reduced *Gli1* expression in the shortened VL and a loss of the labial/buccal-lingual *Gli1* expression pattern (**Qiu *et al.*, 2023**). Conversely, *Evc* mutants display increased *Gli1* expression in the truncated VL and maintain the labial/buccal-lingual expression pattern of *Gli1* **(Fig. 19)**, as well as the corresponding proliferation patterning (**Fig. 18**)

(**Qiu and Tucker, unpublished**). These results indicate that Shh signaling-mediated asymmetrical proliferation plays a critical role in the bending of the VL during early development. Previous research has provided support for this hypothesis that asymmetrical growth rates between neighboring tissues could be the underlying cause of folding and bulging (**Radlanski and Renz, 2006**). This observation could potentially clarify the reduced expression of *Gli1* during normal VL development (**Fig. 19B,C; 20B-D; 21H, Qiu and Tucker, unpublished**). By E14.5, the VL has undergone bending and is approaching the midline (**Qiu and Tucker, 2022**), resulting in a less noticeable buccal-lingual expression and a reduction in *Gli1* expression at the end of the VL. As the VL surrounds the tooth germ and extends towards the midline by E16.5 (**Qiu and Tucker, 2022**), the expression of *Gli1* is further reduced at the top and end regions of the VL. This diminished expression pattern continues through at least to E18. To validate the expression pattern of *Gli1* in the VL, it would be beneficial to investigate *Gli1* expression at earlier developmental stages, such as E13.5, as well as at later postnatal stages. *Gas1* is predominantly expressed in the buccal side of the VL, as well as in the surrounding mesenchyme of the buccal region at E13.5 to E15.5 (**Qiu *et al.*, 2023**; **Fig. S4, Qiu and Tucker, unpublished).** Whereas the expression of *Evc*, shown by the lacZ *Evc* reporter, was observed surrounding the tooth germ and VL, with strong expression at the 1/3 end of VL epithelium at E15.5 **(Ruiz-Perez *et al.*, 2007**). Such differential expression of *Gas1* and *Evc* in the VL may be responsible for the varying

pathological mechanisms observed in the truncated VL of *Gas1* and *Evc* mutants. Additional LacZ staining analysis is required to confirm the expression of *Evc* in orofacial regions, specifically in the tooth germ and VL areas during earlier developmental stages.

Both mutations result in impaired proliferation in the truncated VL at an early developmental stage (E12.5) (**Qiu *et al*., 2023; Fig. 17, Qiu and Tucker, unpublished**). This suggest that the proliferation plays a crucial role in the elongation of the VL but may not be necessary for its initiation. Thus, the disrupted proliferation observed at the end of the truncated VL in *Evc* mutants at E14.5 (**Fig. 18, Qiu and Tucker, unpublished**) may result in the failure of the VL to extend towards the midline. These findings suggest a dual role of Shh signaling-mediated proliferation in VL development. As mentioned, the asymmetrical proliferation promotes the bending of the VL in the middle region, while proliferation at the end of the VL facilitates its extension towards the midline. Therefore, the observed upregulation of *Gli1* expression at the tip of the shortened VL in the *Evc* mutants at E14.5, E16.5, and E18 (**Fig.19;20;21, Qiu and Tucker, unpublished**) may be a result of positive feedback due to the reduced proliferation in this region in the *Evc* mutants.

The bending of the VL in *Gas1* mutants at later stages, starting from E15.5, may related to developmental stalling, where the mutants show early defects

and temporal arrest of development but can recuperate through subsequent accelerated development (**Miletich et al., 2011**). To validate this hypothesis, additional samples of *Gas1* and *Evc* mutants at the same developmental stage should be analyzed. To confirm that the asymmetrical expression pattern remains unchanged, it is necessary to analyze the expression of *Gli1* in the VL of *Evc* mutants at an early developmental stage, preferably before or when the curve occurs, such as at E13.5. Additionally, exploring proliferation in the truncated VL of *Gas1* mutants at a later stage, such as E14.5, would be a compelling area for further investigation.

7.5 VL defects related to disrupted Shh signalling shed light on the pathological mechanisms of ciliopathies, particularly EvC syndrome

EvC syndrome is related to defective primary cilium and disrupted Shh signaling, and our most recent study has confirmed this pathway could be essential for proper VL development (**Qiu *et al.*, 2023**). Vestibule defects are the most common oral clinic manifestations in the individuals of EvC syndrome (see details in the introduction), with the presence of multiple frenula and the attachment of gums to the upper lips and cheeks (**Sasalawad *et al.*, 2013**). Vestibule abnormalities were also expected to be associated in other ciliopathies, and as such, Joubert syndrome (**Penon-Portmann *et al.*, 2022**) and oral-facial-digital (OFD) syndromes (**Bruel *et al.*, 2018**) have been found to exhibit frenula defects. Therefore, my investigation on the VL in *Evc* mouse

models could provide valuable insights.

The *Evc* mutants closely resemble the phenotypes observed in EvC patients, particularly with regards to the oral defects, with the branching of the VL a potential mechanism for the generation of accessory frenula (**Ruiz-Perez *et al.*, 2007; Nakatomi *et al.*, 2013; Fig. 15L; 20F-H**, **Qiu and Tucker, Unpublished**). Attachment of the gums and tissues might be expected to be caused by failure of opening, however, our *Evc* mice were still able to open the anterior VL to create a vestibule, with the presence of small holes in the lower anterior multiple VL of *Evc* mutants at P4 (**Fig. 15L, Qiu and Tucker, Unpublished**), suggesting that the differentiation mechanisms was unaffected. The shallow oral vestibule observed postnatally is therefore likely to be due to incomplete extension of the VL, rather than a failure in the opening of the VL. More in-depth studies on the differentiation process in *Evc* mutants would be necessary to confirm this. Given the reliance of the developing VL on Shh signalling through cilia, vestibule changes, including accessory frenula, changed attachment and other defects could serve as a crucial clinical feature for diagnosing ciliopathies in patients.

The formation of supernumerary tooth germs in the *Evc* mutants is accompanied by an increase in *Gli1* expression in the truncated VL (**Fig. 21, Qiu and Tucker, unpublished**), indicating the potential activation of the non-

canonical Shh signaling pathway. This pathway is characterized by GLI transcription factors acting independently of PTCH1/SMO or Shh ligand and is commonly associated with oncogenic effects due to increased GLI activity (**Pietrobono, Gagliardi and Stecca, 2019**). It would be therefore important to examine the expression of *Ptch1* in both the VL and supernumerary tooth.

Hh has an intricate relationship with Wnt signalling in a number of tissues (**Sarkar *et al.*, 2000; Day and Yang, 2008**; **Kumar *et al.*, 2021**). Therefore, changes in hedgehog signalling may impact Wnt signalling. Aanalysis of RNA-Seq data at E14 highlighted the importance of the Wnt signaling pathway and its interaction with Shh in the early development of the VL and DL (**Fig. S8,9. Qiu *et al.*, Unpublished**). Mesenchymal Wnts have been found to have a suppressive effect on tooth development. In mouse, decreasing Wnt activity in the mesenchyme, led to the formation of ectopic teeth by allowing other regions of the epithelium to contribute to tooth formation (**Järvinen *et al.*, 2018**). In contrast, overactivation of Wnt signalling in the epithelium led to an increase in tooth development (**Järvinen *et al.*, 2006; Popa, Buchtova and Tucker, 2019**). The balance of Wnt signalling in the two different tissues (ectoderm and neural crest derived mesenchyme) is therefore intriguing for future exploration in the context of the VL and supernumerary tooth formation.

Despite the loss of *Gli1* expression in the additional branches of the VL in *Evc*

mutants, there was a significant upregulation of *Gli1* expression in the VL, particularly in the end region (**Fig. 20, Qiu and Tucker, Unpublished**). This suggests that the regulation of *Gli1* via EVC may be context-dependent. Thus, it would be necessary to investigate other Shh readouts, such as *Ptch1* and *Gli1*, in other craniofacial tissues of *Evc* mutant mice.

3D reconstructions of the VL in humans have shown that the VL is not a simple sheet but branches to link up with the DL during human development (**Hovorakova *et al.*, 2005, 2007; Qiu *et. al*., 2020**). In the mouse, however, the anterior VL appears as a single extension (**Hovorakova *et al.*, 2016**). In the *Evc* mutants the epithelium of the VL appeared to branch (**Fig. 15; 20, Qiu and Tucker, Unpublished**). Branching of epithelial tissues occurs in a number of organs (lungs, salivary glands, kidney) and depends on the critical function of Fgf signaling (**Zhang *et al*., 2014; Chatzeli, Gaete, and Tucker, 2017**). It would therefore be interesting to test whether an upregulation of Fgf signaling is responsible for the development of multiple VL formation in the *Evc* mutants.

In summary, my PhD research has addressed a gap in odontogenic studies by providing a comprehensive investigation of the VL and its developmental relationship with the DL, thereby contributing new insights to the field. Specifically, these findings highlight the importance of a previously overlooked structure that plays a crucial role in the development of the oral cavity. The

uncovered mechanisms of normal oral vestibule formation in both mice and human have shown a close developmental relationship between the VL and DL. Additionally, molecular profiling of the VL in relation to the DL has highlighted the involvement of Shh signals from the adjacent tooth germ during VL development, while the VL and DL defects identified in *Gas1* and *Evc* mouse models have provided the basis for further VL studies and enhanced our understanding of disorders linked to this region, such as ciliopathies. In the future it is hoped that increased understanding of the VL and vestibule and its association with ciliopathies will improve the diagnosis and outcomes for patients.

Acknowledgements

I would like to express my heartfelt gratitude to my first supervisor Prof. Abigail Tucker for her invaluable guidance and strongly support throughout my PhD journey. It’s been a steep learning curve for me since I came to King's. My PhD journey began with many challenges as I was a dentist with limited understanding of developmental theory. However, her patient and encouragement enabled me to overcome all obstacles and grow as a researcher. She was always available to offer help and guidance whenever I faced academic or personal hurdles. Even during the pandemic, when I was stuck in China for an extended period, she continued to provide invaluable support despite the distance and time zone differences. Thanks to her strongly support, I was fortunate to have various opportunities to enhance my knowledge and skills. These included attending conferences, applying for grants, and visiting labs in Oxford and China etc. I feel incredibly fortunate to be her student. Not only is she a leading figure in the field, but she is also incredibly kind and supportive. I am very grateful for the invaluable guidance and support she provided me throughout my PhD journey, and her mentorship will have a lasting impact on my future career.

I am grateful for the support of my second supervisor Dr. Isabelle Miletich and the committee panels (Prof. Gordon Proctor, Dr. Ana Angelova Volponi, Dr. Maisa Seppala) throughout my PhD journey, and I would like to express my

sincere appreciation to them.

I would like to express my gratitude to all the collaborators who have supported and contributed to my publications: Prof. Maria Hovorakova (Charles University, Prague, Czech Republic), Prof. Zhi Chen (Wuhan University, China), Dr. Maisa Seppala (KCL, UK), Prof. Marcela Buchtová (Institute of Animal Physiology and Genetics/Masaryk University, Czech Republic), Prof. Martyn T. Cobourne (KCL, UK), Dr. Tathyane H. N. Teshima (UCL, UK), and Dr. Barbora Hutečková (Institute of Animal Physiology and Genetics/Masaryk University, Czech Republic). Their valuable contributions have been instrumental in the success of my research, and I am truly thankful for their support.

I would like to extend my thanks to my supervisors of the host labs at both China and Oxford for their generous support during my lab visits: Prof. Zhi Chen (Wuhan University, China), Prof. Stephen Twigg (University of Oxford, UK), and Prof. Andrew Wilkie (University of Oxford, UK). In particular, I would like to express my gratitude to the CZ group and Clinical genetics group for their invaluable support to my research.

I would like to express my gratitude to Tucker's lab for their help during my PhD journey, especially Dr. Juan Fons Romero, Dr. Neal Anthwal, and Sun Ying. And I am deeply grateful for the opportunity to work with such a dedicated and

knowledgeable team.

I would like to express my sincere appreciation to China, the China Scholarship Council, and King's College London for their generous support throughout my PhD journey. Their support has provided me with the opportunity to pursue my academic goals and has been instrumental in my success.

I owe a debt of gratitude to my family for their unwavering support and encouragement throughout my academic journey. Their belief in me has been a constant source of motivation, and I am immensely grateful for their love and support.

I would like to extend my thanks to my friends and the Centre for Craniofacial and Regenerative Biology for their invaluable assistance. Their support has been instrumental in my academic achievements, and I am deeply grateful for their help and encouragement.

References/Bibliography

Adloff P. (1907). Zur Frage der überzähligen Zähne im menschlichen Gebiss. Deut Monatschr Zahnheilk 22:622–624.

Adloff P. (1909). Überreste einer prälactealen Zahnreihe beim Menschen. Deut Monatschr Zahnheilk 11:828-832.

Adloff P. (1916). Die Entwicklung des Zahnsystems der Säugetiere und des Menschen. Eine kritik der Dimertheorie von Bolk. Meusser, Berlin, Germany.

Alfaqeeh, S. A., and Tucker, A. S. (2013). The slice culture method for following development of tooth germs in explant culture. J. Vis. Exp. 81:e50824. doi:10.3791/50824.

Allen, B. L., Song, J. Y., Izzi, L., Althaus, I. W., Kang, J. S., Charron, F., Krauss, R. S. and Mcmahon, A. P. (2011). Overlapping roles and collective requirement for the coreceptors GAS1, CDO, and BOC in SHH pathway function, *Developmental Cell*, 20(6), pp. 775–787. doi: 10.1016/j.devcel.2011.04.018.

Amack J. D. (2022). Structures and functions of cilia during vertebrate embryo development. Molecular reproduction and development, 89(12), 579–596. https://doi.org/10.1002/mrd.23650.

Aubert-Mucca, M. *et al.* (2022) 'Ellis-Van Creveld Syndrome: Clinical and Molecular Analysis of 50 Individuals', *Journal of Medical Genetics*, pp. 1–9. doi: 10.1136/jmg-2022-108435.

Badri, M. K., Zhang, H., Ohyama, Y., Venkitapathi, S., Alamoudi, A., Kamiya,

N., Takeda, H., Ray, M., Scott, G., Tsuji, T., Kunieda, T., Mishina, Y., & Mochida, Y. (2016). Expression of Evc2 in craniofacial tissues and craniofacial bone defects in Evc2 knockout mouse. Archives of oral biology, 68, 142–152. https://doi.org/10.1016/j.archoralbio.2016.05.002

Bangs, F. and Anderson, K. V. (2017) 'Primary cilia and Mammalian Hedgehog signaling', *Cold Spring Harbor Perspectives in Biology*, 9(5), pp. 1–21. doi: 10.1101/cshperspect.a028175.

Baujat, G. and Le Merrer, M. (2007) 'Ellis-van creveld syndrome', *Orphanet Journal of Rare Diseases*, 2(1), pp. 1–5. doi: 10.1186/1750-1172-2-27.

Beales, P. L. *et al.* (2007) 'IFT80, which encodes a conserved intraflagellar transport protein, is mutated in Jeune asphyxiating thoracic dystrophy', *Nature Genetics*, 39(6), pp. 727–729. doi: 10.1038/ng2038.

Berbari, N. F. *et al.* (2009) 'The Primary Cilium as a Complex Signaling Center', *Current Biology*, 19(13), pp. R526–R535. doi: 10.1016/j.cub.2009.05.025.

Bhaskar SN. Orban's oral histology and embryology, 9th edn.. St Louis, Toronto, London: The CV Mosby Company, 1980.

Blair, H. J. *et al.* (2011) 'Evc2 is a positive modulator of Hedgehog signalling that interacts with Evc at the cilia membrane and is also found in the nucleus', *BMC Biology*, 9, pp. 1–13. doi: 10.1186/1741-7007-9-14.

Boffano, P. *et al.* (2022) 'The epidemiology and management of odontomas: a European multicenter study', *Oral and Maxillofacial Surgery*, (0123456789).

doi: 10.1007/s10006-022-01091-w.

Bolk L. (1914). Supernumerary teeth in the molar region in man. Dent Cosmos 56:154–167.

Bolk, L. (1921). Odontological essays. Journal of Anatomy, 55, 219– 234.

Bolk, L., (1924). Die "Nebenleiste" der Saugetiere und die "Zahndrusenleiste" der Reptilien. Deutsche Monatsschrift fur Zahnheilkunde 7, 129-137.

Bruel, A. L. *et al.* (2017) ‘Fifteen years of research on oral-facial-digital syndromes: From 1 to 16 causal genes’, *Journal of Medical Genetics*, 54(6), pp. 371–380. doi: 10.1136/jmedgenet-2016-104436.

Bruel, A.-L., Levy, J., Elenga, N., Defo, A., Favre, A., Lucron, H., Capri, Y., Perrin, L., Passemard, S., Vial, Y. et al. (2018). INTU-related oral-facial-digital syndrome type VI: A confirmatory report. Clin. Genet. 93, 1205-1209. doi:10.1111/ cge.13238。

Buchtová, M. *et al.* (2013) ‘Odontogenesis in the Veiled Chameleon (Chamaeleo calyptratus)’, *Archives of Oral Biology*, 58(2), pp. 118–133. doi: 10.1016/j.archoralbio.2012.10.019.

Buchtová, M., Handrigan, G. R., Tucker, A. S., Lozanoff, S., Town, L., Fu, K., Diewert, V. M., Wicking, C. and Richman, J. M. (2008). Initiation and patterning of the snake dentition are dependent on Sonic Hedgehog signaling. Dev. Biol. 319, 132-145. doi:10.1016/j.ydbio.2008.03.004.

Cahuana, A. *et al.* (2004) ‘Oral manifestations in Ellis-van Creveld syndrome: Report of five cases’, *Pediatric Dentistry*, 26(3), pp. 277–282.

Caparrós-martín, J. A. *et al.* (2015) 'Specific variants in WDR35 cause a distinctive form of ellis-van creveld syndrome by disrupting the recruitment of the evc complex and smo into the cilium', *Human Molecular Genetics*, 24(14), pp. 4126–4137. doi: 10.1093/hmg/ddv152.

Caparrós-Martín, J. A., Valencia, M., Reytor, E., Pacheco, M., Fernandez, M., Perez-Aytes, A., Gean, E., Lapunzina, P., Peters, H., Goodship, J. A. et al. (2013) 'The ciliary EVC/EVC2 complex interacts with smo and controls hedgehog pathway activity in chondrocytes by regulating Sufu/Gli3 dissociation and Gli3 trafficking in primary cilia', *Human Molecular Genetics*, 22(1), pp. 124–139. doi: 10.1093/hmg/dds409.

Caspary, T., Larkins, C. E. and Anderson, K. V. (2007) 'The Graded Response to Sonic Hedgehog Depends on Cilia Architecture', *Developmental Cell*, 12(5), pp. 767–778. doi: 10.1016/j.devcel.2007.03.004.

Chai, Y., Jiang, X., Ito, Y., Bringas, P., Jr, Han, J., Rowitch, D. H., Soriano, P., McMahon, A. P., & Sucov, H. M. (2000). Fate of the mammalian cranial neural crest during tooth and mandibular morphogenesis. Development (Cambridge, England), 127(8), 1671–1679. https://doi.org/10.1242/dev.127.8.1671.

Chatzeli, L., Gaete, M., & Tucker, A. S. (2017). Fgf10 and Sox9 are essential for the establishment of distal progenitor cells during mouse salivary gland development. Development (Cambridge, England), 144(12), 2294–2305. https://doi.org/10.1242/dev.146019.

Cheng, S. Y. and Michael Bishop, J. (2002) ‘Suppressor of Fused represses Gli-mediated transcription by recruiting the SAP18-mSin3 corepressor complex’, *Proceedings of the National Academy of Sciences of the United States of America*, 99(8), pp. 5442–5447. doi: 10.1073/pnas.082096999.

Chlastakova, I., Lungova, V., Wells, K., Tucker, A.S., Radlanski, R.J., Misek, I. et al. (2011) Morphogenesis and bone integration of the mouse mandibular third molar. European Journal of Oral Sciences, 119, 265–274.

Cobourne, M. T., Miletich, I. and Sharpe, P. T. (2004). Restriction of sonic hedgehog signalling during early tooth development. Development 131, 2875-2885. doi:10.1242/dev.01163.

Coolen, N. A., Schouten, K. C. W. M., Middelkoop, E., and Ulrich, M. M. W. (2010). Comparison between human fetal and adult skin. Arch. Dermatol. Res. 302, 47–55. doi: 10.1007/s00403-009-0989-8.

Cooper, M. K., Porter, J. A., Young, K. E., & Beachy, P. A. (1998). Teratogen-mediated inhibition of target tissue response to Shh signaling. Science (New York, N.Y.), 280(5369), 1603–1607. https://doi.org/10.1126/science.280.5369.1603

Corbit, K. C. *et al.* (2005) ‘Vertebrate Smoothened functions at the primary cilium’, *Nature*, 437(7061), pp. 1018–1021. doi: 10.1038/nature04117.

Coslet, J. G. and Cohen, D. W. (1969) ‘Observations on the Development of the Vestibular Trough in the Human Fetus Part I. The Anterior Portion of the Mouth’, *Journal of Periodontology*, 40(6), pp. 320–329. doi:

10.1902/jop.1969.40.6.320.

Dale, B. A., Holbrook, K. A., Kimball, J. R., Hoff, M., and Sun, T. T. (1985). Expression of epidermal keratins and filaggrin during human fetal skin development. J. Cell Biol. 101, 1257–1269. doi: 10.1083/jcb.101.4.1257.

Danielian, P. S., Muccino, D., Rowitch, D. H., Michael, S. K. and Mcmahon, A. P. (1998). Modification of gene activity in mouse embryos in utero by a tamoxifeninducible form of cre recombinase. Curr. Biol. 8, 1323-1326. doi:10.1016/S0960- 9822(07)00562-3.

Davey, M. G. *et al.* (2014) 'Loss of cilia causes embryonic lung hypoplasia, liver fibrosis, and cholestasis in the talpid3 ciliopathy mutant', *Organogenesis*, 10(2), pp. 177–185. doi: 10.4161/org.28819.

Davideau, J.L., Demri, P., Hotton, D., Gu, T.T., MacDougall, M., Sharpe, P., Forest, N., Berdal, A., (1999). Comparative study of MSX-2, DLX-5, and DLX-7 gene expression during early human tooth development. Pediatric research 46, 650-656.

Day, Timothy F. BS; Yang, Yingzi PhD. Wnt and Hedgehog Signaling Pathways in Bone Development. The Journal of Bone & Joint Surgery 90(Supplement_1):p 19-24, February 2008. | DOI: 10.2106/JBJS.G.01174.

Dietrich, D. R. (1993). Toxicological and pathological applications of proliferating cell nuclear antigen (PCNA), a novel endogenous marker for cell proliferation. Crit. Rev. Toxicol. 23, 77–109. doi: 10.3109/10408449309104075.

Dorn, K. V., Hughes, C. E. and Rohatgi, R. (2012) ‘A Smoothened-Evc2 Complex Transduces the Hedgehog Signal at Primary Cilia’, *Developmental Cell*, 23(4), pp. 823–835. doi: 10.1016/j.devcel.2012.07.004.

Echevarrıá-Andino, M. L. and Allen, B. L. (2020). The hedgehog co-receptor BOC differentially regulates SHH signaling during craniofacial development. Development (Camb.) 147, dev189076. doi:10.1242/dev.189076.

Eckhart, L., Lippens, S., Tschachler, E. & Declercq, W. (2013) Cell death by cornification. Biochimica et Biophysica Acta, 1833, 3471–3480.

Elliott, K. H. and Brugmann, S. A. (2019) ‘Sending mixed signals: Cilia-dependent signaling during development and disease’, *Developmental Biology*, 447(1), pp. 28–41. doi: 10.1016/j.ydbio.2018.03.007.

Ellis, R. W. B. and Van Creveld, S. (1940) ‘A syndrome characterized by ectodermal dysplasia, polydactyly, chondro-dysplasia and congenital morbus cordis: Report of three cases’, *Archives of Disease in Childhood*, 15(82), pp. 65–84. doi: 10.1136/adc.15.82.65.

Fons Romero, J. M., Star, H., Lav, R., Watkins, S., Harrison, M., Hovorakova, M., Headon, D., & Tucker, A. S. (2017). The Impact of the Eda Pathway on Tooth Root Development. Journal of dental research, 96(11), 1290–1297. https://doi.org/10.1177/0022034517725692.

Fons, J.M., Mozaffari, M., Malik, D., Marshall, A.R., Connor, S., Greene, N.D.E. et al. (2020) Epithelial dynamics shed light on the mechanisms underlying ear canal defects. Development, 147, dev194654.

Fraser, A. M. and Davey, M. G. (2019) ‘TALPID3 in Joubert syndrome and related ciliopathy disorders’, *Current Opinion in Genetics and Development*, 56, pp. 41–48. doi: 10.1016/j.gde.2019.06.010.

Fukumoto, S. *et al.* (2004) ‘Ameloblastin is a cell adhesion molecule required for maintaining the differentiation state of ameloblasts’, *Journal of Cell Biology*, 167(5), pp. 973–983. doi: 10.1083/jcb.200409077.

Gaete, M. and Tucker, A. S. (2013) ‘Organized Emergence of Multiple-Generations of Teeth in Snakes Is Dysregulated by Activation of Wnt/Beta-Catenin Signalling’, *PLoS ONE*, 8(9). doi: 10.1371/journal.pone.0074484.

Galdzicka, M. *et al.* (2002) ‘A new gene, EVC2, is mutated in Ellis-van Creveld syndrome’, *Molecular Genetics and Metabolism*, 77(4), pp. 291–295. doi: 10.1016/S1096-7192(02)00178-6.

Galdzicka, M. M., Egeland, J. A. and Ginns, E. I. (2016) ‘Role of EVC and EVC2 in Ellis–van Creveld Syndrome and Weyers Acrofacial Dysostosis’, *Epstein’s Inborn Errors of Development*, pp. 1397–1404. doi: 10.1093/med/9780199934522.003.0214.

García, E. B. G. and Knoers, N. V. (2009) ‘Gardner’s syndrome (familial adenomatous polyposis): a cilia-related disorder’, *The Lancet Oncology*, 10(7), pp. 727–735. doi: 10.1016/S1470-2045(09)70167-6.

George, E., DeSilva, S., Lieber, E., Raziuddin, K., & Gudavalli, M. (2000). Ellis van Creveld syndrome (chondroectodermal dysplasia, MIM 22550) in three siblings from a non-consanguineous mating. Journal of perinatal medicine,

28(6), 425–427. https://doi.org/10.1515/JPM.2000.055.

Ghandehari-Motlagh, M. *et al.* (2016) ‘Ameloblastic fibro-odontoma in a 4-year-old boy’, *Iranian Journal of Pediatrics*, 26(2), pp. 5–8. doi: 10.5812/ijp.3124.

Gritli-Linde, A., Bei, M., Maas, R., Zhang, X. M., Linde, A., & McMahon, A. P. (2002). Shh signaling within the dental epithelium is necessary for cell proliferation, growth and polarization. Development (Cambridge, England), 129(23), 5323–5337. https://doi.org/10.1242/dev.00100.

Hammerschmidt, M., Bitgood, M. J. and McMahon, A. P. (1996) ‘Protein kinase A is a common negative regulator of Hedgehog signaling in the vertebrate embryo’, *Genes and Development*, 10(6), pp. 647–658. doi: 10.1101/gad.10.6.647.

Hanemann, J. A. C. *et al.* (2013) ‘Peripheral compound odontoma erupting in the gingiva’, *Head and Face Medicine*, 9(1), pp. 2–5. doi: 10.1186/1746-160X-9-15.

Hardcastle, Z., Mo, R., Hui, C. C., & Sharpe, P. T. (1998). The Shh signalling pathway in tooth development: defects in Gli2 and Gli3 mutants. Development (Cambridge, England), 125(15), 2803–2811. https://doi.org/10.1242/dev.125.15.2803.

Hattab, F. N., Yassin, O. M. and Sasa, I. S. (1998) ‘Oral manifestations of Ellis-van Creveld syndrome: Report of two siblings with unusual dental anomalies’, *Journal of Clinical Pediatric Dentistry*, 22(2), pp. 159–165.

Haycraft, C. J. *et al.* (2005) ‘Gli2 and Gli3 localize to cilia and require the intraflagellar transport protein polaris for processing and function’, *PLoS Genetics*, 1(4), pp. 0480–0488. doi: 10.1371/journal.pgen.0010053.

Hermans, F. *et al.* (2021) ‘Intertwined Signaling Pathways Governing Tooth Development: A Give-and-Take Between Canonical Wnt and Shh’, *Frontiers in Cell and Developmental Biology*, 9(October). doi: 10.3389/fcell.2021.758203.

Heuzé, Y., Singh, N., Basilico, C., Jabs, E.W., Holmes, G. and Richtsmeier, J. T. (2014). Morphological comparison of the craniofacial pehenotypes of mouse models expressing th Apert FGFR2 S252W muation in neural crest or mesoderm derived tissues. Bone 63, 1001-1109. doi:10.1016/j.bone.2014.03.003.

Hui, C. C., & Angers, S. (2011). Gli proteins in development and disease. Annual review of cell and developmental biology, 27, 513–537. https://doi.org/10.1146/annurev-cellbio-092910-154048.

Hovorakova, M. *et al.* (2005) ‘The developmental relationship between the deciduous dentition and the oral vestibule in human embryos’, *Anatomy and Embryology*, 209(4), pp. 303–313. doi: 10.1007/s00429-004-0441-y.

Hovorakova, M. *et al.* (2007) ‘Early development of the lower deciduous dentition and oral vestibule in human embryos’, *European Journal of Oral Sciences*, 115(4), pp. 280–287. doi: 10.1111/j.1600-0722.2007.00464.x.

Hovorakova, M., Prochazka, J., Lesot, H., Smrckova, L., Churava, S.,

Boran, T. et al. (2011) Shh expression in a rudimentary tooth offers new insights into development of the mouse incisor. Journal of Experimental Zoology. Part B, Molecular and Developmental Evolution, 316, 347–358.

Hovorakova, M. *et al.* (2016) 'One Odontogenic Cell-Population Contributes to the Development of the Mouse Incisors and of the Oral Vestibule', pp. 1–16. doi: 10.1371/journal.pone.0162523.

Hovorakova, M. *et al.* (2020) 'Reawakening of Ancestral Dental Potential as a Mechanism to Explain Dental Pathologies', *Integrative and Comparative Biology*, 60(3), pp. 619–629. doi: 10.1093/icb/icaa053.

Hu, X. *et al.* (2013) 'Expression of SHH signaling molecules in the developing human primary dentition', *BMC Developmental Biology*, 13(1). doi: 10.1186/1471-213X-13-11.

Huangfu, D. *et al.* (2003) 'Hedgehog signalling in the mouse requires intraflagellar transport proteins why less severe than Shh mutants but similar to disruption of L / R nodal assymetry !', *Letters to Nature*, 426(November), pp. 83–87. doi: 10.1038/nature02080.1.

Hunter, M. L. and Roberts, G. J. (1998) 'Oral and dental anomalies in Ellis van Creveld syndrome (chondroectodermal dysplasia): Report of a case', *International Journal of Paediatric Dentistry*, 8(2), pp. 153–157. doi: 10.1046/j.1365-263X.1998.00069.x.

Incardona, J. P., Gaffield, W., Kapur, R. P., & Roelink, H. (1998). The

teratogenic Veratrum alkaloid cyclopamine inhibits sonic hedgehog signal transduction. Development (Cambridge, England), 125(18), 3553–3562. https://doi.org/10.1242/dev.125.18.3553.

Ingham, P. W. and Mcmahon, A. P. (2001) 'Hedgehog signaling in animal development : paradigms and principles', pp. 3059–3087. doi: 10.1101/gad.938601.look.

Ishitsuka, Y., & Roop, D. R. (2020). Loricrin: Past, Present, and Future. International journal of molecular sciences, 21(7), 2271. https://doi.org/10.3390/ijms21072271.

Izzi, L., Lévesque, M., Morin, S., Laniel, D., Wilkes, B. C., Mille, F., Krauss, R. S., Mcmahon, A. P., Allen, B. L. and Charron, F. (2011) 'Boc and gas1 each form distinct shh receptor complexes with ptch1 and are required for shh-mediated cell proliferation', *Developmental Cell*, 20(6), pp. 788–801. doi: 10.1016/j.devcel.2011.04.017.

Järvinen, E. *et al.* (2006) 'Continuous tooth generation in mouse is induced by activated epithelial Wnt/β-catenin signaling', *Proceedings of the National Academy of Sciences of the United States of America*, 103(49), pp. 18627–18632. doi: 10.1073/pnas.0607289103.

Järvinen, E. *et al.* (2018) 'Mesenchymal Wnt/β-catenin signaling limits tooth number', *Development (Cambridge)*, 145(4), pp. 1–12. doi: 10.1242/dev.158048.

Jernvall, J., Aberg, T., Kettunen, P., Keränen, S., & Thesleff, I. (1998). The life

history of an embryonic signaling center: BMP-4 induces p21 and is associated with apoptosis in the mouse tooth enamel knot. Development (Cambridge, England), 125(2), 161–169. https://doi.org/10.1242/dev.125.2.161

Jiang, J. and Struhl, G. (1995) 'Protein kinase A and hedgehog signaling in drosophila limb development', *Cell*, 80(4), pp. 563–572. doi: 10.1016/0092-8674(95)90510-3.

Jin, S., Martinelli, D. C., Zheng, X., Tessier-Lavigne, M. and Fan, C. M. (2015). Gas1 is a receptor for sonic hedgehog to repel enteric axons. Proc. Natl. Acad. Sci. USA 112, E73-E80. doi:10.1073/pnas.1418629112

Kalaskar, R. and Kalaskar, A. R. (2012) 'Oral manifestations of Ellis-van Creveld syndrome', *Contemporary Clinical Dentistry*, 3(5), pp. S55–S59. doi: 10.4103/0976-237X.95106.

Kantaputra, P.N., Wangtiraumnuay, N., Ngamphiw, C., Olsen, B., Intachai, W., Tucker, A.S. et al. (2022) 'Cryptophthalmos, dental anomalies, oral vestibule defect, and a novel FREM2 mutation', *Journal of Human Genetics*, 67(2), pp. 115–118. doi: 10.1038/s10038-021-00972-4.

Kawasaki, M., Porntaveetus, T., Kawasaki, K., Oommen, S., Otsuka-Tanaka, Y., Hishinuma, M., Nomoto, T., Maeda, T., Takubo, K., Suda, T. et al. (2014). Rspondins/ Lgrs expression in tooth development. Dev. Dyn. 243, 844-851. doi:10. 1002/dvdy.24124.

Kim, J., Kato, M. and Beachy, P. A. (2009) 'Gli2 trafficking links Hedgehog-

dependent activation of Smoothened in the primary cilium to transcriptional activation in the nucleus', *Proceedings of the National Academy of Sciences of the United States of America*, 106(51), pp. 21666–21671. doi: 10.1073/pnas.0912180106.

Kochva, E., 1963. Development of the venom gland and trigeminal muscles in Vipera palaestinae. Acta Anat 52, 49-89.

Kochva, E. (1965). The development of the venom gland in the opisthoglyph snake Telescopus fallax with remarks on Thamnophis sirtalis. Copeia 1965, 147–154. doi: 10.2307/1440716.

Kogerman, P. *et al.* (1999) 'Mammalian Suppressor-of-Fused modulates nuclear – cytoplasmic shuttling of GLI-1', 1(September).

Kong, J. H., Siebold, C., & Rohatgi, R. (2019). Biochemical mechanisms of vertebrate hedgehog signaling. Development (Cambridge, England), 146(10), dev166892. https://doi.org/10.1242/dev.166892.

Koster, M.I. & Roop, D.R. (2004) Genetic pathways required for epidermal morphogenesis. European Journal of Cell Biology, 83, 625–629.

Kowal, A. *et al.* (2015) 'EVC gene polymorphisms and risks of isolated hypospadias - A preliminary study', *Central European Journal of Urology*, 68(2), pp. 257–262. doi: 10.5173/ceju.2015.493.

Kuechle, M. K., Presland, R. B., Lewis, S. P., Fleckman, P., and Dale, B. A. (2000). Inducible expression of filaggrin increases keratinocyte susceptibility to apoptotic cell death. Cell Death Differ. 7, 566–573. doi:

10.1038/sj.cdd.4400687.

Kulkarni, A. K. *et al.* (2018) ‘A ciliary protein EVC2/LIMBIN plays a critical role in the skull base for mid-facial development’, *Frontiers in Physiology*, 9(OCT), pp. 1–13. doi: 10.3389/fphys.2018.01484.

Kumar, V. *et al.* (2021) ‘The Role of Notch, Hedgehog, and Wnt Signaling Pathways in the Resistance of Tumors to Anticancer Therapies’, *Frontiers in Cell and Developmental Biology*, 9(April), pp. 1–24. doi: 10.3389/fcell.2021.650772.

Kus-Bartoszek, A., Lipski, M., Jarzabek, A., Manowiec, J. & Drozdzik, A. (2022) Gingival phenotype changes and the prevalence of mucogingival deformities during the early transitional dentition phase-a two-year longitudinal study. International Journal of Environmental Research and Public Health, 19, 3899. doi:10.3390/ijerph19073899.

Larkins, C. E. *et al.* (2011) ‘Arl13b regulates ciliogenesis and the dynamic localization of Shh signaling proteins’, *Molecular Biology of the Cell*, 22(23), pp. 4694–4703. doi: 10.1091/mbc.E10-12-0994.

Leche W. (1893). Nachträge zu Studien über die Entwickelung der Zahnsystems bei Säugertieren. Morph Jahrb 20:113–142.

Lee, C. S., Buttitta, L. and Fan, C. M. (2001a). Evidence that the WNT-inducible growth arrest-specific gene 1 encodes an antagonist of sonic hedgehog signaling in the somite. Proc. Natl. Acad. Sci. U.S.A. 98, 11347-11352. doi:10.1073/pnas. 201418298.

Lee, C. S., May, N. R., & Fan, C. M. (2001b). Transdifferentiation of the ventral retinal pigmented epithelium to neural retina in the growth arrest specific gene 1 mutant. Developmental biology, 236(1), 17–29. https://doi.org/10.1006/dbio.2001.0280.

Lee, S. C., Lee, J. B., Kook, J. P., Seo, J. J., Nam, K. I., Park, S. S., et al. (1999). Expression of differentiation markers during fetal skin development in humans: immunohistochemical studies on the precursor proteins forming the cornified cell envelope. J. Invest. Dermatol. 112, 882–886. doi: 10.1046/j.1523-1747.1999.00602.x.

Levi-Duque, F. and Ardila, C. M. (2019) 'Association between odontoma size, age and gender: Multivariate analysis of retrospective data', *Journal of Clinical and Experimental Dentistry*, 11(8), pp. e701–e706. doi: 10.4317/jced.55733.

Li, J., Chatzeli, L., Panousopoulou, E., Tucker, A. S. and Green, J. B. A. (2016). Epithelial stratification and placode invagination are separable functions in early morphogenesis of the molar tooth. Development (Camb.) 143, 670-681. doi:10. 1242/dev.130187.

Li, Q. *et al.* (2010) 'Genome scan for locus involved in mandibular prognathism in pedigrees from China', *PLoS ONE*, 5(9), pp. 1–4. doi: 10.1371/journal.pone.0012678.

Li, W. *et al.* (1995) 'Function of protein kinase A in hedgehog signal transduction and Drosophila imaginal disc development', *Cell*, 80(4), pp. 553–562. doi: 10.1016/0092-8674(95)90509-X.

Liem, K. F. *et al.* (2009) ‘Mouse Kif7/Costal2 is a cilia-associated protein that regulates Sonic hedgehog signaling’, *Proceedings of the National Academy of Sciences of the United States of America*, 106(32), pp. 13377–13382. doi: 10.1073/pnas.0906944106.

Lippens, S., Kockx, M., Knaapen, M., Mortier, L., Polakowska, R., Verheyen, A. et al. (2000) Epidermal differentiation does not involve the pro-apoptotic executioner caspases, but is associated with caspase-14 induction and processing. Cell Death and Differentiation, 7, 1218–1224.

Louie, K. W., Mishina, Y. and Zhang, H. (2020) ‘Molecular and cellular pathogenesis of ellis-van creveld syndrome: Lessons from targeted and natural mutations in animal models’, *Journal of Developmental Biology*, 8(4), pp. 1–15. doi: 10.3390/jdb8040025.

Martinelli, D. C. and Fan, C. M. (2007) ‘Gas1 extends the range of Hedgehog action by facilitating its signaling’, *Genes and Development*, 21(10), pp. 1231–1243. doi: 10.1101/gad.1546307.

Martin, K. J., Rasch, L. J., Cooper, R. L., Metscher, B. D., Johanson, Z., and Fraser, G. J. (2016). Sox2+ progenitors in sharks link taste development with the evolution of regenerative teeth from denticles. Proc. Natl. Acad. Sci. U. S. A. 113, 14769-14774. doi: 10.1073/pnas.1612354113.

MCKUSICK, V. A., EGELAND, J. A., ELDRIDGE, R., & KRUSEN, D. E. (1964). DWARFISM IN THE AMISH I. THE ELLIS-VAN CREVELD SYNDROME. Bulletin of the Johns Hopkins Hospital, 115, 306–336.

McKusick, V. A. (2000) ‘Ellis-van Creveld syndrome and the Amish’, *Nature Genetics*, 24(3), pp. 203–204. doi: 10.1038/73389.

Miletich, I. and Sharpe, P. T. (2003) ‘Normal and abnormal dental development’, *Human Molecular Genetics*, 12(REV. ISS. 1), pp. 69–73. doi: 10.1093/hmg/ddg085.

Miletich, I., Yu, W.-Y., Zhang, R., Sharpe, P. T., Caixeta De Andrade, S., Pereira, S. F. A., Ohazama, A., Mock, O. B., Buchner, G., Sealby, J. et al. (2011). ‘Developmental stalling and organ-autonomous regulation of morphogenesis’, *Proceedings of the National Academy of Sciences of the United States of America*, 108(48), pp. 19270–19275. doi: 10.1073/pnas.1112801108.

Miller, D. R., Newstead, G. J. and Young, L. W. (1969) ‘Perinatal leukemia with apossible variant of the Ellis-van Creveld syndrome’, *The Journal of Pediatrics*, 74(2), pp. 300–303. doi: 10.1016/S0022-3476(69)80081-8.

Moore, E. R. (2022) ‘Primary Cilia: The New Face of Craniofacial Research’, *Biomolecules*, 12(12). doi: 10.3390/biom12121724.

Moore KL, Persaud TVN (1993) The developing human, 5th edn. WB Saunders, Philadelphia.

Mostafa, M. I. *et al.* (2005) ‘Unusual pattern of inheritance and orodental changes in the Ellis-Van Creveld syndrome’, *Genetic Counseling*, 16(1), pp. 75–83.

Nakatomi, M. (2009) ‘Ellis-van Creveld (EvC) Syndrome: Unusual Oral

Defects in Humans and Evc Mutant Mice', *Journal of Oral Biosciences*, 51(3), pp. 151–157. doi: 10.1016/s1349-0079(09)80023-6.

Nakatomi, M., Hovorakova, M., Gritli-Linde, A., Blair, H. J., MacArthur, K., Peterka, M., et al. (2013). Evc regulates a symmetrical response to Shh signaling in molar development. J. Dent. Res. 92, 222–228. doi: 10.1177/0022034512471826.

Nery, E. B., Kraus, B. S. and Croup, M. (1970) 'Timing and topography of early human tooth development', Archives of Oral Biology, 15(12). doi: 10.1016/0003-9969(70)90020-8.

Nethan, S. T., Sinha, S. and Chandra, S. (2017) 'Ellis-van creveld with an unusual dental anomaly: A case report', *Iranian Journal of Medical Sciences*, 42(5), pp. 501–504.

Nigg, E. A., & Stearns, T. (2011). The centrosome cycle: Centriole biogenesis, duplication and inherent asymmetries. Nature cell biology, 13(10), 1154–1160. https://doi.org/10.1038/ncb2345.

Nüsslein-Volhard, C., & Wieschaus, E. (1980). Mutations affecting segment number and polarity in Drosophila. Nature, 287(5785), 795–801. https://doi.org/10.1038/287795a0.

Okada, A., Charron, F., Morin, S., Shin, D. S., Wong, K., Fabre, P. J., Tessier-Lavigne, M. and Mcconnell, S. K. (2006). Boc is a receptor for sonic hedgehog in the guidance of commissural axons. Nature 444, 369-373. doi:10.1038/ nature05246.

Orban B (1928) Entwicklung und Wachstum der Zahnleiste
und Zahnkeime. Z Anat Entwickl Ges 83:724–733.

Paces-Fessy, M. *et al.* (2004) 'The negative regulator of Gli, Suppressor of fused (Sufu), interacts with SAP18, Galectin3 and other nuclear proteins', *Biochemical Journal*, 378(2), pp. 353–362. doi: 10.1042/BJ20030786.

Pan, Y. *et al.* (2006) 'Sonic hedgehog Signaling Regulates Gli2 Transcriptional Activity by Suppressing Its Processing and Degradation', *Molecular and Cellular Biology*, 26(9), pp. 3365–3377. doi: 10.1128/mcb.26.9.3365-3377.2006.

Pan, Y. and Wang, B. (2007) 'A novel protein-processing domain in Gli2 and Gli3 differentially blocks complete protein degradation by the proteasome', *Journal of Biological Chemistry*, 282(15), pp. 10846–10852. doi: 10.1074/jbc.M608599200.

Pathi, S. *et al.* (2001) 'Comparative biological responses to human Sonic, Indian, and Desert hedgehog', *Mechanisms of Development*, 106(1–2), pp. 107–117. doi: 10.1016/S0925-4773(01)00427-0.

Pavlikova, H., Witter, K., and Misek, I. (1999). Primordium of the upper vestibulum oris in the domestic sheep. Acta Vet. Brno 68, 175–178. doi: 10.2754/avb199968030175.

Pelissier, A., Ouhayoun, J. P., Sawaf, M. H., and Forest, N. (1992). Changes in cytokeratin expression during the development of the human oral mucosa. J. Periodontal Res. 27, 588–598. doi: 10.1111/j.1600-0765.1992.tb01741.x

Peña-Cardelles, J. F. *et al.* (2019) ‘Oral manifestations of ellis-van creveld syndrome. A rare case report’, *Journal of Clinical and Experimental Dentistry*, 11(3), pp. e290–e295. doi: 10.4317/jced.55543.

Penon-Portmann, M., Eldomery, M. K., Potocki, L., Marafi, D., Posey, J. E., Cobanâ€ Akdemir, Z., Harel, T., Grochowski, C. M., Loucks, H., Devine, W. P. et al. (2022). ‘De novo heterozygous variants in SLC30A7 are a candidate cause for Joubert syndrome’, *American Journal of Medical Genetics, Part A*, 188(8), pp. 2360–2366. doi: 10.1002/ajmg.a.62872.

Perlmann, T. and Jansson, L. (1995) ‘A novel pathway for vitamin A signaling mediated by RXR heterodimerization with NGFI-B and NURR1’, *Genes and Development*, 9(7), pp. 769–782. doi: 10.1101/gad.9.7.769.

Peterka, M., Lesot, H., & Peterková, R. (2002). Body weight in mouse embryos specifies staging of tooth development. Connective tissue research, 43(2-3), 186–190. https://doi.org/10.1080/03008200290000673.

Peterková, R. (1985) ‘The common developmental origin and phylogenetic aspects of teeth, rugae palatinae, and fornix vestibuli oris in the mouse.’, *Journal of craniofacial genetics and developmental biology*, 5(1), pp. 89–104. Available at: http://www.ncbi.nlm.nih.gov/pubmed/2580855 (Accessed: 13 April 2020).

Pietrobono, S., Gagliardi, S. and Stecca, B. (2019) ‘Non-canonical hedgehog signaling pathway in cancer: Activation of GLI transcription factors beyond smoothened’, *Frontiers in Genetics*, 10(JUN), pp. 1–20. doi:

10.3389/fgene.2019.00556.

Placek, M., Mskach, M. & Mrklas, L. (1974) Significance of the labial frenum attachment in periodontal disease in man. Part 1. Classification and epidemiology of the labial frenum attachment. Journal Periodontology, 45, 891–894.

Plotnikova, O. V., Pugacheva, E. N., & Golemis, E. A. (2009). Primary cilia and the cell cycle. Methods in cell biology, 94, 137–160. https://doi.org/10.1016/S0091-679X(08)94007-3.

Polymeropoulos, M. H. *et al.* (1996) 'The gene for the Ellis-van Creveld syndrome is located on chromosome 4p16', *Genomics*, 35(1), pp. 1–5. doi: 10.1006/geno.1996.0315.

Popa, E. M., Buchtova, M. and Tucker, A. S. (2019) 'Revitalising the rudimentary replacement dentition in the mouse', *Development (Cambridge, England)*, 146(3). doi: 10.1242/dev.171363.

Presland, R. B., Kuechle, M. K., Lewis, S. P., Fleckman, P., and Dale, B. A. (2001). Regulated expression of human filaggrin in keratinocytes results in cytoskeletal disruption, loss of cell-cell adhesion, and cell cycle arrest. Exp. Cell Res. 270, 199–213. doi: 10.1006/excr.2001.5348.

Qin, J. *et al.* (2011) 'Intraflagellar transport protein 122 antagonizes Sonic Hedgehog signaling and controls ciliary localization of pathway components', *Proceedings of the National Academy of Sciences of the United States of America*, 108(4), pp. 1456–1461. doi: 10.1073/pnas.1011410108.

Qiu, T., Teshima, T. H. N., Hovorakova, M. and Tucker, A. S. (2020). Development of the vestibular lamina in human embryos: morphogenesis and vestibule formation. Front. Physiol. 11, 753. doi:10.3389/fphys.2020.00753.

Qiu, T. and Tucker, A. S. (2022). Mechanisms driving vestibular lamina formation and opening in the mouse. J. Anat. 242, 224-234. doi:10.1111/joa.13771.

Qiu, T., Hutečková, B., Seppala, M., Cobourne, M. T., Chen, Z., Hovořáková, M., Buchtová, M. and Tucker, A. S. (2023). Molecular profiling of the vestibular lamina highlights a key role for Hedgehog signalling. Development. doi:10.1242/dev.201464.

Radlanski, R. J. (1995) 'Morphogenesis of human tooth primordia: The importance of 3D computer-assisted reconstruction', *International Journal of Developmental Biology*, 39(1), pp. 249–256. doi: 10.1387/ijdb.7626413.

Radlanski, R. J., Mocker, E. and Rahlfs, D. (1998) 'Computer-aided graphical reconstructions of the development of murine dental primordia and surrounding structures from day 12 until birth', *European Journal of Oral Sciences*, 106(1 SUPPL.), pp. 71–79. doi: 10.1111/j.1600-0722.1998.tb02156.x.

Radlanski, R. J. and Renz, H. (2006) 'Genes, forces, and forms: Mechanical aspects of prenatal craniofacial development', *Developmental Dynamics*, 235(5), pp. 1219–1229. doi: 10.1002/dvdy.20704.

Rimkus, T. K. *et al.* (2016) 'Targeting the sonic hedgehog signaling pathway:

Review of smoothened and GLI inhibitors', *Cancers*, 8(2), pp. 1–23. doi: 10.3390/cancers8020022.

Rohatgi, R., Milenkovic, L., & Scott, M. P. (2007). Patched1 regulates hedgehog signaling at the primary cilium. Science (New York, N.Y.), 317(5836), 372–376. https://doi.org/10.1126/science.1139740.

Röse C. (1895). Überreste einer vorzeitigen prälactealen und einer vierten Zahnreihe beim Menschen. Öster-ung Vierteljahrschr Zahnheilk 2:45-50.

Rothova, M. *et al.* (2012) 'Lineage tracing of the endoderm during oral development', *Developmental Dynamics*, 241(7), pp. 1183–1191. doi: 10.1002/dvdy.23804.

Roubicek, M. and Spranger, J. (1984) 'Weyers acrodental dysostosis in a family', *Clinical Genetics*, 26(6), pp. 587–590. doi: 10.1111/j.1399-0004.1984.tb01108.x.

Rui, Z. *et al.* (2014) 'Smoothened gene alterations in keratocystic odontogenic tumors', *Head and Face Medicine*, 10(1), pp. 1–7. doi: 10.1186/1746-160X-10-36.

Ruiz-Perez, V. L. *et al.* (2000) 'Mutations in a new gene in Ellis-van Creveld syndrome and Weyers acrodental dysostosis', *Nature Genetics*, 24(3), pp. 283–286. doi: 10.1038/73508.

Ruiz-Perez, V. L. *et al.* (2003) 'Mutations in two nonhomologous genes in a head-to-head configuration cause Ellis-van Creveld syndrome', *American Journal of Human Genetics*, 72(3), pp. 728–732. doi: 10.1086/368063.

Ruiz-Perez, V. L., Blair, H. J., Rodriguez-Andres, M. E., Blanco, M. J.,Wilson, A., Liu, Y.-N., Miles, C., Peters, H. and Goodship, J. A. (2007). Evc is a positive mediator of Ihh-regulated bone growth that localises at the base of chondrocyte cilia. Development 134, 2903-2912. doi:10.1242/dev.007542.

Ruiz-Perez, V. L. and Goodship, J. A. (2009) 'Ellis-van Creveld syndrome and Weyers acrodental dysostosis are caused by cilia-mediated diminished response to Hedgehog ligands', *American Journal of Medical Genetics, Part C: Seminars in Medical Genetics*, 151(4), pp. 341–351. doi: 10.1002/ajmg.c.30226.

Ruiz i Altaba, A. (1997) 'Catching a Gli-mpse of hedgehog', *Cell*, 90(2), pp. 193–196. doi: 10.1016/S0092-8674(00)80325-6.

Sánchez, O. H., Berrocal, M. I. L. and González, J. M. M. (2008) 'Metaanalysis of the epidemiology and clinical manifestations of odontomas', *Medicina Oral, Patologia Oral y Cirugia Bucal*, 13(11), pp. 730–734.

Sanz-Navarro, M., Delgado, I., Torres, M., Mustonen, T., Michon, F. and Rice, D. P. (2019). Dental epithelial stem cells express the developmental regulator Meis1. Front. Physiol. 10, 249. doi:10.3389/phys.2019.00249.

Sarkar, L., Cobourne, M., Naylor, S. and Sharpe, P. T. (2000). Wnt/Shh interactions regulate ectodermal boundary formation during mammalian tooth development. Proc. Natl. Acad. Sci. USA 97, 4520-4524. doi:10.1073/pnas.97.9. 4520.

Sasaki, H., Nishizaki, Y., Hui, C., Nakafuku, M., & Kondoh, H. (1999).

Regulation of Gli2 and Gli3 activities by an amino-terminal repression domain: implication of Gli2 and Gli3 as primary mediators of Shh signaling. Development (Cambridge, England), 126(17), 3915–3924. https://doi.org/10.1242/dev.126.17.3915.

Sasalawad, S. S., Hugar, S. M., Poonacha, K. S., and Mallikarjuna, R. (2013). Ellis-van Creveld syndrome. BMJ Case Rep. 2013:bcr2013009463. doi: 10.1136/bcr-2013-009463.

Satish V, Prabhadevi MC, Sharma R. (2011). Odontome: A Brief Overview. Int. J. Clinical Pediatric Dentistry. 4 (3): 177-185.

Schock, E. N. and Brugmann, S. A. (2017). 'Discovery, diagnosis, and etiology of craniofacial ciliopathies', *Cold Spring Harbor Perspectives in Biology*, 9(9). doi: 10.1101/cshperspect.a028258.

Schroeder HE. Oral structural biology. New York: Georg Thieme Verlag Stuttgart, 1991.

Schour, I. (1929) 'Early human tooth development, with special reference to the relationship between the dental lamina and the lip-furrow band', *Journal of Dental Research*, 9(5), pp. 699–717. doi: 10.1177/00220345290090050801.

Scurlock, D. *et al.* (2005) 'Ellis-van Creveld syndrome and dyserythropoiesis', *Archives of Pathology and Laboratory Medicine*, 129(5), pp. 680–682. doi: 10.5858/2005-129-0680-ecsad.

Seppala, M., Depew, M. J., Martinelli, D. C., Fan, C.-M., Sharpe, P. T. and Cobourne, M. T. (2007). Gas1 is a modifier for holoprosencephaly and

genetically interacts with sonic hedgehog. J. Clin. Investig. 117, 1575-1584. doi:10.1172/ JCI32032.

Seppala, M., Xavier, G. M., Fan, C.-M. and Cobourne, M. T. (2014). Boc modifies the spectrum of holoprosencephaly in the absence of Gas1 function. Biology Open 3, 728-740. doi:10.1242/bio.20147989.

Seppala, M., Fraser, G., Birjandi, A., Xavier, G. and Cobourne, M. (2017). Sonic hedgehog signaling and development of the dentition. Journal of Developmental Biology 5, 6. doi:10.3390/jdb5020006.

Seppala, M., Thivichon-Prince, B., Xavier, G. M., Shaffie, N., Sangani, I., Birjandi, A. A., Rooney, J., Lau, J. N. S., Dhaliwal, R., Rossi, O. et al. (2022). Gas1 regulates patterning of the murine and human dentitions through sonic hedgehog. J. Dent. Res. 101, 473-482. doi:10.1177/00220345211049403

Shaik, S. *et al.* (2016) 'Ellis-van Creveld syndrome with unusual oral and dental findings: A rare clinical entity', *Dental Research Journal*, 13(2), pp. 193–197. doi: 10.4103/1735-3327.178213.

Smith, C. E. L., Lake, A. V. R. and Johnson, C. A. (2020) 'Primary Cilia, Ciliogenesis and the Actin Cytoskeleton: A Little Less Resorption, A Little More Actin Please', *Frontiers in Cell and Developmental Biology*, 8(December). doi: 10.3389/fcell.2020.622822.

Soukup, V., Tazaki, A., Yamazaki, Y., Pospisilova, A., Epperlein, H.-H., Tanaka, E. M. and Cerny, R. (2021). Oral and palatal dentition of axolotl arises from a common tooth-competent zone along the ecto-endodermal

boundary. Front. Cell Dev. Biol. 8, 622308. doi:10.3389/fcell.2020.622308.

Spranger, S. and Tariverdian, G. (1995) ‘Symptomatic heterozygosity in the Ellis‐van Creveld syndrome?’, *Clinical Genetics*, 47(4), pp. 217–220. doi: 10.1111/j.1399-0004.1995.tb03963.x.

Sreekumar, V. and Norris, D. P. (2019) ‘Cilia and development’, *Current Opinion in Genetics and Development*, 56(Figure 1), pp. 15–21. doi: 10.1016/j.gde.2019.05.002.

Susami, T., Kuroda, T., Yoshimasu, H., & Suzuki, R. (1999). Ellis-van Creveld syndrome: craniofacial morphology and multidisciplinary treatment. The Cleft palate-craniofacial journal : official publication of the American Cleft Palate-Craniofacial Association, 36(4), 345–352. https://doi.org/10.1597/1545-1569_1999_036_0345_evcscm_2.3.co_2.

Szymanska, K. and Johnson, C. A. (2012) ‘The transition zone: An essential functional compartment of cilia’, *Cilia*, 1. doi: 10.1186/2046-2530-1-10.

Taipale, J., Chen, J. K., Cooper, M. K., Wang, B., Mann, R. K., Milenkovic, L., Scott, M. P., & Beachy, P. A. (2000). Effects of oncogenic mutations in Smoothened and Patched can be reversed by cyclopamine. Nature, 406(6799), 1005–1009. https://doi.org/10.1038/35023008.

Takeda, H. *et al.* (2002) ‘Positional cloning of the gene LIMBIN responsible for bovine chondrodysplastic dwarfism’, *Proceedings of the National Academy of Sciences of the United States of America*, 99(16), pp. 10549–10554. doi: 10.1073/pnas.152337899.

Tenzen, T., Allen, B. L., Cole, F., Kang, J.-S., Krauss, R. S. and Mcmahon, A. P. (2006). The cell surface membrane proteins cdo and boc are components and targets of the hedgehog signaling pathway and feedback network in mice. Dev. Cell 10, 647-656. doi:10.1016/j.devcel.2006.04.004.

Thesleff, I. (2008) 'Tooth organogenesis and regeneration', *StemBook*, pp. 1–12. doi: 10.3824/stembook.1.37.1.

Thomas, D. C. *et al.* (2022) 'Role of primary cilia and Hedgehog signaling in craniofacial features of Ellis–van Creveld syndrome', *American Journal of Medical Genetics, Part C: Seminars in Medical Genetics*, 190(1), pp. 36–46. doi: 10.1002/ajmg.c.31969.

Tompson, S. W. J. *et al.* (2007) 'Sequencing EVC and EVC2 identifies mutations in two-thirds of Ellis-van Creveld syndrome patients', *Human Genetics*, 120(5), pp. 663–670. doi: 10.1007/s00439-006-0237-7.

Tonge, C. H. (1969) 'The Time-Structure Relationship of Tooth Development in Human Embryogenesis', *Journal of Dental Research*, 48(5), pp. 745–752. doi: 10.1177/00220345690480052301.

Tucker, A. S. (2007) 'Salivary gland development', *Seminars in Cell and Developmental Biology*, 18(2), pp. 237–244. doi: 10.1016/j.semcdb.2007.01.006.

Tucker, A. S. (2010) 'Salivary gland adaptations: Modification of the glands for novel uses', *Salivary Glands: Development, Adaptations and Disease*, 14(April 2010), pp. 21–31. doi: 10.1159/000313705.

Tucker, A. and Sharpe, P. (2004) ‘The cutting-edge of mammalian development; how the embryo makes teeth’, *Nature Reviews Genetics*, 5(7), pp. 499–508. doi: 10.1038/nrg1380.

Tukachinsky, H., Lopez, L. V. and Salic, A. (2010) ‘A mechanism for vertebrate Hedgehog signaling: Recruitment to cilia and dissociation of SuFu-Gli protein complexes’, *Journal of Cell Biology*, 191(2), pp. 415–428. doi: 10.1083/jcb.201004108.

Uma, E. (2017) ‘Compound odontoma in anterior mandible—A case report’, *Malaysian Journal of Medical Sciences*, 24(3), pp. 92–95. doi: 10.21315/mjms2017.24.3.11.

Vonk, F. J., Admiraal, J. F., Jackson, K., Reshef, R., de Bakker, M. A. G., Vanderschoot, K., et al. (2008). Evolutionary origin and development of snake fangs. Nature 454, 630–633. doi: 10.1038/nature07178.

Wang, X. P., O’connell, D. J., Lund, J. J., Saadi, I., Kuraguchi, M., Turbe-Doan, A., Cavallesco, R., Kim, H., Park, P. J., Harada, H. et al. (2009). Apc inhibition of Wnt signaling regulates supernumerary tooth formation during embryogenesis and throughout adulthood. Development 136, 1939-1949. doi:10.1242/dev. 033803.

Wheway, G., Nazlamova, L. and Hancock, J. T. (2018) ‘Signaling through the primary cilium’, *Frontiers in Cell and Developmental Biology*, 6(FEB), pp. 1–13. doi: 10.3389/fcell.2018.00008.

Wilkinson, D. G. (1992). In Situ Hybridisation: A Practical Approach. Oxford:

IRL Press.

Van der Burght, S. N. *et al.* (2020) ‘Ciliary Tip Signaling Compartment Is Formed and Maintained by Intraflagellar Transport’, *Current Biology*, 30(21), pp. 4299-4306.e5. doi: 10.1016/j.cub.2020.08.032.

Verlach, J., Foltan, R., Vlk, M., Szabo, P., and Smetana, K. (2017). Phenotypic chacterisation of oral mucosa: what is normal? J. Oral Pathol. Med. 46, 834–839. doi: 10.1111/jop.12556.

Visel, A., Thaller, C. and Eichele, G. (2004) ‘GenePaint.org: An atlas of gene expression patterns in the mouse embryo’, *Nucleic Acids Research*, 32(DATABASE ISS.), pp. 552–556. doi: 10.1093/nar/gkh029.

Volakakis, N. *et al.* (2010) ‘NR4A orphan nuclear receptors as mediators of CREB-dependent neuroprotection’, *Proceedings of the National Academy of Sciences of the United States of America*, 107(27), pp. 12317–12322. doi: 10.1073/pnas.1007088107.

von Arx, T., Lozanoff, S. (2017). Vestibule and Cheeks. In: Clinical Oral Anatomy. Springer, Cham. https://doi.org/10.1007/978-3-319-41993-0_3

West, C. M. (1924). The development of the gums and their relationship to the deciduous teeth in the human fetus. Contr. Embroyol. Carnegie Inst. 16, 25–45.

Witter, K., Pavlikova, H., Matulova, P., and Misek, I. (2005). Relationship between vestibular lamina, dental lamina, and the developing oral vestibule in the upper jaw of the field vole (Microtus agrestis, Rodentia). J. Morphol. 265,

264–270. doi: 10.1002/jmor.10356.

Xavier, G. M., Sharpe, P. T. and Cobourne, M. T. (2009). Scube1 is expressed during facial development in the mouse. J. Exp. Zool. B Mol. Dev. Evol. 312, 518-524. doi:10.1002/jez.b.21260.

Xavier, G. M. *et al.* (2015) 'Activated WNT signaling in postnatal SOX2-positive dental stem cells can drive odontoma formation', *Scientific Reports*, 5(September), pp. 1–7. doi: 10.1038/srep14479.

Xavier, G. M. *et al.* (2016) 'Hedgehog receptor function during craniofacial development', *Developmental Biology*, 415(2), pp. 198–215. doi: 10.1016/j.ydbio.2016.02.009.

Yang, C. *et al.* (2012) 'Smoothened transduces Hedgehog signal by forming a complex with Evc/Evc2', *Cell Research*, 22(11), pp. 1593–1604. doi: 10.1038/cr.2012.134.

Ye, Q., Bhojwani, A. and Hu, J. K. (2022) *Understanding the development of oral epithelial organs through single cell transcriptomic analysis*, *Development (Cambridge, England)*. doi: 10.1242/dev.200539.

Ye, X. *et al.* (2006) 'A novel heterozygous deletion in the EVC2 gene causes Weyers acrofacial dysostosis', *Human Genetics*, 119(1–2), pp. 199–205. doi: 10.1007/s00439-005-0129-2.

Yoshida, T. *et al.* (2008) 'Cell lineage in mammalian craniofacial mesenchyme', *Mechanisms of Development*, 125(9–10), pp. 797–808. doi: 10.1016/j.mod.2008.06.007.

Yu, F. *et al.* (2018) ‘A novel mutation of adenomatous polyposis coli (APC) gene results in the formation of supernumerary teeth’, *Journal of Cellular and Molecular Medicine*, 22(1), pp. 152–162. doi: 10.1111/jcmm.13303.

Yu, W., Sun, Z., Sweat, Y., Sweat, M., Venugopalan, S. R., Eliason, S., Cao, H., Paine, M. L. and Amendt, B. A. (2020). Pitx2-Sox2-Lef1 interactions specify progenitor oral/dental epithelial cell signaling centers. Development (Camb.) 147, dev186023. doi:10.1242/DEV.186023.

Zhang, H. *et al.* (2015) ‘Generation of Evc2/Limbin global and conditional KO mice and its roles during mineralized tissue formation’, *Genesis*, 53(9), pp. 612–626. doi: 10.1002/dvg.22879.

Zhang, H. *et al.* (2016) ‘Elevated Fibroblast Growth Factor Signaling Is Critical for the Pathogenesis of the Dwarfism in Evc2/Limbin Mutant Mice’, *PLoS Genetics*, 12(12), pp. 1–23. doi: 10.1371/journal.pgen.1006510.

Zhang, X., Martinez, D., Koledova, Z., Qiao, G., Streuli, C. H., & Lu, P. (2014). FGF ligands of the postnatal mammary stroma regulate distinct aspects of epithelial morphogenesis. Development (Cambridge, England), 141(17), 3352–3362. https://doi.org/10.1242/dev.106732.

Zhang, Ziyu *et al.* (2017) ‘Suppressor of Fused Chaperones Gli Proteins To Generate Transcriptional Responses to Sonic Hedgehog Signaling’, *Molecular and Cellular Biology*, 37(3). doi: 10.1128/mcb.00421-16.

Zhao, Y., Tong, C. and Jiang, J. (2007) ‘Hedgehog regulates smoothened activity by inducing a conformational switch’, *Nature*, 450(7167), pp. 252–258.

doi: 10.1038/nature06225.

Zhao, Z., Stock, D. W., Buchanan, A. V. and Weiss, K. M. (2000). Expression of Dlx genes during the development of the murine dentition. Dev. Genes Evol. 210, 270-275. doi:10.1007/s004270050314.

Zihni, C., Mills, C., Matter, K. & Balda, M.S. (2016) Tight junctions: from simple barriers to multifunctional molecular gates. Nature Reviews. Molecular Cell Biology, 17, 564–580.

List of figures

1) Figures in introduction

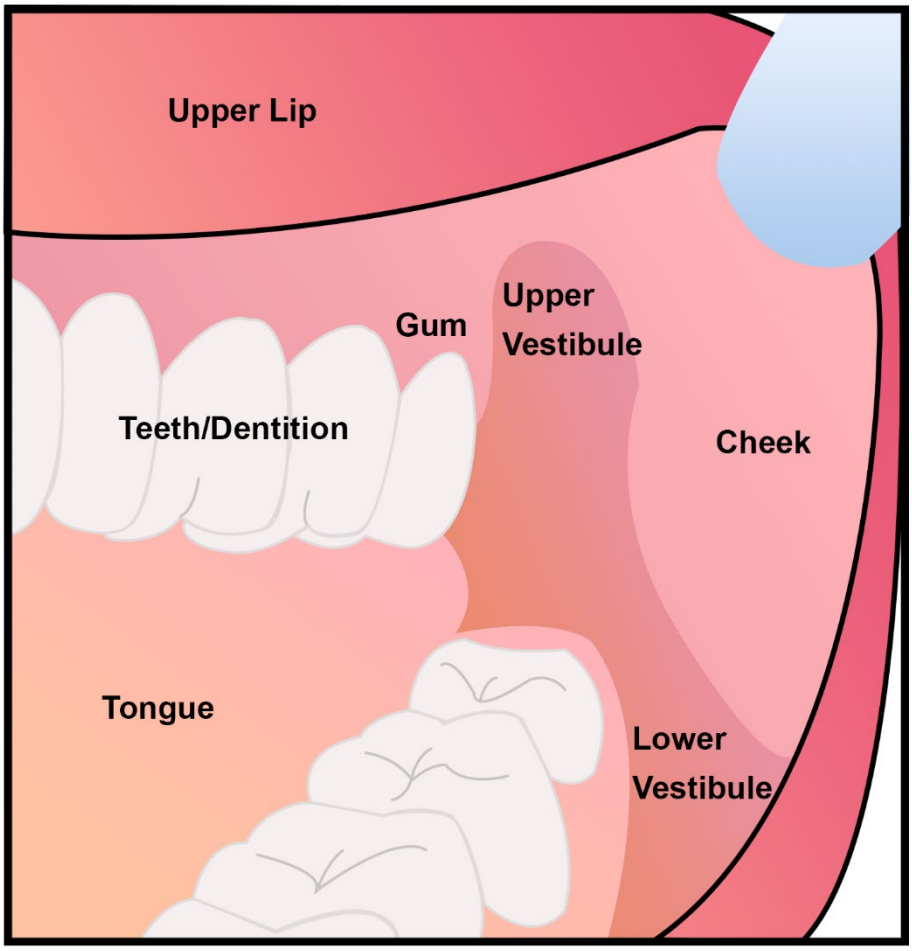

Figure 1. A basic schematic diagram showing the structure of oral cavity. The upper vestibule and lower vestibule are highlighted, which create the sulcus between the cheeks/lips and teeth/gum.

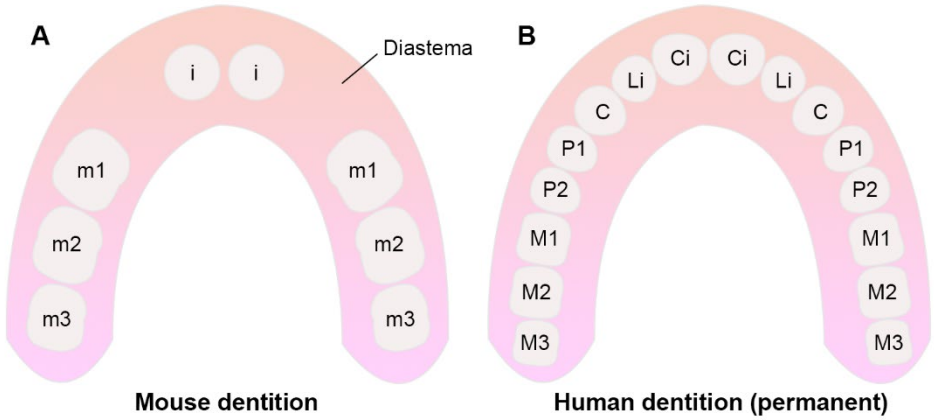

Figure 2. A diagrammatic representation illustrating the arrangement and types of teeth in mice and humans. (**A**) Mouse dentition. In mice, there are one incisor (i) and three molars (m1, m2, m3) positioned in each quadrant, which are distinctly spaced apart by a toothless gap in the dental arch, known as the diastema. (**B**) The human has two sets of dentitions and more complex tooth types. The arrangement of permanent dentition is displayed, which consists eight teeth in each quadrant, including one central incisor (Ci), one lateral incisor (Li), one canine (C), two premolars (P1, P2), and three molars (M1, M2, M3). The third molar (M3) is also called wisdom teeth.

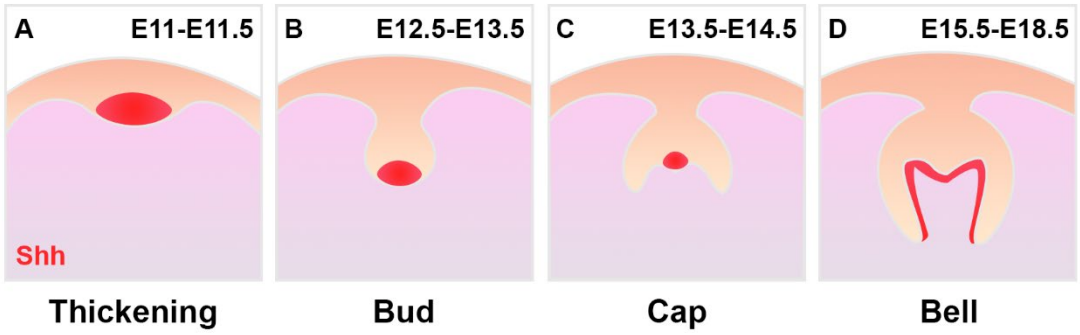

Figure 3. A schematic diagram of *Shh* transcription (red) during early tooth development. (**A**) Thickening/placode. The DL initiates as a thickened epithelium at

embryonic day (E) 11 to E11.5. The *Shh* expression is confined to the epithelial thickening. (**B**) Bud stage at E12.5 to E13.5. The *Shh* expresses in the enamel knot precursor cells located at the tip of the early bud. (**C**) Cap stage at E13.5 to E14.5. The *Shh* expression is observed in the primary enamel knot. (**D**) Bell stage at E15.5 to E18.5. *Shh* expresses is detected in the stratum intermedium, pre-ameloblasts and internal enamel epithelium.

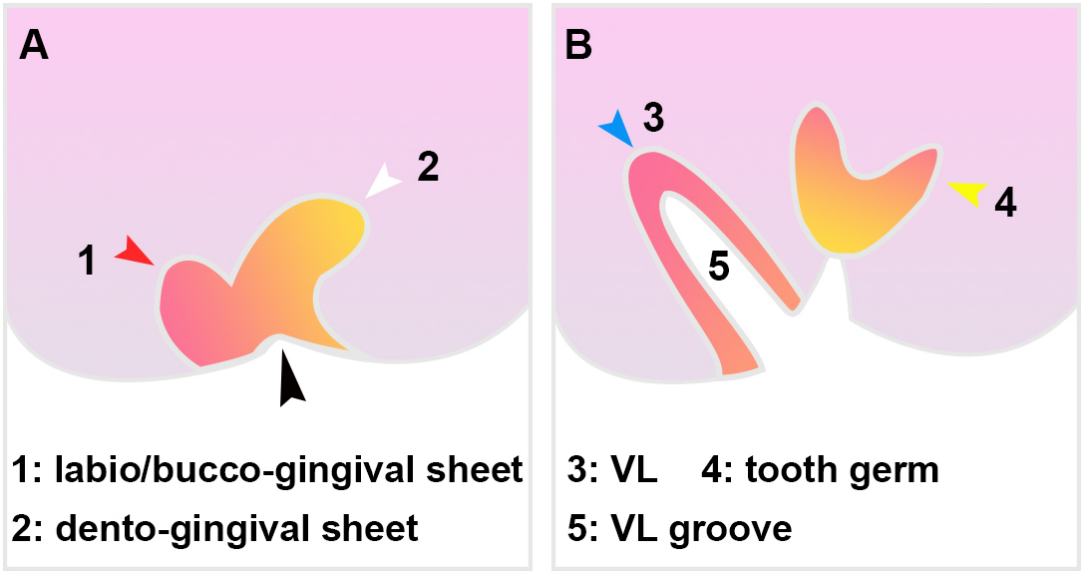

Figure 4. A basic illustration demonstrates the development of dento-gingival sheet and labio-gingival sheet in human embryos. (**A**) During the second month of embryonic development in humans, epithelial thickening grew into the underneath tissue, forming the labio/bucco-gingival sheet (A1) and dento-gingival sheet (A2). The labio-tectal furrow was indicated by a black arrowhead. (**B**) The dento-gingival sheet produced the ectodermal section of tooth germs (B4). Meanwhile, the labio/bucco-gingival sheet developed into the epithelia (B3) that covered the interior surface of the lip and a portion of the gingiva. 1: labio/bucco-gingival sheet (red arrowhead), 2: dento-

gingival sheet (white arrowhead), 3: vestibular lamina (VL) (blue arrowhead), 4: tooth germ (yellow arrowhead), 5: VL groove.

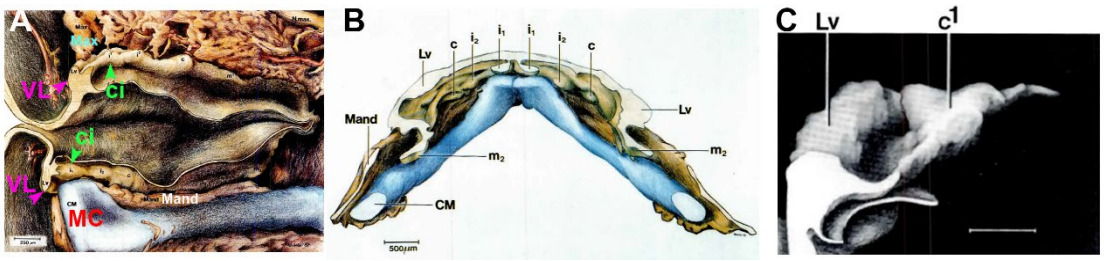

Figure 5. Spatial arrangement of oral cavity and its surrounding structures. (**A**) 37mm crown-rump length (CRL) human embryo. Based on a 3D reconstruction of the right oral cavity and its adjacent tissues, it was observed that the tooth germs i1 in the maxilla region were in the bud stage, the maxilla extended into the groove between the Lv (VL) and Ld (DL). In the lower jaw, i1 had developed to the early cap stage. Additionally, the CM (MC) swell had reached adjacent to the bud i1, and a portion of the Mand was situated in the space between the CM (MC) and other dental germs. (**B**) 21mm CRL human embryo. A 3D reconstruction was used to examine the lower tooth primordia and the surrounding tissues, which revealed that the Lv (VL) runs continuously and externally to the tooth germs. Furthermore, the Lv (VL) was found to be fused with the central incisor. (**C**) 37mm CRL human embryo. A 3D reconstruction of the upper canine primordia and the Lv (VL) showed that the VL was particularly thick in this region. Lv (VL): vestibular lamina; Ld (DL): dental lamina; i1: primary central incisor primordia; i2: primary lateral incisor primordia; c: primary canine primordia; m1: the primary 1st molar primordia; m2: the primary 2nd molar primordia; Mand: mandibular bone; Max: maxilla; CM (MC): Meckel's cartilage (adapted from **Radlanski,**

1995).

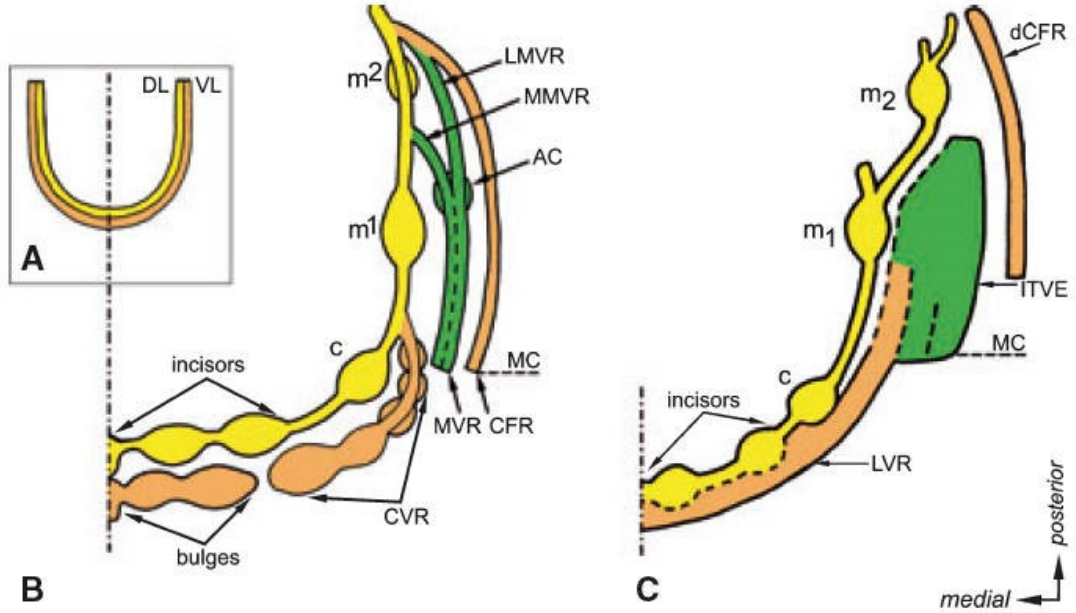

Figure 6. Spatial interactions of the DL and VL in human fetus. The dental epithelium is tinted yellow, and the base of the oral vestibule is shaded in orange. The rest VL epithelium is green. (**A**) The prevailing theory posits that the VL is a continuous entity that runs externally and parallel the DL. (**B**) VL and DL in the upper jaw. Recent findings suggest that the upper VL epithelial bulges initially appear outside of the DL in the lip area. These bulges fuse together and develop into the CVR situated posteriorly. The CVR merges with the dental mound located posterior to the c. Within the cheek area, the vestibular epithelium gives rise to both the MVR and CFR. The CFR refers to the epithelium that lines the mucosal inflection, separating the cheeks and teeth. Posteriorly, the MVR separates into two distinct branches MMVR and LMVR as it extends backwards. (**C**) VL and DL in the lower jaw. The lower vestibular epithelium exhibits several distinct structures, including the LVR, ITVE, and the dCFR. In the lower

incisor region, the vestibular and dental epithelium are fused together. VL: vestibular lamina; DL: dental lamina; CVR: canine vestibular ridge; c: deciduous canine primordium; CFR: cheek-furrow ridge; LMVR: lateral molar vestibular ridge; MMVR: medial molar vestibular ridge; MVR: molar vestibular ridge; AC: accessory epithelial cap; MC: mouth corner; LVR: labial vestibular ridge; ITVE: irregularly thickened vestibular epithelium; dCFR: mandibular cheek furrow ridge; m1: first deciduous molar; m2: second deciduous molar (**Hovorakova *et al.*, 2007**).

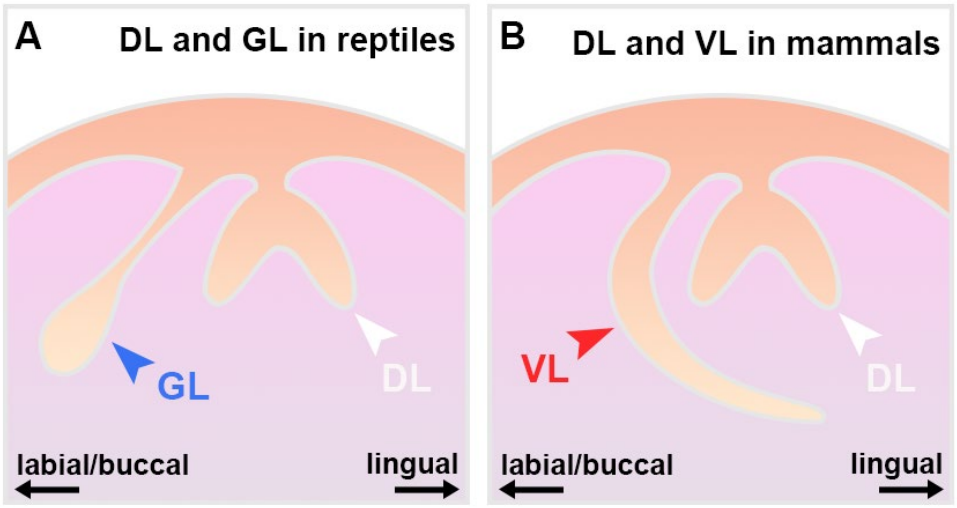

Figure 7. DL-gland lamina in reptiles and DL-VL lamina in mammals. (**A**) In reptiles, the primary epithelial thickening can develop into the DL and an adjacent gland lamina, such as the venom gland in snake and gland in chameleons. (**B**) In mammals, this primary epithelial thickening can develop into the DL and an adjacent vestibular lamina. Both the glands and VL located in the buccal/labial side of the DL. DL: dental lamina; VL: vestibular lamina; GL: gland lamina.

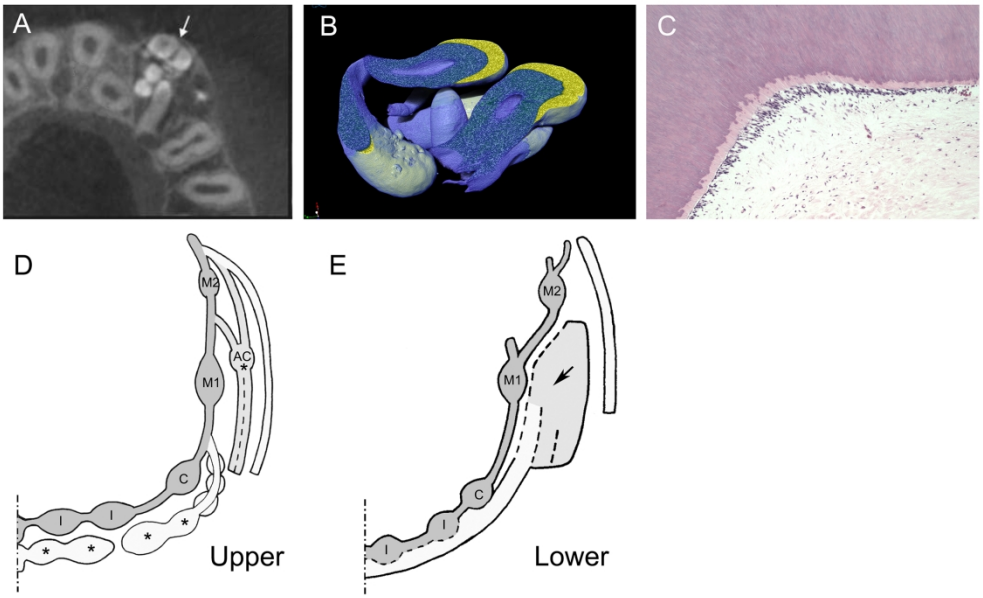

Figure 8. Odontomas formation associated with VL. (**A**) Cone Beam Computed Tomography (CBCT) photograph of a 10-year old patient, showing the odontomas formation located in the anterior upper jaw. (**B**) The MicroCT scan displays the dental structures within odontoma. (**C**) Histological section of odontoma toothlet, which shows a structured odontoblasts layer. (**D, E**) The upper and lower VL/DL in human fetuses are visualized by 3D reconstructions (**Hovorakova *et al.*, 2007**). Dark grey: DL, I: Incisors, C: Canines, M1: the 1st molar, M2: the 2nd molar, AC: accessory cusp. Asterisks: highlights of the areas to form compound odontomas; Arrow: the region where complex odontomas may form (**Hovorakova *et al.*, 2020**).

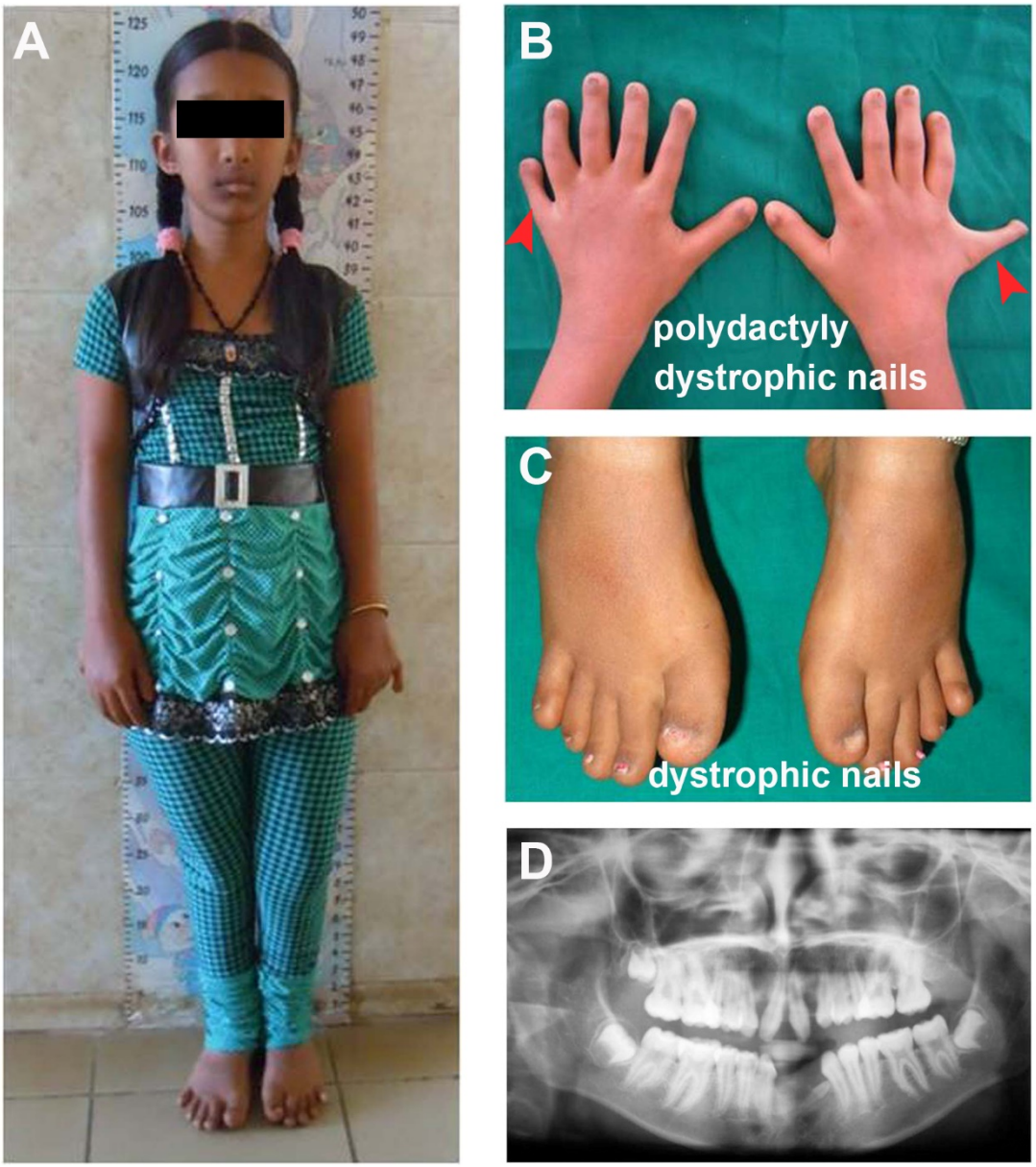

Figure 9. Some typical clinical features of EvC patients. (**A**) The typical characteristics of a 13-year-old patient, who present normal trunk and facial development but with short stature (4 feet). (**B, C**) Supernumerary fingers and hypoplastic, fragile or missing nails. (**D**) A panoramic X-ray displays partial absence of teeth and an impacted incisor in the lower jaw. Red arrowheads point out the supernumerary fingers (adapted from **Sasalawad *et al.*, 2013**).

Figure 10. Oral vestibule and tooth defects seen in EvC patients. (**A**) Multiple broad labial frenula and conical incisors in the upper jaw. White arrowheads point out the accessory labio-gingival frenulum, and blue arrowheads point out the conical incisors. (**B**) Upper broad median frenum (white arrowhead) with highly attachment to the gingival margin, leading to the increased space between the upper incisors. Tooth defects include malocclusion, conical shaped teeth, and the missing or impacted lower incisors (white asterisk). (**C**) Lower broad median frenum (white arrowhead) with highly attachment to the gingival margin. (adapted from **Sasalawad *et al.*, 2013**; adapted from **Kalaskar and Kalaskar, 2012**).

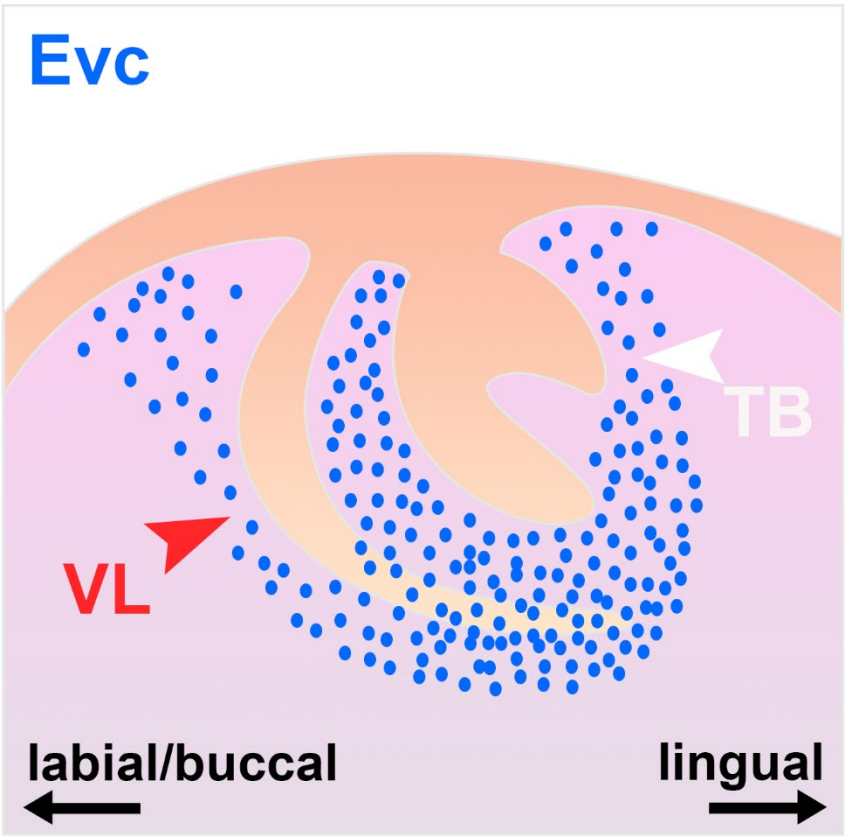

Figure 11. *Evc* expression pattern in the murine VL and TB. At E15.5, the expression of *Evc*, as shown using a reporter for *LacZ*, was mainly concentrated in the mesenchyme surrounding the VL and TB. Within the VL epithelium, robust expression of *Evc* was detected in the distal third region of VL. VL: vestibular lamina; TB: tooth bud.

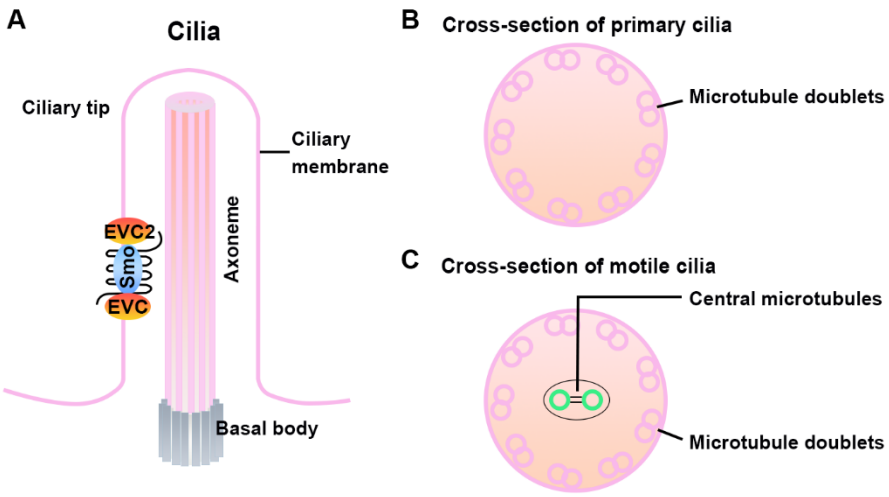

Figure 12. A diagrammatic representation illustrates the structures of primary cilium and motile cilium. (**A**) The cilium's main structural components including ciliary membrane, basal body, axoneme, and EVC zone. (**B**) Specifically, the axoneme within the primary cilium consists of a ring that contains nine microtubule doublets. (**C**) In contrast to primary cilium, the motile cilium exhibits a distinct structural arrangement known as the "9+2" structure, which consists of a central pair of microtubules.

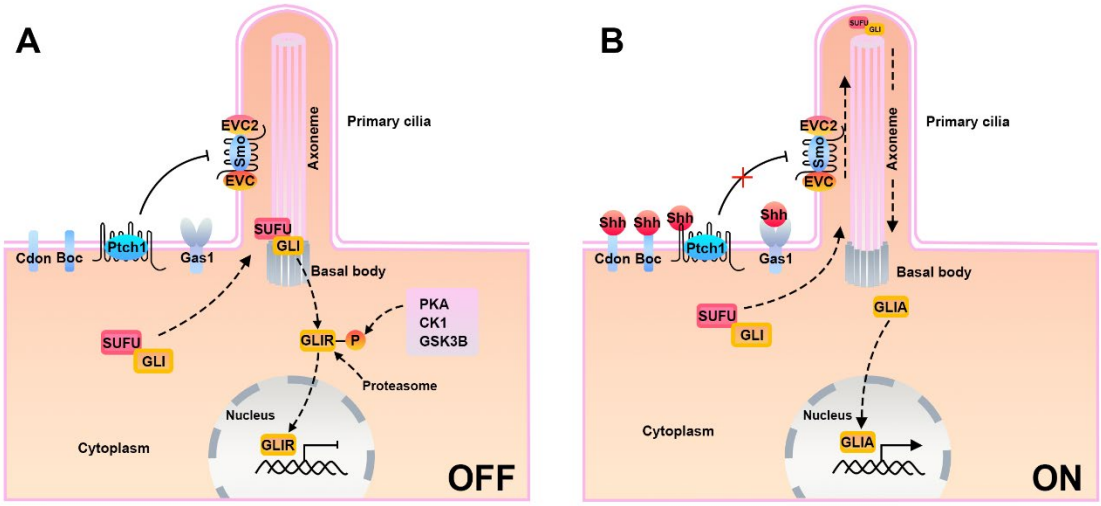

Figure 13. A basic diagram depicting the key steps of Shh signaling transduction in the primary cilium. (**A**) In the inactive (OFF) state, PTCH1 gathers on the primary cilium membrane and suppresses the function of SMO. SUFU sequesters GLI proteins and triggers their phosphorylation by GSK3B, PKA, and CK1. Following phosphorylation, GLI proteins are proteolytically cleaved to truncated repressor forms that suppress the signalling transduction. (**B**) The binding of SHH to PTCH1 activates the Shh signaling pathway (ON), with facilitation from co-receptors CDO, BOC, and GAS1. SMO accumulates in the ciliary membrane and interacts with EVC/EVC2 proteins. The SUFU-GLI complex is transported to the cilium tip and dissociated, full-length GLI then enters into the nucleus to activate the pathway.

2) Figures in chapter 6 (unpublished)

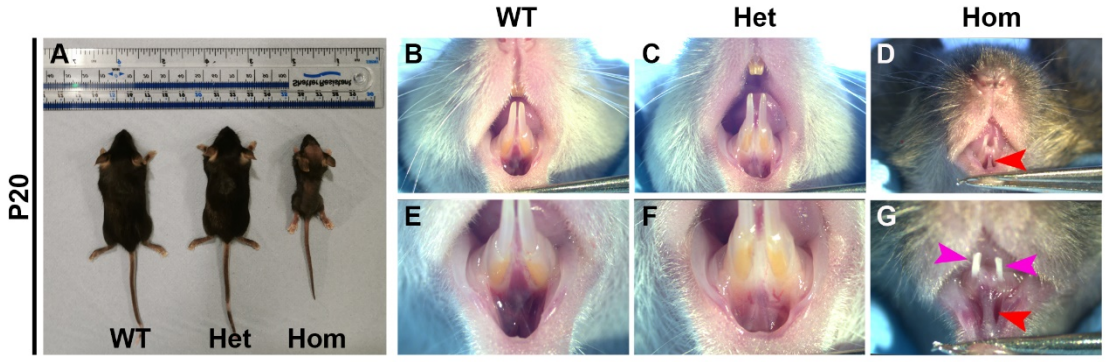

Figure 14. The observed characteristics of the *Evc* mutants at P20. (**A**) Body size differences in *EVC*$^{-/-}$ (N=7), *EVC*$^{+/-}$ (N=7), and WT littermates (N=5). The *Evc* homozygous mutants exhibit a substantially reduced body size compared to the littermate controls, while the body size of *Evc* heterozygous mutants is similar to that of their littermate controls. (**B-G**) Frontal view of the incisors and oral vestibule. (**B, E**) WT littermates; (**C, F**) *Evc* heterozygous mutants (Het); (**D, G**) *Evc* homozygous

mutants (Hom); Observations in *Evc* homozygous mutants (**D, G**) showed the presence of rudimentary incisors (indicated by magenta arrowheads) and a hyperplastic lower medial vestibule that displayed high attachment to the gingival margin (indicated by red arrowheads), resulting in wider spacing between the two incisors. However, the incisors and vestibule in *Evc* heterozygous mutants (**C, F**) appeared normal and comparable to WT littermates (**B, E**). (**Qiu and Tucker, unpublished**)

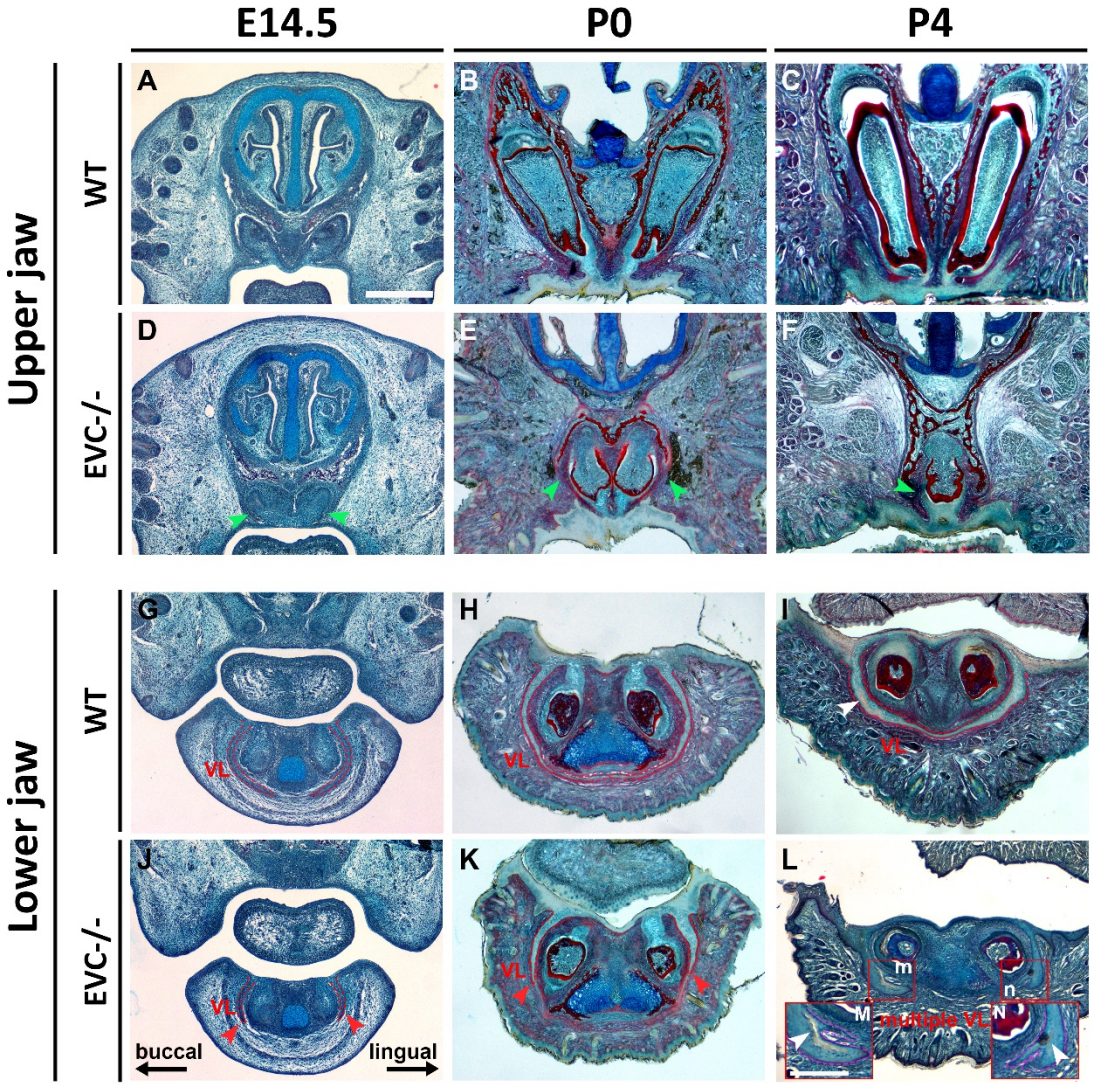

Figure 15. The *Evc*$^{-/-}$ mice exhibit defects in both tooth germ and VL in the

incisor region. (**A-L**) Histological trichrome staining was utilized to examine frontal sections of the VL and tooth germ in the anterior maxilla and mandible at E14.5, P0, and P4. (**A-F**) Anterior upper jaw. Compared to littermate controls with normal incisor tooth germ (A-C), the *Evc*$^{-/-}$ mice displayed fused incisor tooth germs at E14.5, P0, and P4 (**D-F**, green arrowheads). (**G-L**) Anterior lower jaw. (**G-I**) The VL in the littermate controls extends into the mesenchyme and surround the tooth germ, with both sides touching each other at the midline by P0. (**J-L**) A shortened VL is observed in the *Evc*$^{-/-}$ mice (red arrowheads). (**L**) Multiple VLs are observed in the *Evc*$^{-/-}$ mice. (**M, N**) in (**L**) are Higher power view of boxes m and n. VL is outlined by red dashed lines. Lingual-buccal axes are displayed in J, with the same axes utilized for all images. Scale bar in (A-L) = 500μm; Scale bar in (M, N) = 250μm. (**Qiu and Tucker, unpublished**)

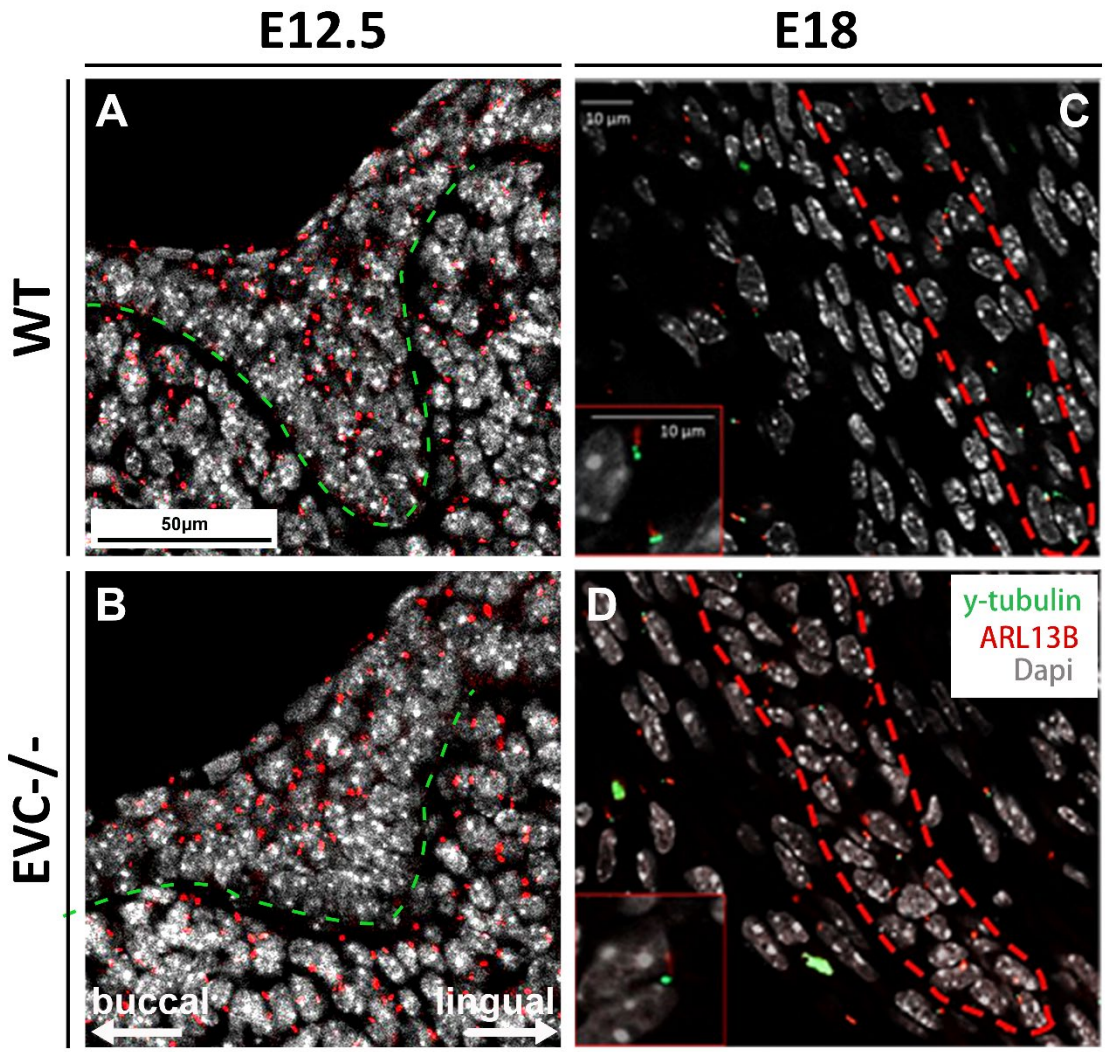

Fig 16. The ARL13B-posive cells are present in the *Evc*$^{-/-}$ mice in comparison to the WT littermates. IF for DAPI (grey), ARL13B (red), and γ-tubulin (green). (**A, B**) E12.5. ARL13B-Positive cells are detected in *Evc*$^{-/-}$ mice compared to their WT littermates. (**C, D**) E18. Magnification (red boxes in C and D) showed that the structure of primary cilia appears normal in the *Evc*−/− mice, as labelled by ARL13B and γ-tubulin. Buccal-lingual axes in panel B shown for all images. Scale bar in (A, B) = 50μm; Scale bar in (C, D) = 10μm; Scale bar in red boxes in panels C and D = 10μm. (**Qiu and Tucker, unpublished**)

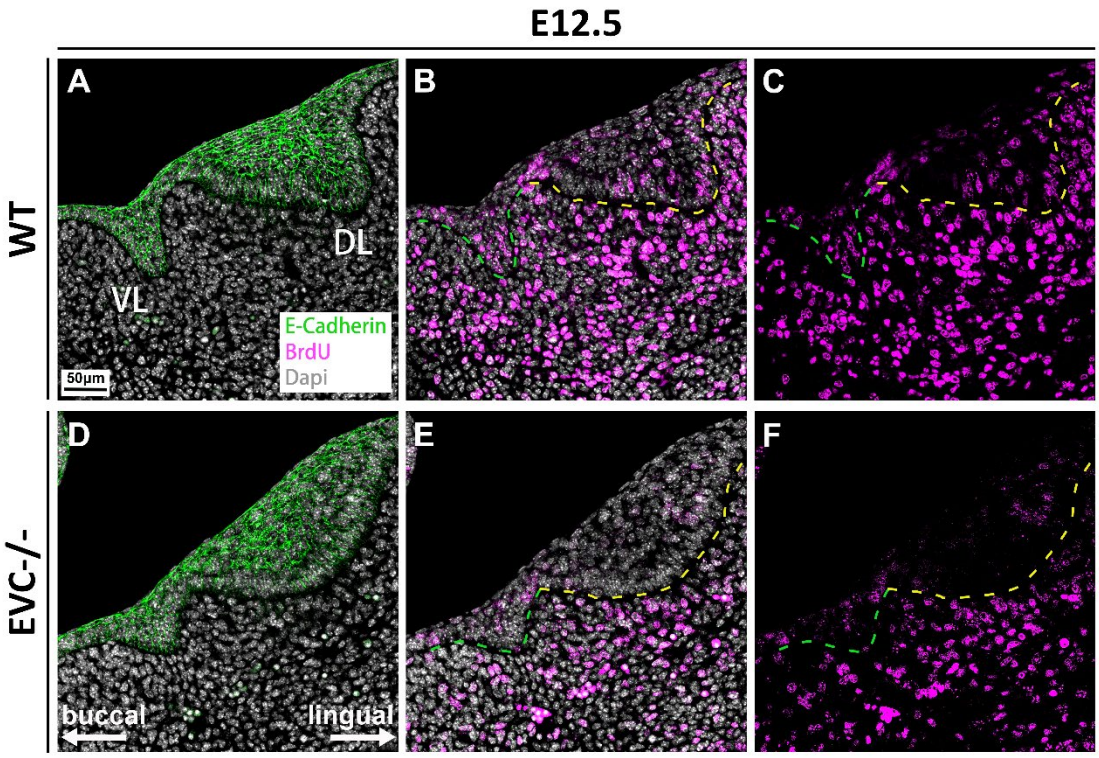

Figure 17. The truncated VL observed in *Evc* homozygous mutants was linked to a decrease in proliferation at E12.5. Immunofluorescence (IF) for BrdU (magenta), DAPI (grey), and E-cadherin (green) in the WT littermates (**A-C**) and *Evc*$^{-/-}$ mice (**D-F**). E-cadherin labelled the VL and DL (**A, D**), and a rudimentary VL was observed in the *Evc*$^{-/-}$ mice. The number of BrdU-positive cells in the VL epithelium was reduced in the *Evc*$^{-/-}$ mice (**E, F**) compared to the WT littermates (**B, C**). Buccal-lingual axes in panel D shown for all images. Scale bar in (A-F) = 50μm. (**Qiu and Tucker, unpublished**)

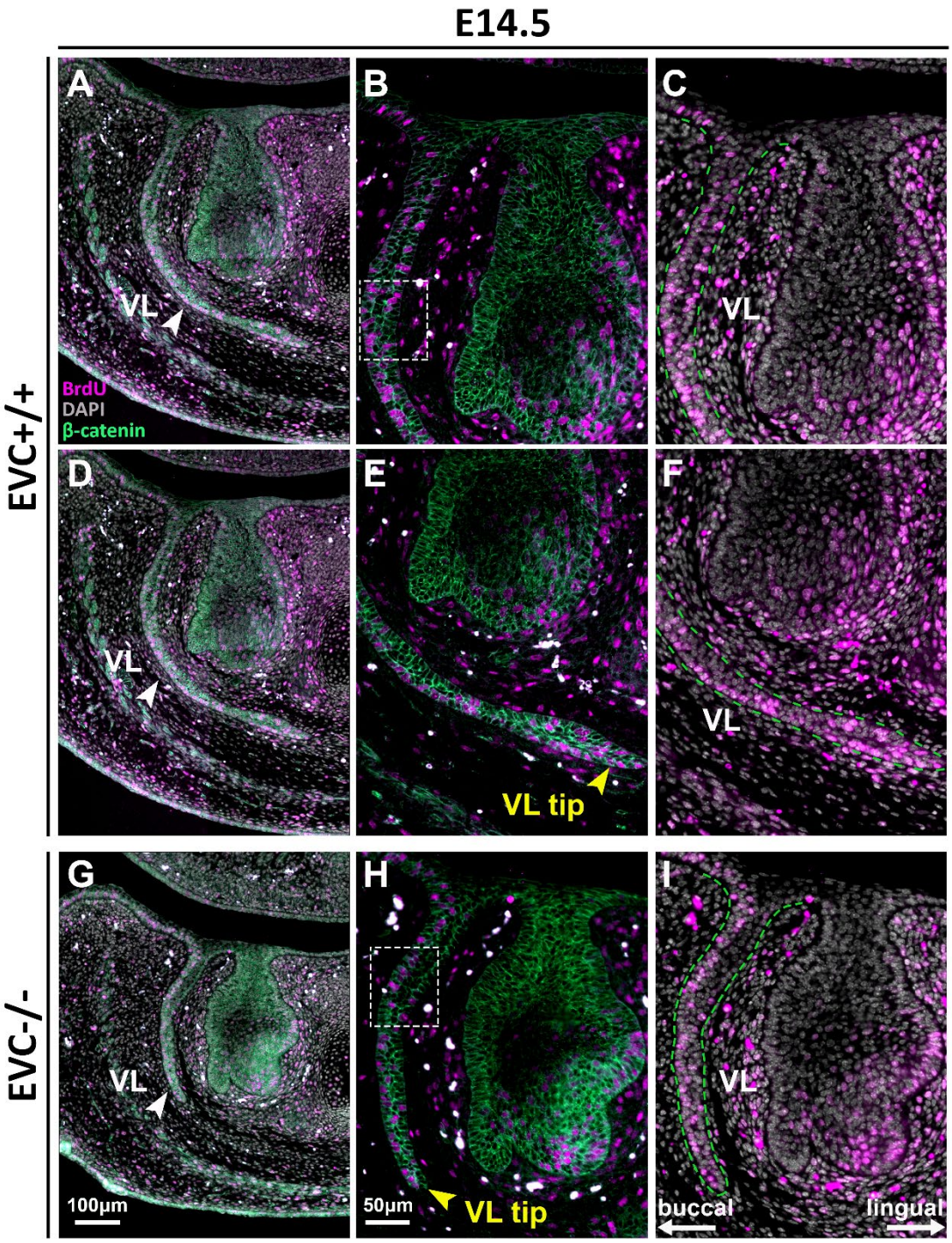

Figure 18. A reduction in proliferation at the tip of the VL at E14.5 is observed in conjunction with the truncated VL of *Evc*$^{-/-}$ mice. (**A-I**) Immunofluorescence staining was performed for β-catenin (green), BrdU (magenta), and DAPI (grey) in both the littermate controls (**A-F**) and *Evc*$^{-/-}$ mice (**G-I**). β-catenin (green) outlines the incisor tooth germ and VL in panels A, B, D, E, G ,H. Compared to the littermate controls, a

shorter VL was observed in the *Evc* homozygous mutants, along with a significant decrease in the number of BrdU-positive cells was observed in the epithelium at the end of the VL in the *Evc*$^{-/-}$ mice (yellow arrowheads). The rectangular boxes in B and H indicate the bending region of the VL, where both the *Evc* homozygous mutants and WT littermates exhibit the buccal-lingual expression pattern of proliferation. The VL is outlined by green dashed lines in panels C, F, and I. Lingual-buccal axes are displayed in I, with the same axes utilized for all images. Scale bar in (A, D, G) = 100μm; Scale bar in (B, C, E, F, H, I) = 50μm. (**Qiu and Tucker, unpublished**)

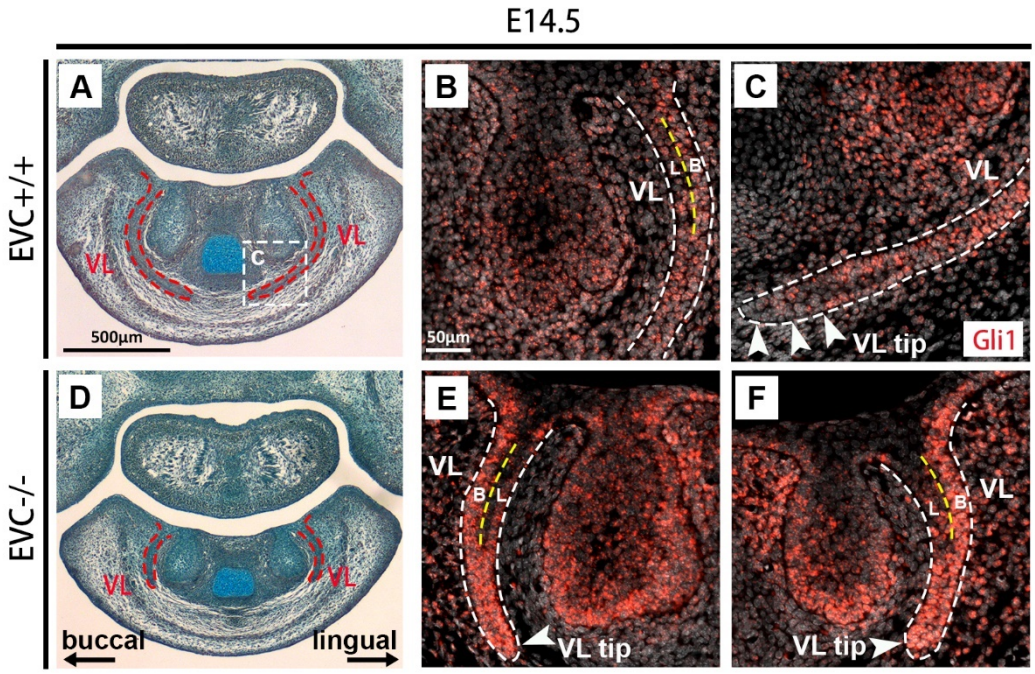

Figure 19. Upregulated expression of *Gli1* in *Evc* mutants at E14.5. (**A**, **D**) Trichrome staining of VL and DL in the lower incisor region at E14.5. Compared to the WT littermates (**A**), a decreased length of the VL was observed in the *Evc*$^{-/-}$ mice. (**B**, **C, E, F**) RNA-Scope for Gli1 (red) and DAPI (grey). (**B, C**) The WT littermates exhibited higher expression of *Gli1* on the buccal side (B) of the VL in the bending region,

compared to the lingual side (L), whereas minimal expression of *Gli1* was observed at the tip of the VL (white arrowheads in C). (**E, F**) Despite the truncated VL observed in *Evc*$^{-/-}$ mice, differential expression of *Gli1* between the buccal (B) and lingual (L) sides in the bending region of the VL was still present. *Gli1* expression at the tip of the VL was significantly increased, as indicated by the white arrowheads in panels E and F. White dashed lines outlined the boundaries of the VL, and yellow dashed lines were added to divide the VL into buccal and lingual sections. Buccal-lingual axes in panel D shown for all images. Scale bar in (A, D) = 500μm; Scale bar in (B, C, E, F) = 50μm. (**Qiu and Tucker, unpublished**)

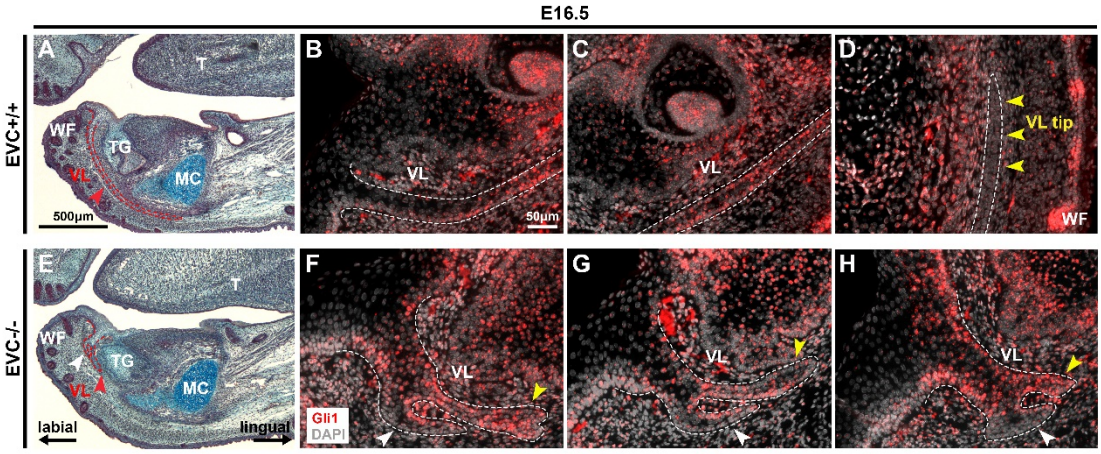

Figure 20. The defective VL of *Evc* homozygous mutant mice showing altered expression of *Gli1* at E16.5. (**A, E**) Trichrome staining performed on sagittal sections of the lower incisor region of mice at E16.5. The VL had extend under the Meckel's cartilage in the WT littermates (**A**); while shorter VL along with the additional VL were observed in the *Evc* mutants (**E**). (**B-D; F-H**) RNA-Scope for Gli1 (red) and DAPI (grey). In WT littermates (**B-D**), *Gli1* expression was mainly detected in the middle region (C) of the VL, with only a few detected in the top (B) and bottom (yellow arrowheads in D)

regions. In *Evc* mutants (**F-H**), the expression of *Gli1* in the additional branches of the VL (white arrowheads in F, G, H) was suppressed, but there was a significant increase in *Gli1* expression in the VL, particularly at the end of the VL. The VL is demarcated by white dashed lines. VL: Vestibular lamina; TG: Incisor tooth germ; MC: Meckel's cartilage; WF: Whisker follicles; T: Tongue. Labial-lingual axes in panel E shown for all images. Scale bars in (A, E) = 500μm; Scale bar in (B-D; F-H) =50μm. (**Qiu and Tucker, unpublished**)

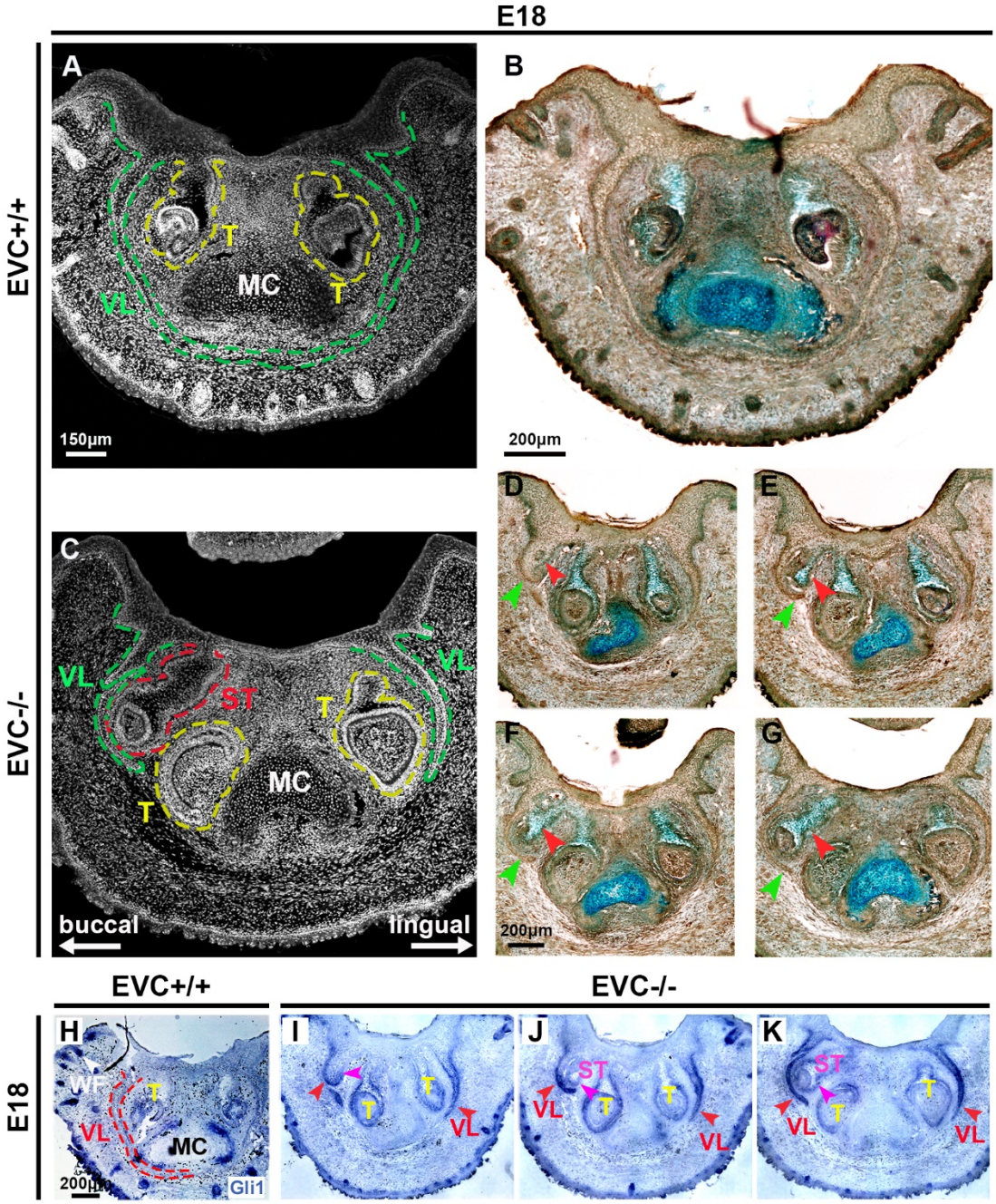

Figure 21. Extra tooth germ formed in the *Evc* homozygous mutants, with upregulated *Gli1* expression in the truncated VL and the normal *Gli1* expression in the extra tooth at E18. (**A, C**) Immunofluorescence for DAPI (grey). (**A**) WT littermate control. (**C**) *Evc* homozygous mutant displays a supernumerary tooth germ on the lingual side of the truncated VL. (**B, D-G**) To provide further insight, histological frontal sections of the anterior mandible were obtained using trichrome staining. (**B**)

WT littermate control. (**D-G**) *Evc* homozygous mutant show an extra tooth germ (pointed by red arrowheads) formed from the VL (indicated by green arrowheads). (**H-K**) Dig insitu hybridization for Gli1, with positive stain in blue. (**H**) WT littermates. *Gli1* expression was notably decreased in the VL, but it continued to be present in other developing regions, including the whisker follicles, Meckel's cartilage, and tooth germ. (**I-K**) *Evc* mutants. There is an upregulation of *Gli1* expression in both the truncated VL and the VL giving rise to the extra tooth germ, especially at the end of the VL. VL: Vestibular lamina; T: Incisor tooth germ; MC: Meckel's cartilage; WF: Whisker follicles; ST: supernumerary tooth germ. Buccal-lingual axes displayed in C shown for all images. Scale bars in (A, C) = 150μm; Scale bar in (B) = 200μm; Scale bar in (D-G) = 200μm; Scale bar in (H-K) = 200μm. (**Qiu and Tucker, unpublished**)

3) Figures in supplementary for chapter 3 (unpublished)

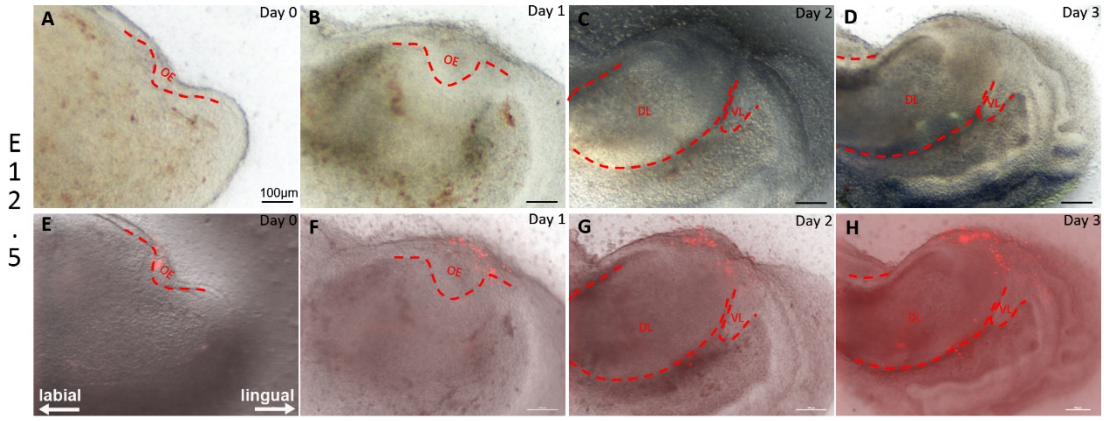

Figure S1. The DiI tracing experiment reveals that the origin of murine VL and DL can be traced back to the same oral epithelial placode. (**A-D**) The development of murine VL and DL at E12.5 after 3 days in culture. At Day0 (E12.5), a single

thickened epithelium was observed. (**E-H**) The corresponding slices of VL and DL labeled with DiI (red fluorescence). The caudal portion of the epithelial thickening was labeled with DiI at Day0 (E12.5). The DiI extended to label the oral epithelium associated with the DL, while the non-labelled portion of the placode gave rise to VL. The VL and DL were outlined with red dashed lines. VL: vestibular lamina; DL: dental lamina; OE: oral epithelium. Scale bar in (A-H) = 100μm. Labial-lingual axes shown in E, same plane for all images. (**Qiu and Tucker, unpublished**)

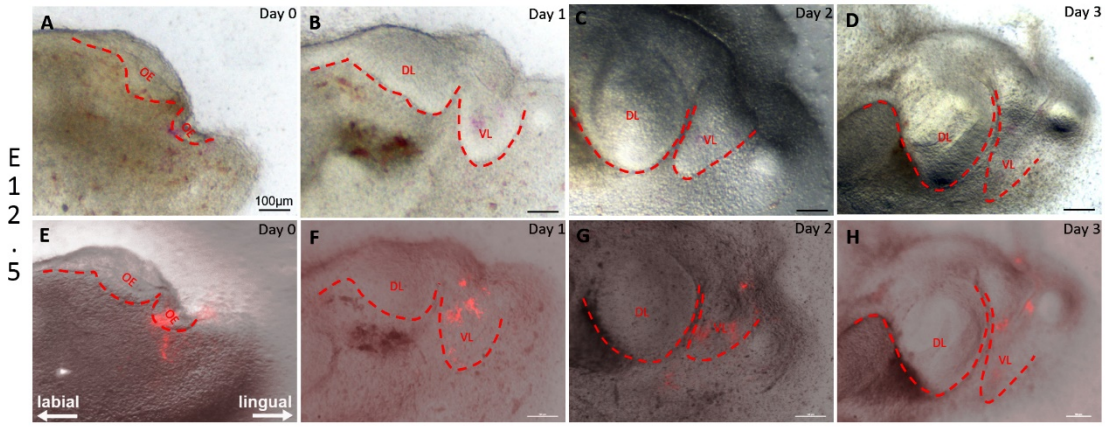

Figure S2. The DiI tracing results demonstrate that VL and DL form from two distinct adjacent thickenings, and the VL is situated at the labial side of the DL. (**A-D**) The development of murine VL and DL at E12.5 after 3 days in culture. By E12.5, the primordia of VL and DL were already discernible as distinct entities when viewed as sagittal slices. (**E-H**) The corresponding slices of VL and DL labeled with DiI (red fluorescence). DiI labeling of the more rostral thickening revealed an extension of DiI downwards, which was associated with the development of VL. No DiI was observed in the DL that originated from the more caudal placode. The VL and DL were outlined with red dashed lines. VL: vestibular lamina; DL: dental lamina; OE: oral epithelium.

Scale bar in (A-H) = 100μm. Labial-lingual axes shown in E, same plane for all images.

(**Qiu and Tucker, unpublished**)

4) Figures in supplementary for chapter 5 (unpublished)

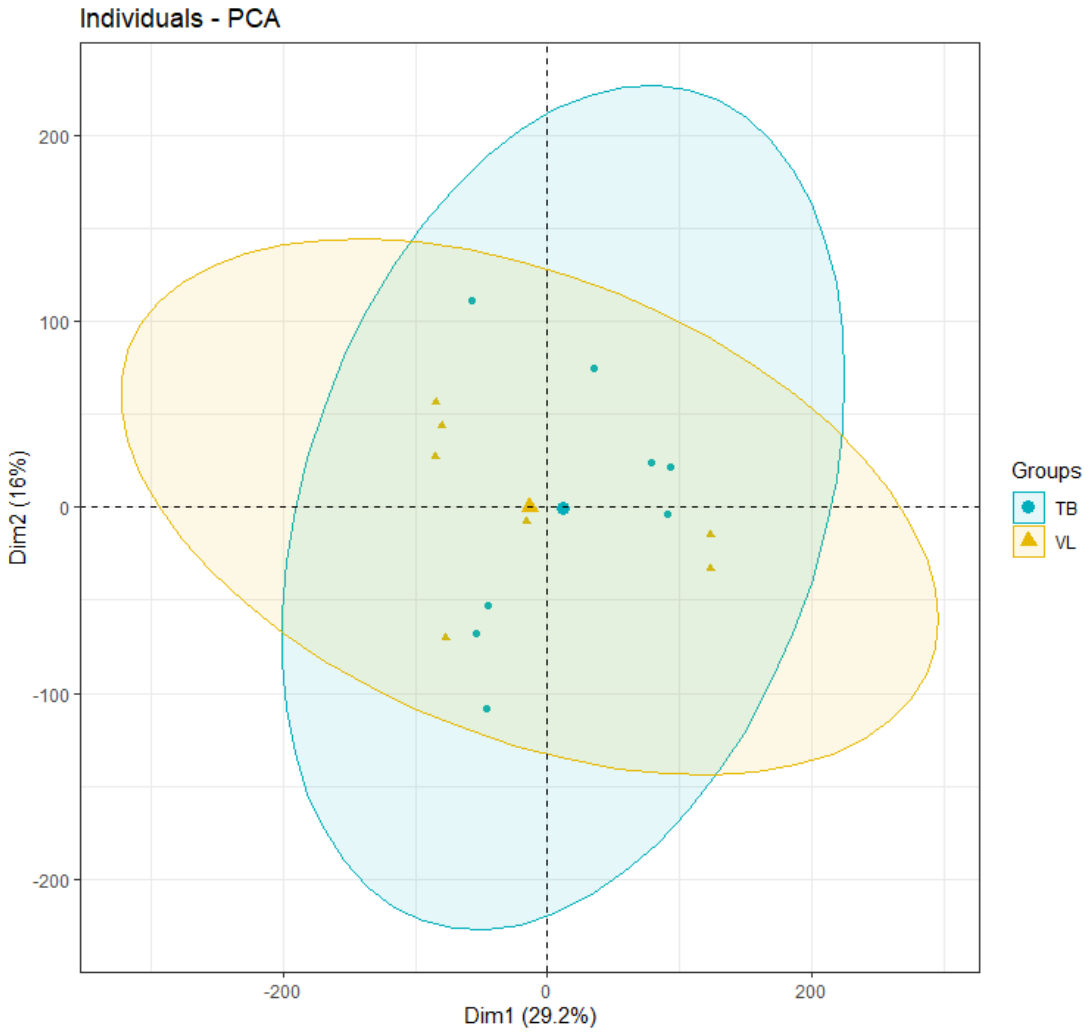

Figure S3. Principal component analysis (PCA) plot exhibited significant overlap of gene expression distributions of VL-TB datasets at E13. The scatterplot displayed blue dots representing TB samples and yellow dots representing VL samples.

The clustering of the samples was shown by ellipses. (**Qiu *et al.*, unpublished**)

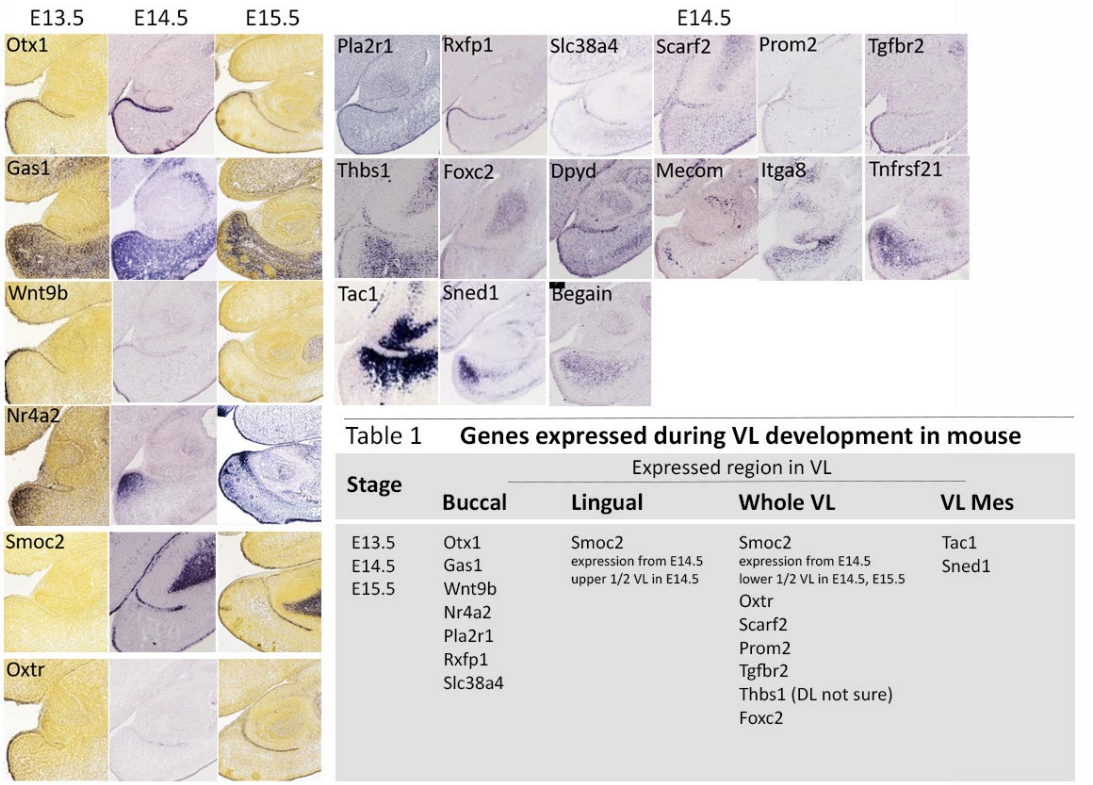

Table 1 **Genes expressed during VL development in mouse**

Stage	Expressed region in VL			
	Buccal	**Lingual**	**Whole VL**	**VL Mes**
E13.5 E14.5 E15.5	Otx1 Gas1 Wnt9b Nr4a2 Pla2r1 Rxfp1 Slc38a4	Smoc2 expression from E14.5 upper 1/2 VL in E14.5	Smoc2 expression from E14.5 lower 1/2 VL in E14.5, E15.5 Oxtr Scarf2 Prom2 Tgfbr2 Thbs1 (DL not sure) Foxc2	Tac1 Sned1

Figure S4. The molecular profile of the murine VL at E13.5, E14.5, and E15.5. The markers specific to VL at E14.5 were identified using Genepaint (https://gp3.mpg.de/) (**Visel, Thaller and Eichele, 2004**), while for E13.5 and E15.5, the datasets available in the Allen Mouse Brain Atlas (mouse.brain-map.org) were referred to. (**Qiu and Tucker, unpublished**)

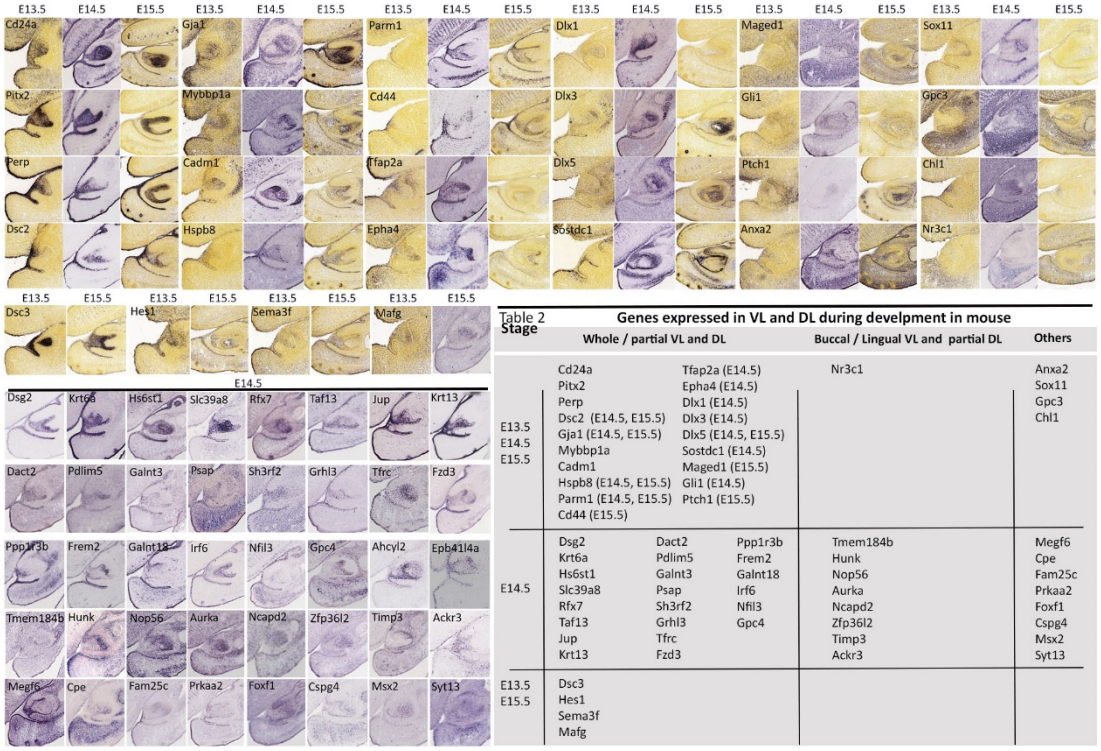

Table 2 **Genes expressed in VL and DL during develpment in mouse**

Stage	Whole / partial VL and DL		Buccal / Lingual VL and partial DL	Others
E13.5 E14.5 E15.5	Cd24a Pitx2 Perp Dsc2 (E14.5, E15.5) Gja1 (E14.5, E15.5) Mybbp1a Cadm1 Hspb8 (E14.5, E15.5) Parm1 (E14.5, E15.5) Cd44 (E15.5)	Tfap2a (E14.5) Epha4 (E14.5) Dlx1 (E14.5) Dlx3 (E14.5) Dlx5 (E14.5, E15.5) Sostdc1 (E14.5) Maged1 (E15.5) Gli1 (E14.5) Ptch1 (E15.5)	Nr3c1	Anxa2 Sox11 Gpc3 Chl1
E14.5	Dsg2 Krt6a Hs6st1 Slc39a8 Rfx7 Taf13 Jup Krt13	Dact2 Pdlim5 Galnt3 Psap Sh3rf2 Grhl3 Tfrc Fzd3	Ppp1r3b Frem2 Galnt18 Irf6 Nfil3 Gpc4	Tmem184b Hunk Nop56 Aurka Ncapd2 Zfp36l2 Timp3 Ackr3	Megf6 Cpe Fam25c Prkaa2 Foxf1 Cspg4 Msx2 Syt13
E13.5 E15.5	Dsc3 Hes1 Sema3f Mafg				

Figure S5. The molecular profile of the murine VL and DL at E13.5, E14.5, and E15.5 (1). Genepaint (https://gp3.mpg.de/) (**Visel, Thaller and Eichele, 2004**) was used to identify the markers that are specific to VL and DL at E14.5. However, for E13.5 and E15.5, the Allen Mouse Brain Atlas datasets (mouse.brain-map.org) was used. (**Qiu and Tucker, unpublished**)

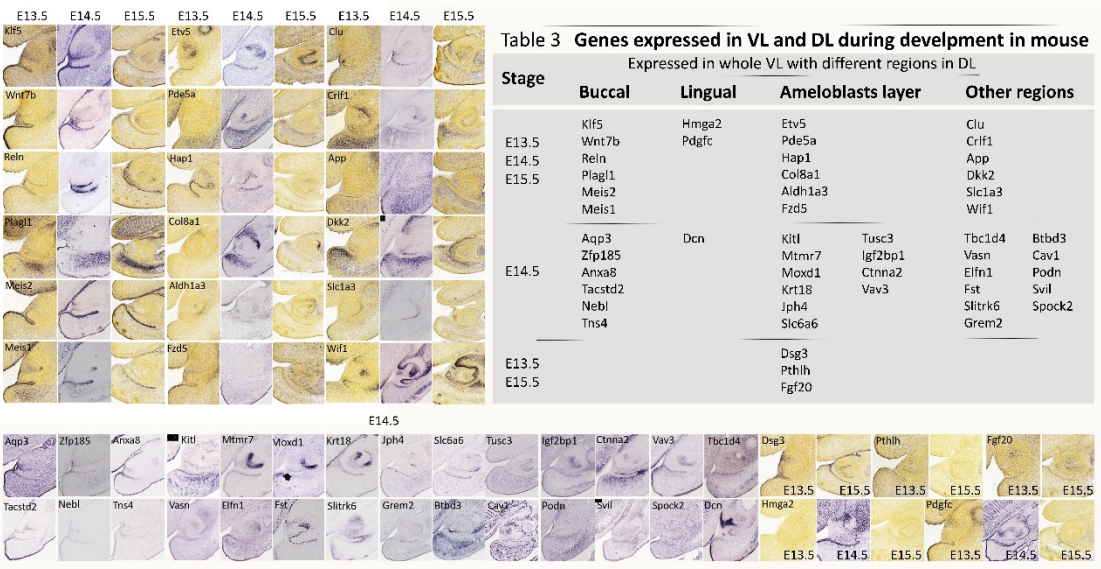

Table 3 **Genes expressed in VL and DL during develpment in mouse**

Stage	Expressed in whole VL with different regions in DL			
	Buccal	**Lingual**	**Ameloblasts layer**	**Other regions**
E13.5 E14.5 E15.5	Klf5 Wnt7b Reln Plagl1 Meis2 Meis1	Hmga2 Pdgfc	Etv5 Pde5a Hap1 Col8a1 Aldh1a3 Fzd5	Clu Crlf1 App Dkk2 Slc1a3 Wif1
E14.5	Aqp3 Zfp185 Anxa8 Tacstd2 Nebl Tns4	Dcn	Kitl Mtmr7 Moxd1 Krt18 Jph4 Slc6a6 Tusc3 Igf2bp1 Ctnna2 Vav3	Tbc1d4 Vasn Elfn1 Fst Slitrk6 Grem2 Btbd3 Cav1 Podn Svil Spock2
E13.5 E15.5			Dsg3 Pthlh Fgf20	

Figure S6. Molecular signature of the murine VL and DL at E13.5, E14.5, and E15.5 (2). To identify the specific markers for VL and DL at E14.5, Genepaint (https://gp3.mpg.de/) (**Visel, Thaller and Eichele, 2004**) was utilized, while the datasets available on the Allen Mouse Brain Atlas (mouse.brain-map.org) were used to identify the specific markers for E13.5 and E15.5. (**Qiu and Tucker, unpublished**)

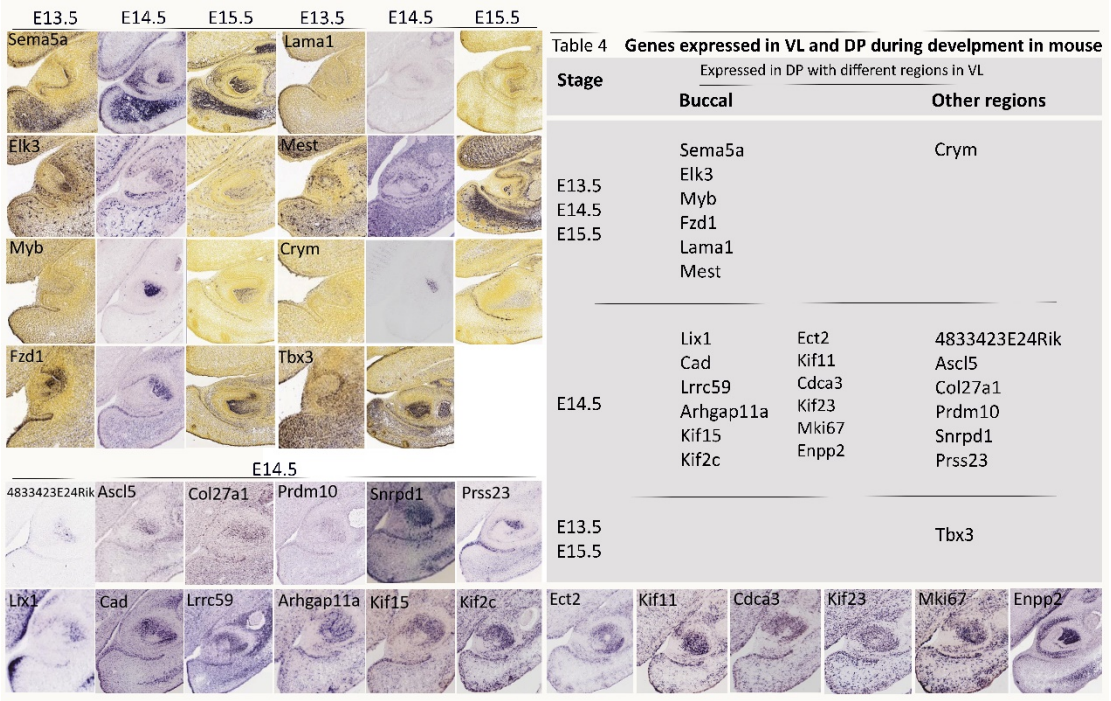

Table 4 **Genes expressed in VL and DP during develpment in mouse**

Stage	Expressed in DP with different regions in VL		
	Buccal		**Other regions**
E13.5 E14.5 E15.5	Sema5a Elk3 Myb Fzd1 Lama1 Mest		Crym
E14.5	Lix1 Cad Lrrc59 Arhgap11a Kif15 Kif2c	Ect2 Kif11 Cdca3 Kif23 Mki67 Enpp2	4833423E24Rik Ascl5 Col27a1 Prdm10 Snrpd1 Prss23
E13.5 E15.5			Tbx3

Figure S7. Molecular signature of the murine VL and DL at E13.5, E14.5, and E15.5 (3). During E14.5, Genepaint (https://gp3.mpg.de/) (**Visel, Thaller and Eichele, 2004**) was used to determine the markers that are specific to VL and DL. On the other hand, for E13.5 and E15.5, the datasets available on the Allen Mouse Brain Atlas (mouse.brain-map.org) was referenced. (**Qiu and Tucker, unpublished**)

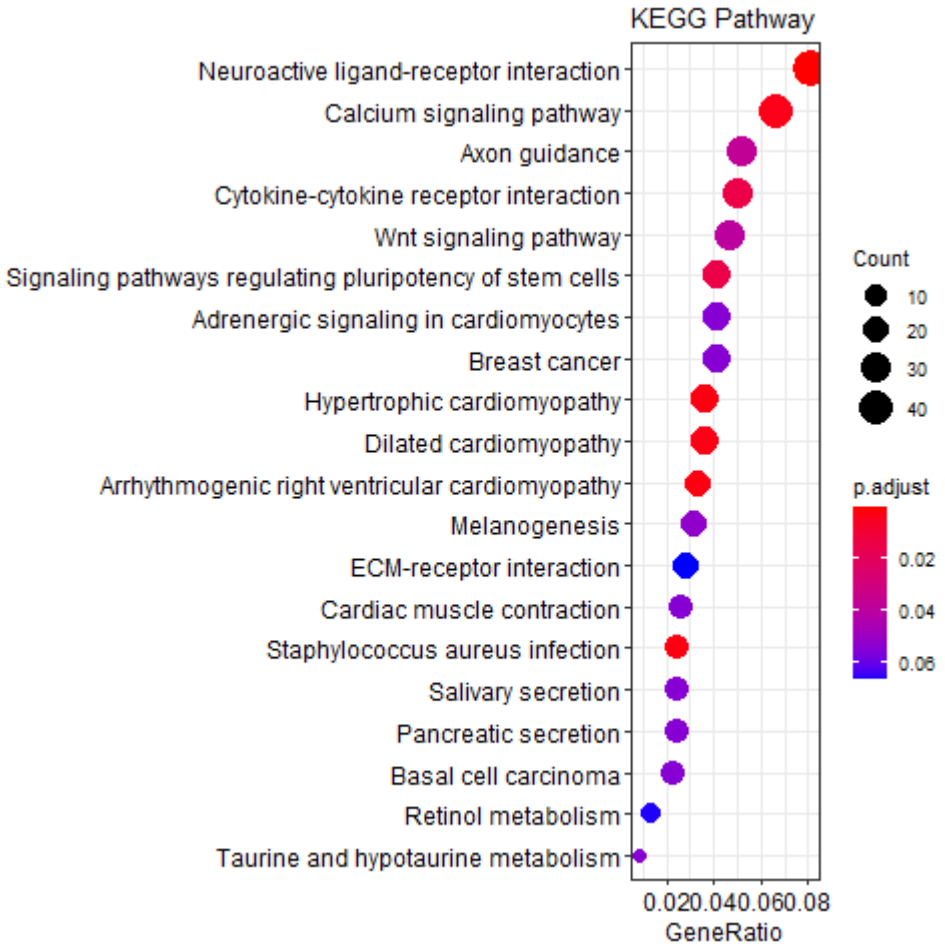

Figure S8. KEGG (Kyoto Encyclopedia of Genes andGenomes) pathway enrichment anlysis highlights the involvement of Wnt signalling pathway during VL and DL early development. (**Qiu *et al*., unpublished**)

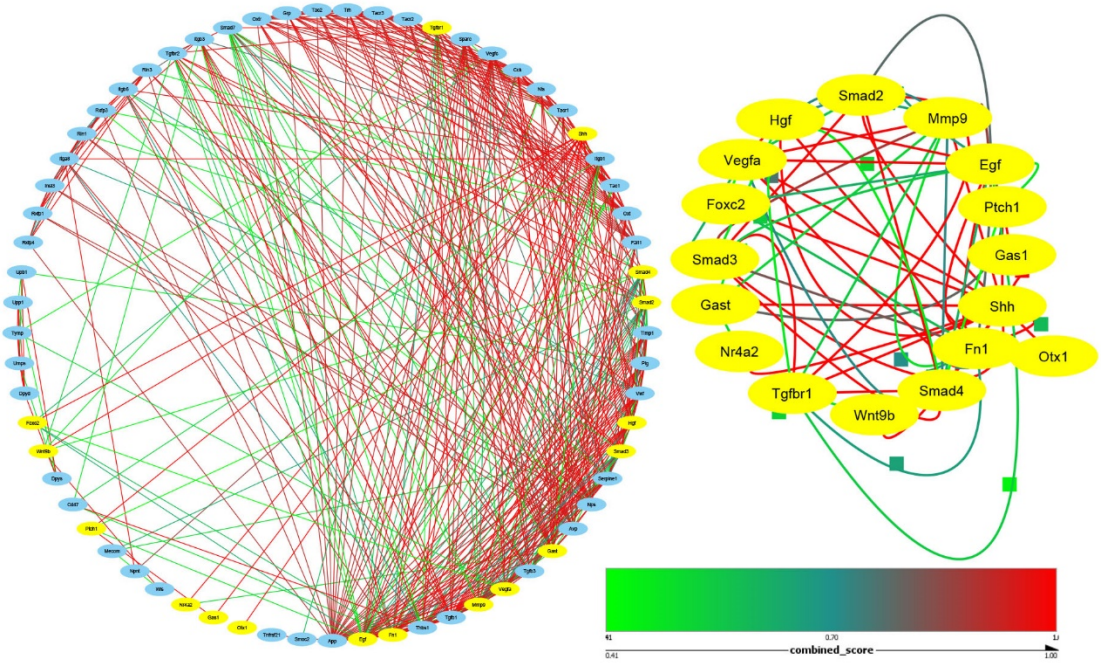

Figure S9. Protein–protein interaction (PPI) network emphasizes the interaction between the Shh and Wnt signaling. (**Qiu *et al*., unpublished**)